



The  
University  
Of  
Sheffield.

**UNIVERSITA' DEGLI STUDI DI PADOVA**  
**THE UNIVERSITY OF SHEFFIELD**



DIPARTIMENTO DI INGEGNERIA CIVILE, EDILE E  
AMBIENTALE

TESI DI LAUREA MAGISTRALE IN INGEGNERIA CIVILE

*Seismic strengthening of RC buildings with FRP  
reinforcement: analysis and feasibility*

Relatore: Prof. Ing. CARLO PELLEGRINO

Correlatore: Senior Lecturer MAURIZIO GUADAGNINI

Laureando: NICOLO' FERRARA

Matricola: 1057043

ANNO ACCADEMICO 2014-2015

## **DECLARATION STATEMENT**

---

The author certifies that all materials contained within this document is his own work except where it is clearly referenced to others.

X

---

Nicolò Ferrara

## **ACKNOWLEDGEMENTS**

---

I would like to thank my supervisor, Professor *Carlo Pellegrino* for the opportunity to work on my dissertation at the University of Sheffield.

I would like to express my gratitude to my supervisor, Senior Lecturer *Maurizio Guadagnini* for his support, patience and constructive comments throughout the preparation of this dissertation.

I would like to thank *Reyes Garcia Lopez* for his valuable assistance.

I would also like to thank all of my friends who supported me.

A special thank goes to my girlfriend *Chiara* for her love, kindness and patience she has shown.

At the end, I would like express appreciation to my family. Words cannot express how grateful I am to my parents *Vittorina* and *Graziano*, for all the sacrifices that you have made on my behalf.

## **ABSTRACT**

---

The aim of this dissertation is to investigate the behaviour of deficient RC structures under seismic action and the strengthening of them. A literature review of the beam-column joints mechanism and the existing strengthening techniques is made, in particular the Carbon Fibre-Reinforced Polymeric confinement of the elements. The seismic performance of a two storey reinforced concrete building with poor detailing in beam-column joints is investigated through non linear dynamic (time-history) analysis. In order to represent joint degradation, pullout fibres and gap properties are added to simulate bond-slip of the reinforcing bars in the beam-column joints and the concrete crushing. The DRAIN-3DX programme is used to model the structure and perform the analysis. CFRP confinement and beam-column joints strengthening have been applied to the bare frame and the global effects on the structure are investigated. The analytical results are compared with the experimental results for both the experiments and it is noted that the models could represent the behaviour of the frame under different PGA.

At the end, the feasibility of the intervention is evaluated with regard to the improving of the performances and the economic evaluating of the intervention. In particular, damage limitation is verified. A new earthquake-proof structure is designed through Straus 7 programme and a time-history analysis is performed, in order to compare the displacements with those of the CFRP retrofitted frame. The performance achieved with CFRP intervention are satisfactory and even the cost estimate is acceptable compared to the new frame.

## **TABLE OF CONTENTS**

---

<b>DECLARATION STATEMENT</b> .....	<b>II</b>
<b>ACKNOWLEDGEMENTS</b> .....	<b>III</b>
<b>ABSTRACT</b> .....	<b>IV</b>
<b>LIST OF FIGURES</b> .....	<b>X</b>
<b>LIST OF TABLES</b> .....	<b>XVII</b>
<b>1. INTRODUCTION</b> .....	<b>1</b>
1.1 Introductory Remarks.....	1
1.2 Aims and Objectives.....	2
<b>2. LITERATURE REVIEW</b> .....	<b>3</b>
2.1 Performance of substandard buildings in earthquakes.....	3
2.2 Beam-column joints.....	6
2.2.1 Exterior joints.....	7
2.2.2 Interior joints.....	9
2.2.3 Mechanic of beam-column joints during earthquakes.....	11
2.2.4 Factor affecting seismic behaviour of joints.....	13
2.2.5 Failure modes of a beam-column joint.....	14
2.2.6 Damage prediction in RC older beam-column joints.....	15
2.2.7 Need for seismic structural retrofitting.....	17
2.2.8 Seismic design aim.....	17
2.2.9 Strong column-weak beam concept.....	18
2.3 Existing strengthening techniques.....	19
2.3.1 Epoxy repair.....	21
2.3.2 Removal and replacement.....	22
2.3.3 Concrete jackets.....	23
2.3.4 Reinforced masonry blocks.....	24
2.3.5 Steel jackets and external steel elements.....	24
2.3.6 Externally bonded Fibre-Reinforced Polymeric reinforcement.....	26
2.4 Fibre-Reinforced Polymeric column confinement.....	31

2.4.1	Introduction.....	31
2.4.2	FRP-confined concrete characteristics.....	33
2.4.3	Lateral confining pressure.....	35
2.4.3.1	Lateral confining pressure in circular sections.....	36
2.4.3.2	Lateral confining pressure in rectangular sections.....	37
2.4.4	Use of confinement to increase ductility in seismic regions.....	38
2.4.5	Stress-strain model for concrete confined with stirrups.....	39
2.4.5.1	Compressive stress-strain model for confined concrete.....	39
2.4.5.2	Tensile stress-strain model for confined concrete.....	41
2.4.6	Stress-strain model for RC rectangular columns confined using FRP jacket.....	42
2.4.6.1	Definition of ultimate condition.....	45
2.4.6.2	Confined concrete compressive strength $f'_{cc}$ .....	45
2.4.6.3	Ultimate axial strain in rectangular columns $\epsilon_{cu}$ .....	47
<b>3.</b>	<b>EXPERIMENTAL INVESTIGATION.....</b>	<b>49</b>
3.1	Introduction.....	49
3.2	Description of the specimen.....	49
3.3	Geometry and details of the specimen.....	50
3.4	Material properties.....	58
3.4.1	Steel bars.....	58
3.4.2	Concrete.....	58
3.5	Additional masses.....	60
3.6	AZALEE shaking table.....	61
3.7	Specimen instrumentation.....	62
3.8	Test sequence and purpose.....	63
<b>4.</b>	<b>CFRP STRENGTHENED FRAME.....</b>	<b>66</b>
4.1	Repairing the damages.....	66
4.2	Carbon fabric for CFRP.....	67
4.3	CFRP reinforcement on BANDIT frame.....	68
4.4	Analysis of sections.....	70
4.4.1	First storey section beam (300 · 260) before strengthening.....	70
4.4.2	First storey section beam (300 · 260) after strengthening.....	71

<b>5. DRAIN-3DX</b> .....	73
5.1 Introduction.....	73
5.2 DRAIN-3DX software.....	73
5.3 Time-history (dynamic) analysis.....	74
5.4 Fiber element type 15.....	74
5.5 Material properties.....	77
5.6 Connection hinge fibers properties.....	78
5.6.1 Pullout properties for connection hinge fibers and degradation parameters.....	78
5.6.2 Gap properties for connection hinge fibers.....	80
<b>6. ANALYTICAL INVESTIGATION</b> .....	82
6.1 Introduction.....	82
6.2 Frame mass.....	82
6.3 Damping of the bare frame.....	83
6.4 Damping of the CFRP retrofitted frame.....	85
6.5 Material properties.....	86
6.5.1 Steel.....	86
6.5.2 Concrete confined with stirrups before test sequence 1.....	86
6.5.3 Concrete confined with stirrups before test sequence 4.....	89
6.5.4 Concrete confined with CFRP sheets before test sequence 4.....	90
6.5.5 TFC composite for CFRP.....	90
6.6 Element segments and cross section fibers.....	93
6.6.1 Bare frame.....	93
6.6.2 CFRP retrofitted frame.....	94
6.7 Analytical geometry of the bare frame.....	95
6.8 Analytical geometry of the CFRP retrofitted frame.....	98
6.9 Connection hinge fibers properties.....	101
6.9.1 Pullout fibers model.....	101
6.9.1.1 Pullout fibers and degradation parameters for bare frame.....	103
6.9.1.2 Pullout fibers for CFRP retrofitted frame.....	105
6.9.2 Gap fibers for bare frame and CFRP retrofitted frame.....	108
6.10 Time-history analysis results.....	109

6.10.1	Displacement time-history in test sequence 1.....	109
6.10.1.1	Response of the bare frame under 0.025g PGA.....	110
6.10.1.2	Response of the bare frame under 0.05g PGA.....	110
6.10.1.3	Response of the bare frame under 0.10g PGA.....	111
6.10.1.4	Response of the bare frame under 0.15g PGA.....	112
6.10.2	Displacement time-history in test sequence 4.....	113
6.10.2.1	Response of the bare frame under 0.05g PGA.....	113
6.10.2.2	Response of the bare frame under 0.10g PGA.....	114
6.10.2.3	Response of the bare frame under 0.20g PGA.....	115
6.10.2.4	Response of the bare frame under 0.30g PGA.....	115
6.10.2.5	Response of the bare frame under 0.35g PGA.....	116
6.11	Analytical and experimental comparisons in terms of period modes.....	117
<b>7.</b>	<b>FEASIBILITY OF THE INTERVENTION.....</b>	<b>118</b>
7.1	Introduction.....	118
7.2	Damage limitation for CFRP retrofitted frame.....	118
7.3	New earthquake-proof structure design.....	119
7.3.1	Design criteria and structural type.....	119
7.3.2	Modal response spectrum analysis with Straus 7.....	120
7.3.3	Design and detailing of beams and columns.....	122
7.3.3.1	Geometrical and reinforcement constraints for columns...126	
7.3.3.2	Geometrical and reinforcement constraints for beams.....126	
7.3.4	Design resistance of the elements.....	126
7.3.5	Damping of the frame.....	130
7.3.6	Material properties.....	130
7.3.6.1	Concrete confined with stirrups for the new frame.....	130
7.3.7	Analytical geometry of the bare frame in DRAIN-3DX.....	131
7.3.8	Time-history analysis results.....	133
7.3.8.1	Displacement time-history in test sequence 4.....	133
7.3.8.1.1	Response of the new frame under 0.05g PGA.....	133
7.3.8.1.2	Response of the new frame under 0.10g PGA.....	134
7.3.8.1.3	Response of the new frame under 0.15 PGA.....	134



7.3.9	Damage limitation for the new frame.....	135
7.4	Economic evaluation of the intervention.....	136
7.5	CFRP retrofitting rough cost estimate.....	136
7.6	New frame rough cost estimate.....	138
<b>8.</b>	<b>CONCLUSIONS.....</b>	<b>139</b>
8.1	Concluding Remarks.....	139
<b>REFERENCES.....</b>		<b>141</b>
<b>APPENDIX A.....</b>		<b>A-1</b>
<b>APPENDIX B.....</b>		<b>B-1</b>
<b>APPENDIX C.....</b>		<b>C-1</b>
<b>APPENDIX D.....</b>		<b>D-1</b>

## **LIST OF FIGURES**

---

Figure (1.1): Global seismic hazard map.....	1
Figure (2.1): Percent of dwelling per year of construction in Italy, Data processing (ISTAT 2001).....	3
Figure (2.2): Flat in Coppito (AQ), L’Aquila, 2009.....	4
Figure (2.3): RC building in Cavezzo (MO), Emilia Romagna, 2012.....	4
Figure (2.4): Typical details in lightly reinforced concrete structures.....	5
Figure (2.5): Examples of joint failures in RC structures.....	6
Figure (2.6): Exterior beam-column joints in plane and space frames.....	8
Figure (2.7): Action and forces on an exterior joint.....	8
Figure (2.8): Interior beam-column joints in plane and space frames.....	9
Figure (2.9): Action and forces on an interior joint.....	9
Figure (2.10): Statics of laterally loaded frame; Detail: Moments and shear gradient through an interior joint.....	11
Figure (2.11): Actions on an interior joint and the corresponding resistance mechanism according to Paulay and Priestley, 1992.....	12
Figure (2.12): Exterior joint specimen exhibits Damage State 9.....	16
Figure (2.13): Joint specimen exhibits Damage State 11.....	16
Figure (2.14): Exterior joint exhibiting Damage State 12.....	17
Figure (2.15): Vacuum impregnation procedure applied by French, Thorp and Tsai.....	21
Figure (2.16): Epoxy resin injection in a damaged joint.....	22
Figure (2.17): Concrete jacketing technique studied by Alcocer and Jirsa. (a) plan, and (b) perspective.....	23
Figure (2.18): Masonry blocks jacketing.....	24
Figure (2.19): Corrugated steel jacketing technique proposed by Ghobarah, Aziz and Bibbah.....	25
Figure (2.20): Retrofitting of the weak column using steel angles and bands (steel jacketing). Designed and applied by BREIN S Structural Care. Building Research Institute, Nepal.....	25
Figure (2.21): FRP-Strengthening applications (Book Composite for Construction, L.C. Bank).....	26

Figure (2.22): Flexural strengthening using CFRP strips of concrete girders in a Cement manufacturing building in Poland. (Book Composite for Construction, L.C. Bank).....	27
Figure (2.23): Installation of prefabricated CFRP L-shaped plates (shear strengthening) over existing CFRP strips (flexural strengthening). (Book Composite for Construction, L.C. Bank).....	27
Figure (2.24): Application of CFRP fabrics to concrete columns for confinement of Reggio Emilia football stadium, Italy. (Book Composite for Construction, L.C. Bank).....	28
Figure (2.25): Stress Strain relationship of matrix, fibers and resulted FRP (CNR-DT200 2004).....	29
Figure (2.26): Uniaxial tension stress-strain diagrams for different unidirectional FRPs (CFRP, GFRP, ARFP) and steel.....	30
Figure (2.27): Comparison of confinement action of steel and FRP materials (Bulletin 14, CEB-FIP 2001).....	33
Figure (2.28): Everyday life example depicting Confinement (Pilakoutas et al., 2014).....	33
Figure (2.29): Strength and ductility enhancement of FRP confined concrete Typical 2-layer AFRP jacket), normalised stress = stress divided by unconfined concrete strength. (Pilakoutas et al., 2014).....	34
Figure (2.30): Typical volumetric ratio for plain concrete under uniaxial loading (Pilakoutas et al., 2014).....	35
Figure (2.31): Confining pressure exerted by the FRP.....	36
Figure (2.32): Confining pressure exerted by the FRP in partially wrapped column.....	37
Figure (2.33): Effectively confined core for non-circular sections (Bulletin 14, CEB-FIP 2001).....	38
Figure (2.34): Lateral force-displacement response of flexure-dominated rectangular columns: (a) as-built; (b) retrofitted with GFRP jacket at the plastic hinge region (Priestley and Seible 1995).....	39
Figure (2.35): Schematic representation of the stress-strain relation for short term loading in uniaxial compression (Model Code for Concrete Structures, 2010).....	40
Figure (2.36): Tension softening and tension stiffening response (Carreira and Chu 1986).....	41
Figure (2.37): Effectively confined concrete in a rectangular column.....	42
Figure (2.38): Lam and Teng's stress-strain model for FRP-confined concrete.....	44

Figure (2.39): Illustration of proposed model for FRP-confined rectangular sections.....	46
Figure (2.40): Variation of the effective confinement area ratio with respect ratio and corner radius. a) Effect of aspect ratio; b) Effect of corner radius-to-section width ratio.....	47
Figure (3.1): BANDIT specimen (Garcia et al. 2012).....	50
Figure (3.2): Clamping of the masses under first slab (Garcia et al. 2012).....	50
Figure (3.3): Clamping of the masses on the second slab (Garcia et al. 2012).....	50
Figure (3.4): BANDIT specimen elevation (Unit: mm), (Garcia et al. 2012).....	52
Figure (3.5): BANDIT specimen top view (Unit: mm), (Garcia et al. 2012).....	52
Figure (3.6): Reinforcement in columns (Unit: mm), (Garcia et al. 2012).....	52
Figure (3.7): Reinforcement in beams (Unit: mm), (Garcia et al. 2012).....	53
Figure (3.8): BANDIT specimen reinforcement (Unit: mm), (Garcia et al. 2012).....	53
Figure (3.9): Reinforcement in upper nodes, 400 mm beam (Unit: mm), (Garcia et al. 2012).....	54
Figure (3.10): Reinforcement in upper nodes, 300 mm beam (Unit: mm), (Garcia et al. 2012).....	54
Figure (3.11): Reinforcement in lower nodes, 400 mm beam (Unit: mm), (Garcia et al. 2012).....	55
Figure (3.12): Reinforcement in lower nodes, 300 mm beam (Unit: mm), (Garcia et al. 2012).....	55
Figure (3.13): Top view of the slabs' reinforcement (Unit: mm), (Garcia et al. 2012).....	56
Figure (3.14): Lateral view of slabs' reinforcement (Unit: mm), (Garcia et al. 2012).....	56
Figure (3.15): BANDIT specimen steel footing (Unit: mm), (Garcia et al. 2012).....	57
Figure (3.16): Specimen foot filled with concrete and ready for the formwork to be bolted (Garcia et al. 2012).....	57
Figure (3.17): Steel specimen foot (Garcia et al. 2012).....	57
Figure (3.18): Instrumented compression testing of a concrete cylindrical sample (Garcia et al. 2012).....	59
Figure (3.19): AZALEE shaking table (Garcia et al. 2012).....	61

Figure (3.20): AZALEE shaking table's 6 DOF (Garcia et al. 2012).....	61
Figure (3.21): Specimen instrumentation (Garcia et al. 2012).....	62
Figure (4.1): Welding of bars in second level nodes (Garcia et al. 2012).....	66
Figure (4.2): Mortar repair at second floor joint and injection ports for crack injection (Garcia et al. 2012).....	66
Figure (4.3): Epoxy resin injection in a damaged joint (Garcia et al. 2012).....	67
Figure (4.4): CFRP strengthening used at beam-column joints of frame A (Garcia et al. 2012).....	69
Figure (4.5): CFRP strengthening in 1 <sup>st</sup> floor (Garcia et al. 2012).....	69
Figure (4.6): CFRP strengthening in 2 <sup>nd</sup> floor (Garcia et al. 2012).....	69
Figure (4.7): 1 <sup>st</sup> floor beam (300) section before strengthening.....	70
Figure (4.8): 1 <sup>st</sup> floor beam (300) section after strengthening.....	72
Figure (5.1): Element Type 15 Model (Powell and Campbell, 1994).....	76
Figure (5.2): Concrete material properties (Powell and Campbell, 1994).....	77
Figure (5.3): Steel material properties (Powell and Campbell, 1994).....	77
Figure (5.4): Pullout fiber basic properties (Powell and Campbell, 1994).....	78
Figure (5.5): Pullout fiber degradation properties (Powell and Campbell, 1994)...	79
Figure (5.6): Gap fiber properties (Powell and Campbell, 1994).....	80
Figure (6.1): Distribution and modelling of the masses in BANDIT frame.....	83
Figure (6.2): Stress-strain model and DRAIN-3DX values for steel.....	86
Figure (6.3): Compressive stress-strain model from CEB (2010) and DRAIN-3DX for confined concrete in 1 <sup>st</sup> floor columns.....	87
Figure (6.4): DRAIN-3DX stress-strain model and values for confined concrete in 1 <sup>st</sup> floor columns.....	88
Figure (6.5): Compressive stress-strain model for all confined concrete elements before test sequence 1.....	88
Figure (6.6): Comparison between stress-strain behaviour for concrete columns in 1 <sup>st</sup> floor before tests sequence 1 and 4 and DRAIN-3DX values for concrete before test sequence 4.....	89
Figure (6.7): DRAIN-3DX compressive stress-strain model for all confined concrete elements before test sequence 4.....	90

Figure (6.8): Comparison between compressive stress-strain model for concrete confined with stirrups and CFRP confined concrete in 1 <sup>st</sup> floor columns.....	91
Figure (6.9): DRAIN-3DX stress-strain model and values for CFRP confined concrete in 1 <sup>st</sup> floor columns.....	91
Figure (6.10): DRAIN-3DX compressive stress-strain model for all CFRP confined concrete elements.....	92
Figure (6.11): Tensile stress-strain model for dry carbon fibres and TFC composite for CFRP.....	92
Figure (6.12): Fibers cross section for 1 <sup>st</sup> floor columns in both bare frame and CFRP retrofitted frame.....	93
Figure (6.13): Fibers cross section for 1 <sup>st</sup> floor columns in CFRP retrofitted frame.....	94
Figure (6.14): Analytical modelling of the bare frame in DRAIN-3DX.....	96
Figure (6.15): Pullout and gap properties for connection hinge fibers for the bare frame in DRAIN-3DX.....	97
Figure (6.16): Analytical modelling of the CFRP retrofitted frame in DRAIN-3DX.....	99
Figure (6.17): Pullout and gap properties for connection hinge fibers for the CFRP retrofitted frame in DRAIN-3DX.....	100
Figure (6.18): Pullout properties for connection hinge fibers in 1 <sup>st</sup> floor columns (bare frame).....	103
Figure (6.19): Pullout properties for connection hinge fibers in 1 <sup>st</sup> floor beams (bare frame).....	104
Figure (6.20): Pullout properties for connection hinge fibers in 2 <sup>nd</sup> floor beams (bare frame).....	104
Figure (6.21): Comparison among pullout properties of the element in bare frame.....	105
Figure (6.22): Welding the bars in Y-direction before test sequence 4 (Garcia et al. 2012).....	106
Figure (6.23): Pullout properties for connection hinge fibers in 1 <sup>st</sup> floor columns (CFRP retrofitted frame).....	106
Figure (6.24): Pullout properties for connection hinge fibers in 1 <sup>st</sup> floor beams (CFRP retrofitted frame).....	107
Figure (6.25): Pullout properties for connection hinge fibers in 2 <sup>nd</sup> floor beams (CFRP retrofitted frame).....	107

Figure (6.26): Comparison among pullout properties of the element in CFRP retrofitted frame.....	108
Figure (6.27): Gap properties for connection hinge fibers (bare frame and CFRP retrofitted frame).....	108
Figure (6.28): 1 <sup>st</sup> floor beam-column joint before test sequence 1 (Garcia et al. 2012).....	109
Figure (6.29): 2 <sup>nd</sup> floor beam-column joint before test sequence 1 (Garcia et al. 2012).....	109
Figure (6.30): Displacement time-history for node 2020 under 0.025g PGA.....	110
Figure (6.31): Displacement time-history for node 3020 under 0.025g PGA.....	110
Figure (6.32): Displacement time-history for node 2020 under 0.05g PGA.....	111
Figure (6.33): Displacement time-history for node 3020 under 0.05g PGA.....	111
Figure (6.34): Displacement time-history for node 2020 under 0.10g PGA.....	111
Figure (6.35): Displacement time-history for node 3020 under 0.10g PGA.....	112
Figure (6.36): Displacement time-history for node 2020 under 0.15g PGA.....	112
Figure (6.37): Displacement time-history for node 3020 under 0.15g PGA.....	112
Figure (6.38): 1 <sup>st</sup> floor joint after test sequence 1 (Garcia et al. 2012).....	113
Figure (6.39): 2 <sup>nd</sup> floor joint after test sequence 1 (Garcia et al. 2012).....	113
Figure (6.40): Displacement time-history for node 2010 under 0.05g PGA.....	113
Figure (6.41): Displacement time-history for node 3010 under 0.05g PGA.....	114
Figure (6.42): Displacement time-history for node 2010 under 0.10g PGA.....	114
Figure (6.43): Displacement time-history for node 3010 under 0.10g PGA.....	114
Figure (6.44): Displacement time-history for node 2010 under 0.20g PGA.....	115
Figure (6.45): Displacement time-history for node 3010 under 0.20g PGA.....	115
Figure (6.46): Displacement time-history for node 2010 under 0.30g PGA.....	115
Figure (6.47): Displacement time-history for node 3010 under 0.30g PGA.....	116
Figure (6.48): Displacement time-history for node 2010 under 0.35g PGA.....	116
Figure (6.49): Displacement time-history for node 3010 under 0.35g PGA.....	116
Figure (7.1): Identification of the site danger with Spettri-NTCver 1.0.03.....	120
Figure (7.2): Identification of the design action with Spettri-NTCver 1.0.03.....	120
Figure (7.3): Inelastic response spectrum with Spettri-NTCver 1.0.03.....	120

Figure (7.4): New frame implemented in Straus 7.....	121
Figure (7.5): Cross-section of first-storey columns.....	122
Figure (7.6): Cross-section of second-storey columns.....	123
Figure (7.7): Cross-section of beams (300 · 260).....	123
Figure (7.8): Cross-section of beams (400 · 260).....	123
Figure (7.9): Longitudinal and transversal reinforcement in the frame (beams 300 · 260).....	124
Figure (7.10): Longitudinal and transversal reinforcement in the frame (beams 400 · 260).....	125
Figure (7.11): Interaction domain M-N for 1 <sup>st</sup> floor columns.....	127
Figure (7.12): Interaction domain M-N for 2 <sup>nd</sup> floor columns.....	127
Figure (7.13): Interaction domain M-N for 1 <sup>st</sup> floor beams (300 · 260).....	128
Figure (7.14): Interaction domain M-N for 2 <sup>nd</sup> floor beams (300 · 260).....	128
Figure (7.15): Interaction domain M-N for 1 <sup>st</sup> floor beams (400 · 260).....	129
Figure (7.16): Interaction domain M-N for 2 <sup>nd</sup> floor beams (400 · 260).....	129
Figure (7.17): DRAIN-3DX model for confined concrete in 1 <sup>st</sup> floor columns outside the critical region.....	130
Figure (7.18): DRAIN-3DX model for confined concrete in 1 <sup>st</sup> floor columns in the critical region.....	131
Figure (7.19): Analytical modelling of the new frame in DRAIN-3DX.....	132
Figure (7.20): Displacement time-history for node 2010 under 0.05g PGA.....	133
Figure (7.21): Displacement time-history for node 3010 under 0.05g PGA.....	133
Figure (7.22): Displacement time-history for node 2010 under 0.10g PGA.....	134
Figure (7.23): Displacement time-history for node 3010 under 0.10g PGA.....	134
Figure (7.24): Displacement time-history for node 2010 under 0.15g PGA.....	135
Figure (7.25): Displacement time-history for node 3010 under 0.15g PGA.....	135



## LIST OF TABLES

---

Table (2-1): Summary of repair procedures.....	20
Table (2-2): Damage states assigned to each repair technique.....	21
Table (2-3): Comparison of typical properties for epoxy adhesive, concrete and steel (Täljsten 1994).....	29
Table (2-4): Comparison between properties of fibers, resins and steel. (typical values).....	31
Table (3-1): Steel bars mechanical properties (Mean values).....	58
Table (3-2): Evaluation of cement and W/C ratio for concretes of 1 <sup>st</sup> and 2 <sup>nd</sup> floor for Bandit specimen (Garcia et al. 2012).....	59
Table (3-3): Concrete average mechanical properties (Garcia et al. 2012).....	60
Table (3-4): Tests sequences (Garcia et al. 2012).....	63
Table (3-5): First test sequence (Garcia et al. 2012).....	64
Table (3-6): Fourth test sequence (Garcia et al. 2012).....	65
Table (4-1): Geometric and mechanical characteristics of dry carbon fibres for CFRP (Garcia et al. 2012).....	67
Table (4-2): Geometric and mechanical characteristics of TFC composite for CFRP (Garcia et al. 2012).....	67
Table (6-1): Mass distribution in each node of the frame.....	83
Table (6-2): Natural frequencies and damping ratios for Bare frame (Garcia et al. 2012).....	84
Table (6-3): Mass damping coefficient and element stiffness coefficient for bare frame.....	84
Table (6-4): Natural frequencies and damping ratios for CFRP retrofitted frame (Garcia et al. 2012).....	85
Table (6-5): Modified natural frequencies and damping ratios for CFRP retrofitted frame.....	85
Table (6-6): Mass damping coefficient and element stiffness coefficient for CFRP retrofitted frame.....	85
Table (6-7): Parameters defining the mean bond stress-slip relationship of ribbed bars (Model Code CEB 2010).....	102
Table (6-8): Adopted degradation properties for both bare frame and CFRP retrofitted frame.....	105

Table (6-9): Gap fibers properties.....	109
Table (6-10): Comparison of modal periods from analytical results during test sequence 1.....	117
Table (6-11): Comparison of modal periods from analytical results during test sequence 4.....	117
Table (7-1): Damage limitation requirement for CFRP retrofitted frame.....	119
Table (7-2): Design action effects for each element of the frame.....	122
Table (7-3): Design bending moment capacity and shear resistance for 1 <sup>st</sup> floor columns.....	127
Table (7-4): Design bending moment capacity and shear resistance for 2 <sup>nd</sup> floor columns.....	127
Table (7-5): Design bending moment capacity and shear resistance for 1 <sup>st</sup> floor beams (300 · 260).....	128
Table (7-6): Design bending moment capacity and shear resistance for 2 <sup>nd</sup> floor beams (300 · 260).....	128
Table (7-7): Design bending moment capacity and shear resistance for 1 <sup>st</sup> floor beams (400 · 260).....	129
Table (7-8): Design bending moment capacity and shear resistance for 2 <sup>nd</sup> floor beams (400 · 260).....	129
Table (7-9): Mass damping coefficient and element stiffness coefficient for the new frame.....	130
Table (7-10): Damage limitation requirement for the new frame and comparison with the CFRP retrofitted frame.....	135
Table (7-11): Retail prices of the materials used for the CFRP intervention on BANDIT frame using Mapewrap C BI-AX.....	137
Table (7-12): Estimate of materials costs for the CFRP intervention on BANDIT frame using Mapewrap C BI-AX.....	137
Table (7-13): Final estimate of costs for the CFRP intervention on BANDIT frame using Mapewrap C BI-AX.....	138
Table (7-14): Final estimate of costs for the new structure.....	138

# 1. INTRODUCTION

---

## 1.1. Introductory remarks

Earthquakes are ground vibrations that are caused mainly by the fracture of the crust of the earth or by sudden movement along an already existing fault (tectonic earthquakes) and they are considered as an independent natural phenomenon. Earthquakes are caused by sudden release of elastic strain energy in the form of kinetic energy along the length of a geological fault. Rarely, earthquakes may be caused by volcanic eruptions. When earthquakes are considered in relation to structures, therefore they are a threat to humans. In some cases an earthquake becomes a really hazardous phenomenon, for instance when it causes major landslides or tsunamis. Although destructive earthquakes are confined to certain geographical areas known as the seismic zones, the large-scale damage that they may cause in densely populated areas and the associated number of deaths is such that they have an impact on the whole world. Figure (1.1) shows the global seismic hazard map. According to a report from the Center for Disaster Management and Risk reduction Technology, in 2011, total damage caused by earthquakes and their secondary hazards, including tsunamis and landslides, cost 365 billion USD, most of which is from the Tohoku earthquake that hit Japan (335 billion USD) making the costliest natural disaster on record. 19300 people died and 450000 lost their homes after tsunami hit the northeast coast of Japan. The Christchurch earthquake in New Zealand caused a total of 20 billion USD in damages.

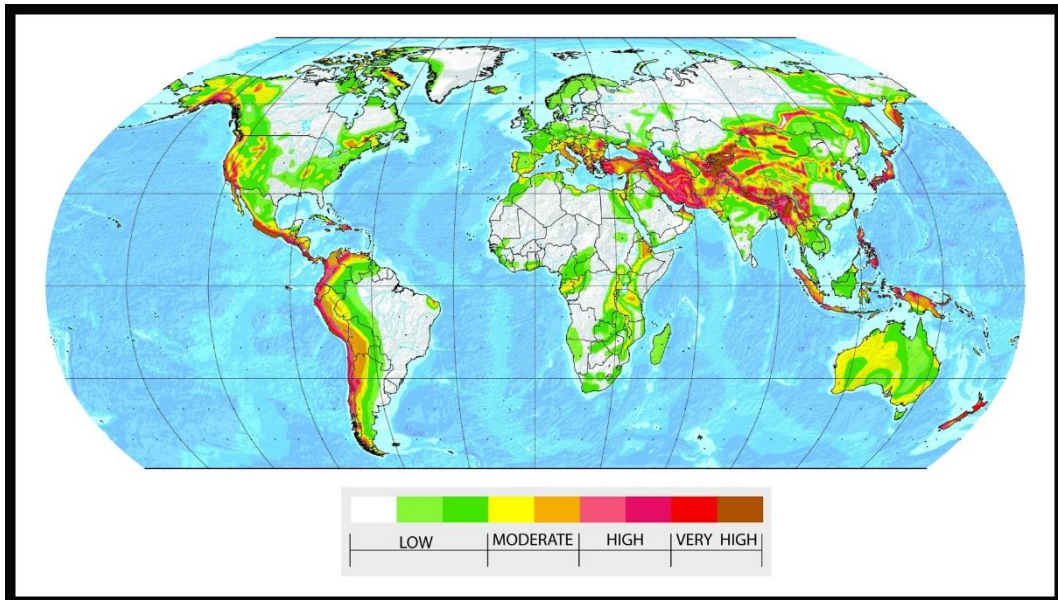


Figure 1.1: Global seismic hazard map

The major factor contributing to both economic and human loss is the collapse of buildings during earthquakes. Many structures built before 1970 were designed only for gravity loads. Therefore, many of the existing buildings may not comply with the recent seismic codes and as a result these buildings represent significant

hazard to the life of the occupants and their investments. When assessing the existing buildings deficiencies such as weak column-strong beam mechanism, absence of joint shear reinforcement, inadequate lap splice of column bars, buckling of flexural reinforcements, and insufficient anchorage of beam bars were usually observed. Seismic rehabilitation of the deficient existing buildings is a key element in the process of mitigating the hazard and achieving seismic safety, as well as for effective disaster prevention. In the conventional seismic retrofitting method using reinforced concrete, not only is the work required very time-consuming but also the weight of such a structure tends to increase due to the strengthening. Retrofitting by steel requires welding work for which special skills may be needed and the retrofitting work is complex as resin must be poured. It is further accompanied by higher construction cost. For this reason, seismic retrofit methods using CFRP were devised. Carbon fiber with high strength, light weight, and high durability has been used for the seismic rehabilitation and strengthening of existing reinforced concrete structure since 1984.

## **1.2. Aims and Objectives**

The aims of this dissertation are two fold. The first part is to analyse the structural behaviour of a simple RC frame, originally the bare frame and then the same frame but retrofitted with CFRP, when subjected to different level of seismic excitations. The last part is to evaluate the efficiency and feasibility of the intervention compared with the built of a new earthquake-proof structure with the same geometry and materials.

The following objectives are identified as essentials for the fulfilment of the aims:

- Understanding the basic principles of structural behaviour in an earthquake, in particular the mechanism of the beam-column joints.
- Understanding the principles of FRP confinement and strengthening of beam-column joints, especially to the case of BANDIT frame.
- Evaluating the dynamic response of RC frame due to different peak ground accelerations.
- Evaluating the performances of the intervention with CFRP compared to the built of a new frame;
- Evaluating the economic feasibility of the intervention.

## 2. LITERATURE REVIEW

### 2.1. Performance of substandard buildings in earthquakes

Many existing reinforced concrete structures were designed before the development of seismic codes or according to earlier versions of seismic codes. Therefore, these structures were designed either for gravity loads or for much lateral load, which were much lower than the loads specified by the current seismic codes. Many of these buildings were designed also employing poor materials and construction practices. The old provisions did not consider the contribution of joints in the overall response of the structures. As a result, these deficient structures usually have inadequate lateral load resistance, insufficient energy dissipation capacity and high strength degradation that can lead to extensive damage and collapse during severe earthquakes.

To mitigate recurring collapse of structures during earthquakes, general guidelines were adopted on the recommendation of Structural Engineers Association of California (SEAOC) in 1968.

These guidelines made three major recommendations:

- The Structure should resist a ground motion due to a minor earthquake without any damage.
- The structure should resist a moderate level of ground motion without structural damage, but possibly may undergo only some non-structural damage.
- The structures should resist a major earthquake of similar intensity of one experienced before or other that have been forecasted in the location, without collapse but minor damages might be inevitable.

In Italy, the seismic classification was introduced with Order P.C.M. n. 3274 of 20/03/2003 and then with the updated of 16/02/2006. Before these dates, not the whole of the territory was considered on a seismic risk.

Furthermore, as we can see from the figure (2.1), more than 60% of dwellings in Italy were built before the mid-1970s, so they have been designed according to old standards and have little or no seismic provision.



Figure 2.1: Percent of dwelling per year of construction in Italy  
Data processing (ISTAT 2001)

Recent earthquakes such as the Northridge 1994, Kobe 1995, Kocaeli, Mexico and Taiwan 1999, Bam 2003, Iran 2004, Pakistan 2005, China 2008, Indonesia and L'Aquila (Italy) 2009, Haiti and Chile 2010, Emilia Romagna (Italy) 2012, brought forth the vulnerability of existing reinforced concrete buildings to strong earthquakes. Failure of beam-column joints was identified as one of the leading causes of collapse of such structures (El-Amoury, 2004).

Figures (2.2) and (2.3) shows the contribution of joints to the overall response of structures and the damage level of substandard detailed structures after Abruzzo (2009) and Emilia Romagna (2012) earthquakes.



Figure 2.2: Flat in Coppito (AQ)  
L'Aquila, 2009



Figure 2.3: RC building in Cavezzo (MO)  
Emilia Romagna, 2012

Beres et al. (1996) conducted seismic experiments on 34 full scale gravity load designed buildings and the main damages were found to be in the joint panel regions followed by the development of diagonal cracks in those regions. This entails the vulnerability of existing buildings in earthquakes due to the beam-column joint failure and thus suggests the need for adapting strengthening techniques in these critical zones.

Through their reviews of detailing manuals and design codes from the past five decades and their consultation with practicing engineers, Beres et al. (1996) identified seven details, shown in Figure (2.4) as typical and potentially critical to the safety of gravity load designed structures in an earthquake.

Furthermore, other typical structural deficiencies of substandard buildings are summarised below (Pampanin et al., 2002 and Adam, 2005):

- Inadequate confining effects in the potential plastic regions.
- Inadequate anchorage detailing for both transverse and longitudinal reinforcements.
- Low quality of materials, low strength of concrete and use of plain bars.
- Strong beam and weak column.

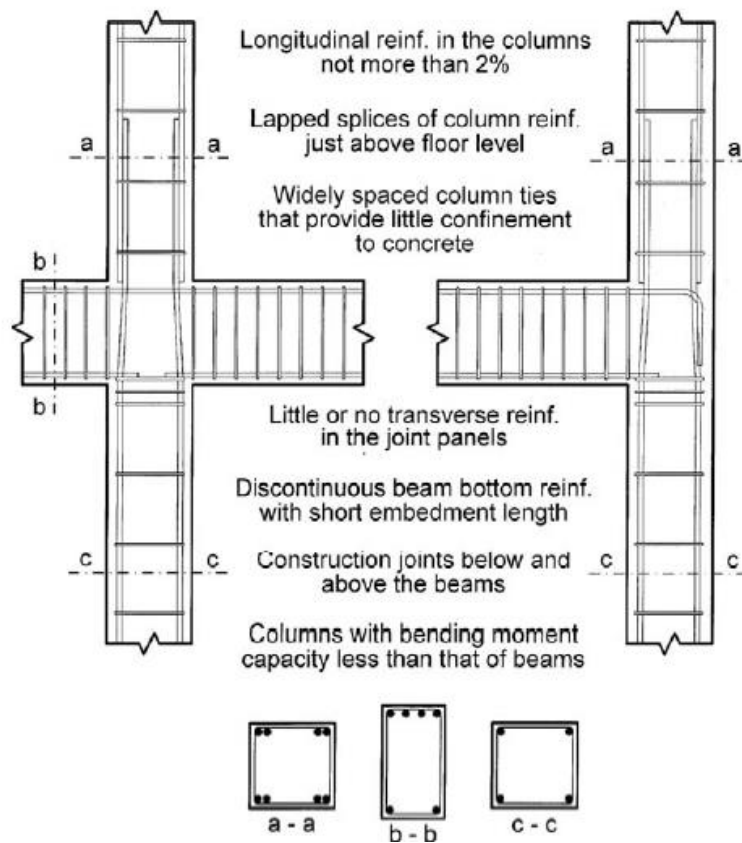


Figure 2.4: Typical details in lightly reinforced concrete structures

Exterior beam–column joints are more vulnerable than interior joints, which are partially confined by beams attached to four sides of the joint and contribute to the core confinement. There are some differences between the shear response of interior and exterior joints (as will be seen in following paragraphs) when subjected to earthquake ground motion due to joint confinement by beams. However, the bond-slip mode of failure of exterior and interior joints is similar (Ghobarah & El-Amoury, 2005).

Figure (2.5) shows some typical examples of joint failures in RC structures:



Joint shear failure



Inadequate joint confinement



Shear failure in column



Local buckling in column



Short columns failure



Short columns failure

Figure 2.5: Examples of joint failures in RC structures

## 2.2. Beam-column joints

A beam-column joint in a reinforced concrete structure is a zone formed by the intersection of beams and columns. A joint is defined as the portion of the column within the depth of the deepest beam that frames into the column (ACI 352 2002). The functional requirement of a joint is to enable the adjoining members to develop and sustain their ultimate capacity.

The behavior of a joint is characterized by a complex interaction of shear, bond and confinement mechanisms taking place in a quite limited area.

With regard to the bond forces acting between concrete and steel, it plays a dominant role with respect to seismic behavior because it affects stiffness and energy dissipation capacity.

The relative slip between the steel bars and the surrounding concrete depends both on steel and concrete strain but Costa, J.L.D. (2003) disregards concrete strain respect to steel strain because of its negligible value.



Bond forces play an important role in the joint mechanism, because they act along joint's perimeter so that a truss mechanism can be mobilized and on a compressed diagonal strut between corners. This mechanism shows the very limited capacity that joints have in dissipating energy and maintaining their strength, so joints can be considered to have a brittle mode of failure.

Tensile forces are transferred through bond during plastic hinge formation. When the longitudinal bars at the joint face are stressed beyond yield splitting cracks are initiate along the bar at the joint face. In order to avoid or retard this phenomenon it is important to give adequate development length for the longitudinal bar within the joint. During earthquakes, the diagonal compression strut deteriorates because of the presence of inelastic cycling, which causes permanent elongation on the beam bars and leads to full depth open cracks at the beam-joint interface. The bond has a very poor response in terms of energy dissipation, stiffness and strength degradation under inelastic cycling.

### 2.2.1. Exterior joints

In case of exterior joints (see figure 2.6), the beam is only on one side of the column in one plane. Therefore, the longitudinal reinforcement of the beam that frames into the column terminates within the joint core and does not go through and through the joint. In figure (2.7a) we can see the actions on a typical exterior beam-column joint. The moments and shears acting due to these actions are shown in figure (2.7b). (Scarpas A., 1981).

Let us assume that the length of columns and shear forces in the columns above and below the joint are equal, i.e.,  $l_c = l'_c$  and  $V_{col} = V'_{col}$  (Generally practically true). (Sharma et al., 2009)

Taking moments about the center of the joint core, we get,

$$M_b + \frac{V_b \cdot h_c}{2} = \frac{V_{col} \cdot l_c}{2} + \frac{V'_{col} \cdot l'_c}{2} = V_{col} \cdot l_c$$

Thus,

$$V_{col} = \frac{\left(M_b + \frac{V_b \cdot h_c}{2}\right)}{l_c}$$

The horizontal shear force in the joint,  $V_{jh}$  can be calculated as,

$$V_{jh} = T - V_{col} = T - \frac{\left(M_b + \frac{V_b \cdot h_c}{2}\right)}{l_c}$$

Similarly, the vertical joint shear force  $V_{jv}$  can be obtained as,

$$V_{jv} = T'' + C'_c + C'_s = T'' + C''_c + C''_s - V_b$$

These shear forces are responsible for diagonal tension and hence cracks in the joint. In order to resist such diagonal tension forces, reinforcement in the joint core is required. With reference to bond behavior, in exterior joints, after a few cycles of inelastic loading, the bond deterioration initiated at the column face due to yield penetration and splitting cracks, progresses towards the joint core. Repeated loading will aggravate the situation and a complete loss of bond up to the beginning of the bent portion of the bar may take place. The longitudinal reinforcement bar, if terminating straight, will get pulled out due to progressive loss of bond.

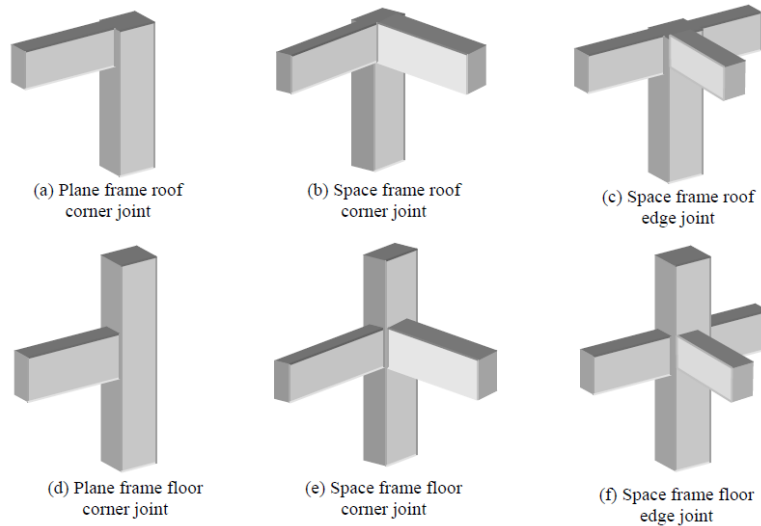


Figure 2.6: Exterior beam-column joints in plane and space frames

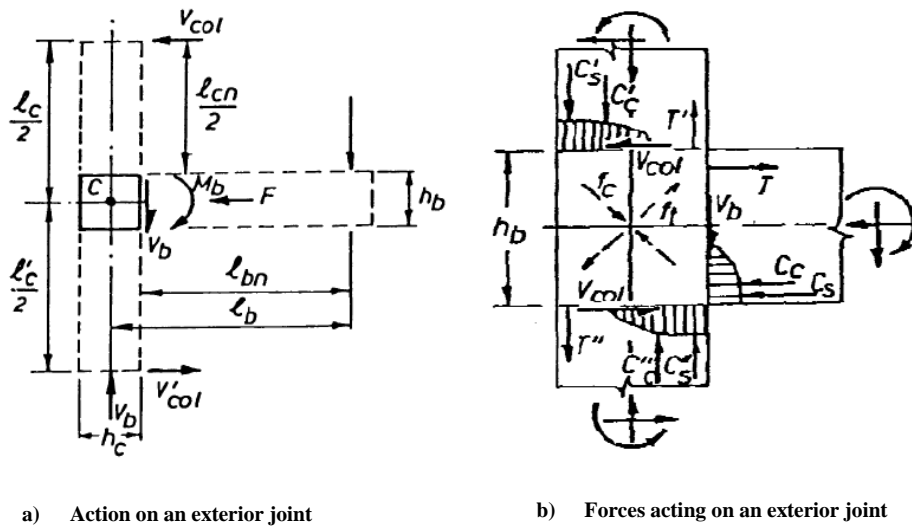


Figure 2.7: Action and forces on an exterior joint

### 2.2.2. Interior joints

In case of interior joints, the beam is running through the column (figure 2.8). Therefore, the longitudinal reinforcement of the beam that frames into the column either can terminate within the joint core without bends or can pass through and through the joint. Consider an interior joint acted upon by a set of actions as shown in figure (2.9a). The bending moment diagram (BMD) is shown in figure (2.8b). In figure (2.8c) we can see the shear force diagram (SFD). (Sharma et al., 2009)

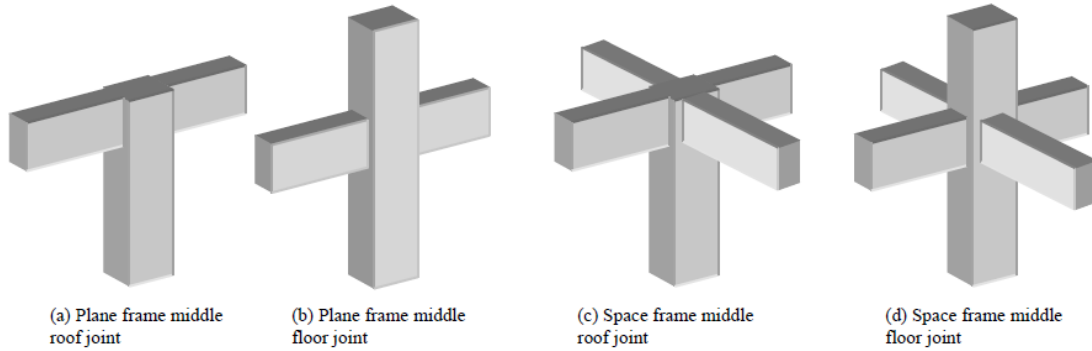


Figure 2.8: Interior beam-column joints in plane and space frames

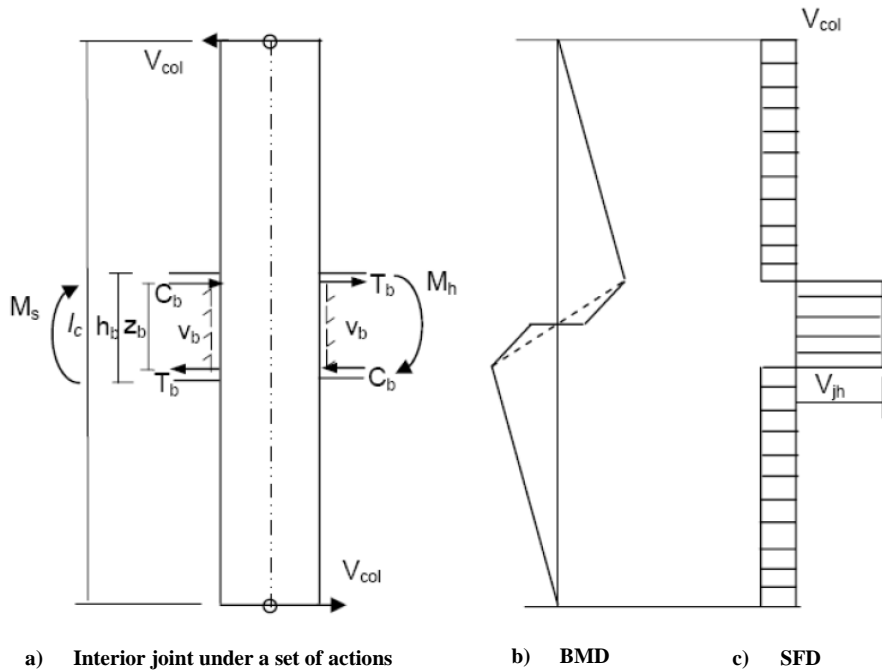


Figure 2.9: Action and forces on an interior joint

From figure (2.9b), it can be noticed that the bending moments just above and below the joint change their nature with a steep gradient within the joint region thus causing large shear forces in the joint compared to that in the column. In order to calculate the horizontal shear force in the joint core, let us consider the equilibrium of the joint. Let  $M_h$  and  $M_s$  be the hogging and sagging moments respectively acting on either side of the joint core as shown in figure (2.9a).  $T_b$  and  $C_b$  are the tensile and compressive forces in the beam reinforcements.  $V_b$  is vertical beam shear and  $V_{col}$  is horizontal column shear.

Again taking moments about the joint core centre, we get,

$$V_{col} \cdot l_c = T_b \cdot Z_b + C_b \cdot Z_b + V_b \cdot h_c$$

Assuming total symmetry and hence,  $T_b = C_b$ , we get,

$$2 \cdot T_b = \frac{(V_{col} \cdot l_c - V_b \cdot h_c)}{Z_b}$$

Where,

$l_c = \text{column height}$

$Z_b = \text{lever arm}$

$h_c = \text{column depth}$

Again, the horizontal joint shear force can be obtained by,

$$V_{jh} = 2 \cdot T_b - V_{col}$$

Substituting, we get,

$$V_{jh} = \frac{(V_{col} \cdot l_c - V_b \cdot h_c)}{Z_b} - V_{col} = V_{col} \cdot \left( \frac{l_c}{Z_b} - 1 \right) - V_b \cdot \left( \frac{h_c}{Z_b} \right)$$

In a similar way, the vertical joint shear force can be obtained.

These shear forces are responsible for diagonal tension and hence cracks in the joint. In order to resist such diagonal tension forces, reinforcement in the joint core is required.

In an interior joint, the force in a bar passing continuously through the joint changes from compression to tension. This causes a push-pull effect which imposes severe demand on bond strength and necessitates adequate development length within the joint. The development length has to satisfy the requirements for compression and for tension forces in the same bar. Insufficient development length and the spread of splitting cracks into the joint core may result in slippage of bars in the joint.

### 2.2.3. Mechanic of beam-column joints during earthquakes

J.L.D. Costa (2003), related to Paulay and Priestley (1992) approach, described on a quality level the mechanic of joints. The behaviour of a joint is characterized by a complex interaction of shear, bond and confinement mechanisms taking place in a quite limited area, the joint core. Thanks to linear static approach, it is possible to represent seismic action with lateral loading, as in figure (2.10). Considering the overall statics of a given two-dimensional frame as shown in Figure (2.10), it appears that lateral loading imposes such a bending moment field in the beams and columns that moments with the same magnitude but of opposite sign will take place on parallel faces of the joint. As a consequence, the joint region is subjected to horizontal and vertical shear forces whose magnitude is  $l_c/d_b$  times the maximum shear force in the columns and  $l_b/d_c$  times the maximum shear force in the beams, respectively.

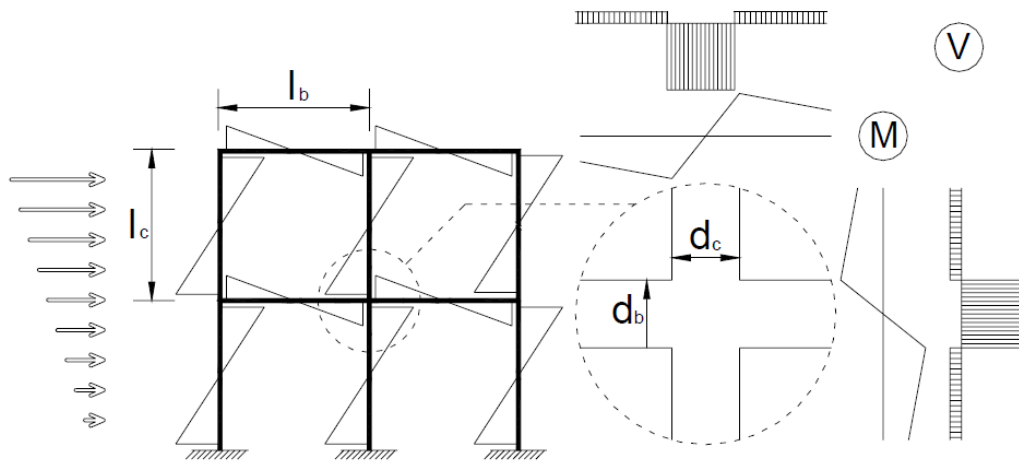


Figure 2.10: Statics of laterally loaded frame;  
Detail: Moments and shear gradient through an interior joint

Consider now the equilibrium of the interior of the joint, represented in Figure (2.11a). It may be seen that the joint core is submitted to two types of actions that combined are generally known as the joint shear:

- Concrete flexural compression from beams and columns at the opposite corner of the joint (Figure 2.11b) and
- Shear flow along its perimeter from beam and column bars by means of bond forces (Figure 2.11c)

The resistance mechanism is composed by a compressed diagonal of concrete roughly limited by the neutral axes of the end sections of the members (Figure 2.11d) and by diagonal compression field – truss mechanism – consisting of horizontal hoops, intermediate column bars (Figure 2.11f) and inclined compressed concrete between shear cracks (Figure 2.11e).

The main component of the resistance mechanism is the compressed diagonal strut, which carries a substantial portion of the joint shear. The rest of the joint shear is transmitted to the joint core through the bond between the longitudinal reinforcement of beams/columns and the surrounding concrete and, therefore, absorbed by the truss mechanism. Depending on the magnitude of the bond forces, diagonal tension cracking takes place. The main crack is developed along the compressed strut but other cracks parallel to it form as well.

To prevent shear failure by diagonal tension, both horizontal and vertical reinforcement are required. Such reinforcement enables a diagonal compression field to be mobilized as shown in Figure (2.11e). This leads to the conclusion that the amount of reinforcement may be significantly higher than would normally be provided by the extension of the reinforcement of beams and columns into the joint core. This is particularly true in the case of joints whose columns are low axially loaded.

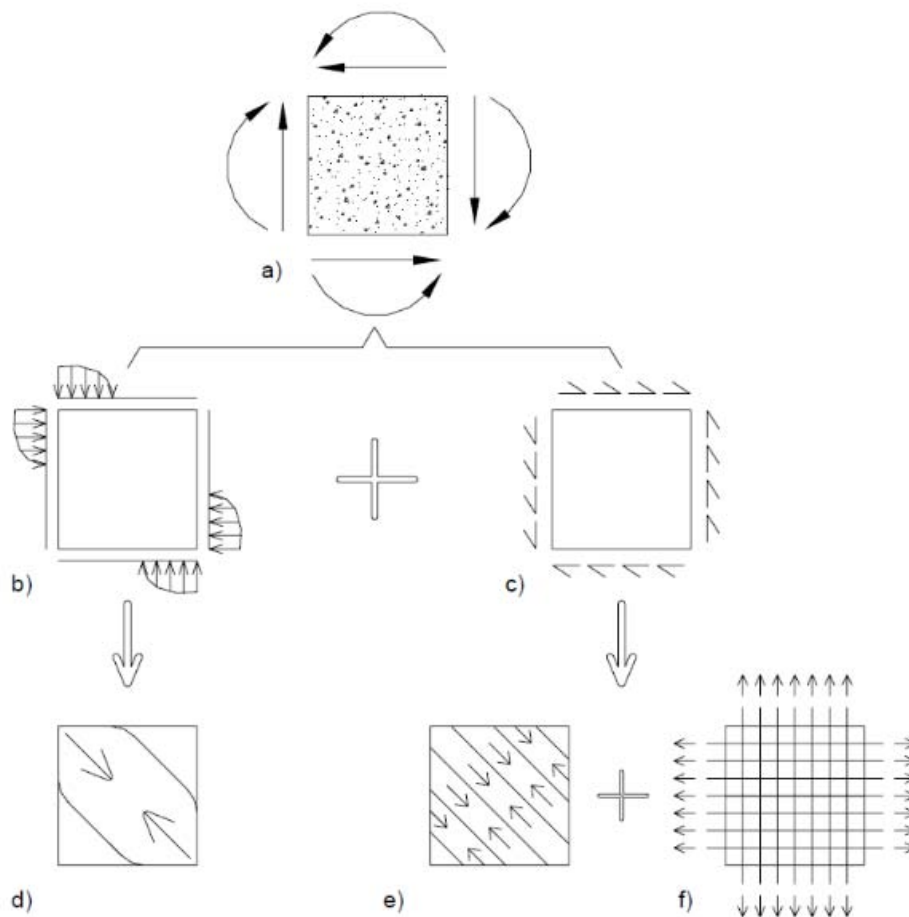


Figure 2.11: Actions on an interior joint and the corresponding resistance mechanism according to Paulay and Priestley, 1992

#### 2.2.4. Factor affecting seismic behaviour of joints

The main important design parameters that affect Beam-Column Joints mechanic are listed below: (CEB, “RC Frames under Earthquake Loading”, 1996)

**Joint volume.** The increase of the joint dimensions would reduce stresses for a given input force demand. Normally, joint dimensions are established in advance by beam and column proportioning in consideration of overall frame performance, so they are not active variable in design of joints. When there is the necessity to change joint dimensions, the dimensions of most interest are usually the depth and width of the column. This is because input to the joint is determined by beam flexural capacity, which, in a strong column/weak beam design, should be kept low enough to prevent development of column flexural hinging. The increase of column depth reduces joint shear stress and lowers bond demand along beam bars passing through a joint.

**Bond resistance.** Bond resistance play an active role in the resistance of a joint. If there is pullout between steel bars and concrete within the joint core, the full joint capacity will not be realized. Bond failure precludes development of full connection capacity.

**Column axial force.** Axial force acting in the column influence the depth of the column flexural compression zone, so even the joint core is influenced. With the increase of the compression zone, a more pronounced diagonal compression strut would be expected to form. But as the vertical stress increases, the strut also becomes less and less diagonal, suggesting that its contribution to shear resistance will become less significant.

**Joint reinforcement.** Both horizontal and vertical reinforcement in the core of the joint will contribute to shear resistance mechanism. The portion of joint shear resistance arising from development of a diagonal compression strut is dependent on confinement of the core to sustain its compressive resistance. Therefore, increasing transverse reinforcement in the joint reduces joint damage and delays joint failure.

**Column-to-beam flexural strength ratio.** This is an important variable when I consider the overall frame structure. In order to know the input demand in the joint it is important to know which element (column or beam) requires the greater capacity.

**Slab effects.** Floor slabs almost always exist at the beam-column joints and they have two important functions in the joint mechanism:

- Slab reinforcement increase joint shear demand by raising the beam hogging moment capacity;
- Slab restrains horizontal joint strain, especially when it surrounds entirely the joint.

**Transverse beams.** They can enhance the joint shear capacity because transverse beams provide a further volume for the joint core. In fact, the joint shear resistance increases with the rising in joint volume.

### **2.2.5. Failure modes of a beam-column joint**

Sharma et al. (2009) presented the classification of beam-column joints and their failure modes.

The reinforced concrete beam-column joints used in frames may be classified in terms of geometric configuration, structural behavior or detailing aspects.

Based on the crack propagation in the joint region and failure mechanism under loading, the joints can be classified as Elastic (joints remain essentially in the elastic range throughout the response of the structure) or Inelastic (inelastic deformation occurring also in parts of the joint).

Based on their behavior under loading, the beam-column joints in a reinforced can be classified as Non-Ductile joints (Brittle joints) or Ductile Joints. Whether a joint will behave in a brittle or ductile manner depends largely on the reinforcement details of the joint.

A beam-column joint primarily consists of three elements viz. beam, column and the joint core (generally considered as a part of column). Each of the three elements can undergo failure under different modes as enlisted below:

- a. Flexural failure of beam.
- b. Flexural failure of column.
- c. Shear failure of beam.
- d. Shear failure of column.
- e. Shear failure of joint core.
- f. Bond failure of reinforcement.
- g. Combinations of various modes listed above.

A failure resulting from single mode is highly uncommon and generally a combination of two or more of the above modes is responsible for the complete failure. Although, joint failure typically means the shear failure of the joint core, but it is quite unlikely that it serve as the weakest link. The failure (or crack propagation) usually initiates from beam or column, whichever is weaker, and then joint cracking occurs. This is primarily due to the penetration of inelastic strains along the reinforcing bars of the beams or columns into the joint. Therefore, if the joint core is not designed for such forces, it is very much possible that ultimate failure results due to excessive shear cracking in joint core. The most favourable condition from seismic design point of view is to have joint core essentially in the elastic range and formation of plastic hinges shall occur in beams. However, when the plastic hinges are developed at the ends of the beams immediately adjacent to a joint, it is not possible to prevent some inelastic deformation occurring in the parts of joint also. Therefore, the ideal situation is to have plastic hinge formation in beams at some distance away from the face of the joint.



### 2.2.6. Damage prediction in RC older beam-columns joints

Pagni and Lowes (2004) performed several experimental tests to predict the damage progression in old beam-column joints. In the study, only laboratory specimens with design details representative of pre-1967 construction were included. Seismic design provisions were introduced into the UBC in 1967 and the ACI code in 1971. Prior to this, design recommendations did not explicitly address joint design. The investigation included five test programmes and twenty-one test specimens.

The results of previous laboratory studies, post-earthquake reconnaissance and field experience were used as the bases for identifying a series of 12 states that define the progression of damage in reinforced concrete beam-column building joints. Damage states were defined based on external, visually observable damage measures such as concrete crack width, the extent of concrete cracking and crushing, and bond degradation as represented by damage to bond-zone concrete or the opening of large flexural cracks at the frame member-joint interface.

The damage states sustained by a beam-column joint in order of increasing earthquake demand are:

0. Initial cracking at the beam-column interface. Cracking occurs at the perimeter of the joint due to flexural loading of the beams.
1. Initial cracking within the joint area. Diagonal cracks occur within the joint due to shear loading of the joint core.
2. Crack width is less than 0.02 in (5 mm).
3. Crack width is greater than 5 mm. Cracks widths greater than 5 mm are at risk for corrosion of the reinforcing steel or will not allow transfer of stresses through the aggregate.
4. Beam longitudinal reinforcement yields. The result of research suggest that after reinforcing steel yields, the strength of the concrete-steel bond is reduced. This is because the Poison effect, which causes the diameter of the bar to decrease under tensile loading, becomes significant in the post-yielding regime
5. Crack width is greater than 0.05 in. (1.3 mm).
6. Spalling of at least 10% joint surface concrete. This state defines the transition from cracking to spalling. Concrete spalling is defined as the breaking off of the concrete layer covering the outermost layer of reinforcing steel. Cracking is no longer measurable where the smooth surface has broken and fallen away. Spalling begins in the center of the joint.
7. Joint shear strength begins to deteriorate. The shear capacity of the joint will reach a maximum and begin to deteriorate before joint is assumed to have lost integrity and failed.

8. Spalling of more than 30% joint surface concrete. Thicker sections of cover concrete break and fall away from the center of the joint exposing the center column longitudinal reinforcement. At the same time, the area of exposed aggregate grows bigger but remains concentrated in the center of the joint surface.
9. Cracks extend into the beam and/or column. Typically, the crack progresses along the reinforcement and may be considered indicative of a splitting-type bond failure.
10. Spalling of more than 80% joint surface concrete. Both the depth and the width of the area of spalling continue to grow, exposing the corner column longitudinal reinforcement.
11. Crushing of concrete extends into joint core. Breaking and falling away of concrete thicker than the cover leads to exposure of the interior aggregate and large sections of the rebar.

Damage states 12a, 12b, 12c, define three types of failure commonly observed in older reinforced concrete joints. These states are not progressive but would occur for the same high earthquake loads.

**12a.** Buckling of longitudinal steel reinforcement. This is the most common among type of failure. After crushing of the core concrete, only longitudinal reinforcement is available to resist the gravity load. This failure is due to loss of gravity-load capacity within the joint.

**12b.** Loss of beam longitudinal steel anchorage within the joint core. The beam appears to pull away from the joint and move without resistance against the lateral loading. The bond between the beam and the joint is lost when a significant amount of the concrete is crushed.

**12c.** Embedded beam longitudinal steel reinforcement pull out. The failure is attributed to pullout of the embedded positive beam reinforcement from the beam-column joint, accompanied by significant damage to the top and bottom columns. (Pessiki et al., 1990)



Figure 2.12: Exterior joint specimen exhibits Damage State 9



Figure 2.13: Joint specimen exhibits Damage State 11



Figure 2.14: Exterior joint exhibiting Damage State 12

### 2.2.7. Need for seismic structural retrofitting

To avoid a strong beam-weak column mechanism, which represent a brittle failure, the columns and beam-column joints can be strengthened to increase their flexural and shear capacities to a higher level than the adjoining beams. Brittle failure modes in the joint zone would significantly reduce the overall ductility of the structure. Rehabilitation of the beam-column joints represents a feasible approach to mitigate the hazard in existing structures and to provide safety to the occupants. Due to the significant contribution of joint failures to the collapse of buildings during earthquakes, it is necessary to develop economical methods to upgrade the joint's capacity, in order to prevent a brittle failure and, instead, shift the failure towards a beam flexural hinging mechanism, which is a more ductile type of behaviour.

The cost of repair/strengthening of the existing RC structures is one of the major factors which make the owners to think twice before choosing a rehabilitation scheme. This has led to the development of several strengthening techniques in the past. During the dissertation one technique will be presented and discussed even under economic aspect, thanks to a cost analysis.

### 2.2.8. Seismic design aims

The philosophy nowadays in the seismic design is to provide the structure with properties that ensure the dissipation of the energy induced by an earthquake. The more energy dissipated, the less strength required by the structure. This means not only safer structures but also more economic ones.

Regions of the primary lateral force resisting mechanism are carefully selected, designed and detailed so that they can dissipate as much as possible the energy transmitted to the structure by the base motions. In frames these regions are generally known as plastic hinges and together they form the energy dissipation mechanism of the structure. The energy is dissipated taking advantage of the ductile properties of the plastic hinges, i.e. their ability to maintain strength in the inelastic range and absorb energy by hysteretic behaviour.

The successful performance of the structure in sustaining large imposed base motions depends mainly on the ability of the energy dissipation mechanism of the structure to hold during the entire seismic action. This is achieved assuring that:

- Each plastic hinge is designed to have strength as close as possible to the required strength and is carefully detailed to maintain its ductility.
- The only mode of failure of a member containing a plastic hinge is the one corresponding to the development of the capacity of the plastic hinge. Therefore all the other modes of failure are inhibited by providing them with strength greater than the capacity of the plastic hinge.
- In the same way, regions not suited to dissipate energy in a stable manner are protected by ensuring that their strengths exceed the requirements from the development of the plastic hinge strength. Therefore these regions are designed to remain elastic.

These three requirements are the basis for the so-called capacity design. (J.L.D. Costa 2003).

In case of ductile structures designed for earthquake resistance, it is possible to highlight some characteristics of the components:

- The strength of the joint should not be less than the maximum demand corresponding to development of the structural plastic hinge mechanism for the frame. This means that the joint should have sufficient strength to enable the maximum capacities to be mobilized in adjoining members. This will eliminate the need for repair in a relatively inaccessible region and for energy dissipation by joint mechanisms.
- The capacity of the column should not be jeopardized by possible strength degradation within the joint. The joint should also be considered as an integral part of the column.
- During moderate seismic disturbances, joint should preferably respond within the elastic range (they do not dissipate energy, as told before).
- Joint deformations should not significantly increase story drift.
- The joint reinforcement necessary to ensure satisfactory performance should not cause undue construction difficulties.

### **2.2.9. Strong column–weak beam concept**

The corollary of the capacity design procedure is the concept of strong column–weak beam and it is of fundamental importance in the design of structures whose seismic resistance system is composed by ductile frames. Considering the structural functions and modes of behaviour of beams and columns, this concept establishes that the energy dissipation mechanism of the structure is composed by flexural plastic hinges taking place in beams and avoided in columns. Therefore, the strength of the beams is limited to the plastic hinge capacity and the columns are supposed to remain in the elastic domain. Column design moments are, according

to this concept, derived at beam-column joints with respect to the actual resisting moments of the plastic hinges in the beams. There are other reasons why columns should always remain in the elastic domain. Columns are not suited to dissipate energy in a stable manner lies, in fact they are submitted to axial compression. Even moderate axial compression affects the ductility of a member in cyclic loading since it leads to requirements regarding concrete strains and therefore induces higher levels of crushing and degradation at the concrete core combined with spalling of the concrete cover. As a consequence members in axial compression experience large drops of strength and are more exposed to brittle modes of failure as the one resulting from buckling of the longitudinal bars. Another reason to avoid the formation of plastic hinges in columns lies in the significant inter-storey drifts resulting from it. High story-drifts have the direct consequence of increasing the P- $\Delta$  effects and therefore the risk of member instability, which compromises the overall safety of the structure.

Columns and joints should always remain in the elastic domain, which is the same to say that they should be provided with strength greater than the maximum demand corresponding to development of the adjacent plastic hinges. This also eliminates the need for repair in a relatively inaccessible region of the structure. Another important reason to prevent damage in these elements is the potential degradation of the capacity of the column due to degradation within the joint. Despite the design principles in the weak beam–strong column concept are quite simple, there are a certain number of situations the designer should carefully evaluate in order to reach a safe structure:

- A high ductility requirement on the beams leads to strain-hardening effects in the longitudinal reinforcement and this may cause an increase of strength between 10 and 25% (Penelis and Kappos, 1997);
- The actual strength of the beam should be assessed considering the reinforcement bars used in the slab since this might increase the flexural strength of the beam;
- During seismic loading the axial load on columns is constantly changing, specially for those in the perimeter of the structure. The range of variation of axial loading must be determined as accurately as possible, since the column strength may be substantially lower than that taken into account.

### **2.3. Existing strengthening techniques**

A comprehensive up-to-date literature search of existing strengthening and repair techniques of nonseismically designed reinforced concrete beam-column joints was made by Engindeniz et al. (2006).

Repairs for earthquake-damaged concrete buildings fall into three generic categories: (FEMA 308)

1. *Cosmetic Repairs.* They are the most exterior repairing and they improve the visual appearance of component damage. These repairs may also restore the non-structural properties of the component, such as weather protection. In this case there are not structural problems and the repair will neglect structural benefits.
2. *Structural Repairs.* In this situation, there are components damage directly. The aim of this action is to restore structural properties.
3. *Structural Enhancements.* They are repairs that comprise supplemental additions, or removal and replacement of existing damaged components. They also include the addition of new components in the structure not necessarily at the site of existing damaged components. The aim of this intervention is to replace structural properties of damaged components rather than to restore them.

Strengthening techniques are listed below:

- Epoxy Repair
- Removal and Replacement
- Concrete Jackets
- Reinforced masonry blocks
- Steel jackets and external steel elements
- Externally bonded Fibre-reinforced polymeric (FRP) reinforcement

Below in table (2-1) there is a summary of repair procedures valid for RC buildings, RM buildings and URM building:

Repair Category	Material			Repair ID	Repair Type
	Reinf. Concrete	Reinf. Masonry	URM		
Cosmetic Repair	✓	✓	✓	CR 1	Surface coating
			✓	CR 2	Repointing
	✓	✓*		CR 3	Crack injection with epoxy
Structural Repair	✓	✓*		SR 1	Crack injection with epoxy
	✓	✓	✓	SR 2	Crack injection with grout
	✓	✓		SR 3	Spall repair
	✓			SR 4	Rebar replacement
	✓	✓	✓	SR 5	Wall replacement
Structural Enhancement	✓	✓	✓	SE 1	Concrete overlay
	✓	✓	✓	SE 2	Composite Fibers
	✓			SE 3	Crack Stitching

Notes: Repairs for concrete walls can also be used for concrete frames in infilled frame systems.

Repairs for steel frames of infill systems are described in the component repair guides.

\* Epoxy injection not recommended for partially-grouted reinforced masonry.

Table 2-1: Summary of repair procedures

With regard to the paragraph 2.2.6., it is possible to suggest some appropriate repairing technique for each damage state, as shown in table (2-2): (Pagni and Lowes 2004)

Method of Repair	Activities	Damage States
0. Cosmetic Repair	Replace and repair finishes.	0-2
1. Epoxy Injection	Inject cracks with epoxy and replace finishes.	3-5
2. Patching	Patch spalled concrete, epoxy inject cracks and replace finishes.	6-8
3. Replace Concrete	Remove and replace damaged concrete, replaces finishes	9-11
4. Replace Joint	Replace damaged reinforcing steel, remove and replace concrete, and replace finishes.	12

Table 2-2: Damage states assigned to each repair technique

Each method of repair or strengthening has advantages and disadvantages with respect to the application details, required labour, disruption of building occupancy and range of applicability. One important point to focus on is the economical aspect, since there is the necessity to evaluate if it is better to repair and strengthen the structure or it is better to pull down the entire structure and build another one. A brief discussion of these techniques is presented here.

### 2.3.1. Epoxy repair

Epoxy Repair can be used both in cosmetic repair and in structural repair. This technique consist of applying a structural binding agent (Epoxy resin) into a crack for the purpose of filling the crack and adhering to the substrate material. There are several methods of epoxy repair, e.g. vacuum impregnation, as shown below in figure (2.15).

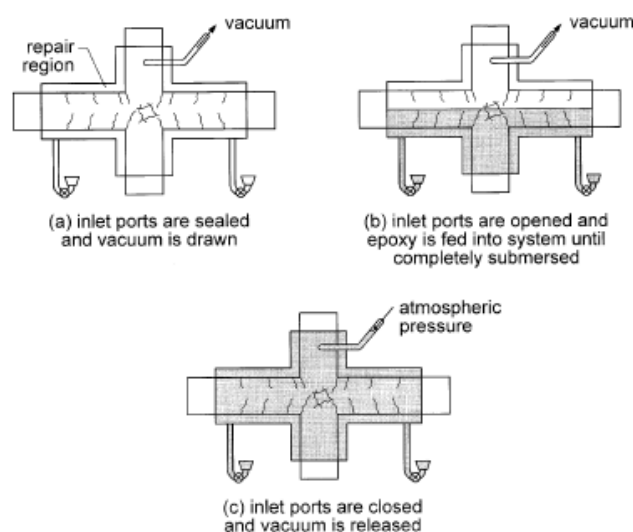


Figure 2.15: Vacuum impregnation procedure applied by French, Thorp and Tsai



Figure 2.16: Epoxy resin injection in a damaged joint  
(Bandit Project 2012)

Many researchers as French, Thorp and Tsai; Beres and al.; Filiatrault and Lebrun; Karayannis, Chalioris and Sideris repaired two, one-way interior joints with vacuum and they obtained different results. The results of the epoxy repair application have shown that the reliability of this technique in restoring the original characteristics of damaged joints is questionable. The bond around the reinforcing bars, once destroyed, does not seem to be completely restored by epoxy injection. The stiffness is only partially recovered and the energy dissipation capacity remained almost unchanged respect to the damaged state. The effectiveness of the epoxy repair is limited by the access to the joint and the epoxy cannot be effectively introduced into the joints surrounded by transverse beam and floor slab. This limitation can possibly be overcome by further advances in the vacuum impregnation technique. This technique requires also a high level of skill for satisfactory execution. (Engindeniz et al. 2006)

### 2.3.2. Removal and replacement

Partial or total removal and replacement of concrete is used for heavily damaged joints with crushed concrete, buckled longitudinal bars, or ruptured ties. Before the removal, the damaged structure must be temporarily supported to ensure stability. Depending on the amount of concrete removed, some additional ties or longitudinal reinforcement may be added. Generally, high-strength, low or nonshrink concrete is used for replacement. Special attention must be paid to achieving a good bond between the new and the existing concrete. In place of concrete, when there are spalls, a repair mortar mix can be used for repairing the structure. Spalls are small sections of wall that become loose or dislodged. The missing material is replaced with a repair mortar mix, which can be based on inorganic materials, such as Portland cement and latex-modified concrete, or organic materials, such as epoxy and polyester. For thick repairs, a mechanical anchorage, using epoxy-embedded dowels, may need to be added to secure the patch. (Engindeniz et al. 2006)



This method of structural strengthening could be costly, time consuming and tedious while structural elements should be replaced by a new similar member with cautious means. Close surveillance might be needed even after replacement to check the probable deflections and buckling of members.

### 2.3.3. Concrete jackets

Concrete jackets is one of the earliest and most common solution for structural enhancement. The method is to encase the existing column, along with the joint region, in new concrete with additional longitudinal and transverse reinforcement. The continuity of the added longitudinal bars through the joint requires opening the slab at the column corners (figure 2.17a).

The addition of the joint transverse reinforcement makes the process even more labor-intensive, in which case the beams are also cored, and in-place bending of the hooks is necessary.

Many tests were performed from different researchers aimed at discovering advantages and disadvantages of this technique.

Corzaao and Durrani, after their tests on two multi-joints specimens, realized that the retrofit was not as effective in improving the behavior of the multi-joint specimens. The results were taken to indicate that jacketing of the columns alone was not adequate in restoring the performance without addressing the problem of load transfer between beams and columns.

Alcocer and Jirsa conducted tests on four three-dimensional beam-column-slab subassemblages subjected to severe bidirectional loading. In those tests, the need to drill holes through the beams for placing joint confinement reinforcement was eliminated by welding a structural steel cage around the joint (figure 2.17b). The cage consisted of steel angles designed to resist the lateral expansion of the joint and flat bars connecting the angles. The studied variables were jacketing the columns only or both beams and columns, jacketing after or prior to first damage, and using bundles or distributed vertical reinforcement around the column. Alcocer and Jirsa recommended that the ACI 352R-76 provisions on joint strength and bond could be used to proportion the jacket and that distributed bars through the slab perforations should be preferred to bundles. The development of bundled bars can be a problem with smaller column-beam strength ratios. (Engindeniz et al. 2006)

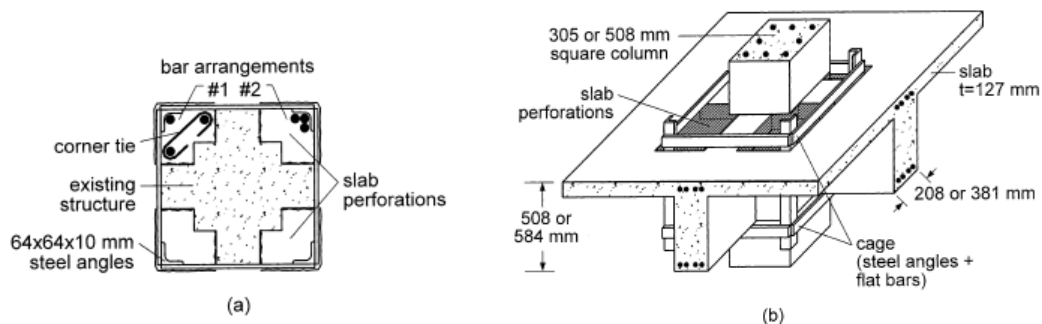


Figure 2.17: Concrete jacketing technique studied by Alcocer and Jirsa. (a) plan, and (b) perspective

### 2.3.4. Reinforced masonry blocks

Reinforced masonry blocks are another solution for structural enhancement. There are several methods to use these blocks. The first method required the existing interior columns to be jacketed by reinforced concrete masonry units, with additional longitudinal reinforcement within the corner cores extending continuously through the slabs and later post-tensioned (figure 2.18(a) and (b)).

Any space between the units and the existing column was then grouted. The shear capacity was increased by providing wire mesh in the mortar bed joints.

The results of the experiments have discovered the same limitations mentioned previously for concrete jacketing. In the case of partial masonry infills, an added functional disadvantage is an increased loss of internal space between the bays. (Engindeniz et al. 2006)

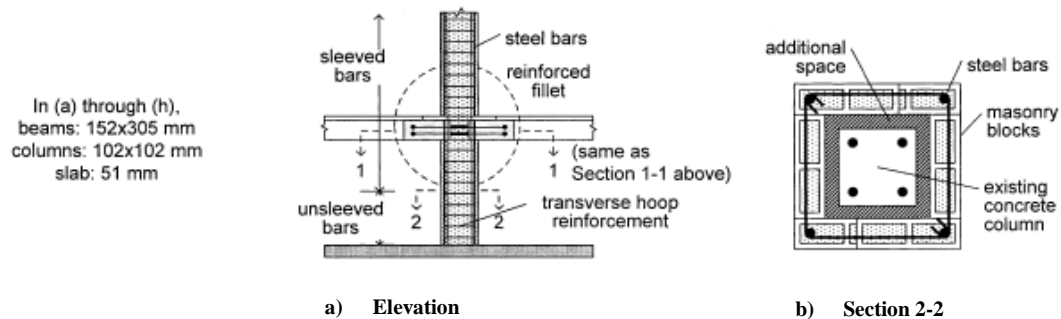


Figure 2.18: Masonry blocks jacketing

### 2.3.5. Steel jackets and external steel elements

There are many possible configurations of steel jackets, plates, shapes (angles, C-sections), size and number of batten plate that have been used to increase the strength and ductility of deficient beam-column joints. Steel jackets consist of flat or corrugated steel plates, or rectangular or circular steel tubes prefabricated in parts and welded in place. The space between the jacket and RC frame is grouted with nonshrink or expansive cement mortar. Steel parts are often mechanically anchored to the concrete to improve confinement. Attaching plates to selected faces of the members using adhesives and bolts, and connecting these plates using rolled shapes (for example, angles) has also been attempted.

Many researchers tested this technique and they disclosed advantages and disadvantages. The authors believe that, when compared with concrete and masonry jackets, the use of steel jackets can significantly reduce the construction time due to prefabrication. Disadvantages, however, such as the potential for corrosion, difficulty in handling the heavy steel plates, objectionable aesthetics in the case of corrugated steel shapes, and loss of floor space in the case of grouted steel tubes, cannot be overlooked. Steel jackets may result in excessive capacity increases, even where only confinement effect is intended, and create unexpected failure modes. Even if these disadvantages are ignored, it seems difficult to apply these schemes to actual three-dimensional joints. The presence of a floor slab, for instance, makes

it difficult, if not unfeasible, to install beam jackets. Although different two-part corrugated steel jackets have been proposed for interior, exterior, and corner joints with floor slab, there are no available data to validate their performance. Prestressing by preheating of externally attached steel straps in a repair scheme has been useful but should not be relied on because it is difficult to control in the field. (Engindeniz et al. 2006)

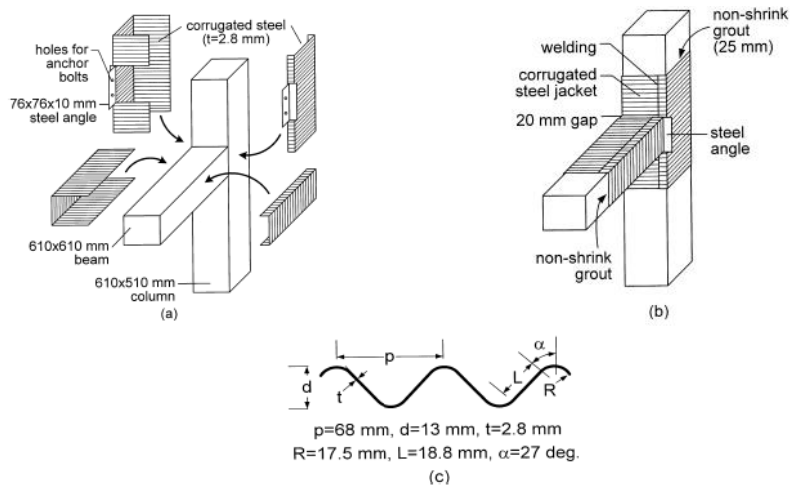


Figure 2.19: Corrugated steel jacketing technique proposed by Ghojarah, Aziz and Bibbah



Figure 2.20: Retrofitting of the weak column using steel angles and bands (steel jacketing). Designed and applied by BREIN S Structural Care. Building Research Institute, Nepal.

### 2.3.6. Externally bonded Fibre-Reinforced Polymeric reinforcement

Fibre-Reinforced Polymer Reinforcements consist of a large number of small, continuous, unidirectional, non-metallic fibres with advanced characteristics, bundled in a resin matrix. Bulletin 14 of fib provide informations about Externally Bonded FRP reinforcement for RC structures. Different systems of externally bonded FRP reinforcement (FRP EBR) exist, as will be discussed later.

There are three main purposes for which FRP can be used:

- Flexural Strengthening
- Strengthening in Shear and Torsion
- Confinement

Strengthening might be required for several reasons, including deterioration due to ageing, crashing of vehicles into bridge components (in the case of bridges), degradation such as corrosion of steel reinforcement, poor initial design and/or construction, lack of maintenance, increase in service loads, change to the structural system, large crack widths, large deformations. FRP system can also be used effectively as seismic reinforcement.

According to the problem of the structure, the FRP-Strengthening application is different, as shown in figure (2.21). Figures (2.22), (2.23) and (2.24) show typical examples of these techniques.

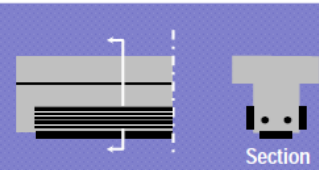
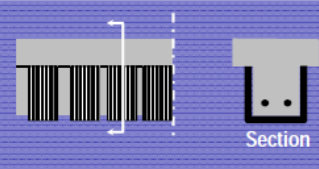
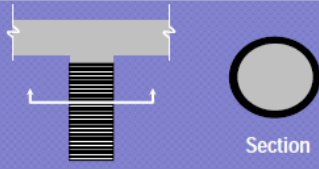
Type	Application	Fibre Dir.	Schematic
Flexural	Tension and/or side face of beam	Along long. axis of beam	
Shear	Side face of beam (u-wrap)	Perpendicular to long. axis of beam	
Confinement	Around column	Circumferential	

Figure 2.21: FRP-Strengthening applications (Book Composite for Construction, L.C. Bank)



**Figure 2.22: Flexural strengthening using CFRP strips of concrete girders in a Cement manufacturing building in Poland. (Book Composite for Construction, L.C. Bank)**



**Figure 2.23: Installation of prefabricated CFRP L-shaped plates (shear strengthening) over existing CFRP strips (flexural strengthening). (Book Composite for Construction, L.C. Bank)**



Figure 2.24: Application of CFRP fabrics to concrete columns for confinement of Reggio Emilia football stadium, Italy.  
(Book Composite for Construction, L.C. Bank)

Composite materials for strengthening of structures are available mainly in the form of thin unidirectional strips (with thickness in order of 1 mm) made by pultrusion, or flexible sheets or fabrics, made of fibres in one or at least two different directions, respectively (and sometimes pre-impregnated with resin).

There are several types of FRP strengthening systems, which are summarised below:

- Wet lay-up systems
- System based on prefabricated elements
- Special systems, e.g. automated wrapping, prestressing etc.

These systems are based on different configurations, types of fibres, adhesives etc. Practical execution and application conditions, for example cleanness and temperature, are very important, in achieving a good bond. A dirty surface will never provide a good bond. FRP can be described as combination of three main components, namely adhesives, resin matrices and fibres. The purpose of the *adhesive* is to provide a shear load path between the concrete surface and the composite material, so that full composite action may develop. The most common type of structural adhesives, namely epoxy adhesive, is the result of mixing an epoxy resin (polymer) with a hardener.

The successful application of an epoxy adhesive system requires the preparation of an adequate specification, which must include such provisions as adherent materials, mixing/application temperatures and techniques, curing temperatures, surface preparation technique, thermal expansion, creep properties, abrasion and

chemical resistance. Table (2-3) provides information for epoxy adhesives, compared with concrete and mild steel.

Property (at 20 °C)	Cold-curing epoxy adhesive	Concrete	Mild steel
Density (kg/m <sup>3</sup> )	1100 – 1700	2350	7800
Young's modulus (GPa)	0.5 - 20	20 - 50	205
Shear modulus (GPa)	0.2 – 8	8 - 21	80
Poisson's ratio	0.3 – 0.4	0.2	0.3
Tensile strength (MPa)	9 - 30	1 - 4	200 - 600
Shear strength (MPa)	10 - 30	2 - 5	200 - 600
Compressive strength (MPa)	55 - 110	25 - 150	200 - 600
Tensile strain at break (%)	0.5-5	0.015	25
Approximate fracture energy (Jm <sup>-2</sup> )	200-1000	100	10 <sup>5</sup> -10 <sup>6</sup>
Coefficient of thermal expansion (10 <sup>-6</sup> /°C)	25 - 100	11 - 13	10 - 15
Water absorption: 7 days - 25 °C (% w/w)	0.1-3	5	0
Glass transition temperature (°C)	45 - 80	---	---

Table 2-3: Comparison of typical properties for epoxy adhesive, concrete and steel (Täljsten 1994)

The *matrix* can be either of thermosetting type (with good processibility and good chemical resistance, the most common) or of thermoplastic type. The function of the matrix is to protect the fibres against abrasion or environmental corrosion, to bind the fibres together and to distribute the load. The matrix has a strong influence on several mechanical properties of the composite, such as transverse modulus and strength, the shear properties and the properties in compression. The most common polymeric matrix materials are epoxy resins, polyester and vinlester.

Figure (2.25) illustrates the stress-strain behaviour of matrix, fibers and resulting FRP.

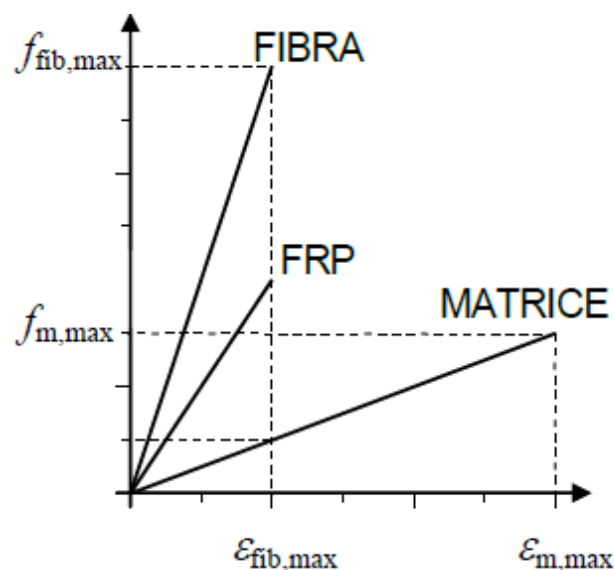


Figure 2.25: Stress Strain relationship of matrix, fibers and resulted FRP (CNR-DT200 2004)

The *fibres* used for strengthening of structures are mainly three types:

- Glass fibres
  - Electrical-glass fibres (E-glass fibres)
  - S-glass fibres
  - Alkali-Resistant glass fibres (AR-glass fibres)
- Aramid fibres
- Carbon fibres

E-glass fibres contain high amounts of boric acid and aluminate and they are disadvantageous in having low alkali resistance. S-glass fibres are stronger and stiffer than E-glass, but still not resistant to alkali. To prevent the problem of cement-alkali erosion, it is necessary to add a considerable amount of zircon.

An important aspect of glass fibres is their low cost.

Aramid fibres were first introduced in 1971. The structure of aramid fibre is anisotropic and gives higher strength and modulus in the fibre longitudinal direction. The diameter of aramid fibre is approximately  $12 \mu\text{m}$ . Aramid fibres respond elastically in tension but they exhibit non-linear and ductile behaviour under compression; they also exhibit good toughness, damage tolerance and fatigue characteristics.

Carbon fibres are normally either based on pitch or PAN, as raw material. Pitch fibres are fabricated by using refined petroleum or coal pitch that is passed through a thin nozzle and stabilised by heating. PAN fibres are made of polyacrylonitrile that is carbonised through burning. The diameter of pitch-type fibres measures approximately  $9\text{-}18 \mu\text{m}$  and that of the PAN-type measures  $5\text{-}8 \mu\text{m}$ . The structure of this carbon fibre varies according to the orientation of the crystals.

Carbon fibres are used for their high performance and are characterized by high Young modulus of elasticity as well as high strength. They have an intrinsically brittle failure behaviour with a relatively low energy absorption; nevertheless, their failure strength are larger compared to glass and aramid fibers. Carbon fibers are less sensitive to creep rupture and fatigue and show a slight reduction of the long-term tensile strength.

Typical properties of various types of fibre materials are provided in table (2-4) and a further comparison is shown in figure (2.26):

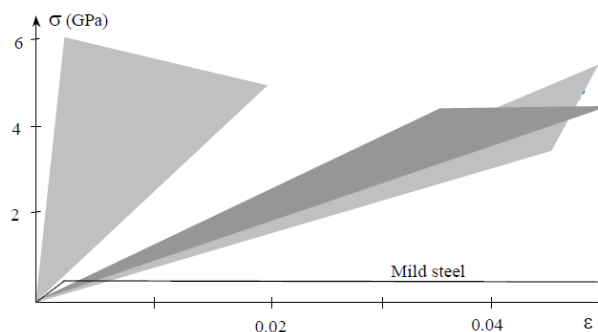


Figure 2.26: Uniaxial tension stress-strain diagrams for different unidirectional FRPs (CFRP, GFRP, ARFP) and steel



	Young's modulus $E$	Tensile strength $\sigma_r$	Strain at failure $\epsilon_r$	Coefficient of thermal expansion $\alpha$	Density $\rho$
	[GPa]	[MPa]	[%]	$[10^{-6} \text{ } ^\circ\text{C}^{-1}]$	$[\text{g}/\text{cm}^3]$
E-glass	70 – 80	2000 – 3500	3.5 – 4.5	5 – 5.4	2.5 – 2.6
S-glass	85 – 90	3500 – 4800	4.5 – 5.5	1.6 – 2.9	2.46 – 2.49
Carbon (high modulus)	390 – 760	2400 – 3400	0.5 – 0.8	-1.45	1.85 – 1.9
Carbon (high strength)	240 – 280	4100 – 5100	1.6 – 1.73	-0.6 – -0.9	1.75
Aramid	62 – 180	3600 – 3800	1.9 – 5.5	-2	1.44 – 1.47
Polymeric matrix	2.7 – 3.6	40 – 82	1.4 – 5.2	30 – 54	1.10 – 1.25
Steel	206	250 – 400 (yield) 350 – 600 (failure)	20 – 30	10.4	7.8

Table 2-4: Comparison between properties of fibers, resins and steel. (typical values)

FRP materials usage as retrofit technique tends to be more advantageous than steel jacketing. After yielding point steel provides uniform and constant confinement pressure. But FRP tend to behave elastically up to failure and higher confinement pressure can be developed at high strain levels. Other advantages of FRP as compared with steel are: light weight and therefore easier application; unlimited availability in FRP sizes; very flexible during installation; high strength; good fatigue resistance; immunity to corrosion; weather resistance; low thermal conductivity; low coefficient of thermal expansion; non magnetic; radar transparency; high dielectric strength (insulator); low maintenance; long term durability; part consolidation; tailored surface finish.

There are also some disadvantages in using FRP in place of steel: bad performance under elevated temperatures; bad effect of UV radiation; application of FRP and adhesives need qualified personnel; adhesives are dangerous for people and environment; high cost; brittle materials (their performance is linear elastic until failure, albeit this happens at a high deformation level); coefficient of thermal expansion is different from that of concrete and masonry; vulnerability to fire and generally high temperatures; reduction of tensile strength and Young Modulus when they are under continuous drench or alkaline environment.

## 2.4. Fibre-Reinforced Polymeric columns confinement

### 2.4.1. Introduction

The confinement of concrete with FRP is based on a well-understood mechanism. When the concrete is subjected to axial compression, it expands laterally. This expansion is resisted by the FRP jacket which provides a confining pressure to the

concrete. Eventual failure occurs when the FRP jacket ruptures, as it will be stated later.

Confining wraps or jackets to rehabilitate and reinforce existing concrete columns or beams represent the principal application of FRP. In the last decade multiple research efforts coupled with field applications of FRP wraps as passive confinement to concrete columns and beams have been carried out exploring all the aspects of technique. Confinement is generally applied to members in compression, with the aim to enhance their load carrying capacity or, in cases of seismic upgrading, to increase their ductility.

Several experimental studies on concrete confined with FRP have been carried out and confirmed the viability of this solution. Current analytical and numerical research (Spoelstra and Monti 1999, Lam and Teng 2003, Ilki et al. 2002, Karbhari and Gao 1997, Moran and Pantelides 2002, Li et al. 2003, Saiidi et al. 2002, Shehata et al. 2002, Vintzileou and Panagiotidou 2007, Yan and Pantelides 2007, Youssef et al. 2007) aims at defining appropriate constitutive laws for FRP-confined models. FRP confinement is used mainly in these cases:

- There is the necessity to improve the initial properties of the concrete member.
- The axial capacity of the structure is less required.
- Any of the concrete member of a structure gets damaged resulting in reduction of axial load capacity.
- There is a need to increase the ductility for resisting greater forces in horizontal direction.

Confinement benefits the elements: to prevent the concrete cover from spalling; to enhance concrete strength and deformation capacities; to provide lateral support to the longitudinal reinforcement.

In case of circular columns, these goals can be achieved by applying external FRP jackets, either continuously all over the surface or discontinuously as strips, because concrete in a circular jacket is uniformly confined.

In case of rectangular columns, concrete is non-uniformly confined. In this case the confinement can be provided with rectangular-shaped reinforcement, with corners rounded before application (the radius is about 15 to 25 mm, depending on the specification given by the FRP jacket supplier).

Rectangular confining reinforcement is less efficient as the confinement action is mostly located at the corners and a significant jacket thickness needs to be used between corners to restrain lateral dilation and column bar buckling. An alternative approach is to enclose the rectangular column within an externally cast circular to oval shape that provides the appropriate shape for the jacket.

As discussed earlier, FRP, as opposed to steel that applies a constant confining pressure after yielding, has an elastic behaviour up to failure and therefore exerts its passive confining action on concrete specimens under axial load in a different way with respect to steel.

In figure (2.27) it is possible to see that steel exerts a constant lateral confining pressure after it reaches a certain value of the normalized axial concrete strain. On the contrary, FRP exerts a continuously increasing confining action.

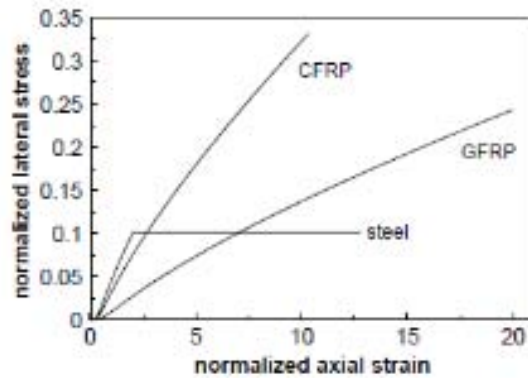


Figure 2.27: Comparison of confinement action of steel and FRP materials (Bulletin 14, CEB-FIP 2001)

An everyday life example can be used to explain the concept of confinement. Considering a weight lifting athlete lifting a heavy weight and the belt that he wears in his abdomen region prevents spine buckling by creating torsional stiffness. The belt provides a lateral confinement pressure, which increases as weights increase (axial force). Thanks to the belt, the athlete is capable of lifting higher amounts of weights. (Pilakoutas et al., 2014)

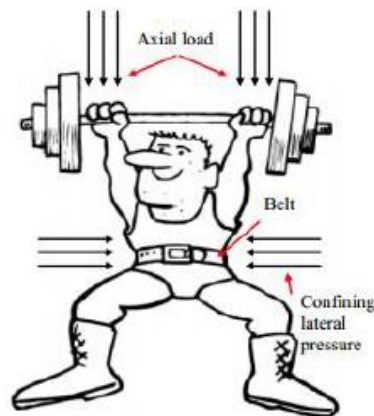


Figure 2.28: Everyday life example depicting Confinement (Pilakoutas et al., 2014)

#### 2.4.2. FRP-confined concrete characteristics

The stress strain relationship of concrete under short-term monotonically increasing uniaxial compressive loading shows gradual deterioration in stiffness, with strain even at a low stress level, caused by development of micro cracks. The failure of concrete is a result of the continuously increasing rate propagation of those cracks. The presence of passive confining reinforcement has a crucial effect on this behaviour of concrete. This kind of reinforcement can be closed steel stirrups or spiral reinforcement or FRP Jacketing. It is characterized as passive because it doesn't participate directly in carrying the imposed vertical load but raises resistance at the induced from the vertical load expansion of bounded concrete. By

doing so, it keeps the cracked pieces of concrete together, limits the progress of expansion and therefore it delays the upcoming failure. The result is that concrete can develop high deformations in the direction of loading without loss of strength (ductility) and the stress-strain curve obtains then characteristics similar to those of an elasto-plastic material.

The stress-strain curve  $\sigma - \varepsilon$  of confined concrete with FRP jackets can be divided into three phases (figure 2.29):

1. Elastic behaviour of concrete, similar to that of unconfined concrete, at the beginning of loading.
2. The development of micro cracks causes concrete expansion, hence the jacket is mobilised and starts confining the concrete core.
3. The gradient of the stress-strain curve changes and stabilises only after significant damage to the confined concrete.

In the first phase, the jacket has not yet been activated, due to low Poisson's ratio of concrete, therefore there is no significant expansion in the concrete core. In the second phase, increased Poisson's ratio causes concrete expansion. When a critical point is reached at critical stress  $f_{cr}$ , there is the end of the second phase. As well as this point, cracking develops at an uncontrollable manner if concrete is not well confined. In the last phase, both stress and strain increase linearly till failure.

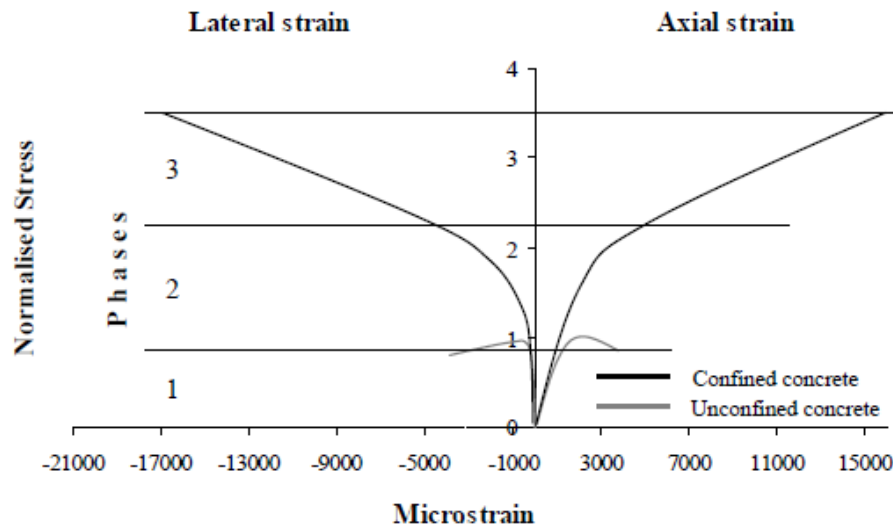


Figure 2.29: Strength and ductility enhancement of FRP confined concrete Typical 2-layer AFRP jacket), normalised stress = stress divided by unconfined concrete strength. (Pilakoutas et al., 2014)

The behaviour of uniaxially loaded concrete is also quantified by the volume change of concrete (as shown in figure 2.30), defined by the volumetric strain ( $\varepsilon_v = \varepsilon_c + 2 \cdot \varepsilon_L$ ), where  $\varepsilon_c$  is the axial strain and  $\varepsilon_L$  is the lateral strain.

Concrete reduces its volume till the onset of the unstable cracking propagation and after that, expansion takes place. The corresponding stress at the minimum volumetric strain is called “critical stress”. Theoretically, the more confinement provided, the higher critical stress is achieved. When volumetric ratio intersects the vertical axis, volume equals to zero and the Poisson’s ratio is equal to 0.5. The corresponding stress is called “zero volumetric stress”.

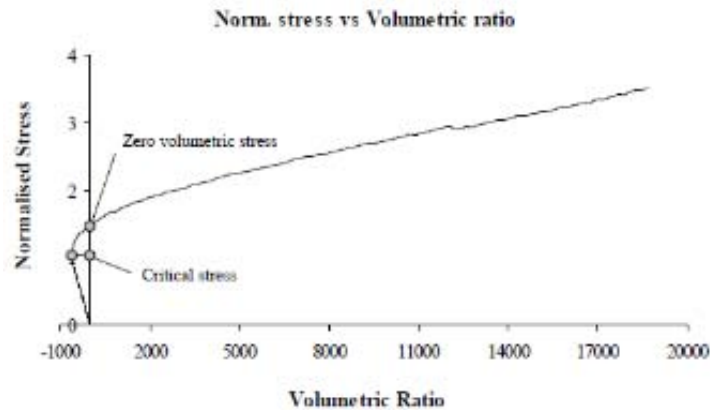


Figure 2.30: Typical volumetric ratio for plain concrete under uniaxial loading (Pilakoutas et al., 2014)

### 2.4.3. Lateral confining pressure

Wrapping reinforcement induce a triaxial state of stress on the concrete under axial compressive loading. Classical experimental study of concrete under triaxial compressive loading was carried out by Richart et al. (1928), at the University of Illinois. The investigation contains a study of concrete specimens loaded in compression in one, in two or in three directions at right angles to each other by means of fluid pressures. Series 3A consisted of tests of sixty-four 4 by 8-in. concrete cylinders in three-dimensional compression, two of the principal stresses being equal, and smaller than the third one. The two smaller stresses were applied by liquid pressure on the sides of the cylinder and the larger axial stress was applied to the cylinder in a testing machine.

This series correctly represent the behaviour of concrete wrapped by FRP and under axial compressive loading. The results of the test show that the strength of concrete is significantly raised by the presence of lateral compressive stresses (increase in strength of about 4.1 times the magnitude of the smallest lateral compression). The results indicate also an increase of ductility, because the specimens were still intact after the test, in spite of the large deformations to which they had been subjected.

The confinement pressure varies according to:

- The type of cross section of the concrete member (whether it is a square section or rectangular section or circular section)

- The amount of wrapping done (whether the FRP is fully wrapped along the concrete member or partially rolled along the concrete member)
- The stiffness of the FRP system
- The direction of orientation of the fibres in the system.

The cross section shape determines the geometric strengthening ratio, which is important in finding the total confinement pressure. Therefore, the confinement pressure varies with the cross sectional shape of the section such as square, rectangular or circular sections.

#### 2.4.3.1. Lateral confining pressure in circular sections

The confinement action exerted by the FRP on the concrete core is of the passive type, that is, it arises as a result of the lateral expansion of concrete under axial load. As the axial stress increases, the corresponding lateral strain increases and the confining device develops a tensile hoop stress balanced by a uniform radial pressure which reacts against the concrete lateral expansion. When an FRP confined cylinder is subject to axial compression, the concrete expands laterally and this expansion is restrained by the FRP.

For uniaxially loaded cylindrical concrete specimens confined with FRP reinforcement, with fibres circumferentially aligned and covering the total concrete surface, the lateral confining pressure comes from figure (2.31) (fib, 2001).

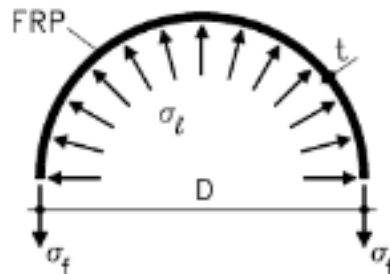


Figure 2.31: Confining pressure exerted by the FRP

The lateral confining pressure  $\sigma_l$  can be expressed as:

$$\sigma_l = \frac{1}{2} \cdot \rho_j \cdot \sigma_j = \frac{1}{2} \cdot \rho_j \cdot E_j \cdot \varepsilon_{j=l} = K_{conf} \cdot \varepsilon_l \quad \text{with} \quad \rho_j = \frac{4 \cdot t_j}{d_j}$$

Where  $\rho_j$  = volumetric ratio of FRP jacket;  $\sigma_j$  = stress in FRP jacket;  $E_j$  = the modulus of the composite material of the jacket;  $K_{conf}$  = stiffness of the FRP confinement;  $\varepsilon_{j=l}$  = circumferential strain in FRP jacket (taken equal to the lateral strain in concrete);  $d_j$  = diameter of FRP jacket.

The lateral confining pressure  $\sigma_l$  exerted by the confining jacket is computed based on its current stress  $\sigma_j = E_j \cdot \varepsilon_j \leq f_j = E_j \cdot \varepsilon_{ju}$ , whilst the maximum lateral confinement  $f_l$  is provided for  $\varepsilon_j = \varepsilon_{ju} =$  FRP jacket effective ultimate circumferential strain:

$$f_j = \frac{1}{2} \cdot \rho_j E_j \cdot \varepsilon_{ju}$$

If the concrete is partially wrapped, less efficiency is obtained as both confined and unconfined zones exist. In this case, the effective lateral confining pressure is obtained by introducing a confinement effectiveness coefficient  $K_{conf} \leq 1$ . The effectiveness coefficient is obtained by considering that the transverse pressure from the confining device is only effective where the confining pressure has fully developed. As illustrated in figure (2.32), the regions of concrete that are not confined can be described by a parabola with initial slope of  $45^\circ$ .

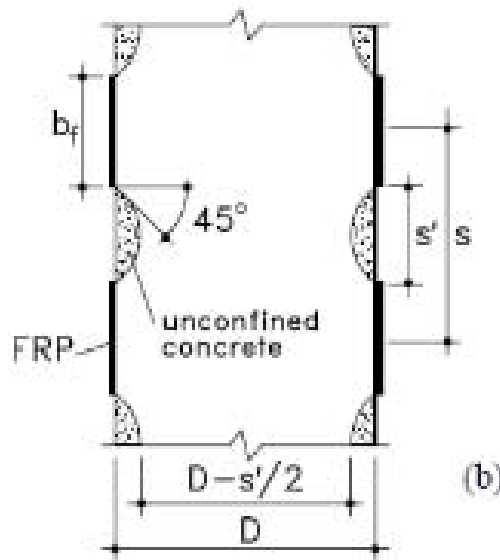


Figure 2.32: Confining pressure exerted by the FRP in partially wrapped column

If the fibres are helically applied, the fibre alignment is less efficient to restrain the lateral expansion of the concrete. Even in this case, this effect can be considered by introducing a corresponding confinement effectiveness coefficient.

#### 2.4.3.2. Lateral confining pressure in rectangular sections

In case of FRP confined rectangular sections, the concrete is non-uniformly confined and the effectiveness of confinement is much reduced. It should be noted that due to the non-uniformity of confinement in a rectangular section, for a given axial strain, the stress sustained by the concrete varies over the section. For a square or rectangular section wrapped with FRP and with corners rounded with a radius

$r_c$ , the parabolic arching action is again assumed for the concrete core where the confining pressure is fully developed. In figure (2.33) it is shown the effectively confined core for rectangular sections.

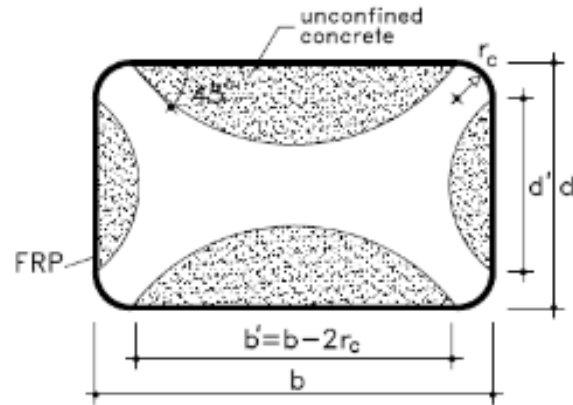


Figure 2.33: Effectively confined core for non-circular sections (Bulletin 14, CEB-FIP 2001)

Lateral confining pressure in rectangular columns will be explained in detail in the following paragraphs, according to the stress-strain model adopted in this dissertation.

#### 2.4.4. Use of confinement to increase ductility in seismic regions

Pilakoutas et al. (2014) expressed the meaning of Ductility: it is the capability of showing inelastic elongation along with no significant decrease in strength. Ductility is expressed as the ratio of elongation at ultimate level to elongation at yield level. Enhancement of deformation capacity of structurally deficient columns in seismic regions is of utmost importance. This enhancement is best achieved through concrete confinement.

According to ACI 440.2R-02 and even ACI 318-02, ductile capacity is taken as “adequate” when the value of the strain of the tension steel at the point of concrete crushing or fracture of FRP is 0.005.

Various researchers state many ductility models. One of them is certainly Triantafillou method (2003), also included in ACI 440.2R-08 guidelines.

According to this model, plastic hinge confinement is crucial, as the unconfined compression strength of concrete is insufficient to enable the development of large displacement or chord rotation ductility factors  $\mu_\theta = \frac{\theta_u}{\theta_y}$ . Experimental results have demonstrated that enhancement of the ductility capacity is easily achieved by properly designed FRP jackets (figure 2.34).



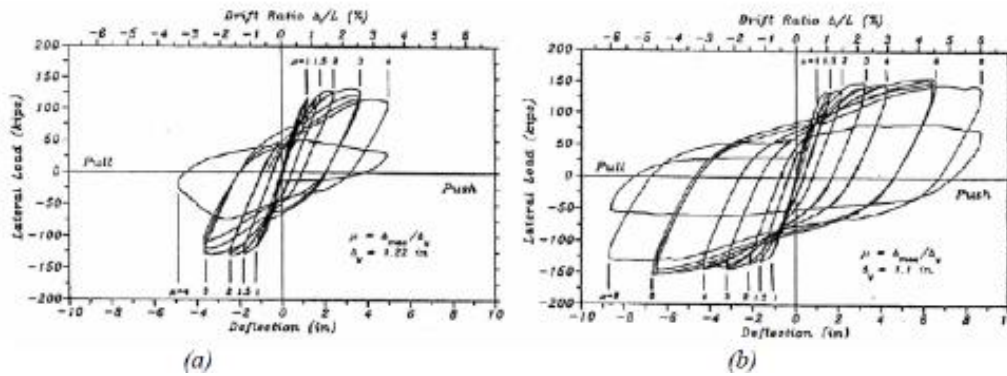


Figure 2.34: Lateral force-displacement response of flexure-dominated rectangular columns: (a) as-built; (b) retrofitted with GFRP jacket at the plastic hinge region (Priestley and Seible 1995)

This model describe a method of selecting the jacket thickness for a specific ductility factor  $\mu_\theta$  required. First the equivalent plastic hinge length  $L_p$  for a given column is calculated based on the yield stress and diameter of longitudinal rebars. From  $L_p$  and  $\mu_\theta$  the curvature ductility factor  $u_\phi = \frac{\phi_u}{\phi_y}$  is established. The yield curvature  $\phi_y$  may be found from moment-curvature analysis of the cross section, whereas the maximum required curvature  $\phi_u$  may be obtained (again from section analysis) in terms of the ultimate concrete strain. Hence the required value for  $\varepsilon_{cu}$  can be established and an appropriate confinement model can be used to solve for the required FRP thickness.

#### 2.4.5. Stress-strain model for concrete confined with stirrups

In literature there are many stress-strain models for stirrups confined concrete. Some models are valid for design, for example parabola-rectangle, triangle-rectangle, rectangle (stress block). These models are accepted and suggested by the normatives such as Eurocode 2 and NTC 2008. They do not consider tensile behaviour of confined concrete. In order to perform an analytical investigation, these models should not be used and nonlinear models should be used instead. Some of the most accepted models are Hognestad (1951), CEB (2010), Saenz (1964), Sargin (1971), Mander et al. (1988), Kwon and Spacone (2002). These models explain the compressive behaviour of confined concrete. In this dissertation, CEB model will be used because it is accepted by Eurocode 2. Tensile behaviour of confined concrete will be discuss later with regard to tension stiffness.

##### 2.4.5.1. Compressive stress-strain model for confined concrete

The non-linear stress-strain relationship for stirrups confined concrete under short-term loading (CEB 2010) is shown in figure (2.35) and it is described below:

$$\frac{\sigma_c}{f_{cm,c}} = - \left( \frac{k \cdot \eta - \eta^2}{1 + (k-2) \cdot \eta} \right) \quad \text{for } |\varepsilon_c| < |\varepsilon_{cu2,c}|$$

Where:

$$\eta = \varepsilon_c / \varepsilon_{c2,c};$$

$$k = E_{ci} / E_{c1};$$

$f_{cm,c}$  is the maximum compressive stress for confined concrete;

$\varepsilon_{cu2,c}$  is the maximum strain for confined concrete;

$\varepsilon_{c2,c}$  is the strain at maximum compressive stress for confined concrete;

$E_{c1}$  is the secant modulus from the origin to the peak compressive stress;

$k$  is the plasticity number.

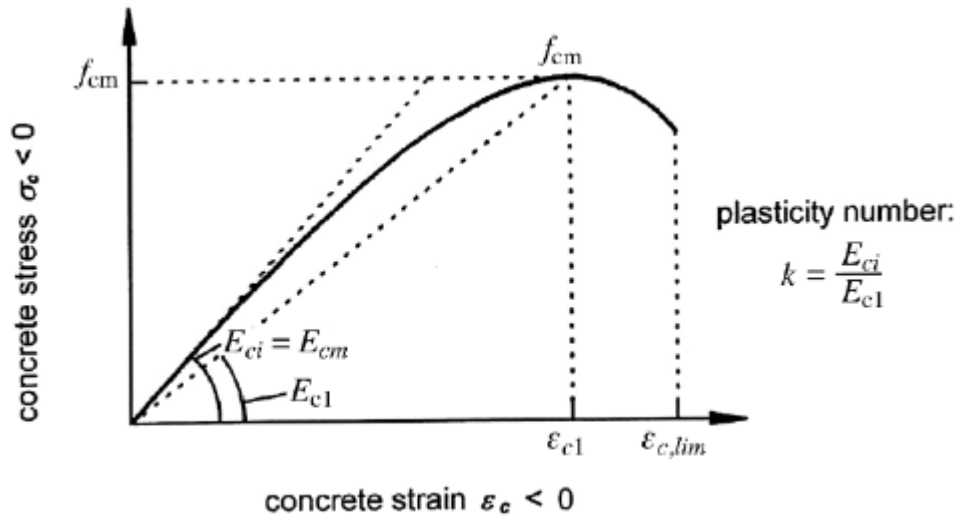


Figure 2.35: Schematic representation of the stress-strain relation for short term loading in uniaxial compression (Model Code for Concrete Structures, 2010)

$f_{cm,c}$ ,  $\varepsilon_{cu2,c}$ ,  $\varepsilon_{c2,c}$  parameters can be found with regard to the characteristics of unconfined concrete and with reference to the confining pressure  $\sigma_2$ :

$$\frac{f_{cm,c}}{f_{cm}} = 1 + 3.5 \cdot \left( \frac{\sigma_2}{f_{cm}} \right)^{\frac{3}{4}}$$

$$\varepsilon_{c2,c} = 0.002 \cdot \left[ 1 + 5 \cdot \left( \frac{f_{cm,c}}{f_{cm}} - 1 \right) \right]$$

$$\varepsilon_{cu2,c} = 0.0035 + 0.2 \cdot \left( \frac{\sigma_2}{f_{cm}} \right)$$

Where:

$f_{cm}$  is the maximum compressive stress for unconfined concrete;

$\sigma_2$  is the confining pressure (with positive sign). This has different expression depending on the cross-section (circular or rectangular). Its value is expressed in CEB “Model Code for Concrete Structures 2010”.

#### 2.4.5.2. Tensile stress-strain model for confined concrete

Although concrete is weak in tension, in order to perform a more accurate analytical investigation, it is necessary to implement even its tensile behaviour. In the case of unconfined concrete, the stress-strain tensile behaviour is represented with tension softening function. With regard to the confined concrete, the existence of reinforcement stiffens and engages the concrete between the cracks through local bond stress transfer associated with local bond-slip. This behavior improves the softening response by introducing the *tension stiffening* effect, which causes the average concrete stress in tension to gradually reduce to zero as the cracking intensifies. Tensile behaviour for both unconfined and confined concrete is shown in figure (2.36).

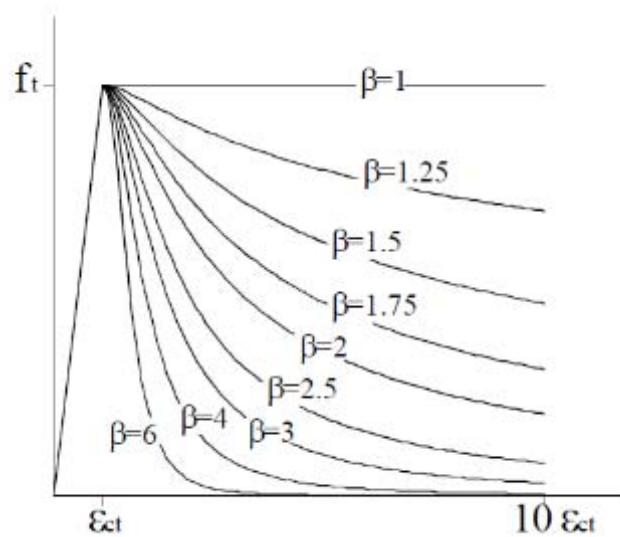


Figure 2.36: Tension softening and tension stiffening response (Carreira and Chu 1986)

According to Carreira and Chu (1986) model, the tensile stress-strain behaviour of confined concrete comprises two functions:

- Linear relationship until the peak of maximum tensile strength ( $f_t$ ) and relative strain ( $\epsilon_{ct}$ ). The slope of the straight line is the modulus of elasticity of the concrete in compression ( $E_c$ ).

- Nonlinear function for softening branch till the maximum tensile strain ( $10 \cdot \varepsilon_{ct}$ ). The function is defined as  $\sigma_{ct}(\varepsilon) = \frac{\beta \cdot f_t \cdot \left(\frac{\varepsilon}{\varepsilon_{ct}}\right)}{\beta - 1 + \left(\frac{\varepsilon}{\varepsilon_{ct}}\right)^\beta}$ , where  $\beta$  is a parameter calibrated on the basis of experimental results ( $1.45 \leq \beta \leq 2.26$ ).

#### 2.4.6. Stress-strain model for RC rectangular columns confined using FRP jacket

In this work, the design-oriented Lam and Teng model (2003) is utilised to define the stress-strain relationship of concrete confined with FRP composites. Due to its simplicity and good prediction of experimental results, the model is widely used in practice and it is included in the most recent version of the Italian FRP guidelines for strengthening RC structures (CNR, 2012). This model is an extension of a design oriented stress–strain model developed for concrete uniformly confined with CFRP based on test results of circular concrete specimens. It should be noted that this model was developed for concrete confined by wrapped FRP with fibers only or predominantly in the hoop direction. CFRP jackets with a significant presence of vertical fibers, however, are seldom used in the retrofit of RC columns. A rectangular column with rounded corners is shown in Figure (2.37), where the width and the depth are respectively  $b$  and  $h$ , ( $b < h$ ). Square columns are considered as a special case of rectangular columns with  $b = h$ .

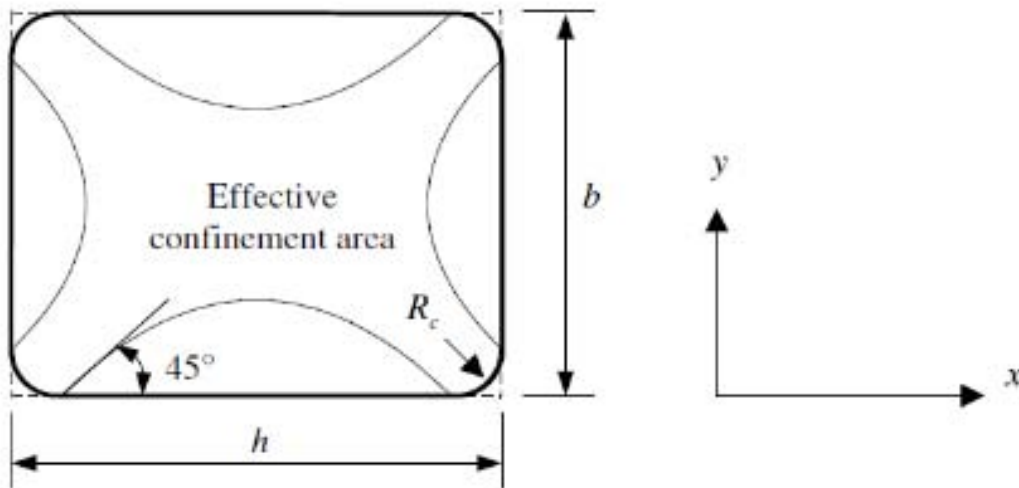


Figure 2.37: Effectively confined concrete in a rectangular column

As it was said earlier, to improve the effectiveness of FRP confinement, corner rounding is generally recommended. Due to the presence of internal steel reinforcement, the corner radius  $R_c$  is generally limited to small values. The reduced effectiveness of an FRP jacket for a rectangular section compared to a circular section has been confirmed by experimental results. Despite this reduced

effectiveness, an FRP-confined rectangular concrete column generally also fails by CFRP rupture.

It should be noted that due to the non-uniformity of confinement in a rectangular section, for a given axial strain, the stress sustained by the concrete varies over the section. The commonly accepted approach is to define the stress as the average axial stress (load divided by cross-sectional area).

The specimens analysed by Lam and Teng have a higher reinforcement ratio respect to those used by other authors. The majority of the existing test results are for low confinement levels which do not cover a sufficiently wide range of confinement levels desirable for assessing the performance of existing theoretical models. The low confinement data have another shortcoming: they are more sensitive to the inherent random variation of the unconfined concrete strength and thus display a relatively large scatter which introduces undesirable uncertainty in the assessment of existing theoretical models.

Fourteen FRP-wrapped specimens were prepared and tested in this experimental program. These included two circular specimens of 152 mm in diameter by 610 mm in height, ten square specimens of 150 · 150 mm in cross section by 600 mm in height, and two rectangular specimens of 150 · 225 mm in cross section by 600 mm in height.

The epoxy primer and resin, and the carbon fiber sheets were supplied by a local firm and formed a proprietary product. The nominal thickness of the fiber sheets was 0.165 mm.

The tensile strength and elastic modulus of the CFRP were found to be 4519 MPa and 257 GPa.

The model presented by Lam and Teng is valid for concrete uniformly confined with CFRP, but it can be applied to rectangular confined concrete columns with the appropriate modifications. This model is based on the following assumptions (see also figure 2.38):

- The stress-strain curve consist of a parabolic first portion and a linear second portion;
- The initial slope of the parabola is the same as the elastic modulus of unconfined concrete  $E_c$ ;
- The non linear part of this portion is affected to some degree by the presence of the FRP jacket;
- The parabolic first portion meets the linear second portion smoothly;
- The linear second portion ends at a point where both the compressive strength  $f'_{cc}$  and the  $\varepsilon_{cu}$  ultimate axial strain of confined concrete are reached.

The first assumption leads to a stress-strain curve which is similar to those adopted by existing design codes for unconfined concrete. The second assumption is to

account for the fact that the initial stiffness of FRP-confined concrete is little affected by the FRP due to the passive nature of confinement.

The third assumption is to reflect the fact that the FRP confinement is activated when the behavior of the concrete becomes non-linear. The fourth assumption ensures a smooth stress–strain curve, while the last assumption is obviously valid for FRP-confined concrete with a monotonically increasing stress–strain curve.

Lam and Teng’s stress-strain model for confined concrete is given by:

$$\sigma_c = E_c \cdot \varepsilon_c - \frac{(E_c - E_2)^2}{4 \cdot f'_{co}} \cdot \varepsilon_c^2 \quad (0 \leq \varepsilon_c \leq \varepsilon_t)$$

$$\sigma_c = f'_{co} + E_2 \cdot \varepsilon_c \quad (\varepsilon_t \leq \varepsilon_c \leq \varepsilon_{cu})$$

- $\sigma_c$  is the axial stress of confined concrete
- $\varepsilon_c$  is the axial strain of confined concrete
- $E_c$  is the elastic modulus of unconfined concrete
- $f'_{co}$  is the unconfined compressive strength
- $f'_{cc}$  is the compressive strength of confined concrete
- $\varepsilon_{cu}$  is the ultimate axial strain of confined concrete
- $\varepsilon_t$  is the axial strain at the transition point  $\left(\varepsilon_t = \frac{2 \cdot f'_{co}}{E_c - E_2}\right)$
- $E_2$  is the slope of the linear second portion  $\left(E_2 = \frac{f'_{cc} - f'_{co}}{\varepsilon_{cu}}\right)$

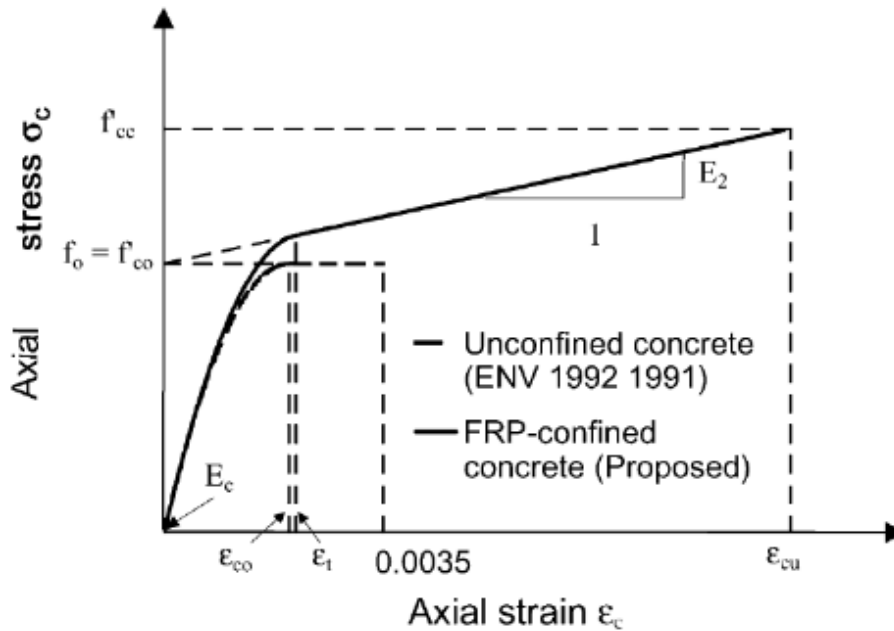


Figure 2.38: Lam and Teng’s stress-strain model for FRP-confined concrete

The difference between Lam and Teng's model for uniformly confined concrete and the model for rectangular confined concrete is given by the definition of the confined concrete compressive strength and the ultimate axial strain.

#### 2.4.6.1. Definition of ultimate condition

The ultimate condition of the element confined with FRP is reached when the FRP ruptures. This ultimate condition is characterized by two parameters:

- Ultimate axial strain;
- Corresponding stress level (generally it is the same of confined concrete compressive strength).

There are two points to make in connection with the ultimate condition of confined concrete. Firstly, the rupture of FRP does not occur when the hoop stress in the FRP jackets reaches the tensile strength determined from material tests. Ultimate condition is dependent on the type of FRP.

Secondly, the stiffness of FRP jacket has an important effect on the ultimate axial strain.

#### 2.4.6.2. Confined concrete compressive strength $f'_{cc}$

The equation for the compressive strength is based on the classical equation proposed by Richart et al. (1928), and then improved, for actively confined concrete:

$\frac{f'_{cc}}{f'_{co}} = 1 + k_1 \cdot \frac{f_l}{f'_{co}}$ , where  $k_1 = 4.1$ ,  $f_l$  is the lateral confining pressure for uniformly confined concrete  $f_l = \frac{2 \cdot f_{FRP} \cdot t}{d}$ .

Lam and Teng's equation proposal for compressive strength of FRP-confined rectangular columns is

$$\frac{f'_{cc}}{f'_{co}} = 1 + k_1 \cdot k_{s1} \cdot \frac{f_l}{f'_{co}}$$

Where  $k_{s1} \cdot \frac{f_l}{f'_{co}}$  is the effective confinement ratio;  $k_1 = 3.3$ ;  $f_l$  is the confining pressure in an equivalent circular column ( $f_l = \frac{2 \cdot E_{frp} \cdot \varepsilon_{h,rup} \cdot t}{D}$ );  $\varepsilon_{h,rup}$  is the ultimate strain of the FRP jacket and it is related to FRP material ultimate tensile strain  $\varepsilon_{frp}$  and the coefficient  $k_\varepsilon$  that vary with the type of FRP ( $\varepsilon_{h,rup} = \varepsilon_{frp} \cdot k_\varepsilon$ ). An average value of 0.586 for  $k_\varepsilon$  has been found for CFRP-confined circular concrete specimens based on the analysis of a large test database assembled from the available literature.

The parameter  $t$  is the total thickness of FRP. In the proposed model, the equivalent circular column is defined to have a diameter  $D$  being the diagonal distance of the section. That is  $D = \sqrt{h^2 + b^2}$ .

The shape factor for strength enhancement  $k_{s1}$  is proposed to depend on two parameters, the effectively confined area and the aspect ratio.

It is well known that in a rectangular section, not the whole of the concrete is confined by FRP. As mentioned earlier, it is assumed that only the concrete contained within the four parabolas which intersect the edges at  $45^\circ$  is effectively confined (see figure 2.39). The effective confinement area ratio  $\frac{A_e}{A_c}$  is therefore given by:

$$\frac{A_e}{A_c} = \frac{1 - \frac{b}{h} \cdot (h - 2 \cdot R_c)^2 + \frac{h}{b} \cdot (b - 2 \cdot R_c)^2}{3 \cdot A_g} - \rho_{sc}$$

In figure (2.39) there is the explanation of the terms used.

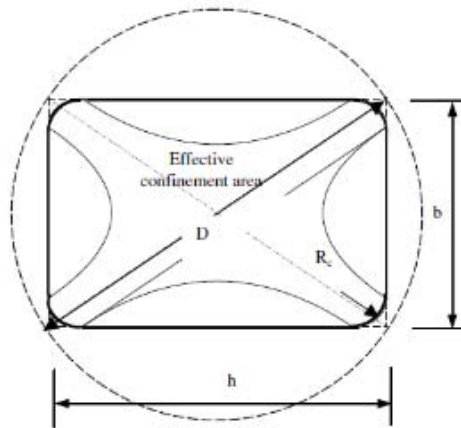


Figure 2.39: Illustration of proposed model for FRP-confined rectangular sections

The term  $\rho_{sc}$  is the cross sectional area ratio of the longitudinal steel reinforcement with respect to the gross cross-sectional area and its expression is given by:

$\rho_{sc} = \frac{A_s}{A_g}$ .  $A_s$  is the total area of longitudinal steel reinforcement and  $A_g$  is the gross area of concrete whose expression is  $A_g = b \cdot h - (4 - \pi) \cdot R_c^2$ .

The effects of the aspect ratio and the corner radius of a rectangular section with a fixed width on the effective confinement area ratio are shown in figure (2.40).



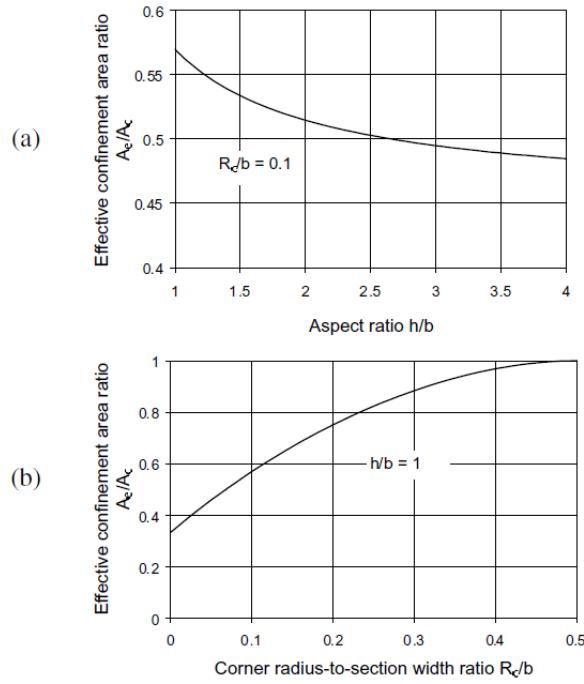


Figure 2.40: Variation of the effective confinement area ratio with respect ratio and corner radius. a) Effect of aspect ratio; b) Effect of corner radius-to-section width ratio

The expression for the shape factor for strength enhancement  $k_{s1}$  is proposed below:

$$k_{s1} = \left(\frac{b}{h}\right)^\alpha \cdot \frac{A_e}{A_c}$$

An appropriate value for the exponent  $\alpha$  is 2, based on the experimental tests.

### 2.4.6.3. Ultimate axial strain in rectangular columns $\epsilon_{cu}$

The equation for the ultimate axial strain in rectangular concrete columns is a modification of the previous equation valid for uniformly confined concrete. Lam and Teng's equation for ultimate axial strain in uniformly confined concrete is:

$\frac{\epsilon_{cu}}{\epsilon_{co}} = 1.75 + k_2 \cdot \frac{f_l}{f'_{co}} \cdot \left(\frac{\epsilon_{h,rup}}{\epsilon_{co}}\right)^{0.45}$ , where  $\epsilon_{co}$  is the axial strain at the compressive strength of unconfined concrete and  $k_2$  is the strain enhancement coefficient and is equal to 12.

The equation for the ultimate axial strain in rectangular concrete columns is given by:

$$\frac{\epsilon_{cu}}{\epsilon_{co}} = 1.75 + k_2 \cdot k_{s2} \cdot \frac{f_l}{f'_{co}} \cdot \left(\frac{\epsilon_{h,rup}}{\epsilon_{co}}\right)^{0.45}$$

Where  $k_{s2}$  is a shape factor depending on the effectively confined area and the aspect ratio. The expression for the shape factor  $k_{s2}$  is proposed below:

$$k_{s2} = \left(\frac{h}{b}\right)^\beta \cdot \frac{A_e}{A_c}$$

An appropriate value for the exponent  $\beta$  is 0.5, based on the experimental tests.

### **3. EXPERIMENTAL INVESTIGATION**

---

#### **3.1. Introduction**

A series of experimental works were performed in a reinforced concrete frame structure using the shaking table test to study the various behavioural aspects of the structure under different level of seismic excitations. The investigated structure is part of the BANDIT European Project SERIES (Seismic Engineering Research Infrastructures for European Synergies). The reference BANDIT program title is “Seismic Strengthening of Deficient RC Buildings Using Ductile Post Tensioned Metal Strips” and it deals with the retrofitting techniques of damaged buildings in reinforced concrete building. In particular, it is investigating the efficiency of the Post Tensioned Metal Strips (PTMS) and Carbon Fibre-Reinforced Polymeric (CFRP) reinforcement techniques at improving the seismic resistance of a seismically deficient two storeys RC building. The building used for the seismic tests on AZALEE shaking table (Saclay, France) is typical from Mediterranean and developing countries architecture design with poor reinforcement in columns and beam–columns joints. The experimental campaign has been efficiently conducted with hundred runs performed on the specimen from February to April 2012 by EMSI experimental team. The bare RC building was initially subjected to a series of shake table tests in two orthogonal directions to produce a desired level of damage and to evaluate the basic performance of the structure. After the initial tests (up to a PGA level of 0.15g), the joints were repaired and strengthened using PTMS, and the building was retested up to a PGA=0.35g. The damaged building was repaired for the second time and retrofitted using CFRP and PTMS on two opposite frames, and was retested to compare the performance of these two strengthening techniques.

Drain-3DX software was used to perform the analysis and analytical responses were compared to the experimental results. Dynamic time-history analysis was performed to analyse the structural behaviours and capacity of the frames.

#### **3.2. Description of the specimen**

The tested building was a one-bay two-storey full-scale reinforced concrete frame regular in plan and elevation. It was designed using typical old pre-seismic construction practice of southern Europe.

To replicate old construction practices, no transverse stirrups were provided at beam-column joints so as to produce damage in these components during the first tests on the original bare building. The anchorage of reinforcement in the joint was just adequate according to the old standards but not adequate enough according to modern standards (Eurocode 8 and even Norme Tecniche per le Costruzioni 2008) The main objective of the project was to investigate experimentally the seismic behaviour of the building repaired and strengthened with external reinforcement using CFRP or PTMS. This dissertation only deals with the use of CFRP reinforcement to rehabilitate the building after damage produced by a series of earthquakes.

The total height of the specimen was 6870 mm.

To simulate permanent and variable design loads, additional masses of 13.5 and 11.0 t were fixed beneath the 1<sup>st</sup> and 2<sup>nd</sup> floor slabs using steel plates and concrete blocks.

Figure (3.1) represent BANDIT building in bare condition, before the application of the additional masses. Figures (3.2), (3.3) shows the preparation of the additional masses under the slabs.



Figure 3.1: BANDIT specimen (Garcia et al. 2012)



Figure 3.2: Clamping of the masses under first slab (Garcia et al. 2012)



Figure 3.3: Clamping of the masses on the second slab (Garcia et al. 2012)

### 3.3. Geometry and details of the specimen

According to Garcia et al. (2012), the geometry of the structure is summarised as follows:

- Four columns, section  $260 \cdot 260 \text{ mm}$ ;
- Two square slabs,  $4260 \cdot 4260 \text{ mm}$  and  $120 \text{ mm}$  thick;
- Four beams for each slab with two different sections:  $400 \cdot 260 \text{ mm}$  in X direction,  $300 \cdot 260 \text{ mm}$  in Y direction;
- Four feet consisting in welded steel boxes dedicated to the fixing of the specimen on the AZALEE table.

The reinforcement details of the specimen can be summarised below and it is shown in figures (3.4)÷(3.17): (Garcia et al. 2012)

- 8  $\phi 14$  mm longitudinal deformed bars and  $\phi 6/200$  mm spacing in lower columns, as shown in figure (3.6);
- 4  $\phi 14$  mm longitudinal deformed bars and  $\phi 6/200$  mm spacing in upper columns, as seen in figure (3.6);
- 8  $\phi 14$  mm longitudinal deformed bars and  $\phi 8/250$  mm spacing in beams, as shown in figure (3.7);
- For the slabs, two steel nets with a  $100 \cdot 100$  mm mesh made of 10 mm diameter bars welded together. These two nets were intended to be in one piece, and fixed on top of each other with a 40 mm gap. In reality,  $4200 \cdot 4200$  mm nets were not available, so, each net has been made of two  $4200 \cdot 2400$  mm nets with a 600 mm overlap. See figures (3.13) and (3.14) for details.

The four feet of the specimen were manufactured from welded steel plates. The description of the feet are shown in figures (3.15), (3.16) and (3.17). They were dedicated to the fixation of the specimen on the AZALEE shaking table by four M36 bolts on each foot's base plate (49 mm thick,  $700 \cdot 700$  mm). These feet formed boxes full of concrete with, to ensure the link between the steel foot and the specimen's column:

- Eight transverse M16 steel rods fixed with screws,
- The eight verticals reinforcement bars of the column,  $90^\circ$  bent and welded in bottom of the foot's base steel plate.

As mentioned previously, the frame was designed according to old provisions of building codes. As shown in figures (3.9), (3.10), (3.11), (3.12), no transverse stirrups were provided at beam-column joints. The beams were designed stronger than the columns, which leads the structure to follow strong beam-weak column behaviour, therefore there is the development of plastic hinges in the columns before they develop in the beams. Furthermore, the beam lower bars are straight with no hooks or bends and in the upper beams, even the beam upper bars are straight.

Longitudinal reinforcement ratios was  $\rho_1 = 1.82\%$  for the first floor columns and  $\rho_2 = 0.91\%$  for the second floor columns. The reduction of longitudinal column reinforcement ratio between floors is a typical construction practice adopted in many developing countries to save material costs. In columns, the stirrups were closed with  $90^\circ$  bends instead of  $135^\circ$  hooks required by current seismic codes.

Between first and second level, the mechanical continuity is ensured by a bars overlap of 350 mm. There are no overlap of the upper columns longitudinal bars under the slab joint.

The top and bottom beam reinforcement has longitudinal reinforcement ratios of 0.65% for the beams 400 mm high and 0.90% for the beams 300 mm height.

The concrete cover is 20 mm thick from the centre of the steel bars in every location of the specimen.

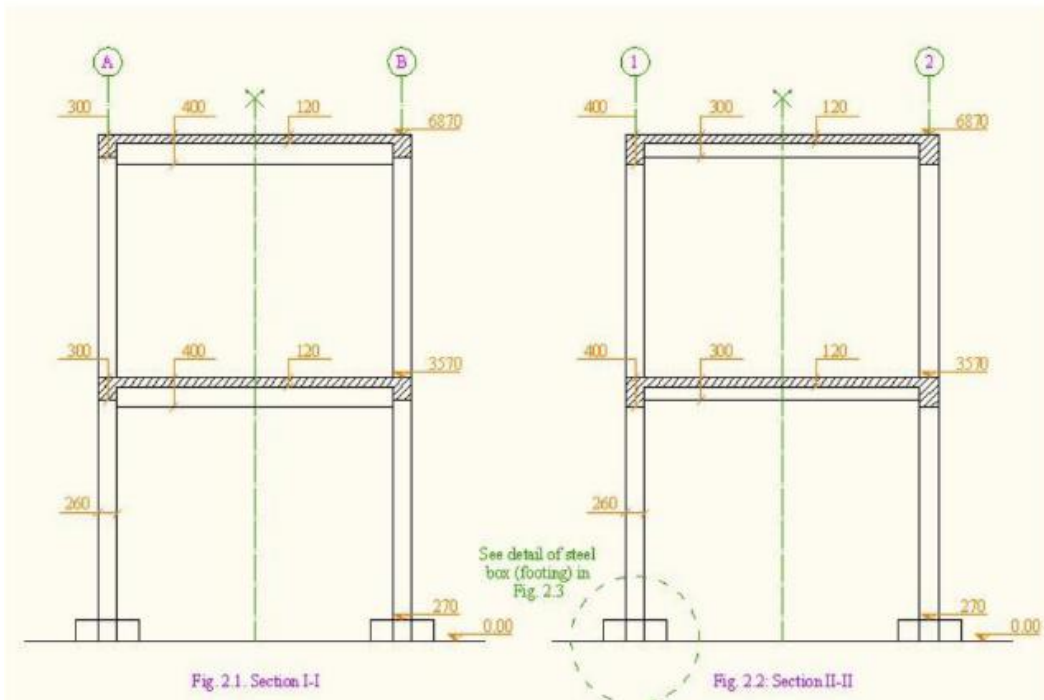


Figure 3.4: BANDIT specimen elevation (Unit: mm), (Garcia et al. 2012)

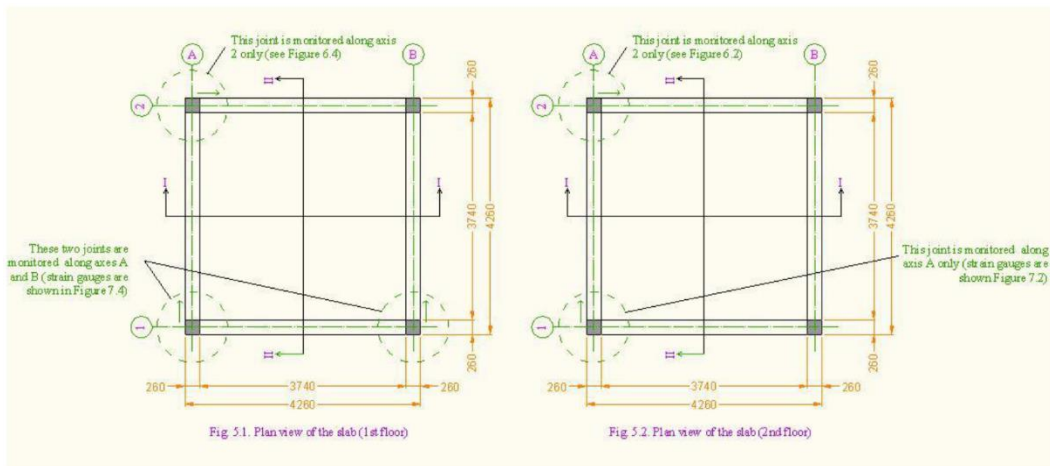


Figure 3.5: BANDIT specimen top view (Unit: mm), (Garcia et al. 2012)

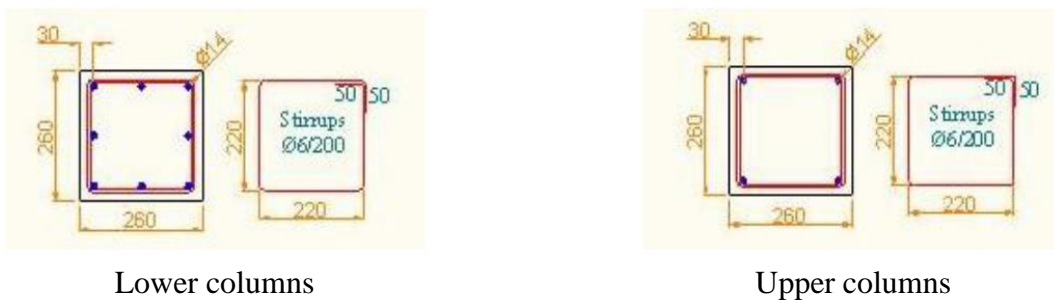


Figure 3.6: Reinforcement in columns (Unit: mm), (Garcia et al. 2012)

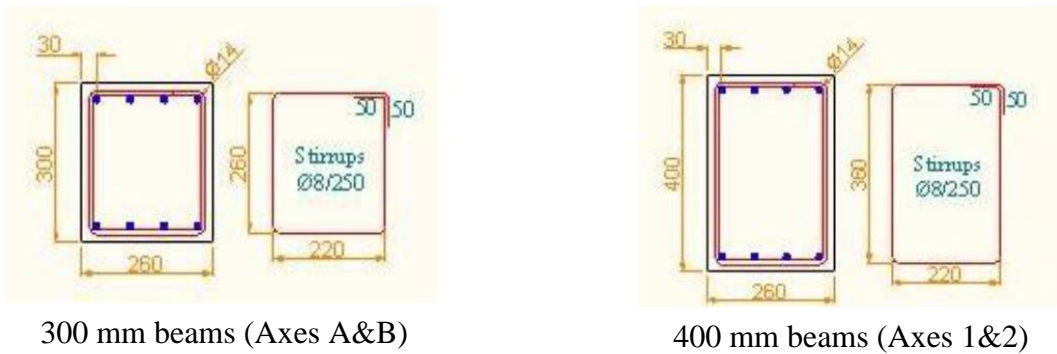


Figure 3.7: Reinforcement in beams (Unit: mm), (Garcia et al. 2012)

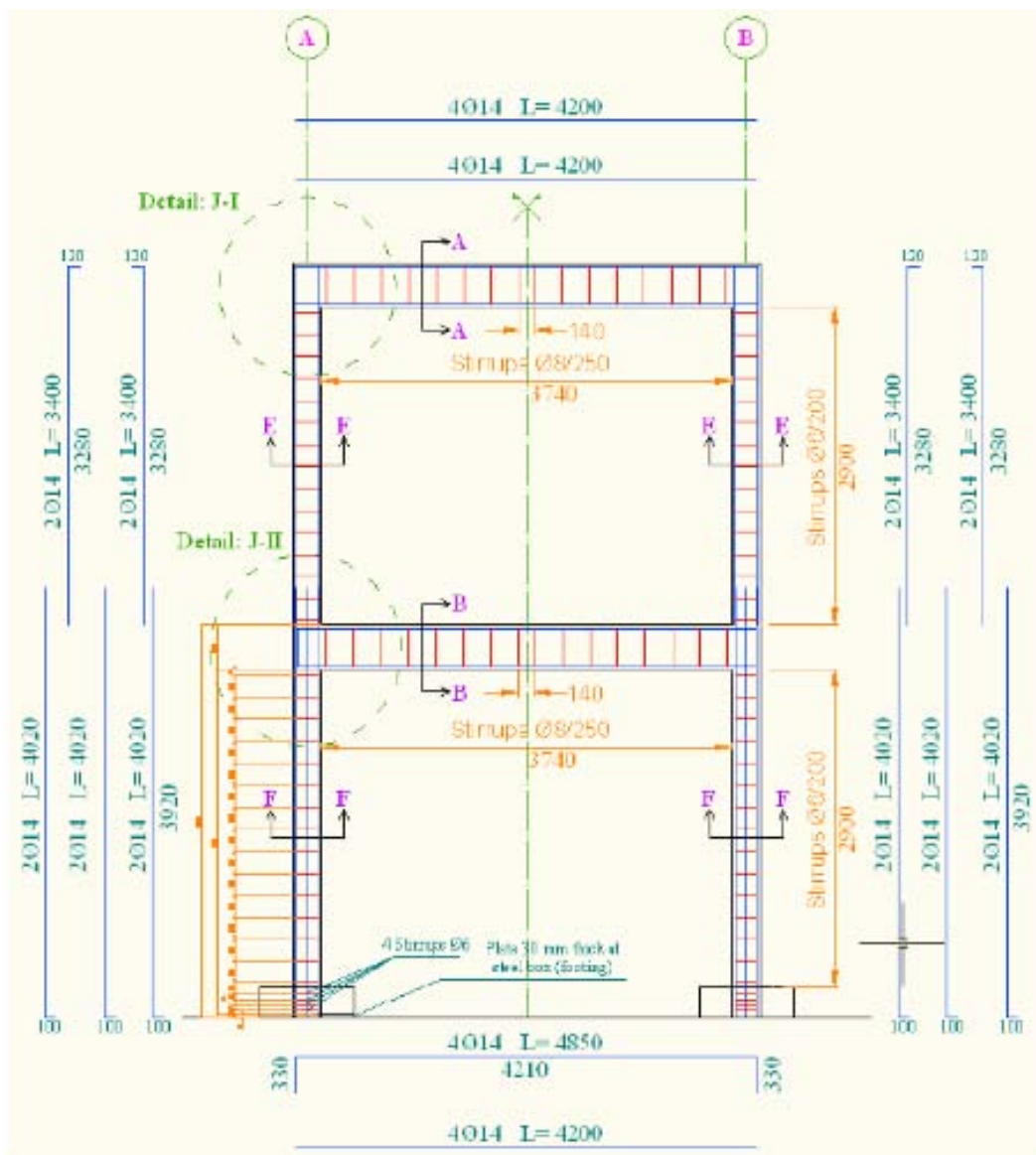


Figure 3.8: BANDIT specimen reinforcement (Unit: mm), (Garcia et al. 2012)

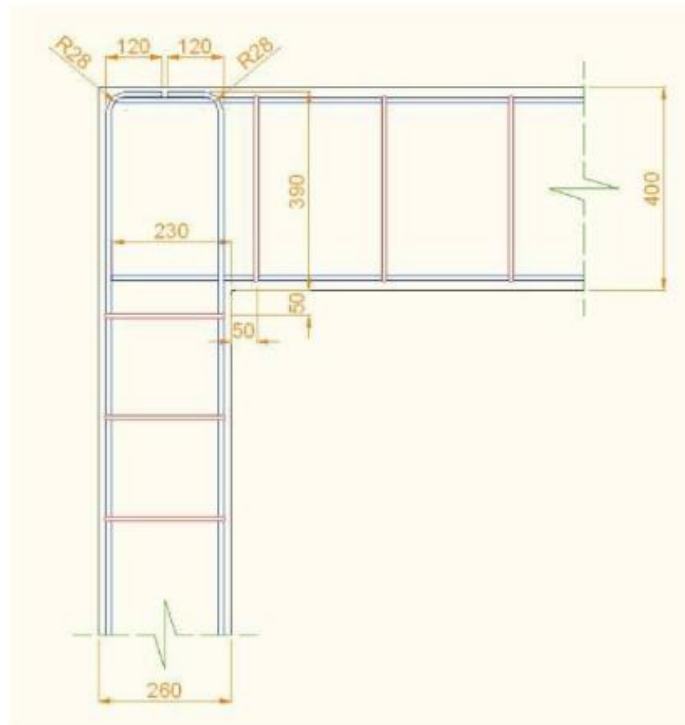


Figure 3.9: Reinforcement in upper nodes, 400 mm beam (Unit: mm), (Garcia et al. 2012)

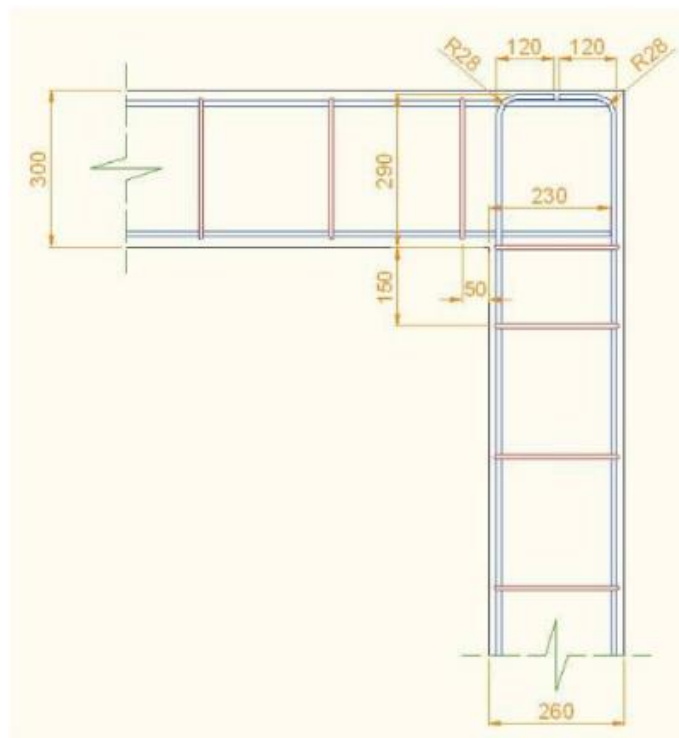


Figure 3.10: Reinforcement in upper nodes, 300 mm beam (Unit: mm), (Garcia et al. 2012)



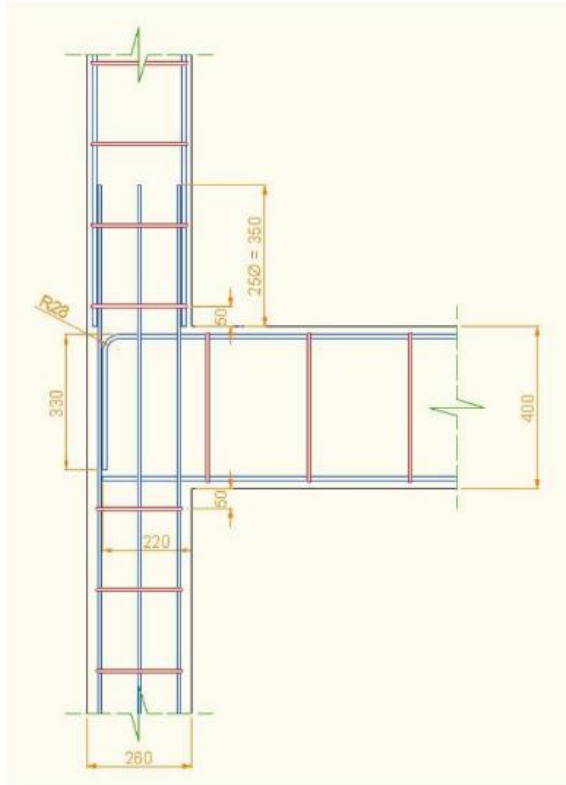


Figure 3.11: Reinforcement in lower nodes, 400 mm beam (Unit: mm), (Garcia et al. 2012)

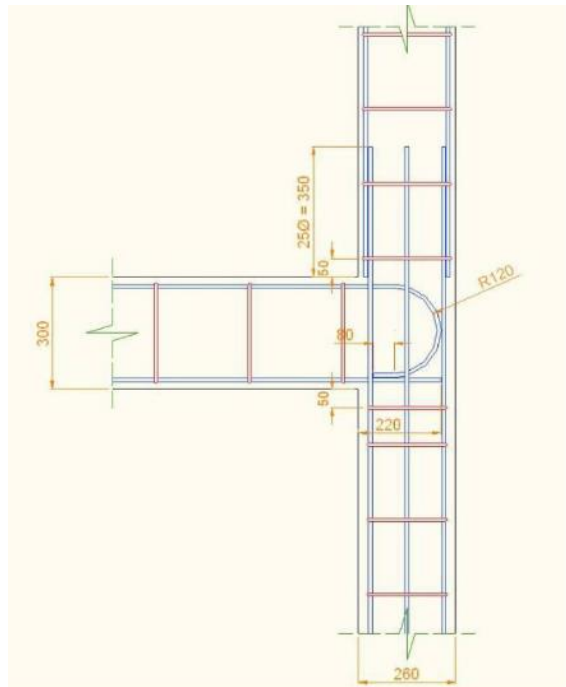


Figure 3.12: Reinforcement in lower nodes, 300 mm beam (Unit: mm), (Garcia et al. 2012)

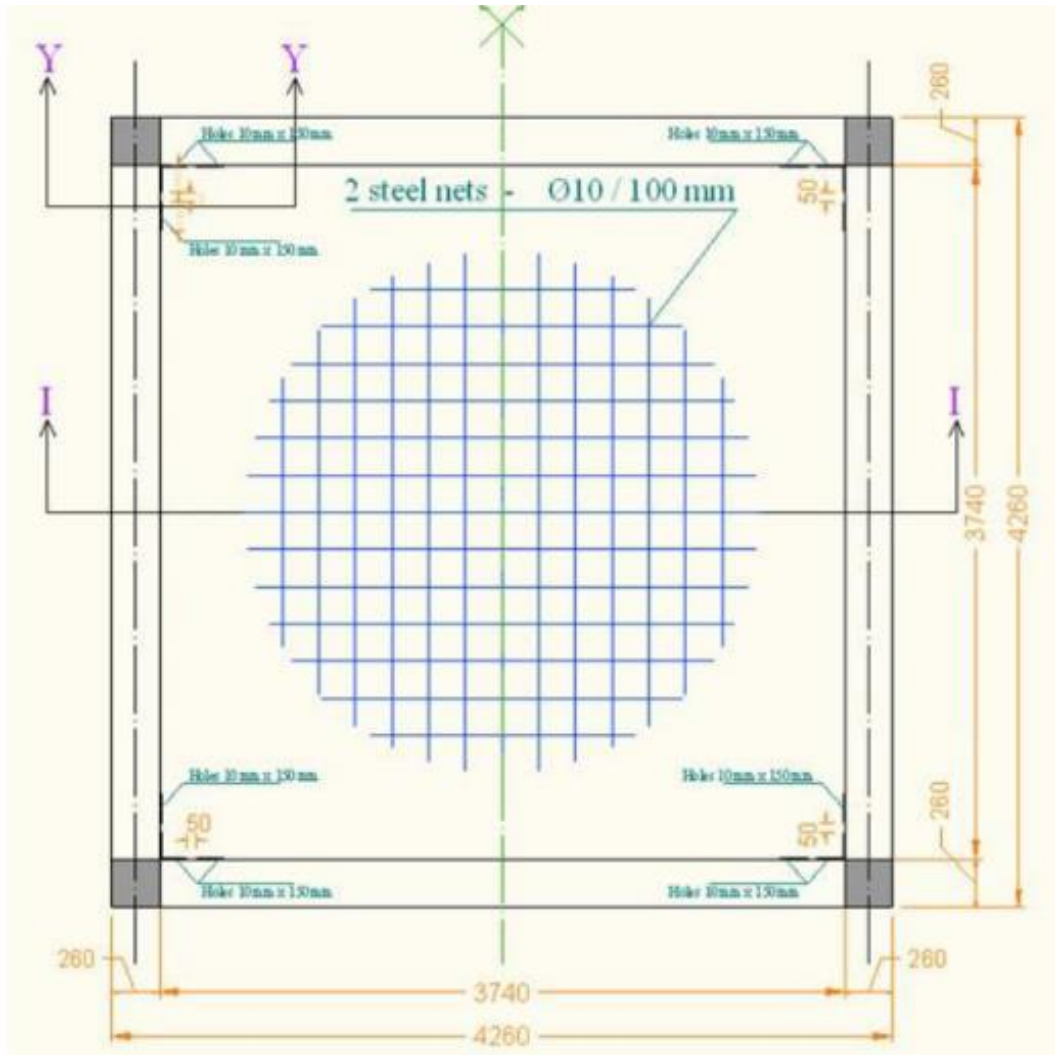


Figure 3.13: Top view of the slabs' reinforcement (Unit: mm), (Garcia et al. 2012)

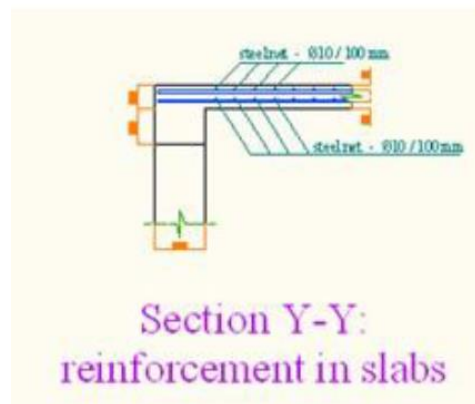


Figure 3.14: Lateral view of slabs' reinforcement (Unit: mm), (Garcia et al. 2012)

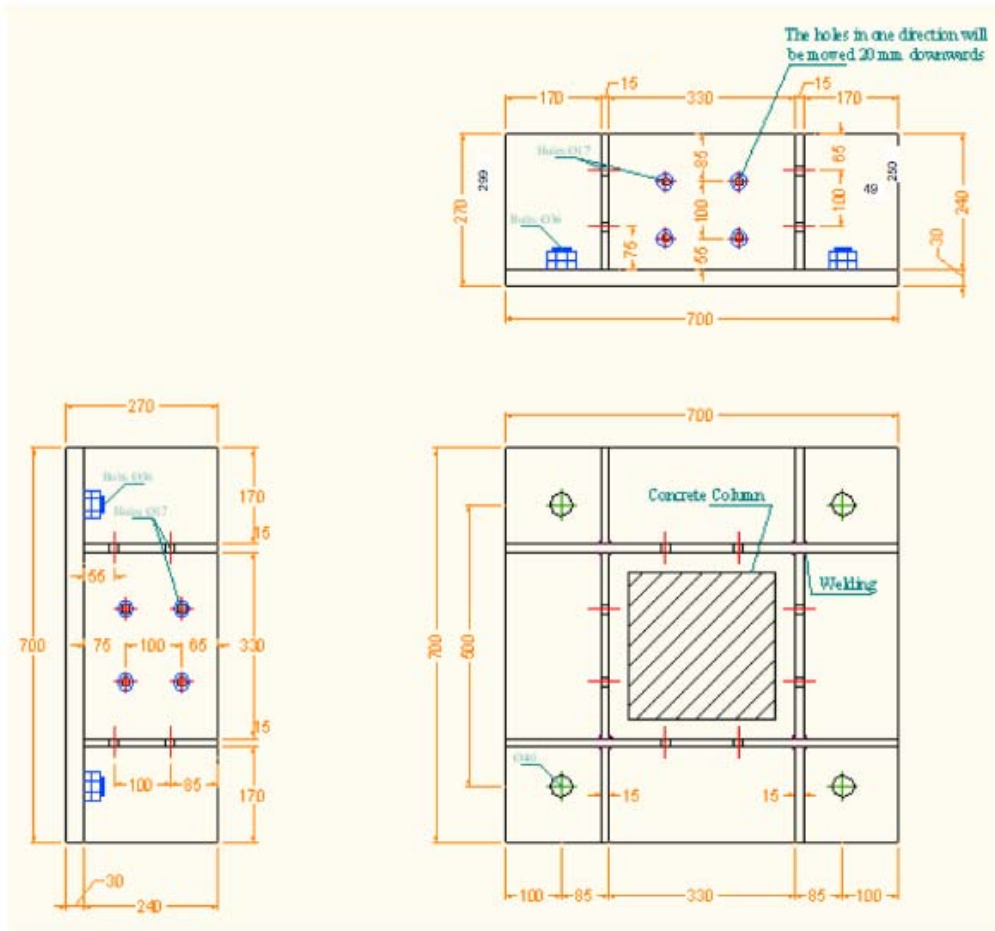


Figure 3.15: BANDIT specimen steel footing (Unit: mm), (Garcia et al. 2012)



Figure 3.16: Specimen foot filled with concrete and ready for the formwork to be bolted (Garcia et al. 2012)



Figure 3.17: Steel specimen foot (Garcia et al. 2012)

### 3.4. Material properties

#### 3.4.1. Steel bars

Deformed B500 steel bars have been used for the reinforcement of the specimen. The mechanical properties were determined in CEBTP laboratory through tensile tests. Three tests have been performed for each diameter. The average values of  $f_y$  (yield strength),  $f_u$  (maximum tensile strength) and  $\varepsilon_{su}$  (conventional elongation after test) are given in table (3-1):

Diameter (mm)	$f_y$ (MPa)	$f_u$ (MPa)	$\varepsilon_{su}$ (%)
6	574	604	18
8	544	572	15
10	513	587	20
14	526	616	19

Table 3-1: Steel bars mechanical properties (Mean values)

#### 3.4.2. Concrete

The specimen was built using two different batches of ready mixed concrete, one for each floor. Concrete of 1<sup>st</sup> floor is more resistant than concrete of 2<sup>nd</sup> floor. BANDIT specimen is representative to old buildings, therefore the concrete chosen was a very low strength concrete (15 MPa).

Several mixes have been designed in order to obtain a low strength concrete suitable for the project. 24 normalized cylinders (diameter 160 mm and height 320 mm) have been cast for each mix in classical cardboard moulds. The concrete was checked by its delivery slip and by the concrete slump test using an Abrams cone. It was then vibrated in the specimens' moulds as well as in the formwork with an electric vibrator. The formwork has been taken off the building three days after cast (for each storey).

A physical examination of the concrete in 1<sup>st</sup> and 2<sup>nd</sup> floor was performed using the core samples extracted before tests. The results of the concrete mix up (content in cement and water) for each cast, compared with the theoretical value, are given in table (3-2).

A test campaign has been realised consisting in a compression tests on normalized cylinders at 14, 21, 28, 40 and 60 days after casting. All the cylinders have been kept at ambient condition in their mould until the date of test.

To provide a complete mechanical characterisation of the concrete, several mechanical tests were performed on cylindrical (diameter 160 mm and height 320 mm) and parallelepipedal (100 · 100 · 500 mm) samples:

- Simple compression tests on cylindrical specimen to determine compressive strength;

- Instrumented compression tests on cylindrical specimen to determine the stress-strain curve and the elastic modulus  $E_c$  (see figure 3.18);
- Four points bending tests to determine the concrete resistance in pure bending condition;
- Splitting or Brazilian tests (transverse compression test) to determine the tension strength.

	<b>Concrete 1<sup>st</sup> floor</b> (measured)	<b>Concrete 2<sup>nd</sup> floor</b> (measured)	<b>Theoretical mix up</b>
<b>Cement content</b> ( $kg/m^3$ )	240±10%	215±10%	180
<b>W/C</b> (water versus cement ratio)	0.80-0.95	0.90-1.05	1.22

**Table 3-2: Evaluation of cement and W/C ratio for concretes of 1<sup>st</sup> and 2<sup>nd</sup> floor for Bandit specimen (Garcia et al. 2012)**

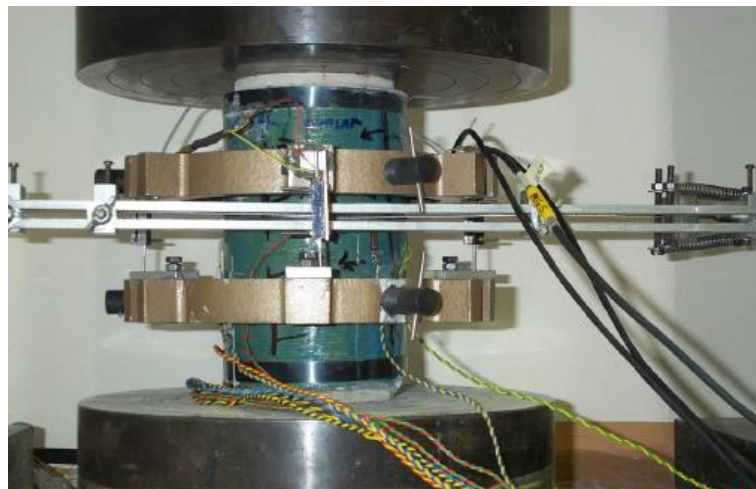


**Figure 3.18: Instrumented compression testing of a concrete cylindrical sample (Garcia et al. 2012)**

Further investigations were performed to provide additional informations on concrete:

- Sclerometer measurements on a concrete surface;
- Mechanical tests on core samples taken from the building, before and after seismic tests;
- Physical analysis of specimen's concrete;

- Ultrasonic Pulse Velocity (UPV) investigation.

In table (3-3) the average values of the compressive and tensile strength for the two cast's concretes are presented:

	Testing step	Age from cast (Days)	Compressive Strength (MPa)	Tensile Strength (MPa)	Elastic Modulus (MPa)
<b>1<sup>st</sup> floor</b>	Standard 28 days after cast	28	24.0		
	Specimens moved on the table	102	30.5		25200
	Before first test sequence (damage X)	120	31.5	2.3	24900
	Before last test sequence (retrofitted Y)	181	29.5	3.0	22800
	After last test sequence (core samples)	250	25.5		19800
<b>2<sup>nd</sup> floor</b>	Standard 28 days after cast	25	19.0		
	Specimens moved on the table	88	23.0		20400
	Before first test sequence (damage X)	106	26.5	2.3	22100
	Before last test sequence (retrofitted Y)	167	24.0	2.3	21200
	After last test sequence (core samples)	250	19.5		18800

Table 3-3: Concrete average mechanical properties (Garcia et al. 2012)

### 3.5. Additional masses

In order to simulate additional permanent and variable loads, one additional masses (13.5 t) was bolted underneath the first floor slab using post-tensioned high strength bolts and another one (11 t) was clamped on the top of the second floor slab. The additional mass for BANDIT specimen was 25 t, consisting in:

- Three steel plates (3 · 3 m, 4.5 t) under the first slab, fixed by four M36 threaded rods passing through the slab;
- One steel plates (3 · 3 m, 4.5 t) and one concrete mass (2 · 2 · 1 m, 6.5 t) fixed on the second slab, on the top of the building. The steel plate is fixed by four M36 threaded bars passing through the slab and the concrete mass is tightly bolted to the steel plate.

### 3.6. AZALEE shaking table

The tests on BANDIT specimen were performed on the six degrees of freedom (as shown in figure 3.20) AZALEE shaking table (EMSI laboratory, TAMARIS facility in CA Saclay, France).

The table is fixed in a pit, situated in the middle of a 2700 tons concrete reaction massif, by eight hydraulic actuators. Its maximum payload is 100 tons. Its square plate is 6 m side. Each horizontal actuator has a maximum force of 1000 kN and the vertical ones a capacity of 1000 kN. Four static pneumatic supports are placed under the table to support and balance the weight of the table and the specimen. The maximum displacement amplitude range is  $\pm 125$  mm for the two horizontal axis and  $\pm 100$  mm for the vertical axis.

The table has been built by welding aluminium plates in a rigid caisson. For tightening the specimens to the plate, 144 M36 threaded steel inserts have been fixed in the aluminium plate with a 500 mm step in both directions. This shaking table is showed in figure (3.19) and (3.20):

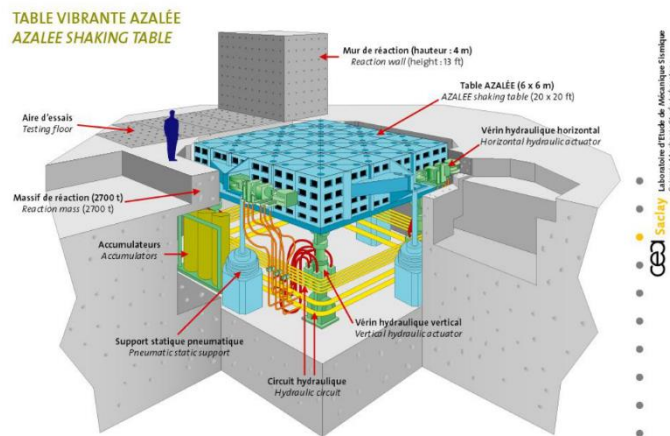


Figure 3.19: AZALEE shaking table (Garcia et al. 2012)

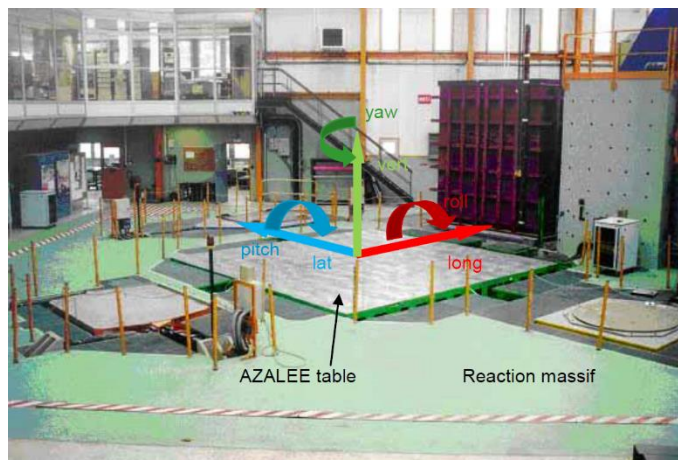


Figure 3.20: AZALEE shaking table's 6 DOF (Garcia et al. 2012)

### 3.7. Specimen instrumentation

The response of the BANDIT structure during excitation was recorded by installing conventional instrumentation, stereovision instrumentation (stereovision sensor and stereo correlation system) and videocameras. The conventional instrumentation is composed of accelerometers, displacement transducers (cable sensors and inductive ones) and strain gages. Displacement transducers are necessary to perform a Dynamic time-history analysis. The initial instrumentation of the specimen is the following one:

- Three accelerometers fixed on AZALEE shaking table;
- Eight accelerometers fixed on the specimen;
- Four displacement transducers measuring the absolute displacement of the specimen;
- Four displacement transducers measuring the absolute displacement of the top of the specimen;
- Four displacement transducers measuring the relative displacement of masses;
- Three displacement transducers measuring the shaking table displacement;
- Eight displacement transducers measuring the relative displacement on Z axis of the specimen;
- 59 gages glued on reinforcement bars of the columns and the beams of the first and second levels.

Figure (3.21) shows the exact location of the instrumentation:

Specimen sensors					
sensor type	frame	measurement point position (height from steel box)	name		drawing detail
accelerometer	B	3150	Ax811	Ax821	B
		6450	Ax812	Ax822	A
	I	3150	Ay1A1	Ay1B1	B
		6450	Ay1A2	Ay1B2	A
displacement sensor (cable)	B	3150	Dx811	Dx821	B
		6450	Dx812	Dx822	A
	I	3150	Dy1A1	Dy1B1	B
		6450	Dy1A2	Dy1B2	A
displacement sensor (cable)	I	0	Dz1A	Dz1B	C
	2	0	Dz2A	Dz2B	
	A	0	DzA1	DzA2	
	B	0	DzB1	DzB2	
displacement sensor			Dxmas1		D
			Dymas1		
			Dxmas2 Dymas2		

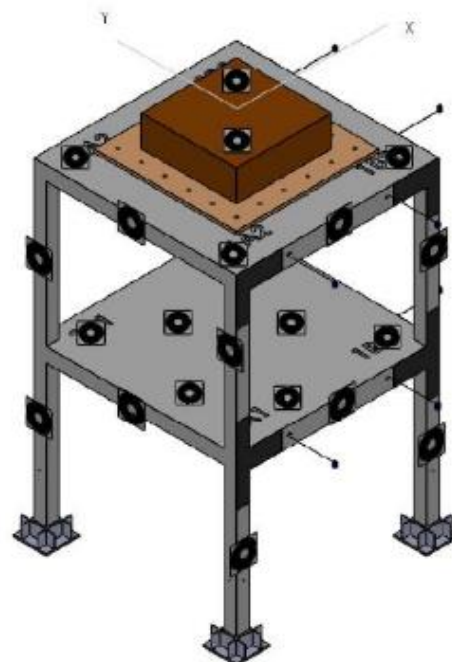


Figure 3.21: Specimen instrumentation (Garcia et al. 2012)



### 3.8. Tests sequence and purpose

AZALEE shaking table provided a series of unidirectional horizontal artificial ground motion based on Eurocode 8 soil type C spectrum as input. The record length was 30s, with a frequency of 0.7-30 Hz. The ground motion record was scale to apply different and increasing (for each test sequence) levels of peak ground acceleration (PGA).

Tests sequence and purposes are listed in the following table:

Direction	Tests sequence	Condition of the test	Purpose
X-direction (Axes 1&2)	1	Specimen without retrofit	Damaging the specimen
	The building is retrofitted with PTMS (frames 1&2)		
	2	Specimen retrofitted with PTMS	Checking the strengthening
Y-direction (Axes A&B)	3	Specimen retrofitted with PTMS	Checking the strengthening
	The building is retrofitted using CFRP and PTMS		
	4	Specimen retrofitted with CFRP + PTMS	Checking the strengthening
Triaxial (X + Y + Z)	5	Specimen retrofitted with PTMS + CFRP	Checking the strengthening

Table 3-4: Tests sequences (Garcia et al. 2012)

Natural frequencies of the structure were obtained using white noise before and after each test, with the purpose of measuring the drop of frequency. For this purpose, a low intensity excitation (maximum PGA= 0.05 g) containing a frequency range of 0.7–50 Hz and with the duration of 50s was used. This signal was computed with the SIGNALSTAR software. The response recorded at each floor was then used to identify the natural frequencies of the relevant vibration modes. All data were monitored for 50s and collected by a data acquisition system at a sampling frequency of 600 Hz.

The criteria to stop a tests sequence were:

- The drop of natural frequencies of the specimen;
- The increase of the interstorey drift ratio (which is the differential displacement between the two slabs divided by the height of the storey), which is an indicator of damages of the joints;
- For high PGA levels, a visual check of the damages of the joints and the elements with the purpose of stopping tests before the collapse of the specimen.

This dissertation will deal with the first and the fourth (with reference to the frame A, strengthened with CFRP) tests sequence.

In particular, the first test sequence was designed in several phases, as shown in the following table:

<b>Test sequence 1 – BARE FRAME</b>			
<b>Direction</b>	<b>Run Number</b>	<b>Type</b>	<b>PGA (g)</b>
X-direction (Axes 1&2)	5	White noise	0.05
Y-direction (Axes A&B)	6	White noise	0.05
X-direction (Axes 1&2)	7	Pretest level adjustment	
X-direction (Axes 1&2)	8	Pretest 0.03g	
X-direction (Axes 1&2)	9	Seism	0.025
X-direction (Axes 1&2)	10	White noise	0.05
X-direction (Axes 1&2)	11	Seism	0.05
X-direction (Axes 1&2)	12	White noise	0.05
X-direction (Axes 1&2)	13	Seism	0.10
X-direction (Axes 1&2)	14	White noise	0.05
X-direction (Axes 1&2)	15	Seism	0.15
X-direction (Axes 1&2)	16	White noise	0.05
X-direction (Axes 1&2)	17	Seism	0.15
X-direction (Axes 1&2)	18	White noise	0.05

Table 3-5: First test sequence (Garcia et al. 2012)

On run 15 at 0.15g, the hydraulic system encountered a high frequency resonance due to oil column and there was a risk that the specimen may have collapsed. Therefore, this test has been repeated with the same consequence.

Before the performing of the fourth test, PTMS strengthening was completely removed and then the building has been retrofitted mixing CFRP and PTMS techniques in this way:

- For the frame A, the CFRP technique;
- For the frame B, the PTMS technique.

The CFRP technique with regard to the BANDIT specimen will be described in the next chapter.

The fourth sequence is composed of these phases, as shown in the table below:

<b>Test sequence 4 – PTMS and CFRP retrofitted FRAME</b>			
<b>Direction</b>	<b>Run Number</b>	<b>Type</b>	<b>PGA (g)</b>
X-direction (Axes 1&2)	56	White noise	0.05
Y-direction (Axes A&B)	57	White noise	0.05
Y-direction (Axes A&B)	58	Pretest level adjustment 0.02g	
Y-direction (Axes A&B)	59	Seism	0.05
Y-direction (Axes A&B)	60	White noise	0.05
Y-direction (Axes A&B)	61	Seism	0.10
Y-direction (Axes A&B)	62	White noise	0.05
Y-direction (Axes A&B)	63	Seism	0.20
Y-direction (Axes A&B)	64	White noise	0.05
Y-direction (Axes A&B)	65	Seism	0.30
Y-direction (Axes A&B)	66	White noise	0.05
Y-direction (Axes A&B)	67	Seism	0.35
Y-direction (Axes A&B)	68	White noise	0.05

Table 3-6: Fourth test sequence (Garcia et al. 2012)

## 4. CFRP STRENGTHENED FRAME

### 4.1. Repairing the damages

Before testing phase 4, the specimen was repaired with a novel “hybrid” strengthening solution with CFRP and PTMS. Columns and joints of frame A were strengthened with externally bonded CFRP sheets, whereas frame B was strengthened with PTMS. The layout and amount of CFRP sheets used to strengthen the building were aimed at improving ductility of columns and beams, and the shear capacity of the joints. With the continuation of the tests, joints started to damage. Before the application of CFRP sheets, the damaged beam-column joints were repaired by:

- Only in X-direction of the second-floor joints, severely damaged by the test, external bars were welded to the bottom beam reinforcement to the column reinforcement to prevent bar pullout. To achieve this, short bar segments 20-30 mm long were inserted between the column and beam longitudinal reinforcement bars. This operation implied to break the concrete to open the junction between the bars, then to weld them and finally to refill the hole. This operation is represented in figure (4.1).
- Damaged and spalled concrete was replaced with high-strength repair mortar, as seen in figure (4.2).
- The main cracked areas were repaired with the injection of epoxy resin, as shown in figure (4.3).

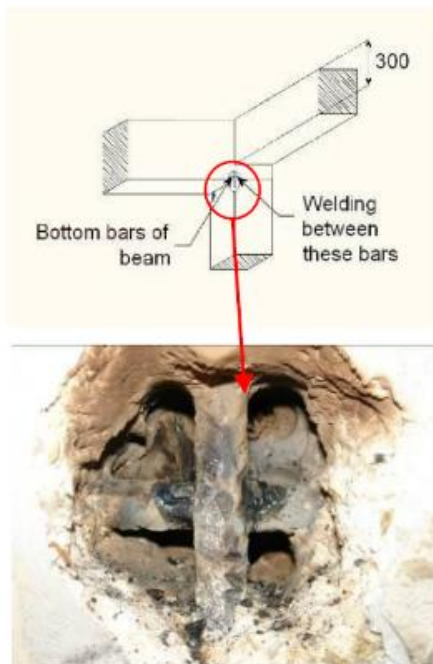


Figure 4.1: Welding of bars in second level nodes (Garcia et al. 2012)



Figure 4.2: Mortar repair at second floor joint and injection ports for crack injection (Garcia et al. 2012)



Figure 4.3: Epoxy resin injection in a damaged joint (Garcia et al. 2012)

#### 4.2. Carbon fabric for CFRP

The carbon fibres used for the strengthening are high strength fibres. Dry fibres characteristics are described in table (4-1). The complete system used for CFRP system is called TFC (Tissu Fibre Carbone) comprising woven carbon fibres (70% fibres in warp direction and 30% in weft direction), particular resins plus hardener. Mechanical characteristics of the composite (referred to one sheet) are shown in table (4-2):

Diameter	Number of fibres in a tuft	Ultimate tensile strength	Elastic modulus	Elongation to break
$\mu m$		MPa	GPa	%
8	12000	4900	230	2.1

Table 4-1: Geometric and mechanical characteristics of dry carbon fibres for CFRP (Garcia et al. 2012)

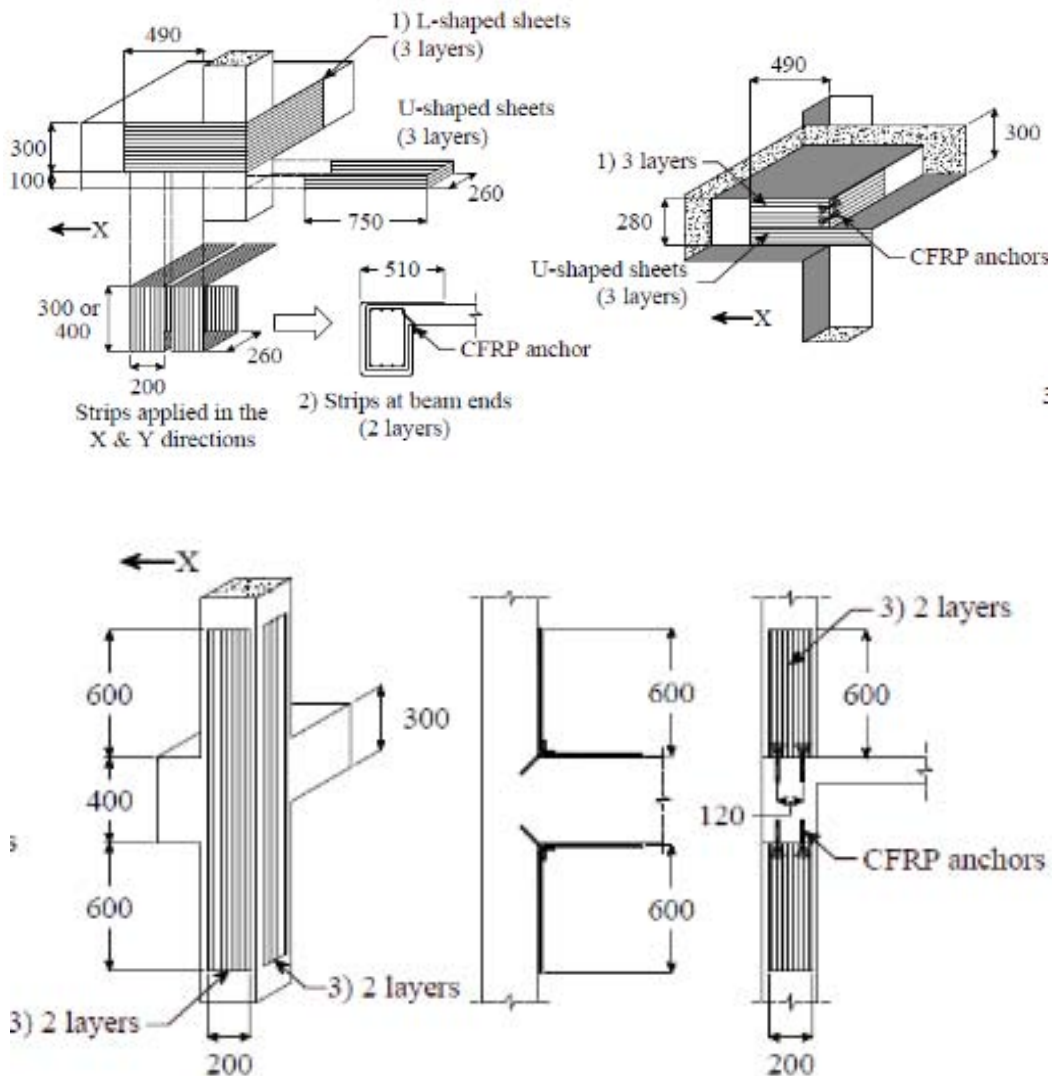
Average thickness	Ultimate tensile strength	Elastic modulus	Ultimate tensile load (warp direction / 10 mm wide)	Ultimate tensile load (weft direction / 10 mm wide)
$mm$	MPa	GPa	kN	kN
0.48	1350	105	8.15	3.50

Table 4-2: Geometric and mechanical characteristics of TFC composite for CFRP (Garcia et al. 2012)

### 4.3. CFRP reinforcement on BANDIT frame

The application of CFRP sheets on the surface of joints, columns and beams, required a prior preparation of the surface and continue with subsequent stages. First of all it was necessary to prepare the surface by grinding the concrete. Secondly, there was the application of the bi components resin on the surface. Then the first sheet of TFC was applied in one direction. Thereafter, it had to alternate glue and carbon layer in directions according to the drawings. Finally, it was necessary to put resin again on all applied sheets.

The CFRP drawings are in the following figure (4.4) and the results are in figures (4.5) and (4.6):



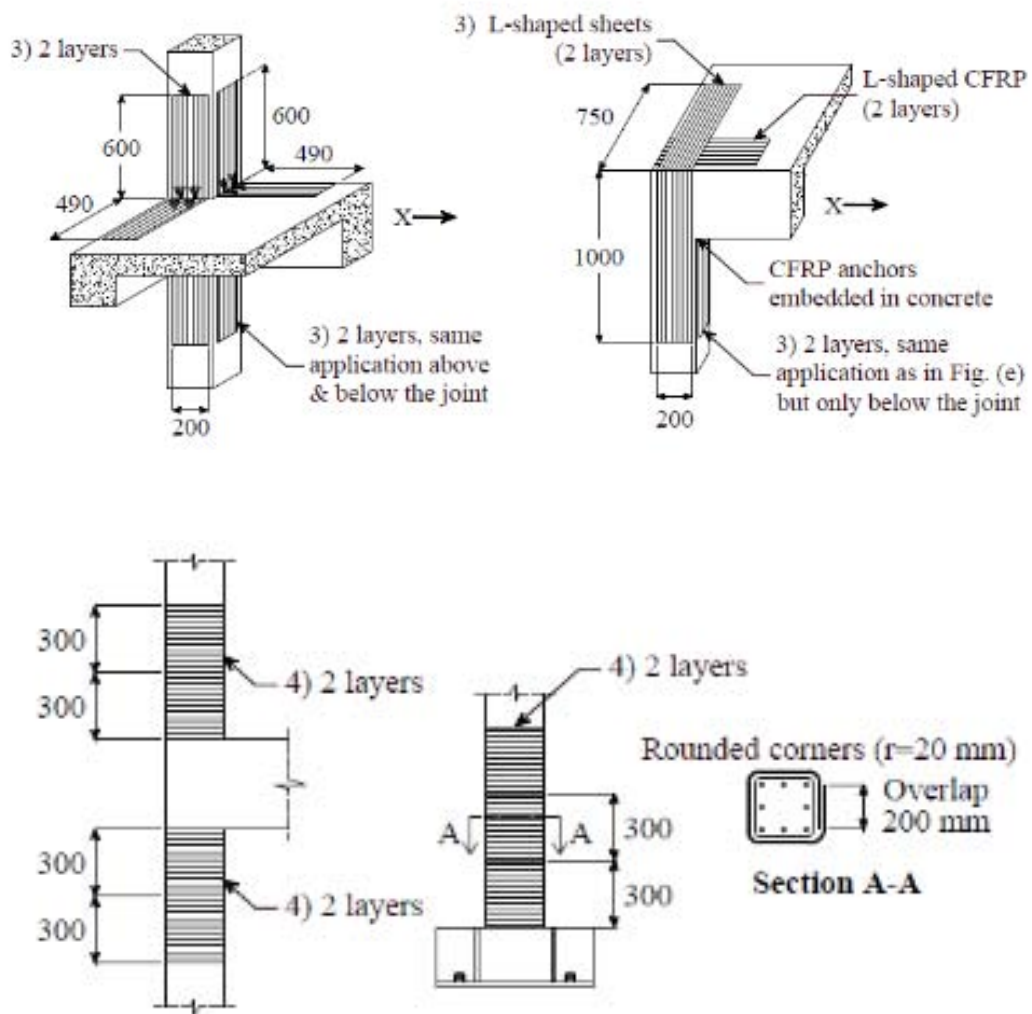


Figure 4.4: CFRP strengthening used at beam-column joints of frame A (Garcia et al. 2012)



Figure 4.5: CFRP strengthening in 1<sup>st</sup> floor (Garcia et al. 2012)



Figure 4.6: CFRP strengthening in 2<sup>nd</sup> floor (Garcia et al. 2012)

#### 4.4. Analysis of sections

In order to understand the real benefit of the intervention, the calculation of the members should be considered before and after strengthening. In this paragraph, a 1<sup>st</sup> floor beam (300 · 260) is analysed before and after the intervention. Theory of plasticity and equilibrium are used to evaluate ultimate capacity of the section under external bending moment. No load safety factors are applied, in order to evaluate the effective resistance of the sections. The evaluation is based on a cracked section because normally the service moment is larger than the cracking moment. Stress-block is the concrete model used for the analysis in the ultimate conditions.

##### 4.4.1. First storey section beam (300 · 260) before strengthening

With reference to the section shown in figure (4.7), from the equilibrium between compression and tension zone in ultimate conditions, the neutral axis depth  $x_0$  can be found. The ultimate conditions are achieved when the extreme compression fibers of concrete reach the ultimate strain  $\epsilon_{cu}$  and the longitudinal reinforcement  $A_{s2}$  is yielded:

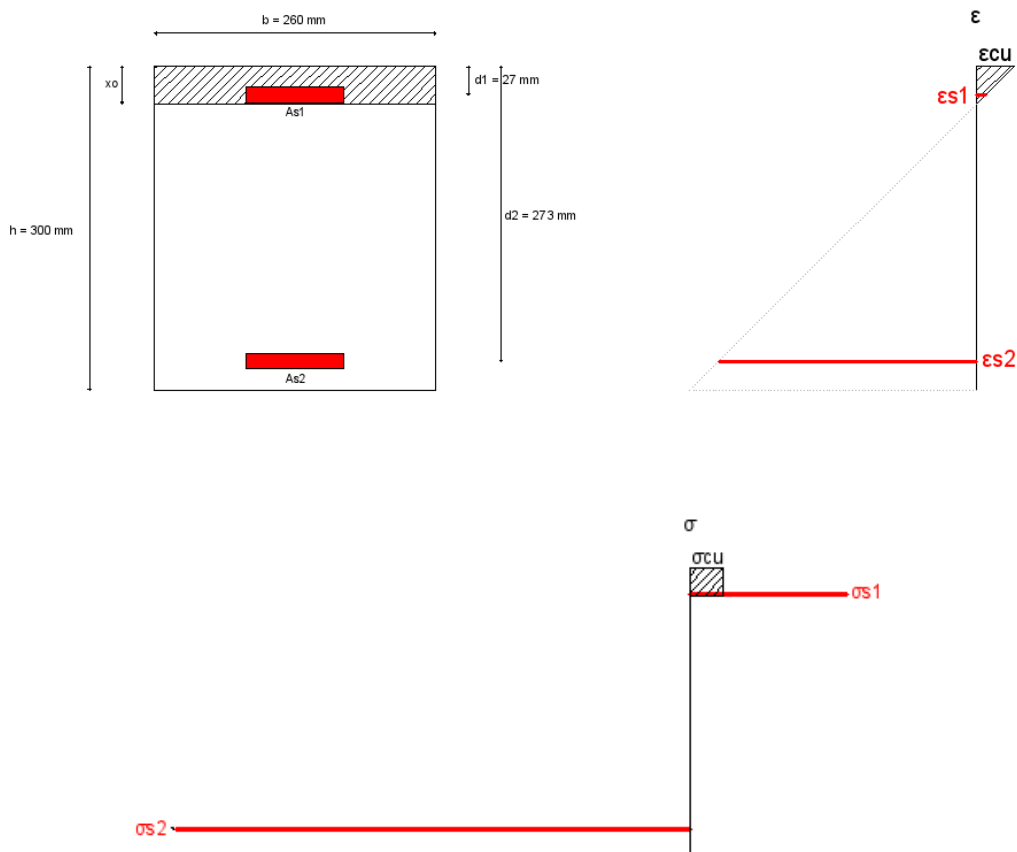


Figure 4.7: 1<sup>st</sup> floor beam (300) section before strengthening



From forces in compression zone = forces in tension zone, the neutral axis depth  $x_0$  is calculated:

$$0.8 \cdot b \cdot x_0 \cdot f_{cm} + A_{s1} \cdot \sigma_{s1}(\varepsilon_{s1}) = A_{s2} \cdot \sigma_{s2}(\varepsilon_{s2})$$

$\varepsilon_{s1}$  and  $\varepsilon_{s2}$  can be calculated using similar triangles:

$$\varepsilon_{s1} = \frac{(x_0 - d_1)}{x_0} \cdot \varepsilon_{cu} \quad ; \quad \varepsilon_{s2} = \frac{(d_2 - x_0)}{x_0} \cdot \varepsilon_{cu}$$

$\sigma_{s1}$  and  $\sigma_{s2}$  are calculated using constitutive model for steel:

$$\sigma_{s1} = E_s \cdot \varepsilon_{s1} = E_s \cdot \frac{(x_0 - d_1)}{x_0} \cdot \varepsilon_{cu}$$

$$\sigma_{s2} = f_y + E_h \cdot \varepsilon_{s2} = f_y + E_h \cdot \frac{(d_2 - x_0)}{x_0} \cdot \varepsilon_{cu}$$

Where  $f_y = 526 \text{ MPa}$  is the value of yield strength of steel,  $E_h = 480.26 \text{ MPa}$  is steel hardening modulus,  $E_s = 202308 \text{ MPa}$  is steel elastic modulus,  $\varepsilon_{cu} = 0.0035$  is the maximum strain for concrete and  $f_{cm} = 31.522 \text{ MPa}$  is the maximum compressive stress for concrete.

With the appropriate substitutions, the neutral axis depth is  $x_0 = 35.11 \text{ mm}$ .

The design bending moment capacity comes from the rotational equilibrium and it is  $M_u = 82.05 \text{ KNm}$ .

#### 4.4.2. First storey section beam (300 · 260) after strengthening

In connection with the figure (4.8), the neutral axis depth  $x_0$  is calculated through equilibrium between compression and tension zone in ultimate conditions. The failure modes of a reinforced concrete element strengthened with externally bonded FRP reinforcement may be divided into two classes: a) those where full composite action of concrete and FRP is maintained until the concrete reaches crushing in compression or the FRP fails in tension (such failure modes may also be characterized as “classical”) and b) those where composite action is lost prior to class a) failure, e.g. due to peeling-off of the FRP. In this case, during the tests there have been no bond-slip between concrete and CFRP sheets wrapped around RC elements. Therefore, the ultimate condition of the beam is reached when the longitudinal CFRP sheets fail in tension. The steel reinforcement  $A_{s1}$  is not yielded whereas the longitudinal bars  $A_{s2}$  are yielded. Concrete in compression is not crushed.

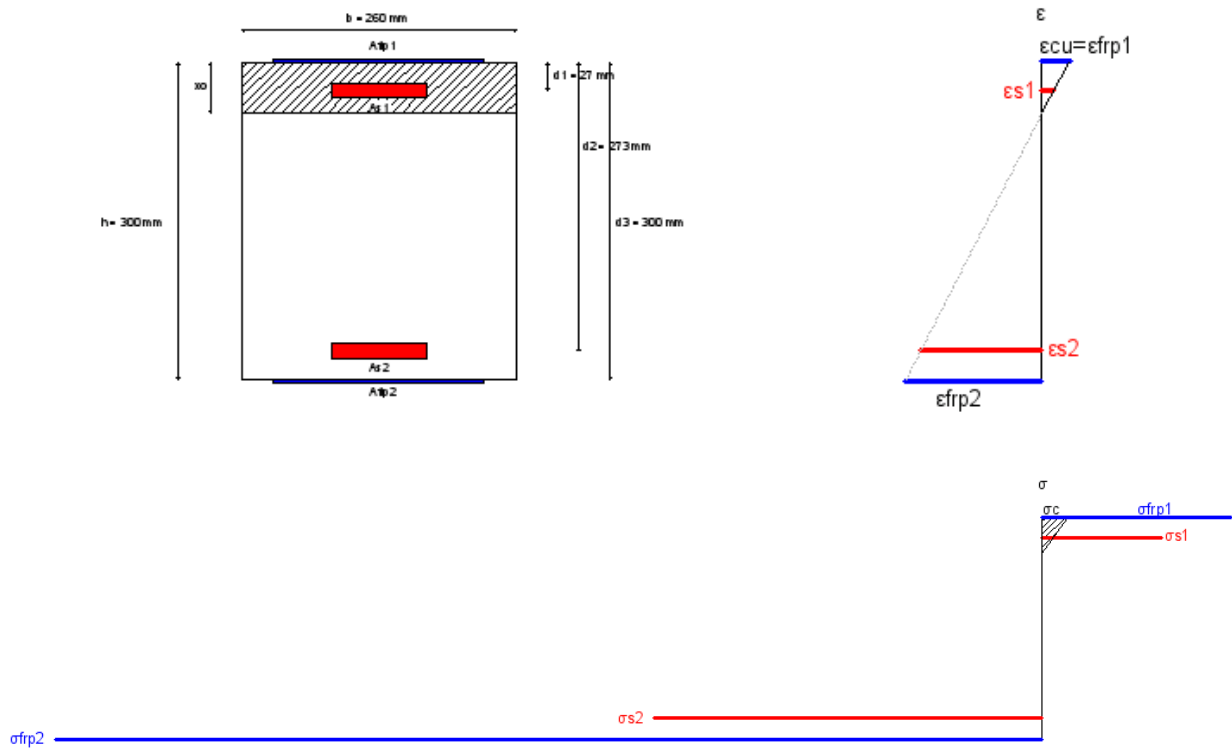


Figure 4.8: 1<sup>st</sup> floor beam (300) section after strengthening

Even in this case forces in compression zone = forces in tension zone, therefore:

$$A_{frp1} \cdot \sigma_{frp1}(\varepsilon_{frp1}) + \frac{b \cdot x_0 \cdot \sigma_{cs}(\varepsilon_{cs})}{2} + A_{s1} \cdot \sigma_{s1}(\varepsilon_{s1}) = A_{s2} \cdot \sigma_{s2}(\varepsilon_{s2}) + A_{frp2} \cdot \sigma_{frp2}$$

$\varepsilon_{frp1}$ ,  $\varepsilon_{cs}$ ,  $\varepsilon_{s1}$ , and  $\varepsilon_{s2}$  are calculated using similar triangles:

$$\varepsilon_{frp1} = \varepsilon_{cs} = \frac{x_0}{d_3 - x_0} \cdot \varepsilon_{frpu} ; \varepsilon_{s1} = \frac{x_0 - d_1}{d_3 - x_0} \cdot \varepsilon_{frpu} ; \varepsilon_{s2} = \frac{x_0 - d_2}{d_3 - x_0} \cdot \varepsilon_{frpu}$$

$\sigma_{frp1}$ ,  $\sigma_{cs}$ ,  $\sigma_{s1}$ ,  $\sigma_{s2}$  are calculated through the constitutive models of the materials. In this case the properties of the concrete are those of the CFRP confined concrete described in the previous paragraphs.

With the appropriate substitutions, the neutral axis depth is  $x_0 = 48.09 \text{ mm}$ .

Here too the design bending moment capacity comes from the rotational equilibrium and it is  $M_u = 144.37 \text{ KNm}$ .

## 5. DRAIN-3DX

---

### 5.1. Introduction

In order to investigate the seismic behaviour of BANDIT specimen, it is necessary to model the frame through a finite element programme. Both bare frame and CFRP retrofitted frame are analysed with DRAIN-3DX software programme and the analytical results are compared with the experimental results, in order to understand the damage mechanism of the specimen here in particular, but more commonly of sub-standard buildings.

As part of this dissertation, a non-linear dynamic (time-history) analysis is performed on the structure. Furthermore, some parametric studies are conducted to examine the effects of those parameters on the response of the structure. One of the most important parameters proves to be the pullout properties of the longitudinal rebars and the gap properties of the concrete. Relevant analytical parameters are compared with the experimental ones, in order to obtain an experimental validation of the theoretical proofs.

### 5.2. DRAIN-3DX software

DRAIN-3DX is a finite element programme capable of performing static and dynamic analysis, both linear and non-linear. The only drawback of this programme is its lack of graphic interface and it is not user friendly. In order to obtain simple and successful results, the output files have been processed with Microsoft Excel. In DRAIN-3DX, the structure is modelled as a 3D assemblage of nonlinear elements connected at nodes. Nodes do not need to be numbered sequentially and they are identified by numbers, the Cartesian coordinates.

Unless specified otherwise, each node has six degrees of freedom (X, Y, Z translations and X, Y, Z rotations). In this case, thanks to the plane symmetry of the building, not the whole structure is modelled, but only a 2D frame. Therefore, each node has three degrees of freedom (X, Y, translations and Z rotation).

The elements must be divided into groups and all elements in a group must be of the same type. The programme has a library of element types to model the elements and joints and to consider the elastic and plastic properties of materials.

Here, the frame is modelled with distributed plasticity approach using *fiber element type 15*. The element type in question will be described later in the chapter. In DRAIN-3DX it is possible to consider  $P - \Delta$  effects and they have been considered in this analysis.

$P - \Delta$  effects can be taken into account by adding a geometric stiffness matrix to the stiffness matrix for each element, and accounting for  $P - \Delta$  effects in the resisting force computation. The geometry stiffness is changed at each event in a static analysis, whereas it can also be kept constant for dynamic analysis.

In this programme, it is also possible to perform energy calculation, for both static and dynamic analyses. The calculation accounts for external work on the nodes, static elastic-plastic work on the elements, kinetic energy, and viscous damping work. If there is a significant energy unbalance, the analysis results are likely to be inaccurate. In this case no energy calculation is performed.

### **5.3. Time-history (dynamic) analysis**

The dynamic non-linear (time-history) analysis is the most accurate seismic analysis. According with Eurocode 8, a time domain response of the structure can be obtained by direct numerical integration of the equation of motion, using accelerograms to represent the ground motions. In the time-history analysis, the response of the structure is calculated at each time step, using the final condition of the previous step as an initial condition of the next step.

This type of analysis allows to know the distribution of plastic hinges through the structure and the failure mechanism. In a dynamic analysis, the time step may be specified to be constant or variable. In this analysis, a constant time step, equal to 0.001667 s, is considered. The program computes an error measure in each step. If this measure exceeds the upper tolerance in any step, the time step is reduced and the step is repeated. If the measure is less than the lower tolerance for some specified number of steps, the time step is increased in the following step.

According with the norm, the seismic motion may be represented in terms of ground acceleration Time-Histories and related quantities (velocity and displacement). In this experiment, accelerograms in terms of ground displacement are used.

The structural element models should be supplemented with rules describing the element behaviour under post-elastic unloading-reloading cycles. These rules should realistically reflect the energy dissipation in the element over the range of displacement amplitudes expected in the seismic design situation.

Eurocode 8 requires to use as a minimum, a bilinear force-deformation relationship for the element level. In reinforced concrete buildings, the elastic stiffness of a bilinear force-deformation relation should correspond to that of cracked sections. In this case, geometric and material nonlinearities are taken into account.

Geometric nonlinearity is mainly caused by large deformation. This source of nonlinearity is numerically given by the change of the stiffness (which is a function of both material and geometry) during the simulation.

Material nonlinearity is caused by nonlinear relationship between stress and strain for the material used. During the analysis procedure, contrary to the design phase, real nonlinear stress-strain relationships for concrete have to be used.

### **5.4. Fiber element type 15**

In order to represent the material nonlinearity, in particular the nonlinear behaviour of concrete, there is the question of how to consider the region which yield and the region which remain elastic in the structural components during the dynamic analysis.

The most common and simple approach is the lumped plasticity model, which consider the yielding of the element (inelastic behaviour) to be localized in the zero length region in the elements' ends, known as plastic hinges. Here, the energy is dissipated. The problems of this model are the need to experimental calibration of the constitutive moment-rotation models, the problem of finding constitutive parameters and the fact that lumped plasticity at element ends is just an approximation of the true plastic hinge zone, which may distribute both in the member and in the joint.

A more advanced modelling approach, called distributed plasticity model, assumes the plastic hinges to form in the members' ends but allows some parts of the length of the element to go into inelastic deformation. (Kyriakides, 2007)

For this reason and others explained later, as well as the good result in comparison to other types of element, the fiber beam-column element of distributed plasticity type 15 has been used for modelling the frame.

Figure (5.1) shows the element model type 15. The element can be used to model both steel and reinforced concrete beams and columns. It can be used to model a single cross section of a beam or column, a single beam or column member, or beams and columns in a larger structure. The location of each fiber depends on a local axis system defined at the beginning of the analysis. The cross-section characteristics are defined by assembling these fibers based on their coordinates and sectional area. The deformable part of the element is divided into a number of segments. The behaviour is monitored as the center cross section in each segment. The cross section properties are assumed to be constant within each segment, but can vary from segment to segment. Naturally, it is also possible to define elastic cross section types. It is possible to include  $P - \Delta$  effects, as has already been said.

The element is based on many simplifying assumptions, and it focus on some important aspects of beam-column behaviour. The main assumption, limitations and characteristics are the followings: (Powell and Campbell, 1994)

- Plane sections are assumed to remain plane.
- Shear deformations can be included, but the shear behaviour is assumed to be elastic, based on a specific shear modulus and effective shear area.
- The behaviour in torsion is assumed to be elastic, based on a specified shear modulus and effective torsional area.
- It is not possible to consider prestressed concrete members.
- The model assumes constant slice properties over each segment, based on the properties of the monitored slice at the segment center. The computed behaviour of the element can be sensitive to the number of segments that are specified, and to the segment length. In finite element terms this is a "low order" element. A higher order element has been considered, with linear property variation over each segment, based on monitored slices at the segment end. The lower order element was chosen mainly because it has more stable behaviour if negative material moduli are specified.
- There is no provision for element loads (loads can be applied only at nodes).
- Rigid end zones can be defined at element ends, both fiber sections and elastic sections. These connections keep rigid the rotation among the components, so they have the relative rotation equal to zero.

- Connection hinges can be specified at any location in the element, to model deformation that occur in beam-to-column or column-to-footing connections. Plastic deformations are distributed along the element length and through the element cross section.
- For reinforced concrete members, reinforcement bond-slippage (called pullout properties) and concrete crack opening (called gap properties) can be considered at connection hinge fibers. For steel members the fiber properties can be chosen to model the deformations of framing angles.
- Concrete strength degradation and reinforcing bar strength degradation are considered.

In DRAIN-3DX, the structure mass is lumped at nodes, and the mass matrix is diagonal. A viscous damping matrix ( $C = \sum \alpha \cdot M + \sum \beta \cdot K_{\beta}$ ) that is proportional to the element stiffness ( $\beta \cdot K_{\beta}$ ) and nodal masses ( $\alpha \cdot M$ ) can be specified. In effect, mass dependent damping introduces translational and/or rotational dampers at each node, with damping coefficients ( $\alpha \cdot M$ ). Different values of  $\alpha$  can be specified for each node if desired. Different values of  $\beta$  can be specified for each element group. The damper stiffness  $K_{\beta}$  remains constant for any element.

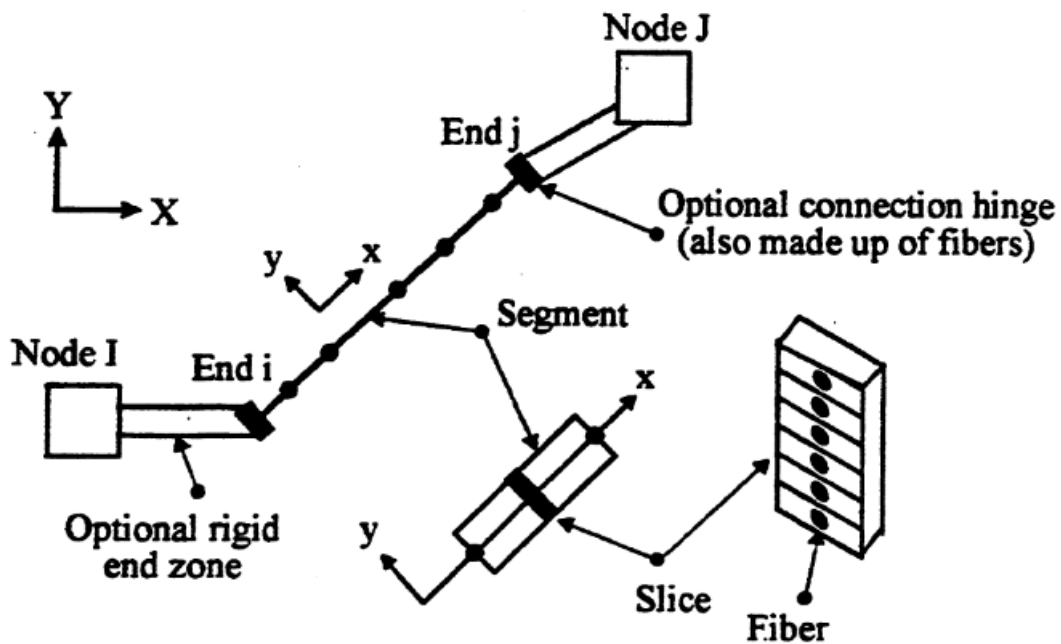


Figure 5.1: Element Type 15 Model (Powell and Campbell, 1994)

## 5.5. Material properties

The material library includes both concrete and steel models. In Elastic Cross Sections Types, the materials are defined through Young's modulus, Shear modulus, etc.

In Fiber Cross Section Types, real stress-strain relationship can be defined for concrete and steel for each segment.

Nonlinear material stress-strain relationships are approximated with a series of straight lines. The material models account for the yield of the steel including strain hardening, for cracking and crushing of concrete including post-crushing strength loss, and for tension stiffening of concrete.

Concrete behaviour for compression can be performed with a maximum of five stress-strain points. Here it is also possible to define an unloading factor, which is an index that represent the response of concrete under different hysteresis loops. Concrete behaviour for tension can be performed with a maximum of two stress-strain points. Steel behaviour can be represent with a maximum of five stress-strain points for compression and tension.

Figures (5.2) and (5.3) show the material models of element type 15 for both concrete and steel.

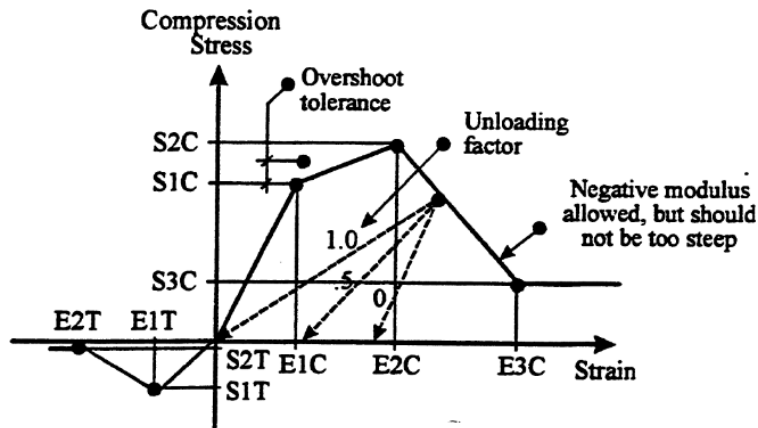


Figure 5.2: Concrete material properties (Powell and Campbell, 1994)

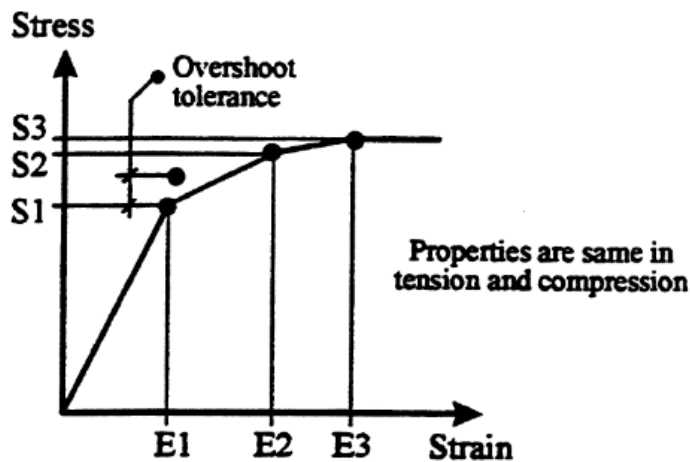


Figure 5.3: Steel material properties (Powell and Campbell, 1994)

## 5.6. Connection hinge fibers properties

For concrete members, the fiber properties can be chosen to model effects such as bond-slip within the connection (Pullout properties) and crack opening (Gap properties) at the connection face. Therefore, pullout and gap fibers replace steel and concrete at member ends.

### 5.6.1. Pullout properties for connection hinge fibers and degradation parameters

According to Powell and Campbell (1994), pullout fibers can be used to model slip movement of the reinforcement bars in the connection region. The bar pullout hysteretic behaviour model included in DRAIN-3DX is represented with a monotonic stress-displacement envelope both in compression and in tension, as shown in figure (5.4). The monotonic stress-displacement envelope consists of trilinear tensile and compressive portions representing the relationship between slip in bar reinforcement with increased bar stress. This is a normal stress  $\sigma$ , not a shear stress  $\tau$ . The stiffness of the trilinear portion is the same in both tension and compression, while the strength may vary. It is necessary to define the following parameters:

- Modulus  $K1$  ( $K1 > 0$ );
- Modulus  $K2$  ( $K1 > K2 > K3$ );
- Modulus  $K3$  ( $K3 < K2$ );
- Yield stress  $S1T > 0$  in tension;
- Yield stress  $S2T > 0$  in tension;
- Yield stress  $S1C > 0$  in compression;
- Yield stress  $S2C > 0$  in compression.

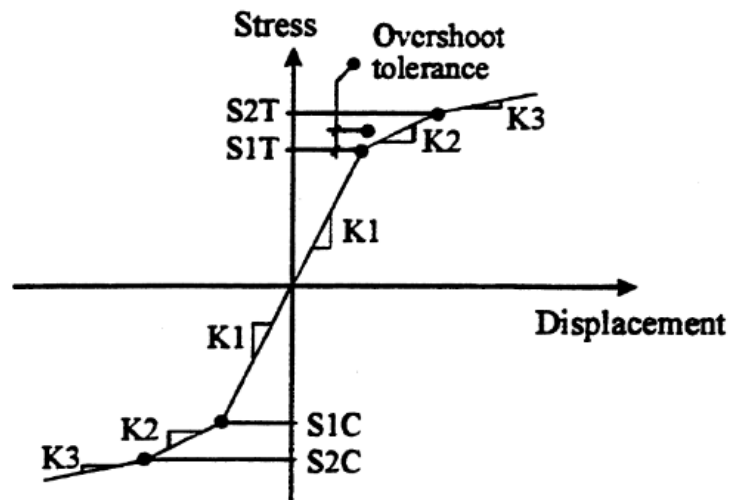


Figure 5.4: Pullout fiber basic properties (Powell and Campbell, 1994)



In order to define the complete hysteretic behaviour of the fiber, furthermore, it is possible to define the degradation parameters accounting for the effects of repeated loading and unloading cycles. These parameters are capable of capturing degradation in strength, stiffness and pinching behaviour in the unloading branch of each cycle.

Figures (5.5a), (5.5b), (5.5c), (5.5d) illustrate pullout fiber degradation properties.

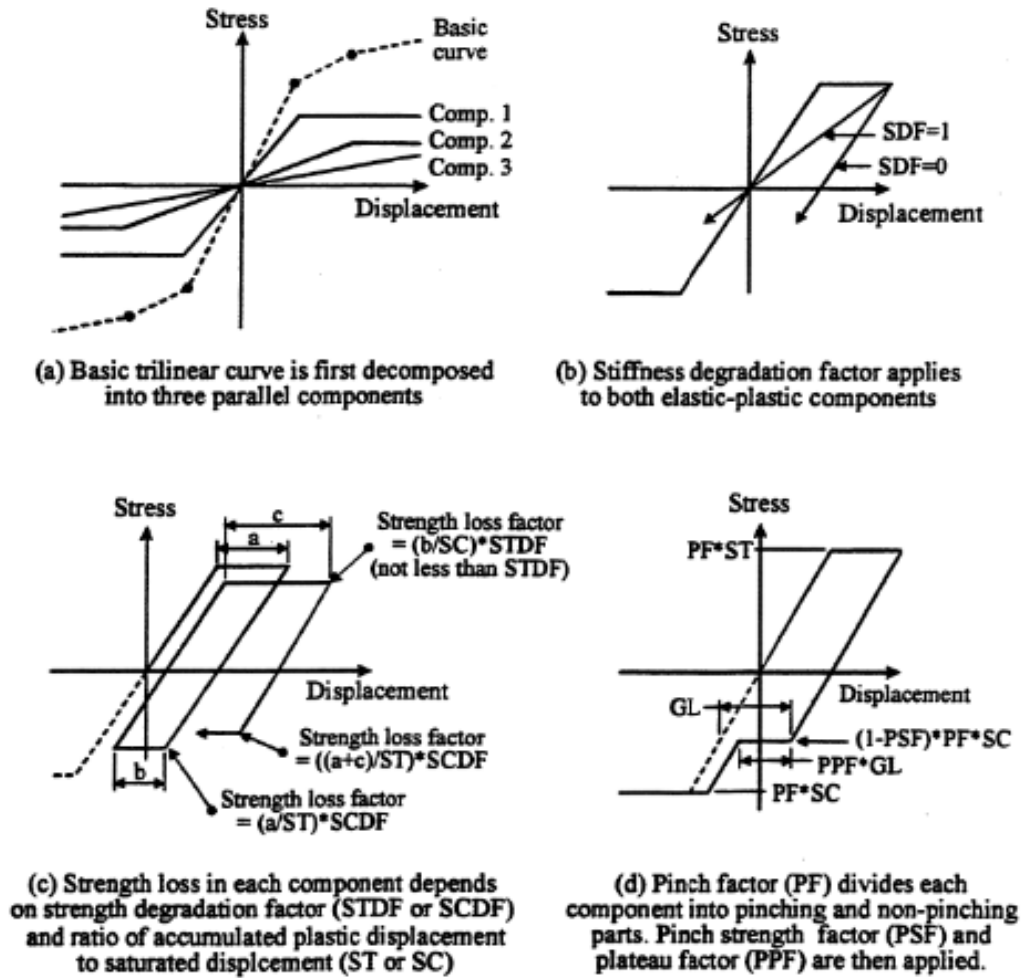


Figure 5.5: Pullout fiber degradation properties (Powell and Campbell, 1994)

The process for applying degradation starts with the decomposition of the trilinear curve (Figure 5.4) into three components, two bilinear (elastic-plastic) curves and one elastic curve acting in parallel as shown in figure (5.5a).

Stiffness degradation factor (SDF) is the parameter that controls the unloading/reloading stiffness of the elastic-plastic curves, as shown in figure (5.5b). SDF can take a value between and one. A value of zero for SDF means that there is no degradation of stiffness (unload at initial stiffness). A value of one for SDF means that the curve unload along a line passing through the point where the curve last crossed the zero stress axis, as shown in figure (5.5b). Values between zero and

one cause a linear interpolation of the stiffness between the two extremes. Strength loss in each component depends on the strength degradation factor in tension or compression (STDF or SCDF) and the ratio of accumulated plastic displacement to saturated displacement (ST or SC), as shown in figure (5.5c). Strength degradation can have a value between zero which means no loss of strength, and one, which accounts for strength degradation. Thus, degradation rate is controlled only with the ST and SC values, which correspond to bar slip in tension and compression at full debonding conditions. Pinching behaviour is controlled by three parameters, as shown in figure (5.5d).

The first is the pinch factor (PF) which divides each component into a pinching and non-pinching part and it can have a value between zero and one. The other two parameters are the pinch strength factor (PSF) and the pinch plateau factor (PPF). PSF controls the strength at which pinching occurs, whereas, after pinching begins, PPF determines the length of the plateau. A value of one indicates that the plateau extends until it meets the last unloading curve. (Kyriakides, 2007)

It is necessary to define the following parameters so as to perform degradation of pullout properties:

- Stiffness Degradation Factor ( $0 \leq SDF \leq 1$ );
- Tension Strength Degradation Factor ( $0 \leq STDF \leq 1$ );
- Compression Strength Degradation Factor ( $0 \leq SCDF \leq 1$ );
- Saturated strain in Compression ( $SC > 0$ );
- Saturated strain in Tension ( $ST > 0$ );
- Pinch Factor ( $0 \leq PF \leq 1$ );
- Pinch Strength Factor ( $0 \leq PSF \leq 1$ );
- Pinch Plateau Factor ( $0 \leq PPF \leq 1$ );

### 5.6.2. Gap properties for connection hinge fibers

Gap fibers can be used to simulate crack opening at the joint interface, which cause additional deformation of the joints. In figure (5.6), gap properties in DRAIN-3DX are presented.

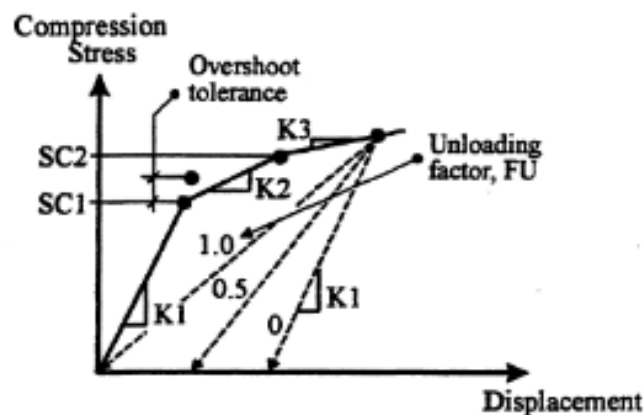


Figure 5.6: Gap fiber properties (Powell and Campbell, 1994)

The gap fiber hysteretic behaviour is represented with a monotonic stress-displacement envelope in compression. It is necessary to define the following parameters:

- Crushing stress  $SC1 > 0$ ;
- Crushing stress  $SC2 > SC1$ ;
- Modulus  $K1 (K1 > 0)$ ;
- Modulus  $K2 (K1 > K2 > K3)$ ;
- Modulus  $K3 (K3 < K2)$ .

As in the previous case, it is necessary to define the Unloading Factor ( $0 \leq UF \leq 1$ ), which represent the behaviour of concrete under hysteretic cycles.

## 6. ANALYTICAL INVESTIGATION

---

### 6.1. Introduction

In this chapter, analytical investigation of both bare frame and CFRP reinforced frame will be presented. So as to understand how the structures behave under seismic loads, it is necessary to model the frames, representing correctly the characteristics of beams, columns and joints. First, analytical results of the bare frame will be compared with the experimental results per every PGA. Secondly, the same thing will be done for the CFRP reinforced frame.

### 6.2. Frame mass

With regard to the geometry description of the bare frame (§ 3.3), the mass of each element of the specimen is as follows:

- Column:  $M_{column} = (0.26 \text{ m} \cdot 0.26 \text{ m} \cdot 3.3 \text{ m}) \cdot \left(24 \frac{\text{kN}}{\text{m}^3}\right) / g = 0.55 \text{ t}$
- Beam (400):  $M_{beam400} = (0.4 \text{ m} \cdot 0.26 \text{ m} \cdot 3.74 \text{ m}) \cdot \left(24 \frac{\text{kN}}{\text{m}^3}\right) / g = 0.95 \text{ t}$
- Beam (300):  $M_{beam300} = (0.3 \text{ m} \cdot 0.26 \text{ m} \cdot 3.74 \text{ m}) \cdot \left(24 \frac{\text{kN}}{\text{m}^3}\right) / g = 0.71 \text{ t}$
- Slab:  $M_{slab} = (4 \text{ m} \cdot 4 \text{ m} \cdot 0.12 \text{ m}) \cdot \left(24 \frac{\text{kN}}{\text{m}^3}\right) / g = 4.70 \text{ t}$
- Additional mass 1<sup>st</sup> floor:  $M_{add1} = 13.5 \text{ t}$
- Additional mass 2<sup>nd</sup> floor:  $M_{add2} = 11.0 \text{ t}$

The structure is modelled as a 2D frame, therefore only half of the mass is calculated and assigned to the frame. The mass of the structure is modelled as lumped mass at nodes.

The mass of the frame is divided among four nodes, two at each corner in the 1<sup>st</sup> floor (nodes 2010 and 2020) and two at each corner in the 2<sup>nd</sup> floor (nodes 3010 and 3020), as shown in figure (6.1). The criterion in which the mass is assigned at each node is based on the area of influence of the elements. The mass of each level was calculated by adding the self weight of half of the slab, two beams and the half storey height of the columns above and below for the first level. For the second level only the self weight of the half storey height of the columns below was added. Additionally, half of the mass of the relative additional mass was added at each level. Bare frame and CFRP retrofitted frame can be considered to have the same

weight, because the weight of CFRP reinforcement is very low compared to the weight of the structure.

The calculated mass for each floor is summarised below:

- $m_1 = \left(\frac{1}{2} \cdot M_{slab}\right) + 4 \cdot \left(\frac{1}{2} \cdot M_{columns}\right) + 2 \cdot \left(\frac{1}{2} \cdot M_{beam300}\right) + M_{beam400} + \left(\frac{1}{2} \cdot M_{add1}\right) = 11.86 t$
- $m_2 = \left(\frac{1}{2} \cdot M_{slab}\right) + 2 \cdot \left(\frac{1}{2} \cdot M_{columns}\right) + 2 \cdot \left(\frac{1}{2} \cdot M_{beam300}\right) + M_{beam400} + \left(\frac{1}{2} \cdot M_{add2}\right) = 10.06 t$

The mass born by each node is given in table (6-1):

	1 <sup>st</sup> floor		2 <sup>nd</sup> floor	
Node	2010	2020	3010	3020
Mass (t)	5.93	5.93	5.03	5.03

Table 6-1: Mass distribution in each node of the frame

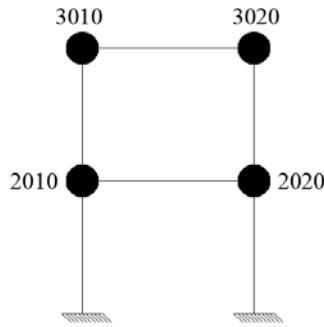


Figure 6.1: Distribution and modelling of the masses in BANDIT frame

### 6.3. Damping of the bare frame

DRAIN-3DX accounts for the effect of linear damping through Rayleigh damping model, in fact, a viscous damping matrix that is linearly proportional to the element stiffness and nodal masses is specified:

$$C = \sum \alpha \cdot M + \sum \beta \cdot K_{\beta}$$

Where C is the viscous damping matrix,  $\alpha$  is the mass damping coefficient and  $\beta$  is the element stiffness coefficient.

In addition, the damping ratio ( $\zeta$ ) of mode  $n^{th}$  is calculated as follows:

$$\zeta_n = \frac{\alpha}{2} \cdot \frac{1}{\omega_n} + \frac{\beta}{2} \cdot \omega_n$$

$\zeta_n$  is the damping ratio for mode  $n$  and  $\omega_n$  is the natural angular frequency for mode of vibration ( $\omega_n = 2 \cdot \pi \cdot f$ ).

According to Chopra (2001), the coefficients  $\alpha$  and  $\beta$  can be calculated for the corresponding modal damping ratios  $\zeta_1$  and  $\zeta_2$  of the 1<sup>st</sup> and 2<sup>nd</sup> mode of vibration (because in this analysis only the first two modes of vibrations are considered) by solving the following matrix equation:

$$\frac{1}{2} \cdot \begin{bmatrix} \frac{1}{\omega_1} & \omega_1 \\ \frac{1}{\omega_2} & \omega_2 \end{bmatrix} \cdot \begin{bmatrix} \alpha \\ \beta \end{bmatrix} = \begin{bmatrix} \zeta_1 \\ \zeta_2 \end{bmatrix}$$

The coefficients  $\alpha$  and  $\beta$  can be calculated from the above equations:

$$\begin{bmatrix} \alpha \\ \beta \end{bmatrix} = 2 \cdot \frac{\omega_1 \cdot \omega_2}{\omega_1^2 - \omega_2^2} \cdot \begin{bmatrix} \omega_1 & -\omega_2 \\ \frac{1}{\omega_1} & \frac{1}{\omega_2} \end{bmatrix} \cdot \begin{bmatrix} \zeta_1 \\ \zeta_2 \end{bmatrix}$$

Chopra (2001) recommends that the damping ratio for the first mode should be greater than the second mode ( $\zeta_1 > \zeta_2$ ). For the bare frame, test sequence 1 – run 5 provides the experimental natural frequencies of the building in X-direction and the results are shown in the following table:

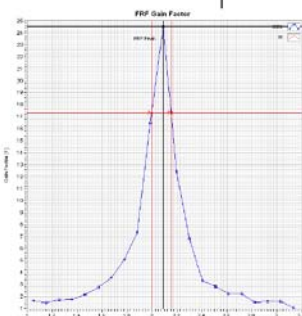
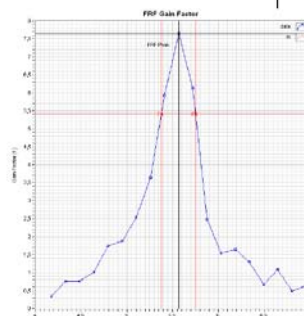
Run	Frequency 1 (Hz)	Damping 1 (%)	Frequency 2 (Hz)	Damping 2 (%)
	AxB1-2		AxB1-1	
5	2.09	3.74	5.57	3.36
				

Table 6-2: Natural frequencies and damping ratios for Bare frame (Garcia et al. 2012)

Therefore, from the values of the experimental results for 1<sup>st</sup> and 2<sup>nd</sup> mode of vibration, the damping coefficient values are calculated. Table (6-3) below shows the results:

Mass Damping Coefficient ( $\alpha$ )	Element Stiffness Coefficient ( $\beta$ )
0.757841	0.001301

Table 6-3: Mass damping coefficient and element stiffness coefficient for bare frame

#### 6.4. Damping of the CFRP retrofitted frame

In this case the process needed to find the coefficients  $\alpha$  and  $\beta$  is the same than in previous case, but the natural frequencies and the damping ratios for the first two modes are different. In table (6-4) natural frequencies and damping ratios for the first two modes are shown for the CFRP retrofitted frame, test sequence 4 – run 57.

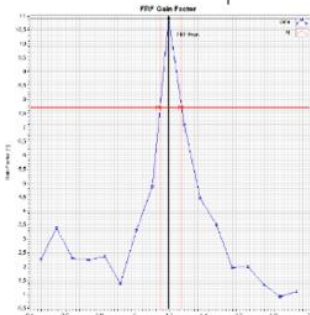
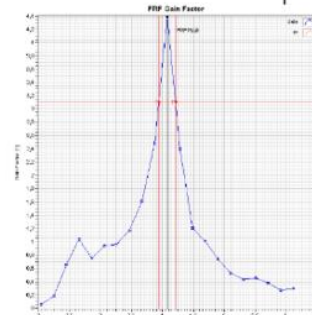
Run	Frequency 1 (Hz)	Damping 1 (%)	Frequency 2 (Hz)	Damping 2 (%)
	Ay1A-2		Ay1A-1	
	1.19	5.20	4.08	3.30
57				

Table 6-4: Natural frequencies and damping ratios for CFRP retrofitted frame (Garcia et al. 2012)

The frequencies and dampings shown above cannot be used even if they have been derived from experimental results. In fact, the analytical investigation of the frame is performed only for the first and the fourth test sequence. In the first case (bare frame), frequencies and dampings can be used in order to find coefficients  $\alpha$  and  $\beta$ , because the frame was not damaged. In the second case (CFRP retrofitted frame), the frame was damaged, therefore these structural weaknesses must be taken into account. One solution lies in increasing the period of the first two modes of vibrations, providing the best fit between analytical and experimental results. The values of frequencies and dampings are shown in table (6-5):

Frequency 1 (Hz)	Damping 1 (%)	Frequency 2 (Hz)	Damping 2 (%)
0.8	5.20	3	3.30

Table 6-5: Modified natural frequencies and damping ratios for CFRP retrofitted frame

From the modified values of the results for 1<sup>st</sup> and 2<sup>nd</sup> mode of vibration, the damping coefficient values are calculated. Table (6-6) below shows the results:

Mass Damping Coefficient ( $\alpha$ )	Element Stiffness Coefficient ( $\beta$ )
0.467541	0.002186

Table 6-6: Mass damping coefficient and element stiffness coefficient for CFRP retrofitted frame

## 6.5. Material properties

According with §5.5, the material properties for cross section fibres are approximated with a series of straight lines. Thereafter, stress-strain relations for steel, stirrups confined concrete, CFRP confined concrete and CFRP sheets used in both bare and CFRP retrofitted frame will be presented.

### 6.5.1. Steel

The bilinear stress-strain model with hardening behaviour is used to describe the behaviour of steel used as longitudinal bars. This model is accepted by both Eurocode 2 and NTC 2008. This relationship is valid for both compressive and tensile behaviour. The characteristics of the material have been presented in § 3.4.1. Figure (6.2) shows the stress strain-model for steel and the values used in DRAIN-3DX:

DRAIN-3DX		
Compression and Tension		
Point	$\sigma$ (MPa)	$\epsilon$
1	526	0.0026
2	616	0.19

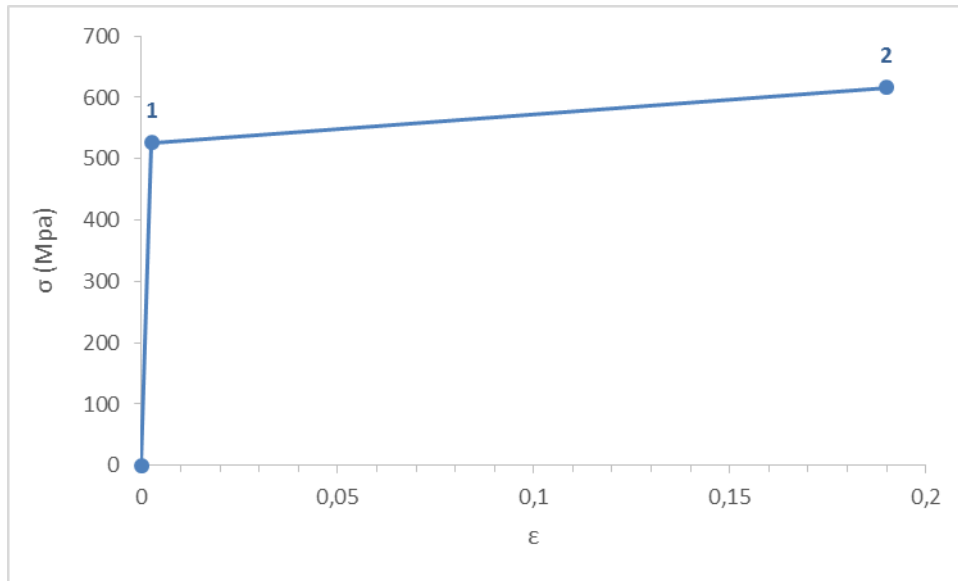


Figure 6.2: Stress-strain model and DRAIN-3DX values for steel

### 6.5.2. Concrete confined with stirrups before test sequence 1

As was mentioned in §2.4.5, the stress-strain relationship used for confined concrete fibers is CEB model (2010) for compression and Carreira and Chu model (1986) for tension, with  $f_t = 2.3 \text{ MPa}$  and  $\beta = 2.26$ . According with §5.5, in DRAIN-3DX five points or less can be used to describe compressive concrete behaviour and two points or less are used to describe tensile concrete behaviour.



Stress-strain model for compression is a non-linear function, so there is a need to approximate a nonlinear function with five or less straight lines. Another problem is the negative material moduli. In fact, the strength of the concrete fibers can be specified to decrease after a maximum strength is reached. If this is done, the material tangent modulus becomes negative, and it is possible for the stiffness of a slice or a complete element also to become negative. If this happens, the element, and possibly the structure, becomes unstable, and it may not be possible to obtain a solution. Powell and Campbell (1994) suggest to try specifying a less rapid rate of strength loss for the concrete materials.

This problem is present in the compressive stress-strain behaviour of concrete. In order to solve this problem, after the peak of strength ( $f_{cm,c}$ ), a value of  $0.85 \cdot f_{cm,c}$  is proposed referred to the maximum strain of confined concrete.

Figure (6.3) shows stress-strain compressive models for 1<sup>st</sup> floor columns: CEB (2010) model with blue line and four-linear model adopted in DRAIN-3DX with black line. Figure (6.4) displays DRAIN-3DX model for both compression and tension and relative values. A visual comparison of the constitutive model among all the elements of the frame is shown in Figure (6.5). Stress-strain models for all the other elements can be found in Appendix A1.

### 1<sup>st</sup> Floor columns

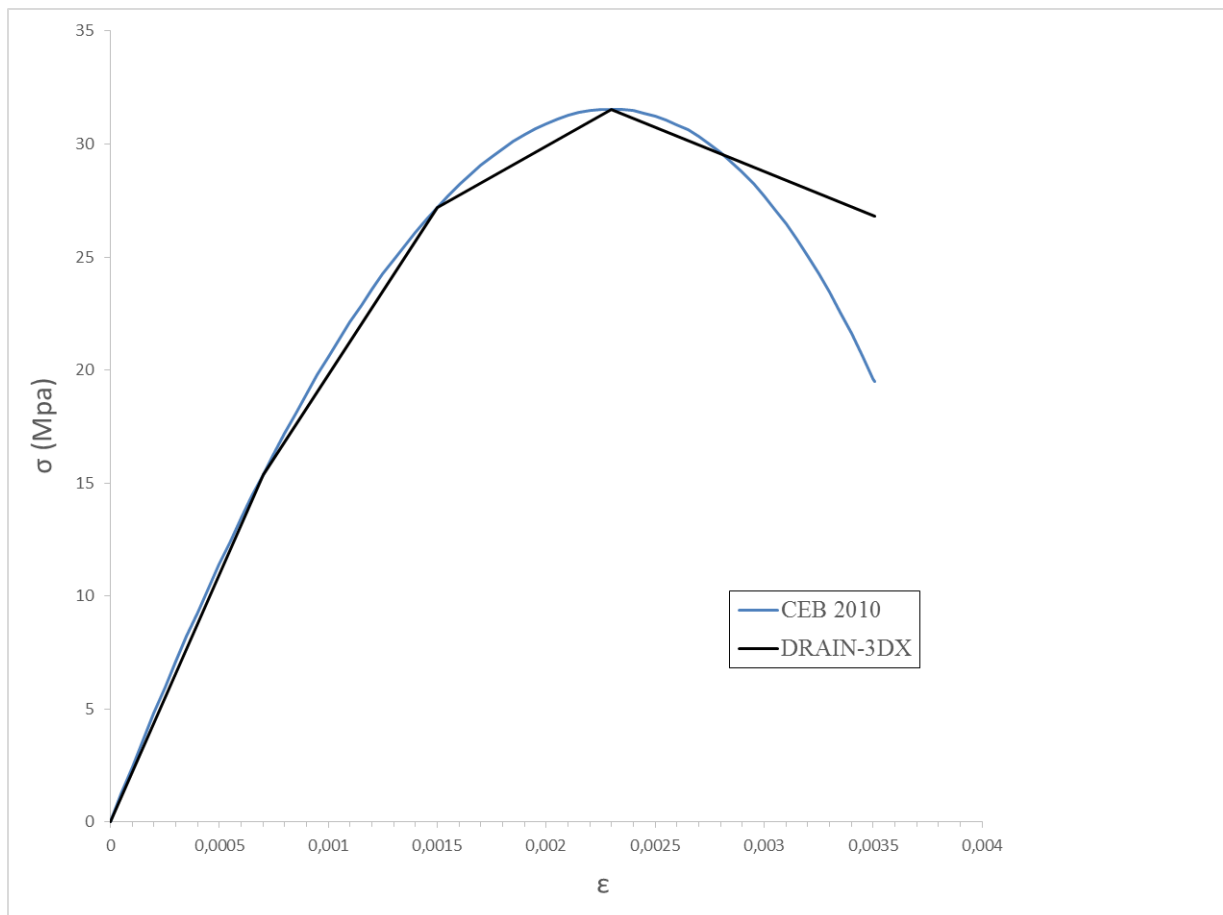


Figure 6.3: Compressive stress-strain model from CEB (2010) and DRAIN-3DX for confined concrete in 1<sup>st</sup> floor columns

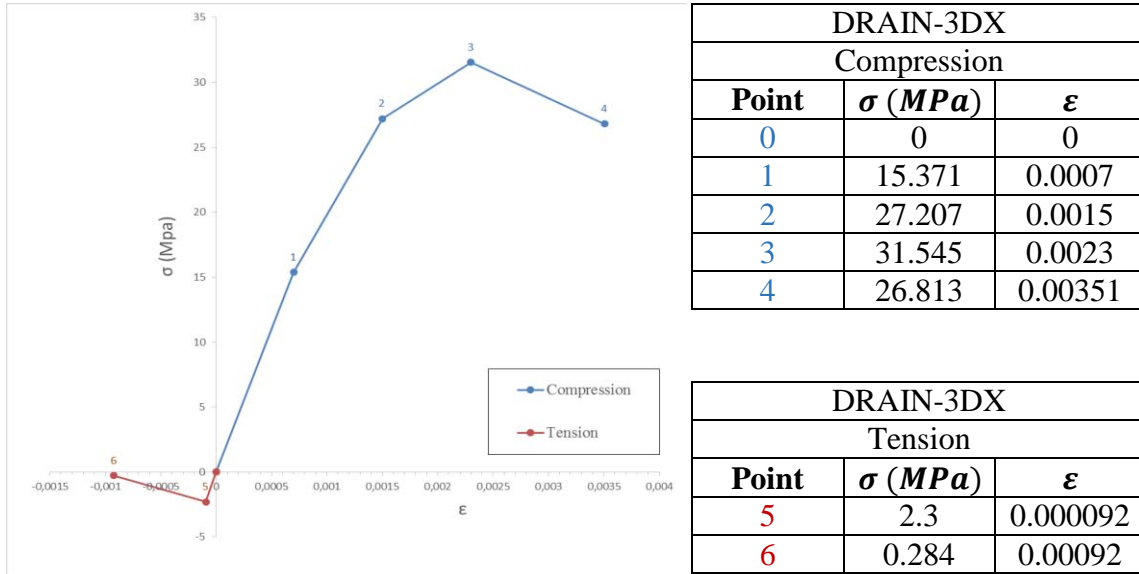


Figure 6.4: DRAIN-3DX stress-strain model and values for confined concrete in 1<sup>st</sup> floor columns

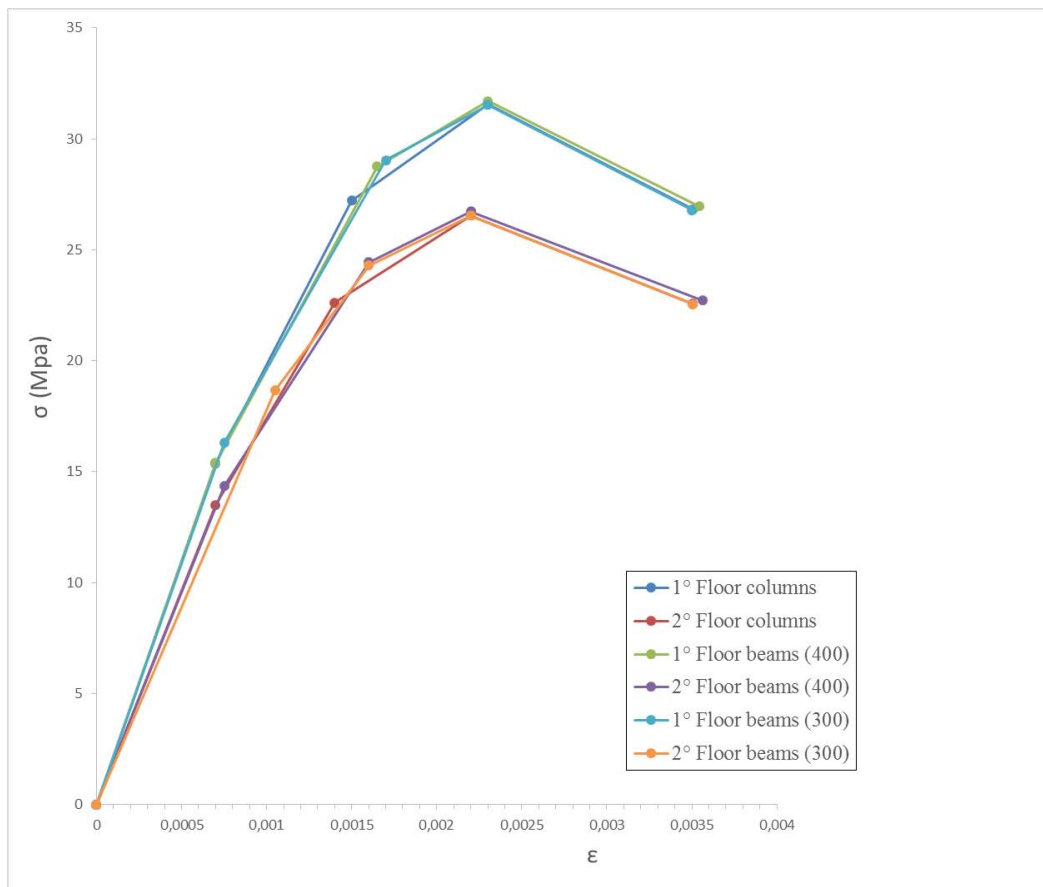


Figure 6.5: Compressive stress-strain model for all confined concrete elements before test sequence 1

### 6.5.3. Concrete confined with stirrups before test sequence 4

After the first three test sequences, described in §3.8, hysteretic cycles arising from artificial earthquakes have damaged the concrete, therefore it is necessary to consider new characteristics of concrete in order to perform the analysis of test sequence 4. As shown in table (3-3) in §3.4.2, elastic modulus  $E_c$  and maximum compressive strength  $f_{cm}$  of concrete have decreased before the last test sequence. The elastic modulus has decreased by 8.43% and maximum compressive strength has decreased by 6.35% for the concrete used in the 1<sup>st</sup> floor. The elastic modulus has decreased by 4.07% and the maximum compressive strength has decreased by 9.43% for the concrete used in the 2<sup>nd</sup> floor. With regard to the tensile behaviour of concrete, before the test sequence 4, the maximum tensile strength has increased for concrete used in 1<sup>st</sup> floor (+30%) and it has been the same for the concrete used in the 2<sup>nd</sup> floor. Figure (6.6) shows stress-strain model for 1<sup>st</sup> floor columns before test sequence 4 against stress-strain model before test sequence 1 and the values adopted in DRAIN-3DX for concrete during test sequence 4. The models used are the same of the previous paragraph. The values for the other elements are shown in Appendix A2. A visual comparison of the constitutive model among all the elements of the frame before test sequence 4 is shown in Figure (6.7).

DRAIN-3DX		
Compression		
Point	$\sigma$ (MPa)	$\epsilon$
0	0	0
1	14.196	0.0007
2	25.355	0.0015
3	29.544	0.0023
4	25.113	0.00351

DRAIN-3DX		
Tension		
Point	$\sigma$ (MPa)	$\epsilon$
5	3	0.000132
6	0.37	0.00132

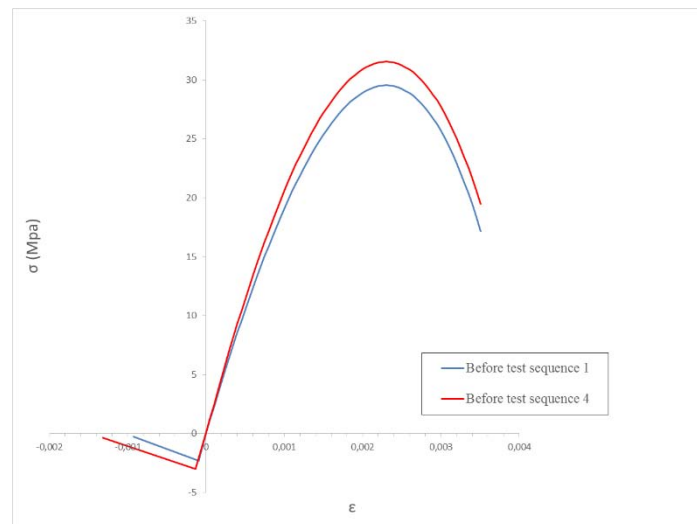


Figure 6.6: Comparison between stress-strain behaviour for concrete columns in 1<sup>st</sup> floor before tests sequence 1 and 4 and DRAIN-3DX values for concrete before test sequence 4

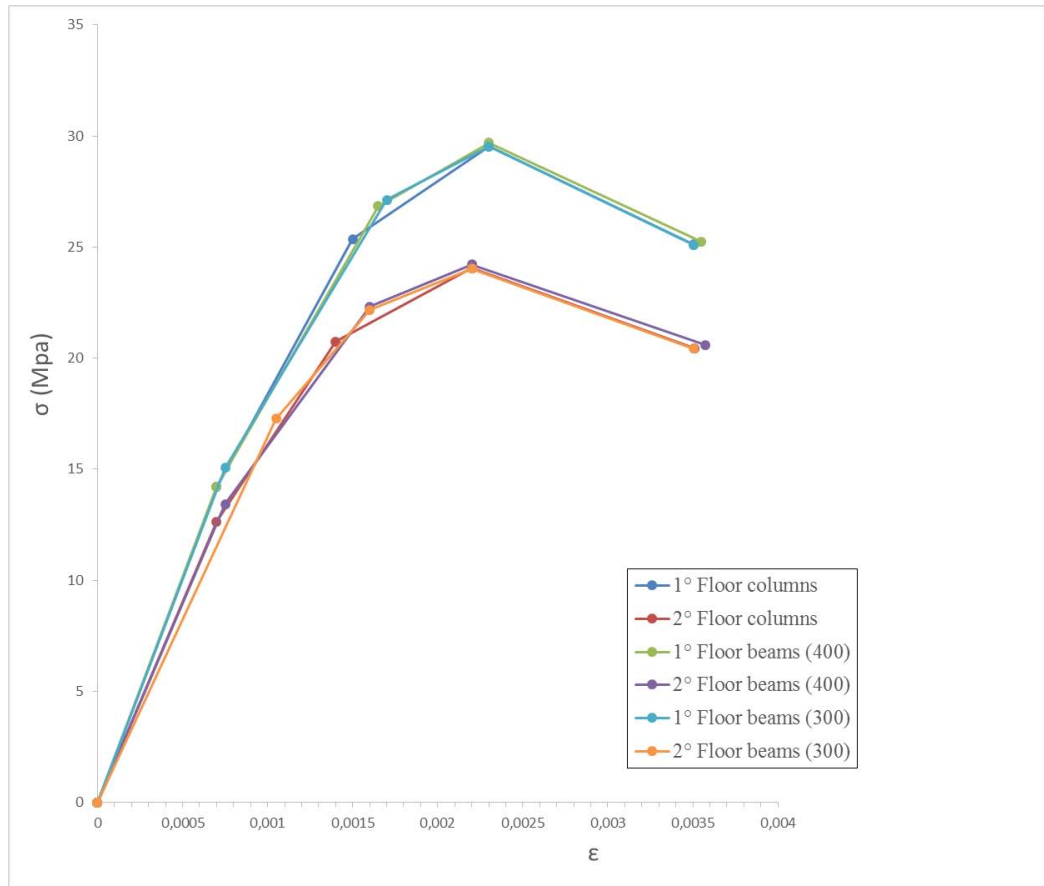


Figure 6.7: DRAIN-3DX compressive stress-strain model for all confined concrete elements before test sequence 4

#### 6.5.4. Concrete confined with CFRP sheets before test sequence 4

The stress-strain relationship used for CFRP confined concrete comes from Lam and Teng's model (2003) for compressive behaviour, as said in §2.4.6. This model is based on concrete's characteristics described in §6.5.3, because the frame has been retrofitted before test sequence 4, therefore concrete had previously been damaged. Tensile behaviour is represented with Carreira and Chu model (1986), with  $f_t = 3.0 \text{ MPa}$  for the 1<sup>st</sup> floor elements,  $f_t = 2.3 \text{ MPa}$  for the 2<sup>nd</sup> floor elements, and  $\beta = 1.70$  for all the elements. The non-linear relationship in Lam and Teng's model was approximated with five straight lines. In figure (6.8) the stress-strain behaviour of 1<sup>st</sup> floor columns concrete confined with CFRP is compared with the constitutive model of the same elements before the retrofitting. DRAIN-3DX model for those elements and the relative values are then shown in figure (6.9). The constitutive model for all the other elements confined with CFRP sheets can be found in appendix C. Figure (6.10) shows the stress-strain behaviour in compression among all CFRP confined elements.

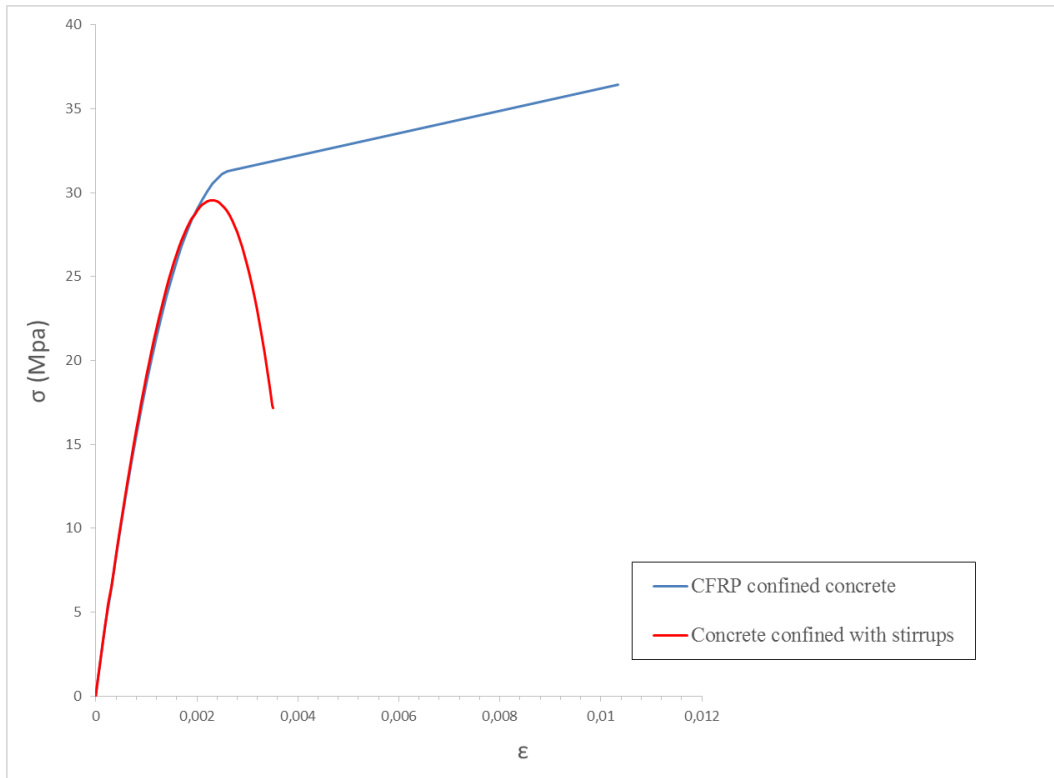


Figure 6.8: Comparison between compressive stress-strain model for concrete confined with stirrups and CFRP confined concrete in 1<sup>st</sup> floor columns

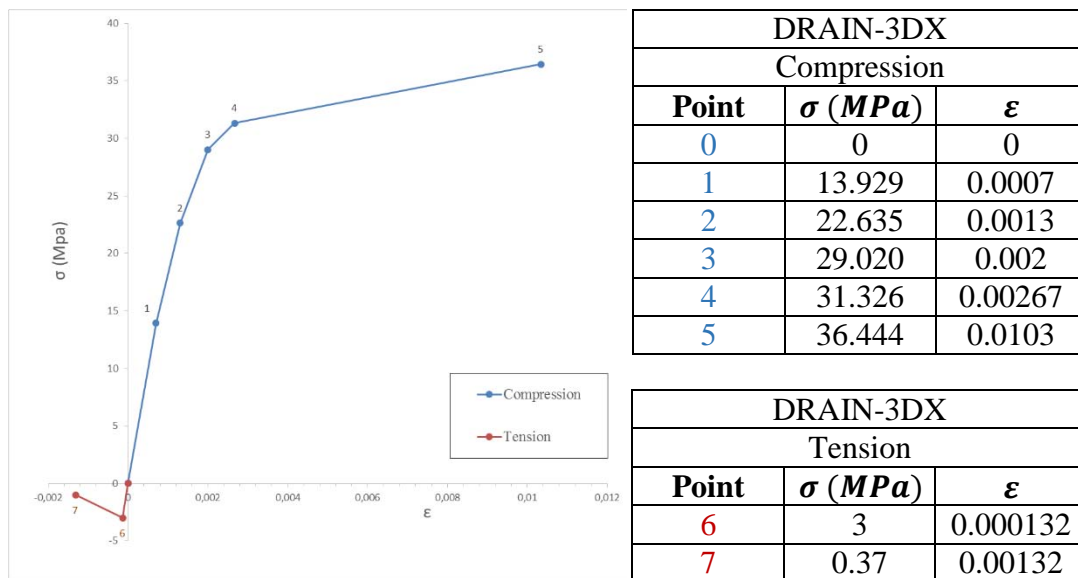


Figure 6.9: DRAIN-3DX stress-strain model and values for CFRP confined concrete in 1<sup>st</sup> floor columns

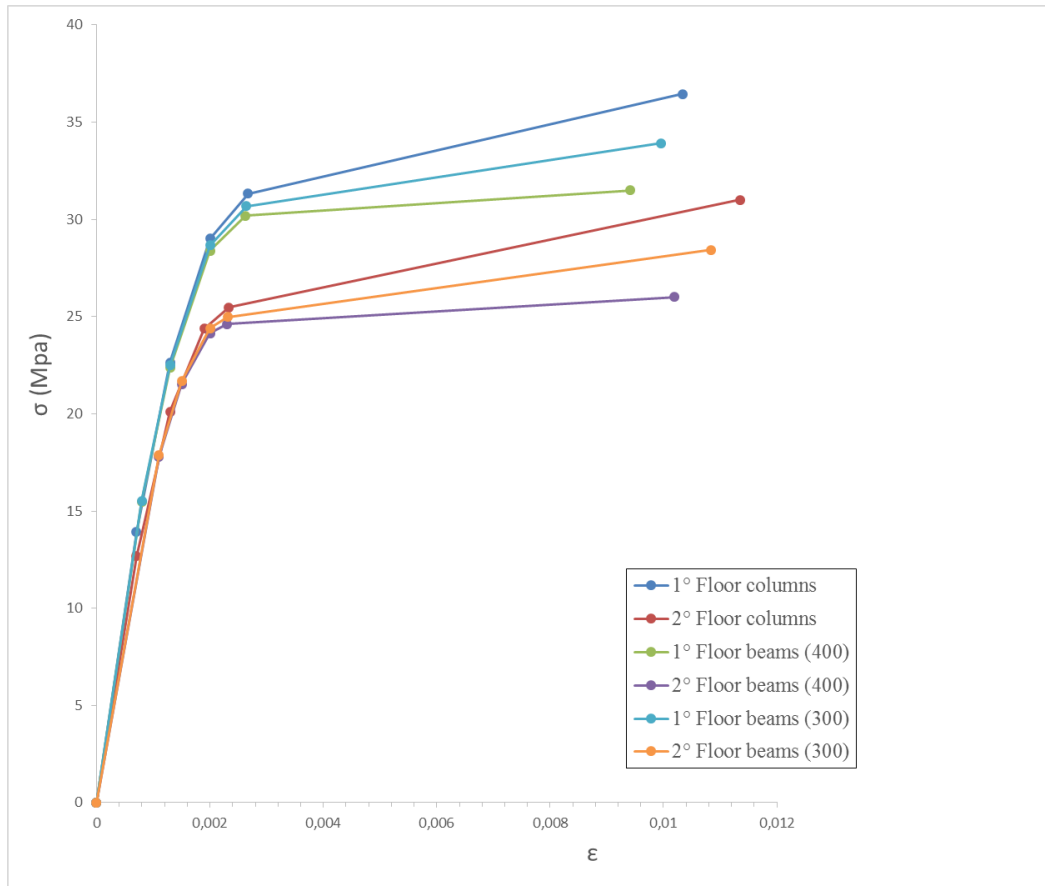


Figure 6.10: DRAIN-3DX compressive stress-strain model for all CFRP confined concrete elements

### 6.5.5. TFC composite for CFRP

Stress-strain tensile behaviour for the fibres is linear elastic up to failure and do not have a pronounced yield plateau as for steel, as said in §2.3.6. The main characteristics of CFRP are described in §4.2. Figure (6.11) shows constitutive stress-strain models for both dry carbon fibres and TFC composite for CFRP.

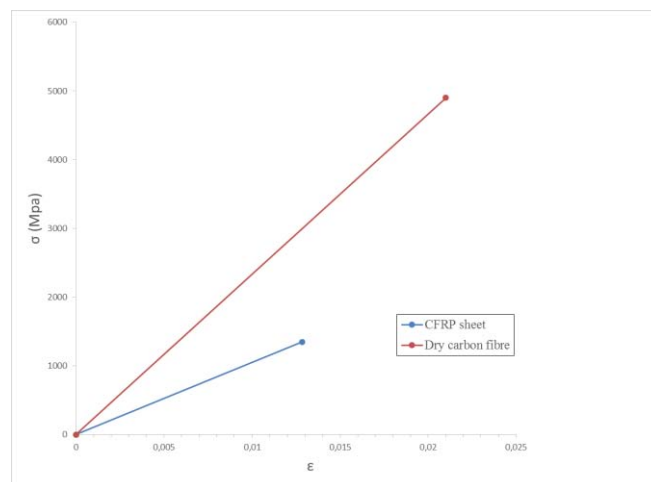


Figure 6.11: Tensile stress-strain model for dry carbon fibres and TFC composite for CFRP

## 6.6. Element segments and cross section fibers

Fiber elements type 15 are chosen to model the elements of both the frames, bare and CFRP retrofitted. The reasons for this choice are explained in §5.4. These elements are used to model single cross section of beams and columns, as will be seen later. Some of the beams and columns are divided into three segments, in order to avoid problems with the numerical convergence of the solution. The length of each segment is proportional to the length of the element (10%, 80%, 10%).

Each cross section of the element is divided into sub sections of steel, concrete and CFRP fibers for the frames. The cross section characteristics are defined by assembling these fibers based on their coordinates and cross sectional area. The response of each fiber is concentrated at its centre of gravity which results in the stiffness and strength of the section depending on the number and location of fibers (Kyriakides, 2007). The number of steel fibers depends upon the number of longitudinal reinforcement bars in the structure and the concrete section is divided into different number of equal parts. CFRP longitudinal sheets are represented with the number of six fibers for each side.

### 6.6.1. Bare frame

According with §3.8, test sequence 1 has been performed in X-direction, therefore only beams (400 · 260) are represented in the 2-D frame. Figure (6.12) shows the concrete and the steel fibers for the 1<sup>st</sup> floor columns. The discretization of other elements is presented in Appendix C. The location of each fiber is dependent upon the local axis system defined in the analysis, as seen in figure (5.1).

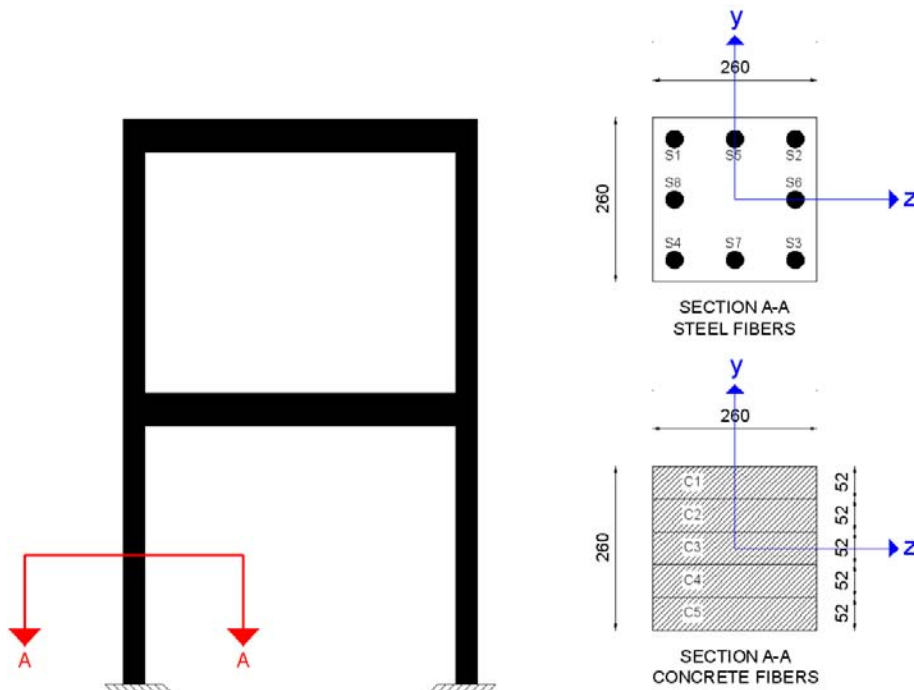


Figure 6.12: Fibers cross section for 1<sup>st</sup> floor columns in both bare frame and CFRP retrofitted frame

### 6.6.2. CFRP retrofitted frame

According with §3.8, test sequence 4 has been performed in Y-direction. In order to perform analytical investigation only beams (300 · 260) are represented in the 2-D frame. An example of fibers cross section is shown in figure (6.13). Here, steel, concrete, and CFRP fibers for the 1<sup>st</sup> floor columns are represented. Fibers cross sections for all the new elements are presented in Appendix C.

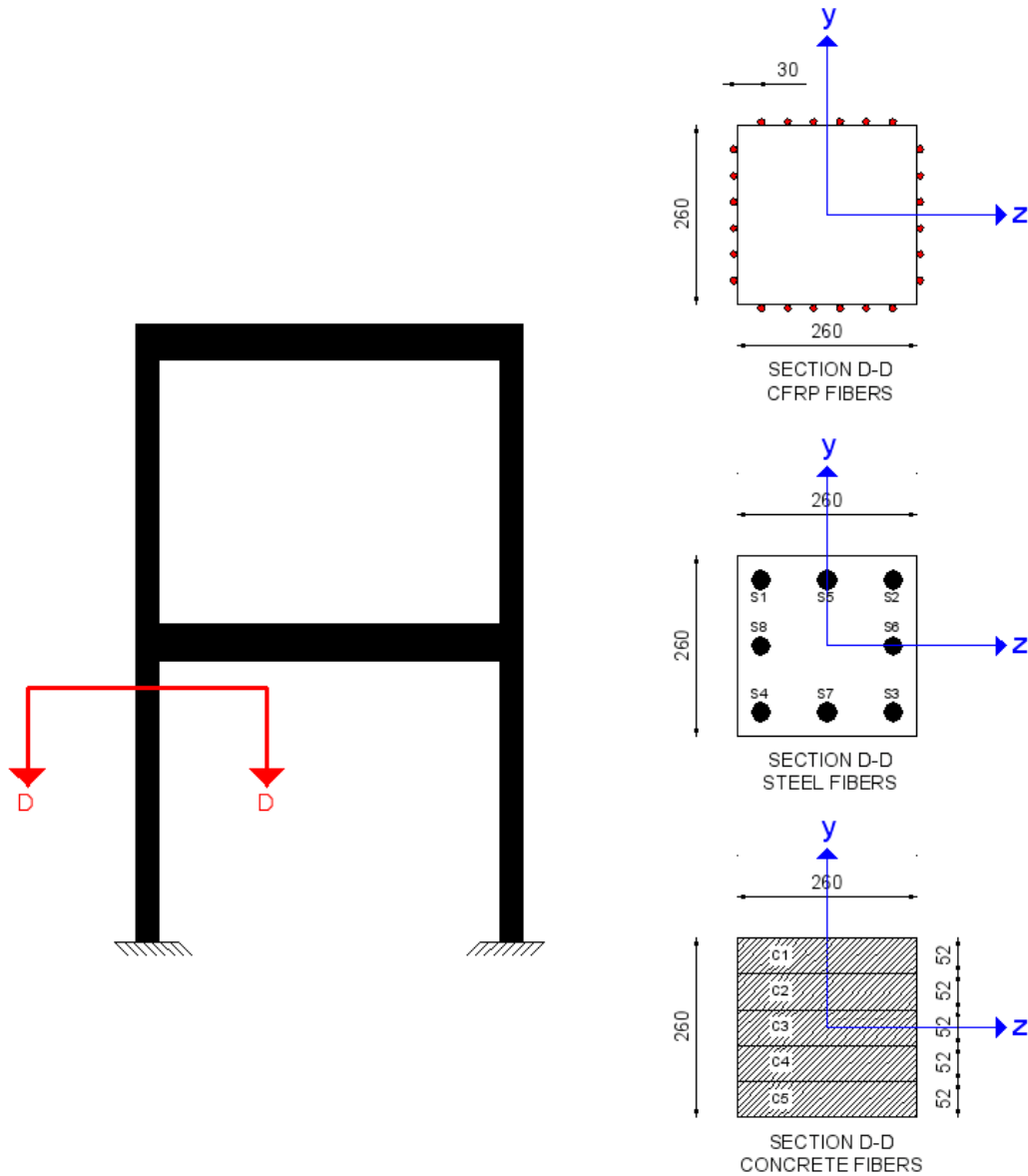


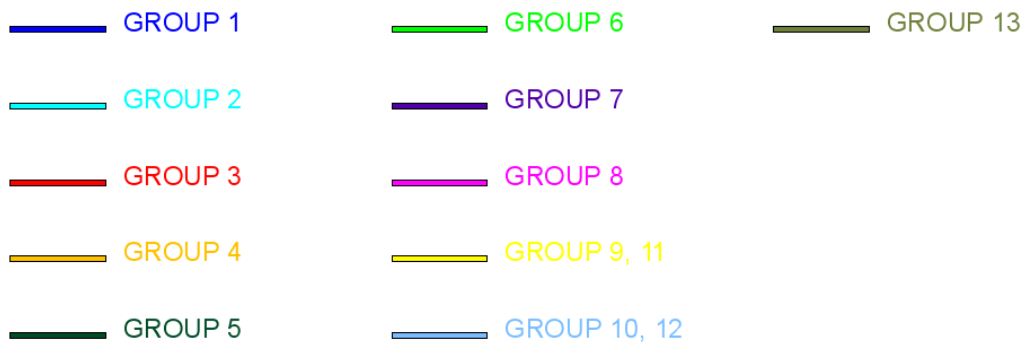
Figure 6.13: Fibers cross section for 1<sup>st</sup> floor columns in CFRP retrofitted frame



## 6.7. Analytical geometry of the bare frame

The structure is modelled in DRAIN-3DX as a two dimensional frame, with columns (260 · 260) and beams (400 · 260). This is because the first damage sequence is in X-direction. The frame is divided into a number of nodes and elements. The nodes are assumed to be at the center line of both beams and columns. At each node six degrees of freedom are defined (translation in X, Y, Z direction and rotation in X, Y, Z direction). Furthermore, restraints are applied to each node so that the frame acts as a two dimensional structure. Node 1010 is considered to be the origin of the global axes. The foundation nodes (1010, 1020) are restrained by a stiff support spring which allows the frame to move with no relative displacement to the ground. The programme refuses to run the analysis if the supports are fixed, because of singularity in stiffness matrix.

Figure (6.14) describes nodes, elements and groups of the bare frame. 1<sup>st</sup> floor column consists of two segments: one represents the column from the ground till the joint and the other represent the 1<sup>st</sup> floor beam-column joint in vertical direction. 2<sup>nd</sup> floor column consists of three segments: one represents the column from the 1<sup>st</sup> floor beam-column joint till the 2<sup>nd</sup> floor beam-column joint and the other two represent the 1<sup>st</sup> and 2<sup>nd</sup> floor beam-column joint in vertical direction. Regarding the beams, both beams of 1<sup>st</sup> and 2<sup>nd</sup> floor are divided into 9 intermediate points, which gives a better understanding of the elementary response of the structure, and also enable to distribute the loads at nodes. Lateral segments are used to represent beam-column joints in horizontal direction. These segments are rigid joints, so relative rotations between beam and column are kept rigid. As explained in §5.6, pullout and gap properties for connection hinge fibers are used in appropriate element groups (5, 7, 8, 10, 12). This choice is supported by the pictures of the frame taken after run 18, at the end of the first test sequence and the correlation between analytical and experimental results, as will be seen later. The model used for pullout properties and the choice of the gap properties are explained in the next paragraphs. Figure (6.15) shows pullout and gap properties for connection hinge fibers in the bare frame.



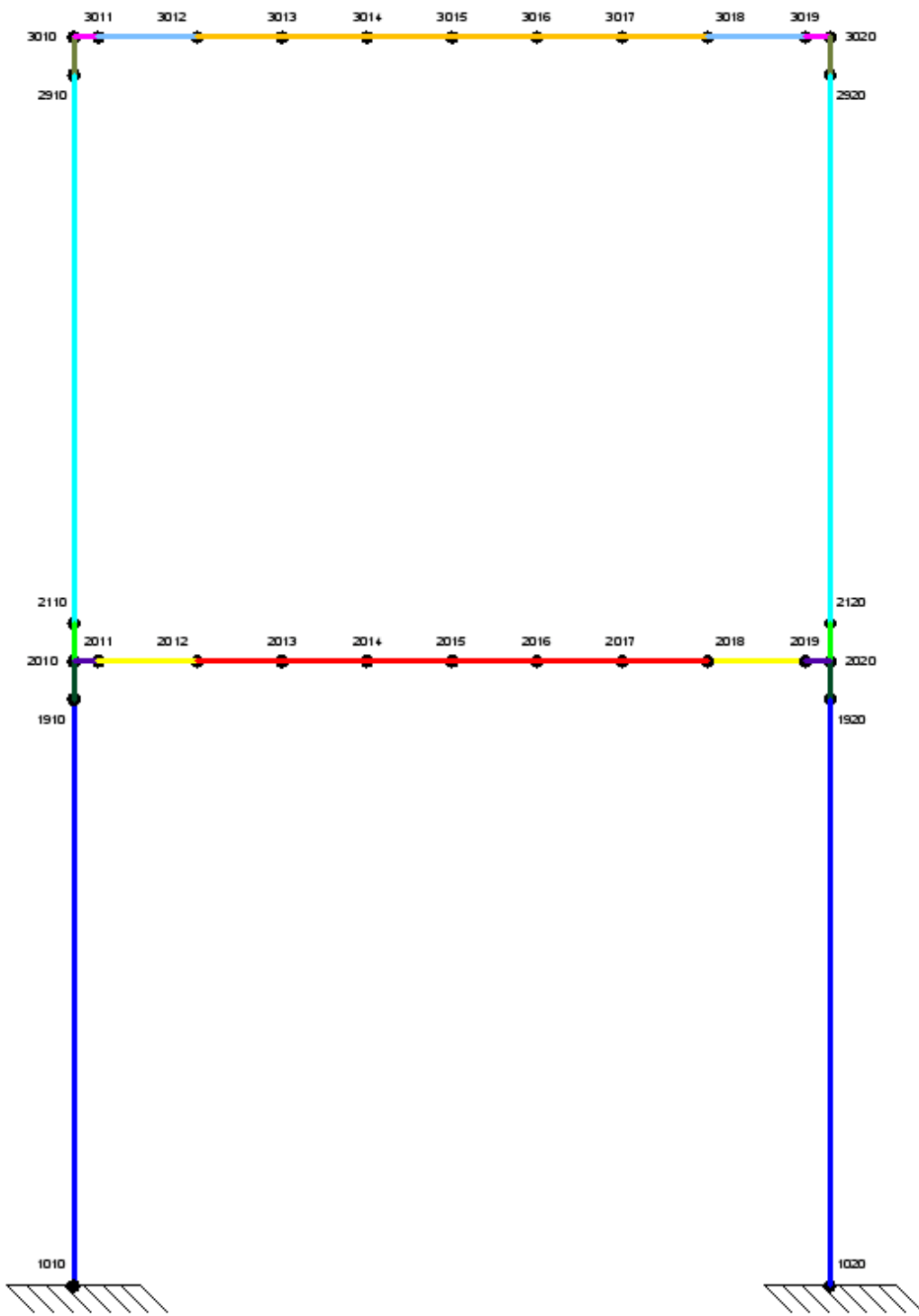
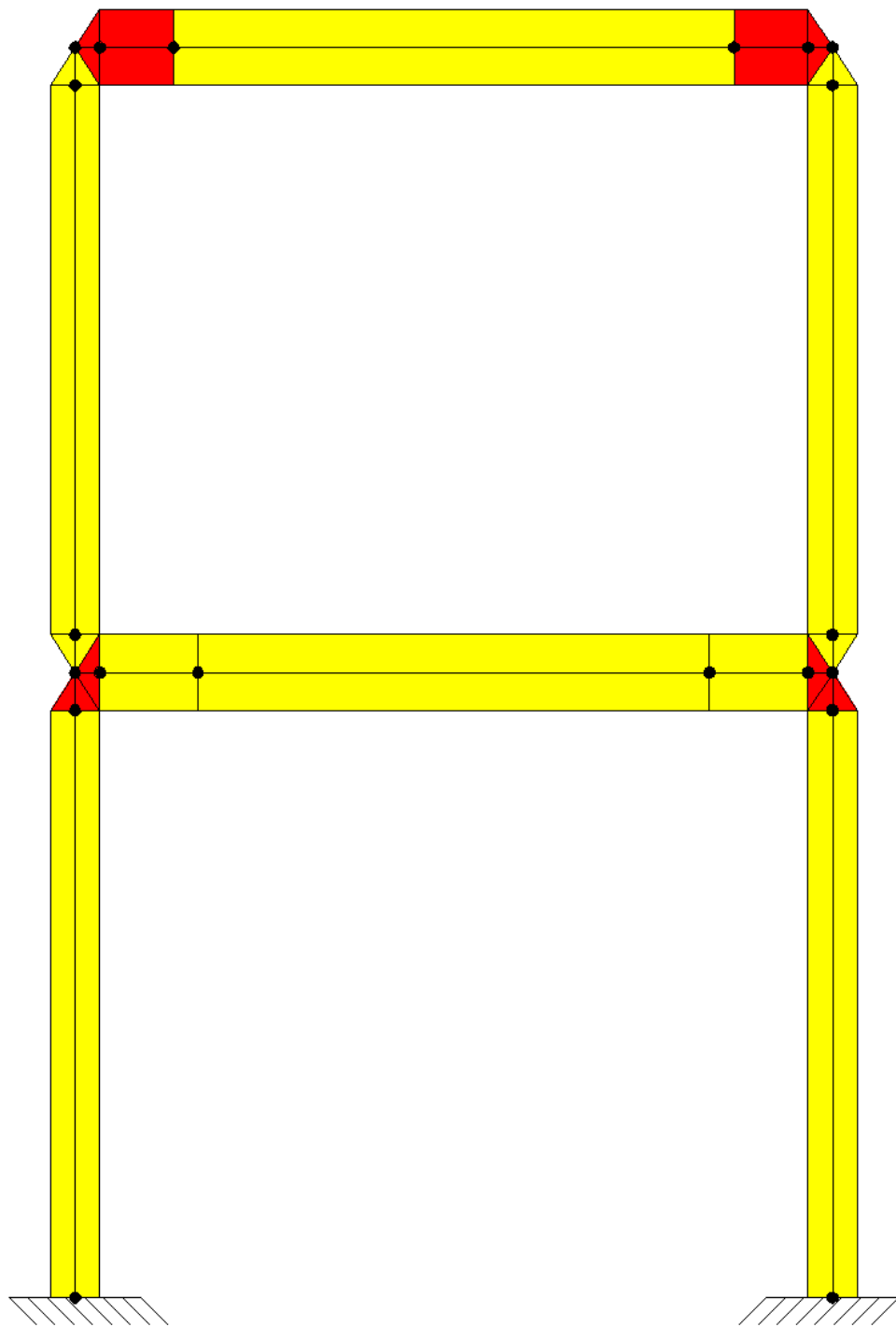


Figure 6.14: Analytical modelling of the bare frame in DRAIN-3DX



**PULLOUT AND GAP PROPERTIES FOR CONNECTION HINGE FIBERS**

Figure 6.15: Pullout and gap properties for connection hinge fibers for the bare frame in DRAIN-3DX

## 6.8. Analytical geometry of the CFRP retrofitted frame

In this case the structure is modelled as a two dimensional frame, with columns (260 · 260) and beams (300 · 260). This is because the fourth damage sequence is in Y-direction. Boundary conditions and restraint are the same as in the previous case. In order to represent CFRP confined elements and also CFRP longitudinal sheets, extra nodes are added to the columns and beams to model the beam-column joints.

Figure (6.16) describes nodes, elements and groups of the CFRP retrofitted frame. 1<sup>st</sup> floor column consists in four segments (groups 1, 2, 4, 7):

- Group 1 represents CFRP confined column from the ground till the height of 90 cm;
- Group 2 represents middle stirrugged column;
- Group 4 represents CFRP confined column under 1<sup>st</sup> floor beam-column joint and here there are CFRP longitudinal sheets.
- Group 7 represents 1<sup>st</sup> floor beam-column joint in vertical direction. This section is not confined but there are CFRP longitudinal sheets.

2<sup>nd</sup> floor column consists in five segments (groups 8, 5, 3, 6, 15):

- Group 8 represents 1<sup>st</sup> floor beam-column joint in vertical direction. This section is not confined but there are CFRP longitudinal sheets;
- Group 5 represents CFRP confined column above 1<sup>st</sup> floor beam-column joint;
- Group 3 represents middle stirrugged column;
- Group 6 represents CFRP confined column under 2<sup>nd</sup> floor beam-column joint. Here there are also CFRP longitudinal sheets;
- Group 15 represents 2<sup>nd</sup> floor beam-column joint in vertical direction. This section is not confined but there are CFRP longitudinal sheets.

Regarding the beams, both beams of 1<sup>st</sup> and 2<sup>nd</sup> floor are divided into 9 intermediate points. Lateral segments are used to represent beam-column joints in horizontal direction. In contrast to bare frame, these segments are not rigid joints, therefore there are relative rotations between beam and columns during the simulation. This can be explained by the fact that PGA levels are higher for CFRP retrofitted frame than for the bare frame.

1<sup>st</sup> and 2<sup>nd</sup> floor beams consists in five segments each (groups 9, 11, 13 for 1<sup>st</sup> floor beams and groups 10, 12, 14 for 2<sup>nd</sup> floor beams):

- Group 9 (and group 10) represents middle stirrugged beam;
- Group 11 (and group 12) represents 1<sup>st</sup> (and 2<sup>nd</sup>) floor beam-column joint in horizontal direction. This section is not confined but there are CFRP longitudinal sheets.
- Group 13 (and group 14) represents CFRP confined beam and there are also CFRP longitudinal sheets.

Figure (6.17) shows pullout and gap properties for connection hinge fibers in CFRP retrofitted frame. In this case it has not been possible to see pictures of the frame after the tests, because CFRP sheets prevent the vision of the damaged parts.

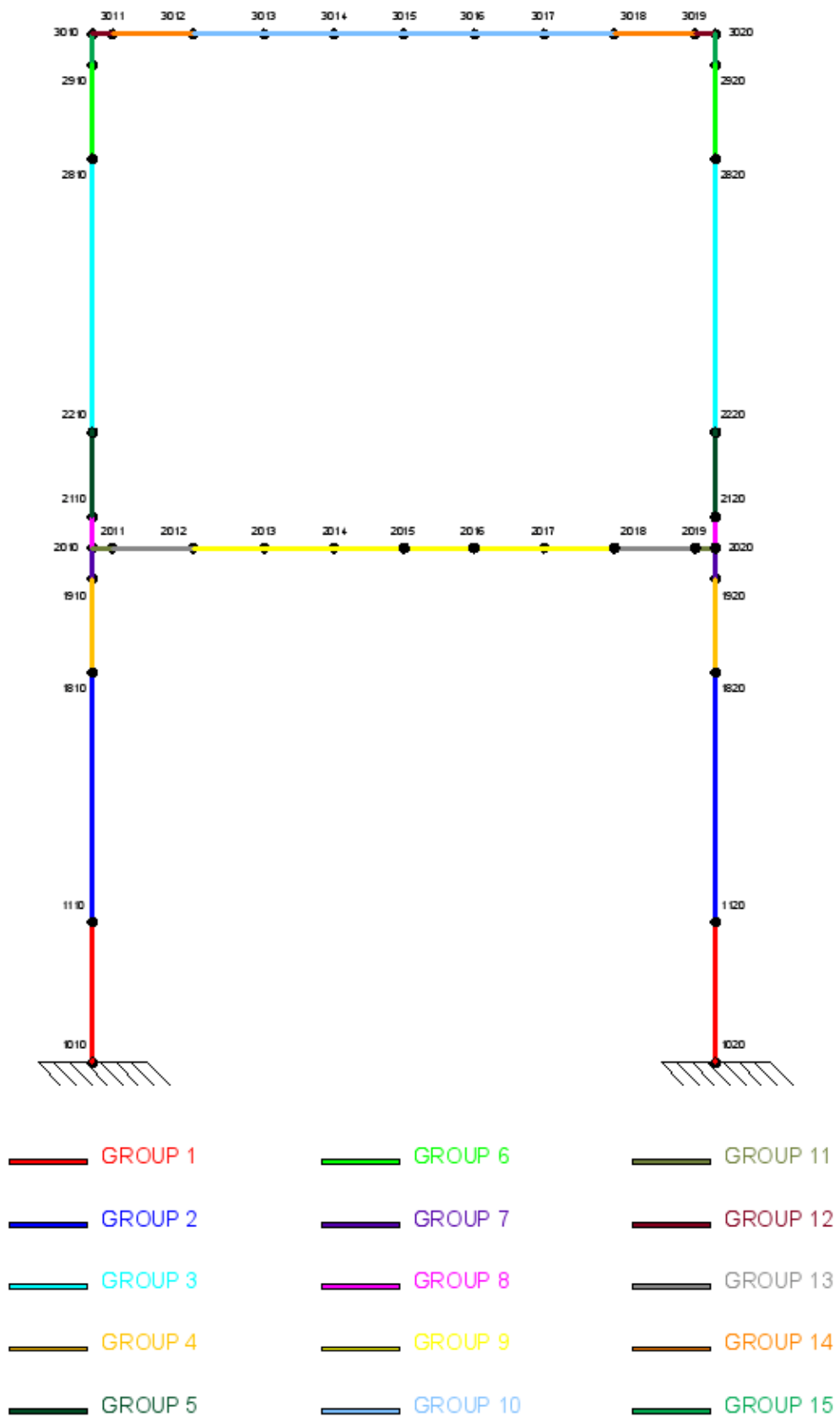
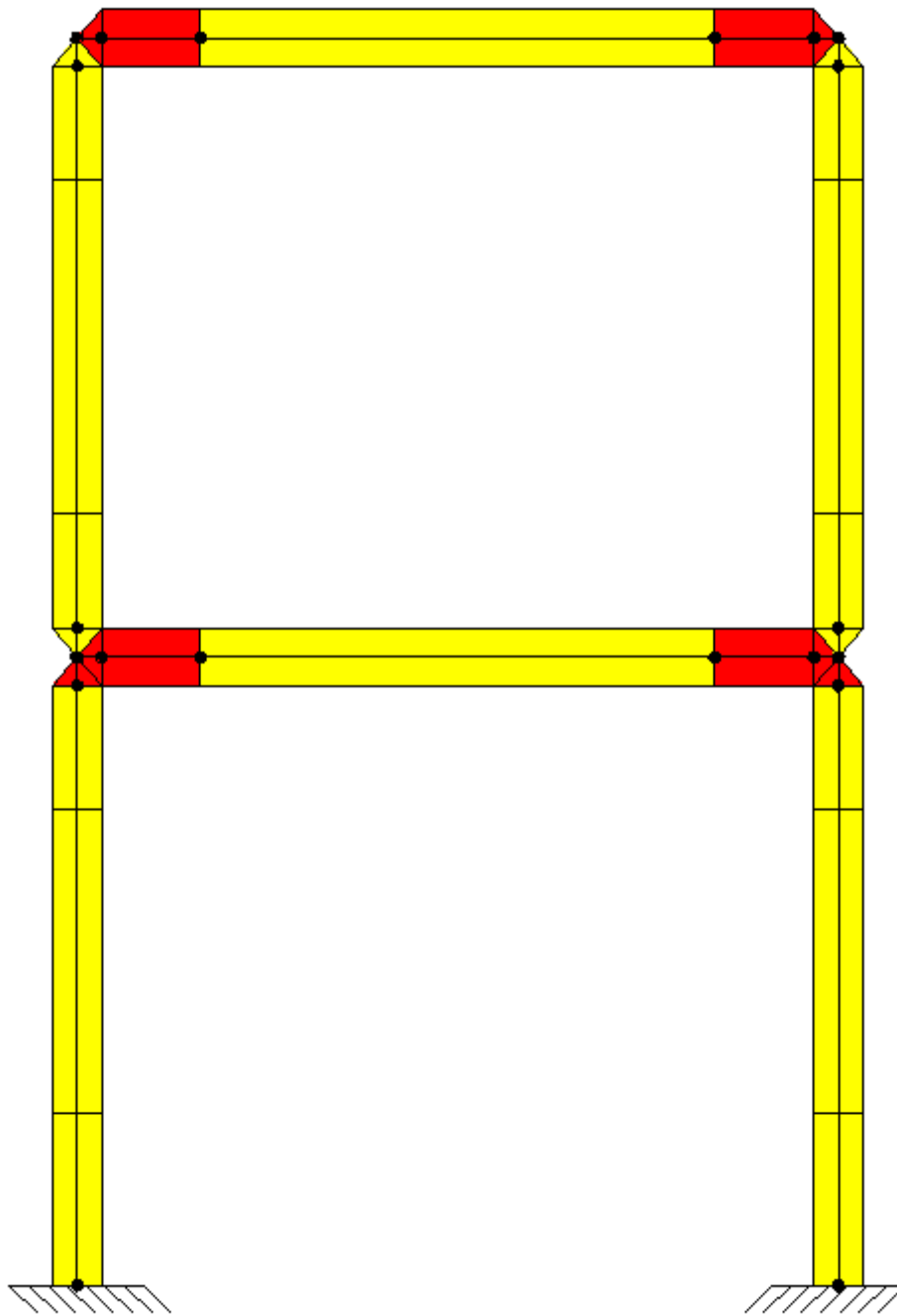


Figure 6.16: Analytical modelling of the CFRP retrofitted frame in DRAIN-3DX



 PULLOUT AND GAP PROPERTIES FOR CONNECTION HINGE FIBERS

Figure 6.17: Pullout and gap properties for connection hinge fibers for the CFRP retrofitted frame in DRAIN-3DX

## 6.9. Connection hinge fibers properties

According to Kwak and Filippou (1990), the force transfer from steel to concrete during the bond can be attributed to three different phenomena:

- Chemical adhesion between mortar paste and bar surface;
- Friction and wedging action of small dislodged sand particles between the bar and the surrounding concrete;
- Mechanical interaction between concrete and steel.

Bond-slip of deformed bars, like in this case, is better than plain bars because most of the steel force is transferred through the lugs to concrete. Friction and chemical adhesion forces are not negligible, but secondary and tend to decrease as the reinforcing bars start to slip. As has been said before, Bandit specimen has been built with inadequate reinforcement detailing in columns and joints to replicate old construction practices. Short bar anchorage length (and even the lack of hooks or bends) in beam-column joints increases significantly bond of bars, because it is considered insufficient to develop the yielding capacity of the 14 mm bars according to current design recommendations. Connection hinge properties in DRAIN-3DX have been discussed in §5.6. . These connection hinges at member ends are defined as fibers having both pullout and gap characteristics. Pullout fibers can model slip movement of the reinforcement bars whereas gap fibers are used to account for gap opening of concrete. These properties play an important role in the deformation of the whole structure. Kwak and Filippou (1990) analysed the deformations on an interior joint and concluded that bond-slip of the reinforcing bars in the joint contributed approximately 33% of the total deformation near the ultimate load. Sezen (2002) also monitored slip deformations on columns and concluded that these contribute were between 25-40% of the total lateral displacement. The model used for the pullout properties is a modification of the CEB model (2010) and it will be described in the next paragraphs.

### 6.9.1. Pullout fibers model

According to §5.6.1., the parameters  $K1$ ,  $K2$ ,  $K3$ ,  $S1T$ ,  $S2T$ ,  $S1C$ ,  $S2C$  have to be defined in order to calibrate the trilinear backbone curve in figure (5.4). The stiffness of the tri-linear portion is the same both in tension and compression while the strength may vary. The trilinear curve is defined for each longitudinal bar or for every group that has the same characteristics, such as anchorage length. In accordance with Kyriakides (2007), the initial stiffness  $K1$  defines the bond conditions prior to yielding of the reinforcement and it is defined as the ratio between steel yield strength ( $S1T$ ) and elastic bar slip ( $s_1$ ). First it must be realised if anchorage failure occurs before or after bar yielding,  $S1T$  is defined as the maximum stress that can be achieved in the bar for the provided anchorage length and derived from a simple equilibrium of forces acting on the bar:

$$S1T = \frac{4 \cdot \tau_{max} \cdot l}{d}$$

where  $d$  is the bar diameter,  $l$  is the anchorage length and  $\tau_{max}$  is the maximum bond strength that can be achieved in the bar. For the definition of the maximum bond strength, many researchers like Eligehausen et al. (1983), Model Code CEB (2010), Wu and Zhao (2013) made their proposals. Model Code CEB (2010) was found to best approximate the experimental results obtained from the tests on BANDIT. Both the bare frame and the CFRP retrofitted frame have shown pullout failure mode of the longitudinal bars instead of splitting. Furthermore, bond conditions can be considered to be bad and  $\tau_{max} = 1.25 \cdot \sqrt{f_{cm}}$  was used in the analysis. Elastic bar slip  $s_1$  is shown in table (6-7).

	1	2	3	4	5	6
	Pull-out (PO)		Splitting (SP)			
	$\varepsilon_s < \varepsilon_{s,y}$		$\varepsilon_s < \varepsilon_{s,y}$			
	Good bond cond.	All other bond cond.	Good bond cond.		All other bond con.	
Unconfined			Stirrups	Unconfined	Stirrups	
$\tau_{bmax}$	$2.5 \cdot \sqrt{f_{cm}}$	$1.25 \cdot \sqrt{f_{cm}}$	$2.5 \cdot \sqrt{f_{cm}}$	$2.5 \cdot \sqrt{f_{cm}}$	$1.25 \cdot \sqrt{f_{cm}}$	$1.25 \cdot \sqrt{f_{cm}}$
$\tau_{bu,split}$	-	-	$7.0 \cdot \left(\frac{f_{cm}}{25}\right)^{0.25}$	$8.0 \cdot \left(\frac{f_{cm}}{25}\right)^{0.25}$	$5.0 \cdot \left(\frac{f_{cm}}{25}\right)^{0.25}$	$5.5 \cdot \left(\frac{f_{cm}}{25}\right)^{0.25}$
$s_1$	1.0 mm	1.8 mm	$s(\tau_{bu,split})$	$s(\tau_{bu,split})$	$s(\tau_{bu,split})$	$s(\tau_{bu,split})$
$s_2$	2.0 mm	3.6 mm	$s_1$	$s_1$	$s_1$	$s_1$
$s_3$	$c_{clear}$	$c_{clear}$	$1.2 \cdot s_1$	$0.5 \cdot c_{clear}$	$1.2 \cdot s_1$	$0.5 \cdot c_{clear}$
$a$	0.4	0.4	0.4	0.4	0.4	0.4
$\tau_{bf}$	$0.40 \cdot \tau_{max}$	$0.40 \cdot \tau_{max}$	0	$0.40 \cdot \tau_{bu,split}$	0	$0.40 \cdot \tau_{bu,split}$

Table 6-7: Parameters defining the mean bond stress-slip relationship of ribbed bars (Model Code CEB 2010)

In case anchorage failure occurs after bar yielding, K2 is defined as  $(f_u - f_y) / (s_2 - s_1)$ . The nonlinear bar slip value  $s_2$  is defined as:  $s_2 = \frac{f_y^2 \cdot d}{8 \cdot E_s \cdot \tau_e} + \frac{(f_s - f_y) \cdot f_y \cdot d}{4 \cdot \tau_y \cdot E_h} + \frac{(f_s - f_y)^2 \cdot d}{8 \cdot \tau_y \cdot E_h}$ , where  $E_h$  is steel hardening modulus and  $\tau_y$  is the yielded bond strength in steel and  $\tau_e$  is the uniform elastic bond strength. For the definition of  $\tau_y$  and  $\tau_e$ , proposals from various researchers have been made. Eligehausen et al. (1983) experimentally defined  $\tau_y = 1.8 \cdot \sqrt{f_{cm}}$  and  $\tau_e = 2.5 \cdot \sqrt{f_{cm}}$  for steel moderately confined that remains in the elastic region. In case where anchorage failure precludes yielding, stiffness K2 is set to zero. In this case values S2T and S2C are just over to S1T and S1C.



### 6.9.1.1. Pullout fibers and degradation parameters for bare frame

Figures (6.18), (6.19), (6.20) show parameters K1, K2, K3, S1T, S2T, S1C, S2C and relative graphs  $\sigma = \sigma(s)$  for the elements of the bare frame affected by bond-slip, as shown in figure (6.15). The elements of the bare frame were subjected to bad bond conditions, so elastic bar slip  $s_1$  is set to 1.8 mm. In figure (6.21) a comparison among the pullout properties of the elements affected by bond-slip. This graph shows that 2<sup>nd</sup> floor beams are the most affected by bond-slip. This fact is visible in the photos of the frame after the first test sequence, as will be seen in the next paragraphs. Contrary to the columns, in the case of the beams, anchorage failure precludes yielding. In table (6-8) adopted degradation properties are shown. These values are kept the same in both the analyses. Stiffness degradation factor is set to the maximum value (1), therefore there is the highest level of stiffness degradation during hysteretic cycles. Tension and compression strength degradation factors are also set to the maximum value (1), therefore there is a big loss of strength during the tests. Pinching behaviour is present.

Unit	K1	K2	K3	S1C	S2C	S1T	S2T
$KN/m^3$	$2.92 \cdot 10^8$	$6.56 \cdot 10^7$	0.01				
<i>Mpa</i>				526	616	526	616

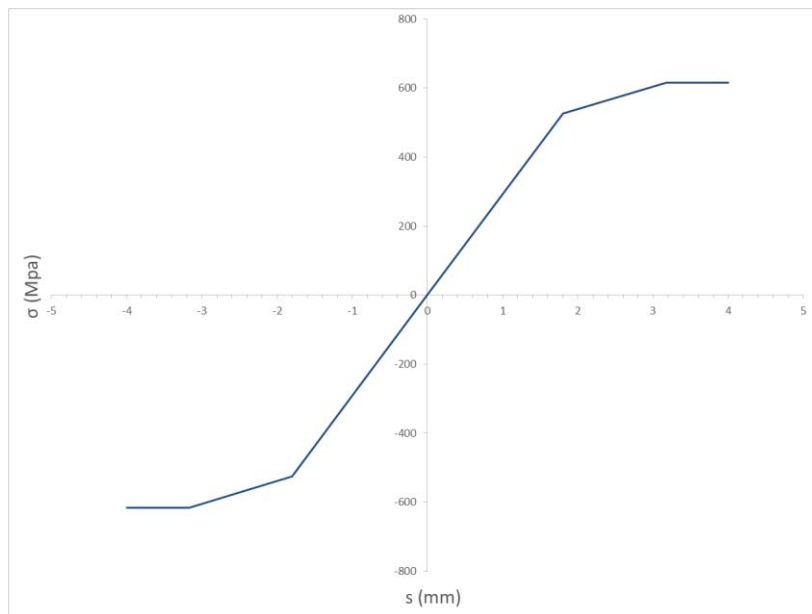


Figure 6.18: Pullout properties for connection hinge fibers in 1<sup>st</sup> floor columns (bare frame)

Unit	K1	K2	K3	S1C	S2C	S1T	S2T
$KN/m^3$	$2.92 \cdot 10^8$	1	0.01				
$Mpa$				467	468	467	468

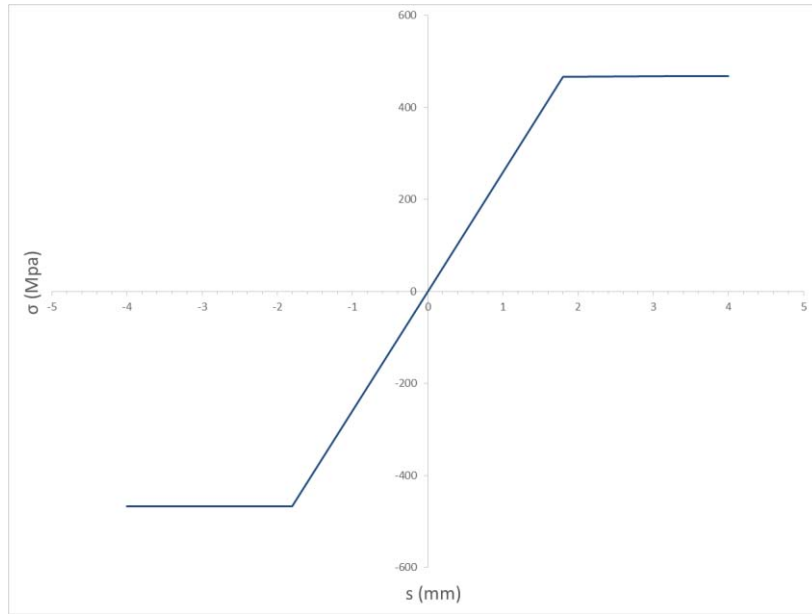
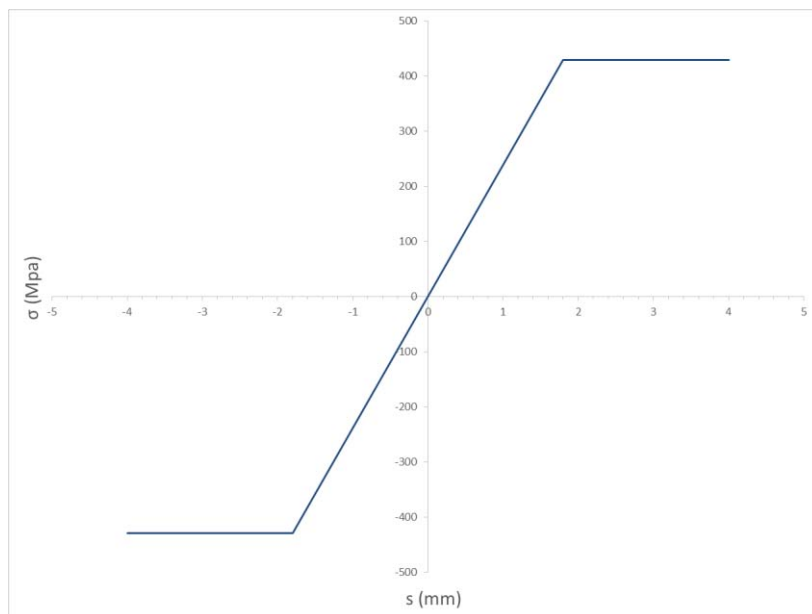


Figure 6.19: Pullout properties for connection hinge fibers in 1<sup>st</sup> floor beams (bare frame)

Unit	K1	K2	K3	S1C	S2C	S1T	S2T
$KN/m^3$	$2.92 \cdot 10^8$	1	0.01				
$Mpa$				428	429	428	429



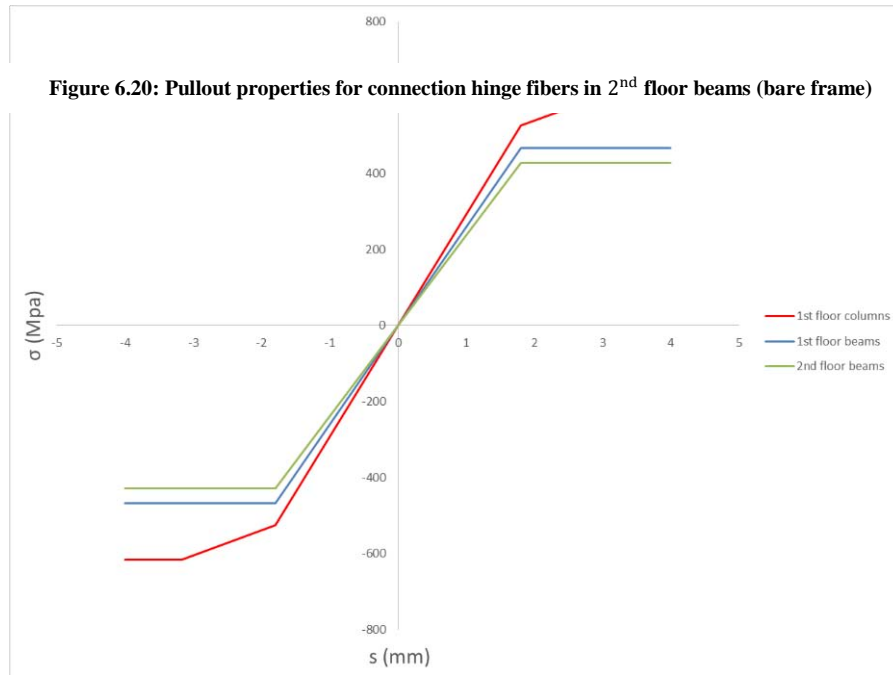


Figure 6.21: Comparison among pullout properties of the element in bare frame

SDF	SDTF	SCDF	ST	SC	PF	PSF	PPF
1	1	1	0.005	0.005	1	1	1

Table 6-8: Adopted degradation properties for both bare frame and CFRP retrofitted frame

### 6.9.1.2. Pullout fibers for CFRP retrofitted frame

Figures (6.23), (6.24), (6.25) show parameters  $K1$ ,  $K2$ ,  $K3$ ,  $S1T$ ,  $S2T$ ,  $S1C$ ,  $S2C$  and relative graphs  $\sigma = \sigma(s)$  for the elements of the CFRP retrofitted frame affected by bond-slip, as shown in figure (6.17). As for the bare frame, even in this case the elements were subjected to bad bond conditions, so elastic bar slip  $s_1$  is set to  $1.8 \text{ mm}$ . In this case, bond-slip of the reinforcing bars in the beam-column joints is activated later than in the bare frame. This is due to the improvement of the general conditions of the bars after CFRP confinement. Besides, before test sequence 4, it has been decided to improve the reinforcement resistance in Y-direction by welding horizontal bars to vertical ones in second level nodes, as shown in figure (6.22). In figure (6.26) a comparison among the pullout properties of the elements affected by bond-slip. This graph has the same characteristics of that of the bare frame. In fact, 2<sup>nd</sup> floor beams are the most affected by bond-slip.



Figure 6.22: Welding the bars in Y-direction before test sequence 4 (Garcia et al. 2012)

Unit	K1	K2	K3	S1C	S2C	S1T	S2T
$KN/m^3$	$2.92 \cdot 10^8$	$7.82 \cdot 10^7$	0.01				
$Mpa$				526	616	526	616

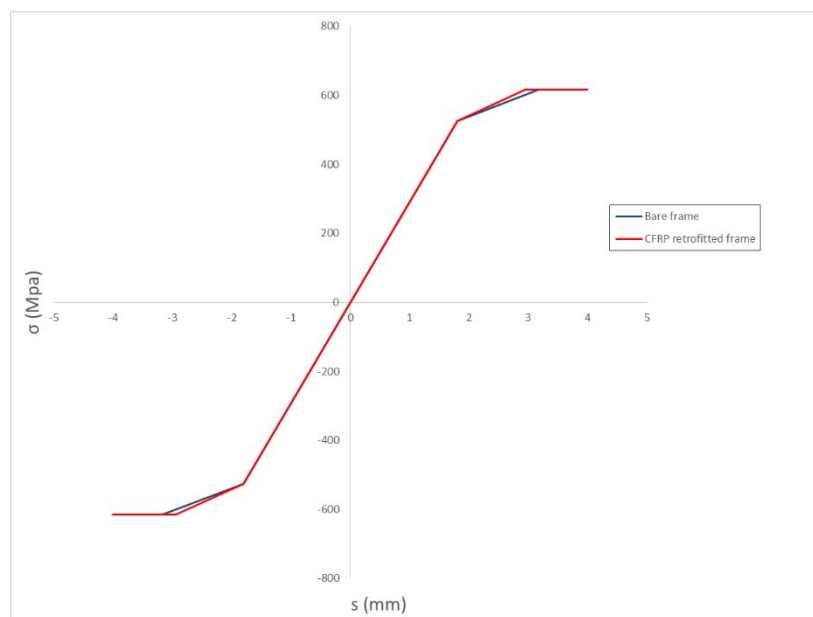


Figure 6.23: Pullout properties for connection hinge fibers in 1<sup>st</sup> floor columns (CFRP retrofitted frame)

Unit	K1	K2	K3	S1C	S2C	S1T	S2T
$KN/m^3$	$2.92 \cdot 10^8$	1	0.01				
$Mpa$				478	479	478	479

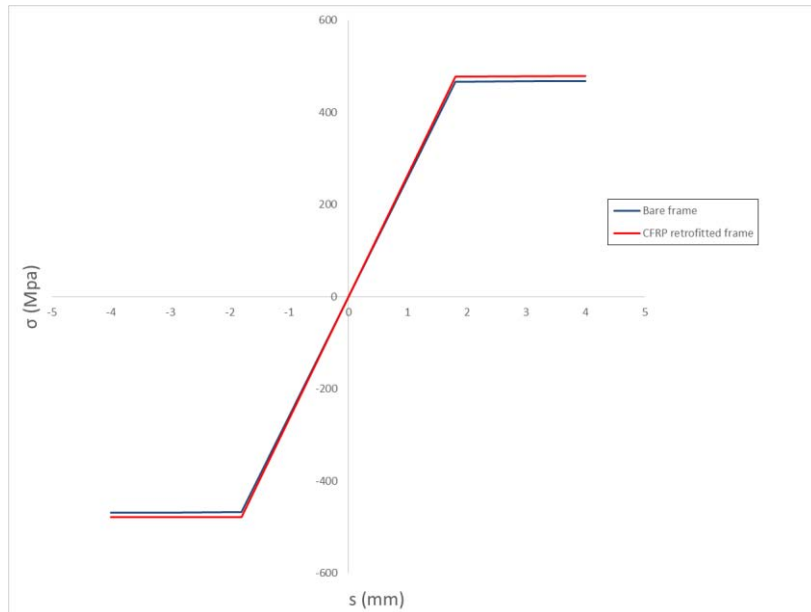


Figure 6.24: Pullout properties for connection hinge fibers in 1<sup>st</sup> floor beams (CFRP retrofitted frame)

Unit	K1	K2	K3	S1C	S2C	S1T	S2T
$KN/m^3$	$2.92 \cdot 10^8$	1	0.01				
$Mpa$				438	439	438	439

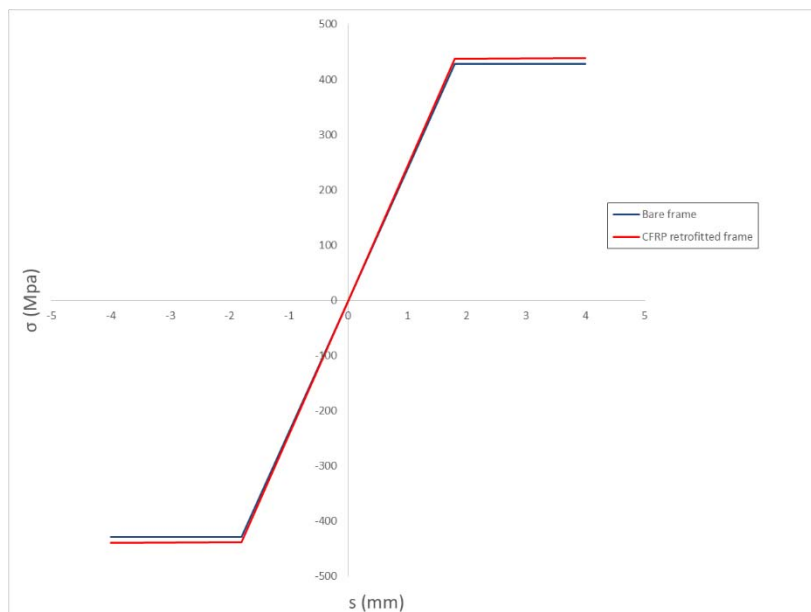


Figure 6.25: Pullout properties for connection hinge fibers in 2<sup>nd</sup> floor beams (CFRP retrofitted frame)

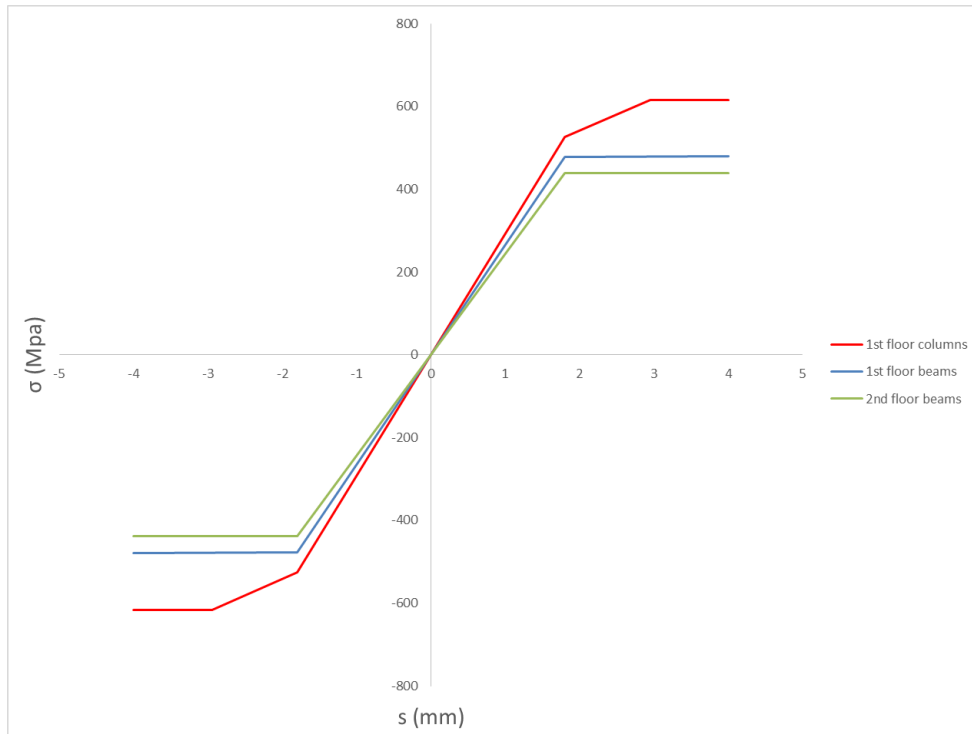


Figure 6.26: Comparison among pullout properties of the element in CFRP retrofitted frame

### 6.9.2. Gap fibers for bare frame and CFRP retrofitted frame

As reported in §5.6.2., gap fibers are used to simulate crack opening at the joint interface. Figure (6.27) shows the model for gap fibers used in both bare and CFRP retrofitted frame and table (6-9) illustrates the values of the adopted parameters.

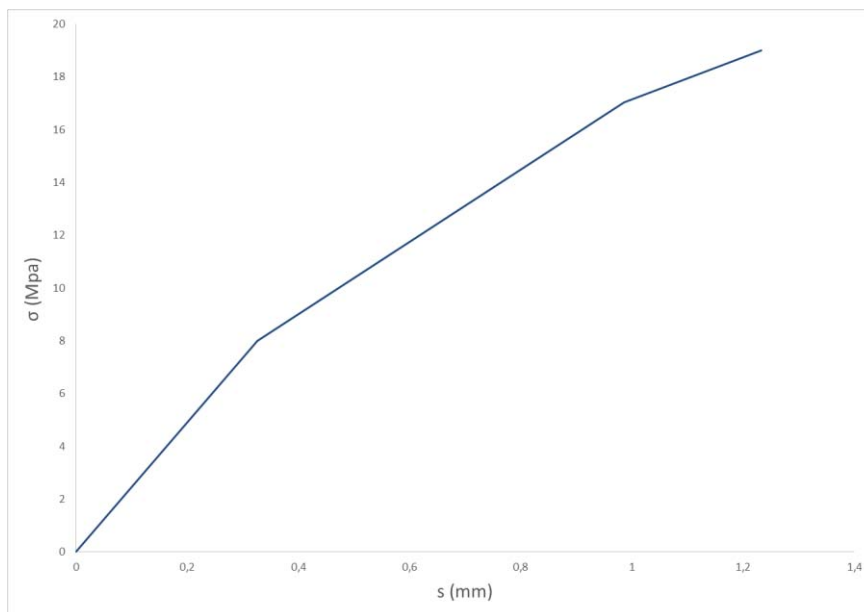


Figure 6.27: Gap properties for connection hinge fibers (bare frame and CFRP retrofitted frame)

Unit	K1	K2	K3	SC1	SC2	FU
$KN/m^3$	$2.45 \cdot 10^7$	$1.37 \cdot 10^7$	$7.95 \cdot 10^6$			
$Mpa$				8	17.033	
						0.5

Table 6-9: Gap fibers properties

## 6.10. Time-history analysis results

As the analysis has been performed based on the peak ground accelerations obtained from shake table tests, displacement time histories have been obtained for each level of test with varying PGA level. In the next paragraphs the time-history response is presented first for the bare frame and then for CFRP retrofitted frame under different PGA, as said in §3.8. Analytical results are compared with experimental results for nodes 2020 and 3020 in bare frame, and 2010 and 3010 in CFRP retrofitted frame.

### 6.10.1. Displacement time-history in test sequence 1

Figures (6.28) and (6.29) illustrate damages on bare frame before test sequence 1. No structural damages are clearly visible but there are only small cracks on the surface. The time-history input file for the bare frame can be found in Appendix D1.



Figure 6.28: 1<sup>st</sup> floor beam-column joint before test sequence 1 (Garcia et al. 2012)



Figure 6.29: 2<sup>nd</sup> floor beam-column joint before test sequence 1 (Garcia et al. 2012)

### 6.10.1.1. Response of the bare frame under 0.025g PGA

Figures (6.30) and (6.31) represent the Time-Displacement history response of the frame for 0.025g PGA. The response is presented for both nodes (2020 and 3020). As can be seen from the figures, overall the analytical results agree well with the experimental results, although generally providing a stiffer response. This can be expected, however, at low values of PGA when local non-linearities can already affect structural response but are difficult to capture numerically.

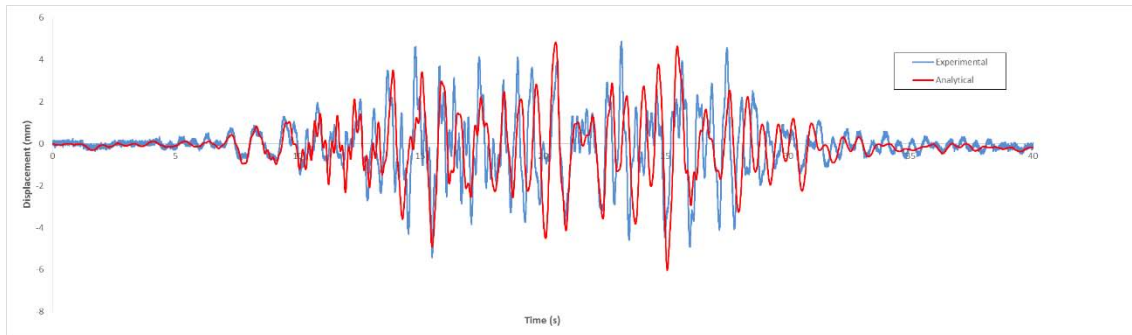


Figure 6.30: Displacement time-history for node 2020 under 0.025g PGA

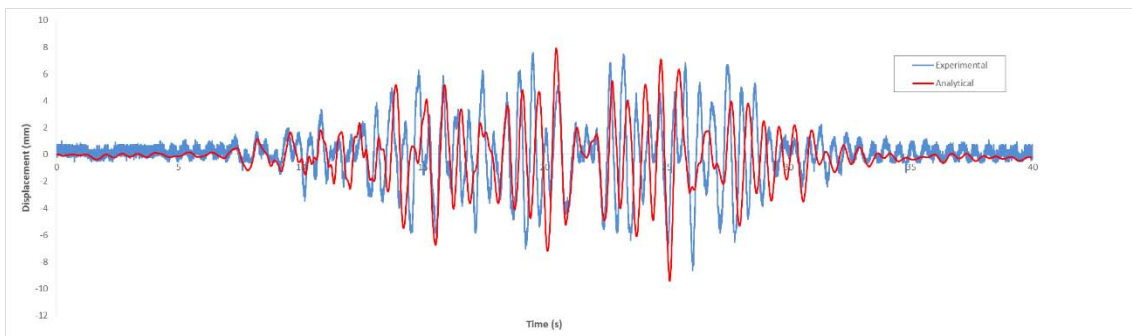
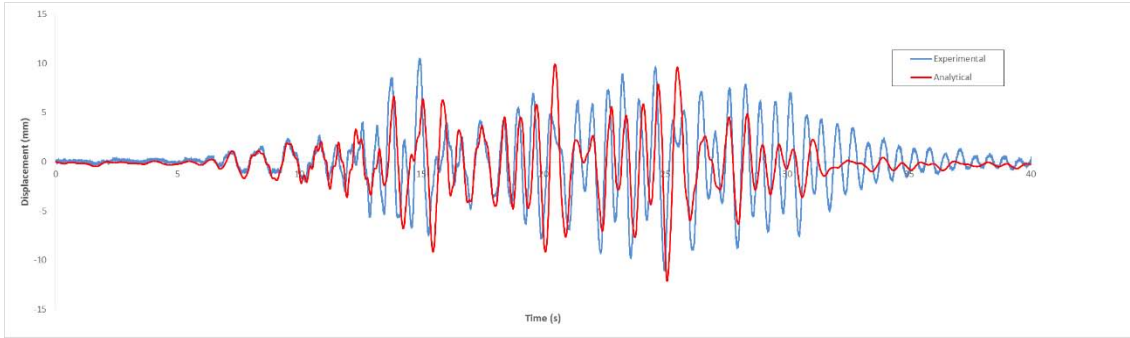


Figure 6.31: Displacement time-history for node 3020 under 0.025g PGA

### 6.10.1.2. Response of the bare frame under 0.05g PGA

Figures (6.32) and (6.33) represent the Time-Displacement history response of the frame for 0.05g PGA. In contrast to 0.025g, the analytical results agree with the experimental results at the beginning of the analysis. In the final part of the analysis, the experimental results for both nodes have a higher amplitude than the analytical results. The analytical frame seems to be stiffer than the real frame.





**Figure 6.32: Displacement time-history for node 2020 under 0.05g PGA**

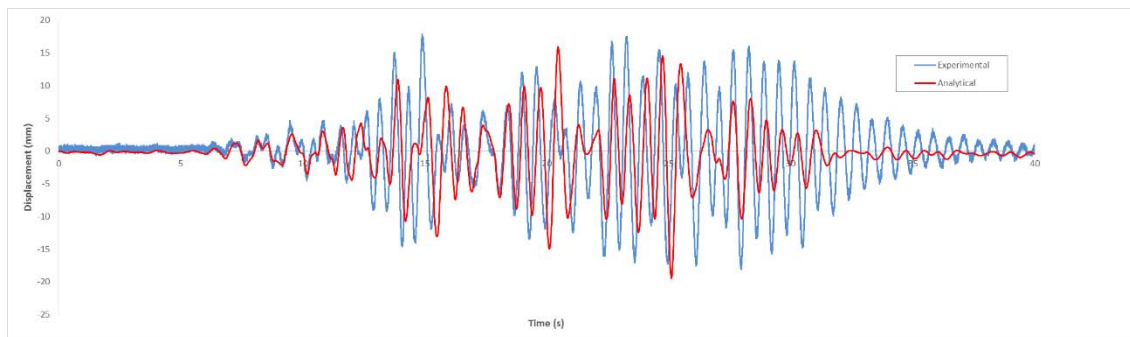


**Figure 6.33: Displacement time-history for node 3020 under 0.05g PGA**

### **6.10.1.3. Response of the bare frame under 0.10g PGA**

Figures (6.34) and (6.35) represent the Time-Displacement history response of the frame for 0.10g PGA. The analytical results are concurrent with the experimental results during the analysis. At some points, in particular in 2<sup>nd</sup> storey, the experimental response is higher than the analytical results. The analytical model is able to predict the global behaviour of the frame.

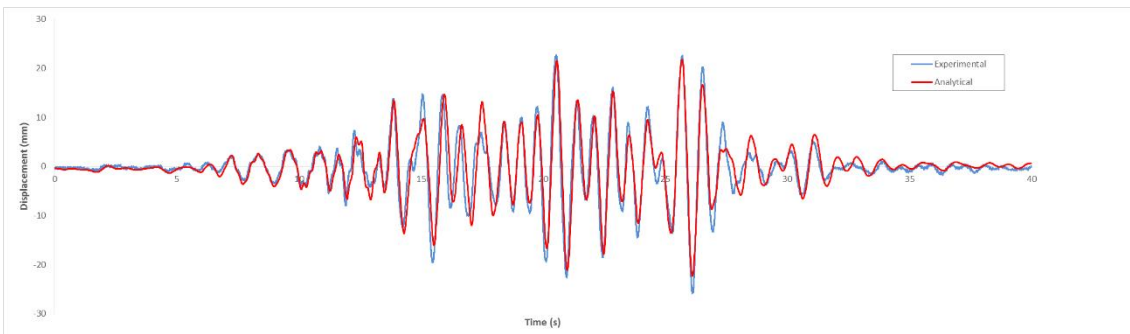


**Figure 6.34: Displacement time-history for node 2020 under 0.10g PGA**

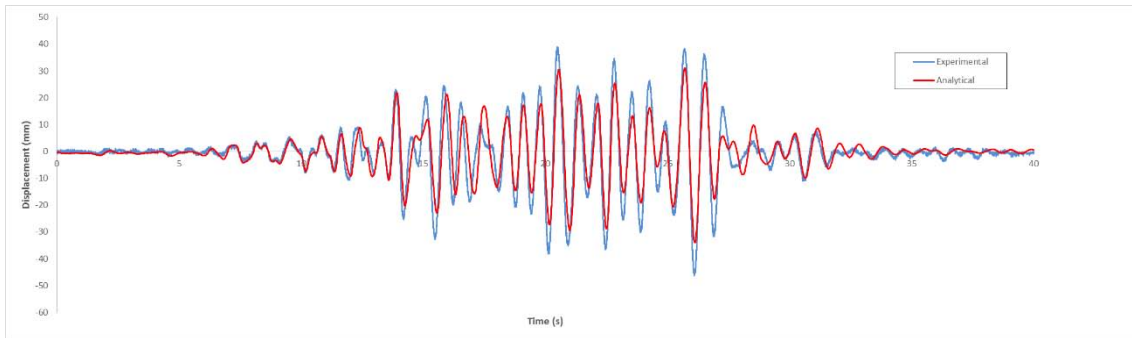


Figure 6.35: Displacement time-history for node 3020 under 0.10g PGA

#### 6.10.1.4. Response of the bare frame under 0.15g PGA

Figures (6.36) and (6.37) represent the Time-Displacement history response of the frame for 0.15g PGA. The analytical results compare well with the experimental results. As can be noticed from the figures, the analytical results do not always reach the peaks of the experimental results, especially for node 3020. On run 15 at 0.15g, about 22s after the test starting, the hydraulic system encountered a high frequency resonance due to oil column. After that time the experimental results were no longer reliable, so the results have been analysed only for 22s. After test sequence 1 damages were clearly visible in all the joints at both levels, but mainly in the second level joint. There, big cracks have opened and concrete was split. Figures (6.38) and (6.39) shows damages at joints after test sequence 1.

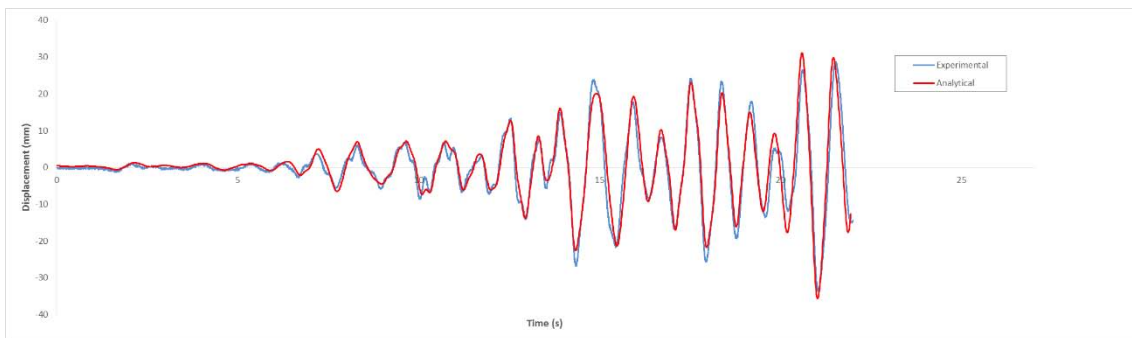


Figure 6.36: Displacement time-history for node 2020 under 0.15g PGA

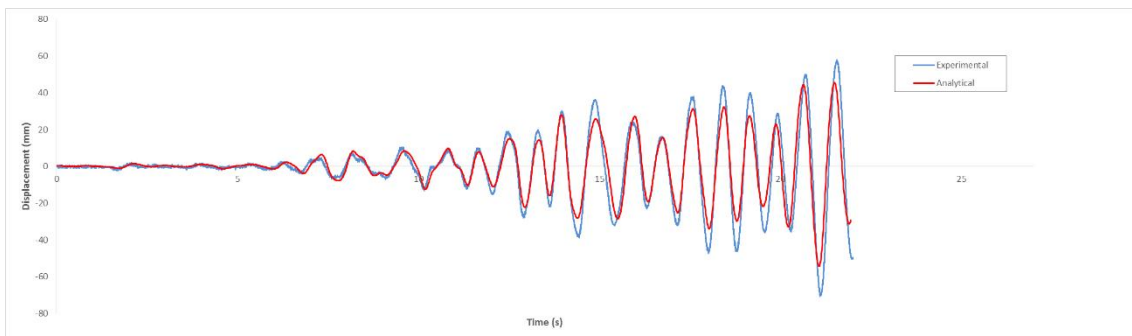


Figure 6.37: Displacement time-history for node 3020 under 0.15g PGA



Figure 6.38: 1<sup>st</sup> floor joint after test sequence 1 (Garcia et al. 2012)



Figure 6.39: 2<sup>nd</sup> floor joint after test sequence 1 (Garcia et al. 2012)

## 6.10.2. Displacement time-history in test sequence 4

Before the strengthening of the structure, the holes have been filled with grout and the crack system have been filled up with epoxy resin. After that, frame A has been strengthened with CFRP and then test sequence 4 has been performed. The results of the analysis are presented in the following paragraphs. The time-history input file for the CFRP retrofitted frame can be found in Appendix D2.

### 6.10.2.1. Response of the CFRP retrofitted frame under 0.05g PGA

The analytical and experimental displacement time-history for nodes 2010 and 3010 under 0.05g PGA are shown in figures (6.40) and (6.41) respectively. The analytical results are very close to the experimental results for both nodes but do not reach the peaks, especially for node 2010. This means that the model is stiffer than the actual frame.

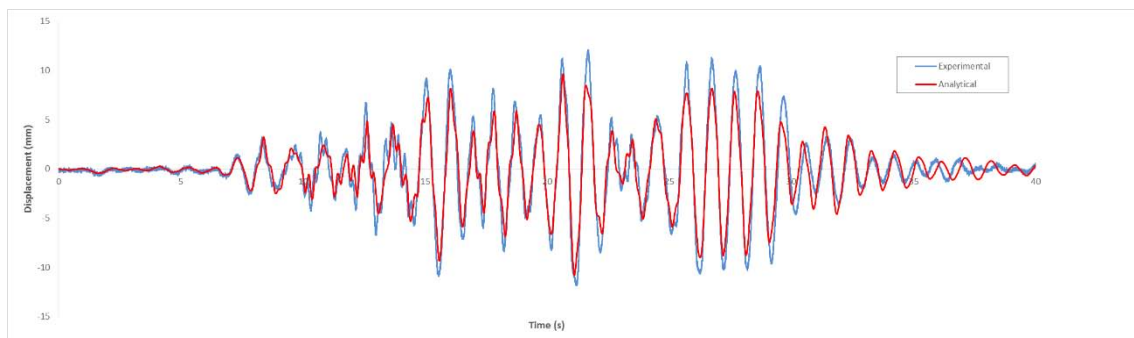


Figure 6.40: Displacement time-history for node 2010 under 0.05g PGA

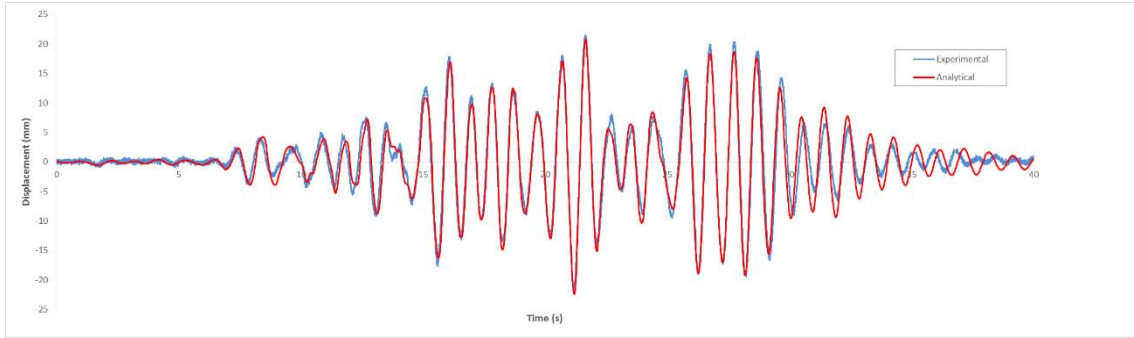


Figure 6.41: Displacement time-history for node 3010 under 0.05g PGA

### 6.10.2.2. Response of the CFRP retrofitted frame under 0.10g PGA

The analytical and experimental displacement time-history for nodes 2010 and 3010 under 0.10g PGA are shown in figures (6.42) and (6.43) respectively. As can be seen from the figures, the analytical results are almost identical to the experimental results. As in the previous frame, peaks values are not reached by the analytical results, especially for node 2010 but the differences are very low.

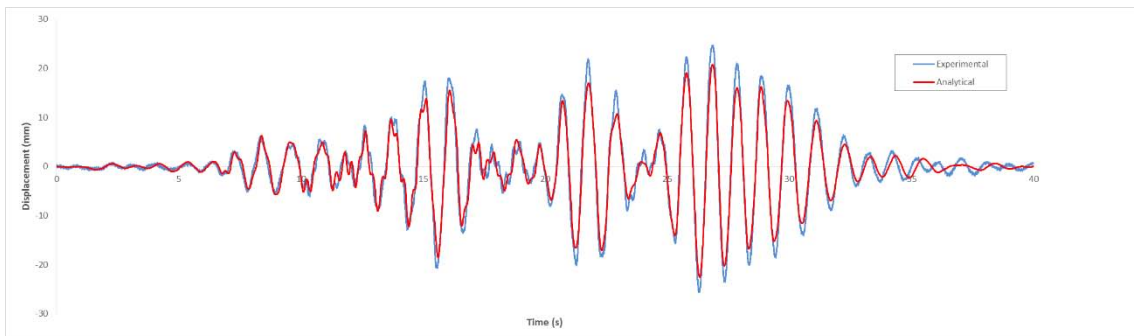


Figure 6.42: Displacement time-history for node 2010 under 0.10g PGA

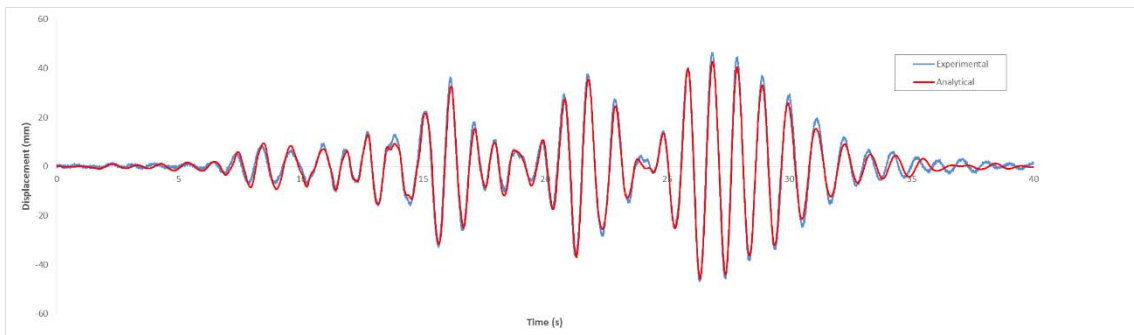


Figure 6.43: Displacement time-history for node 3010 under 0.10g PGA

### 6.10.2.3. Response of the CFRP retrofitted frame under 0.20g PGA

The analytical and experimental displacement time-history for nodes 2010 and 3010 under 0.20g PGA are shown in figures (6.44) and (6.45) respectively. As it can be seen from the graphs, the analytical results are very close to the experimental ones for both storeys.

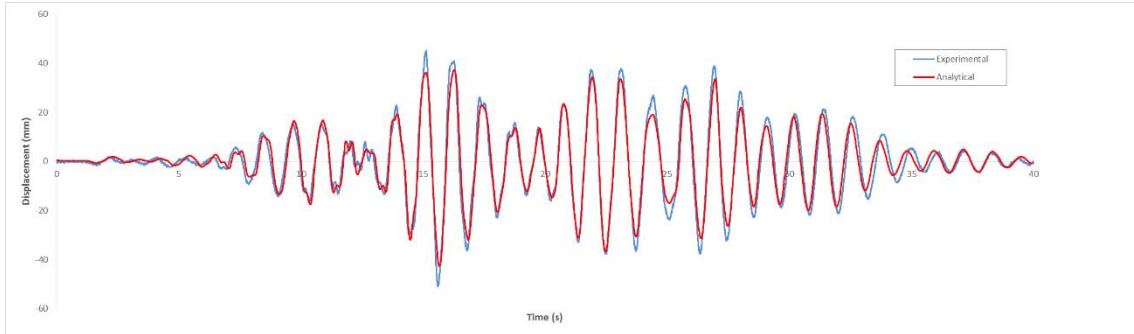


Figure 6.44: Displacement time-history for node 2010 under 0.20g PGA

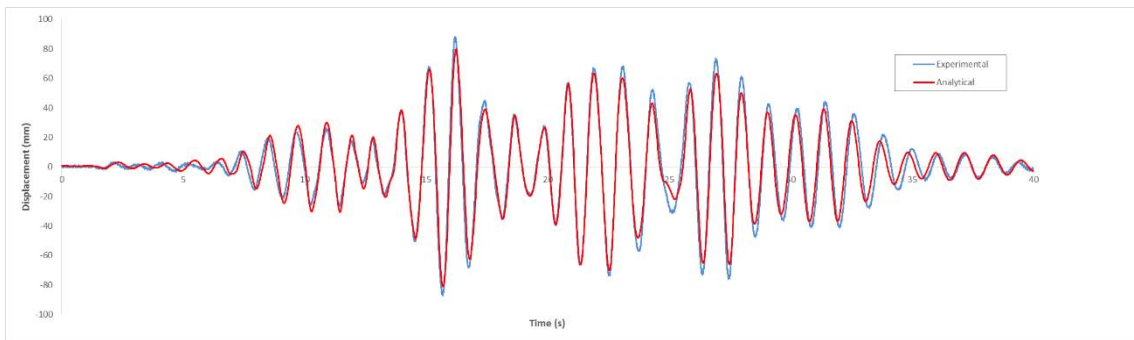


Figure 6.45: Displacement time-history for node 3010 under 0.20g PGA

### 6.10.2.4. Response of the CFRP retrofitted frame under 0.30g PGA

Comparisons between the analytical and experimental results for nodes 2010 and 3010 under 0.30g PGA can be seen in figures (6.46) and (6.47) respectively. Here too, the analytical results are very close to the experimental results.

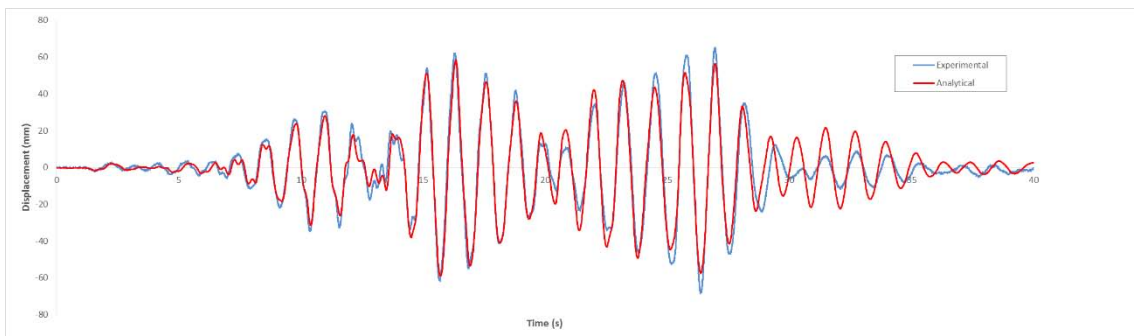


Figure 6.46: Displacement time-history for node 2010 under 0.30g PGA

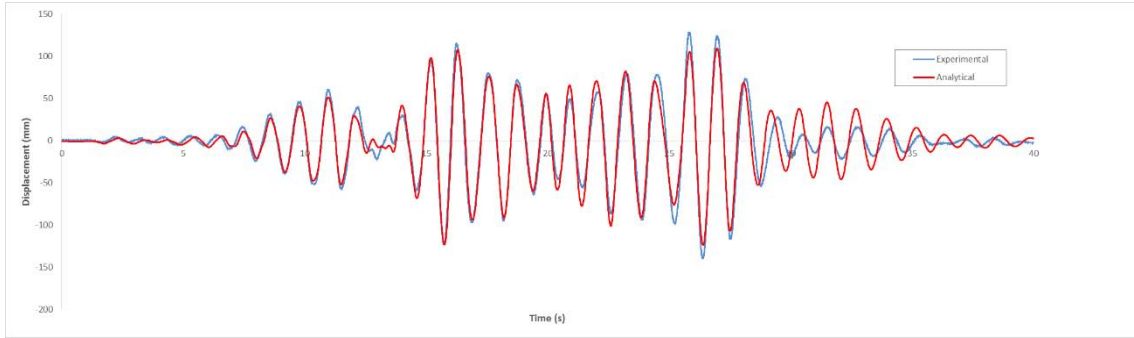


Figure 6.47: Displacement time-history for node 3010 under 0.30g PGA

### 6.10.2.5. Response of the CFRP retrofitted frame under 0.35g PGA

Figures (6.48) and (6.49) below show the analytical and experimental time-history results of first storey and roof displacements at 0.35g PGA. The analytical results are close to the experimental results for both nodes but peaks are not reached by the analytical results. The differences are very low. During this test sequence, all the retrofitting materials remains sound and in place. The damages in the concrete were hidden by the strengthening materials.

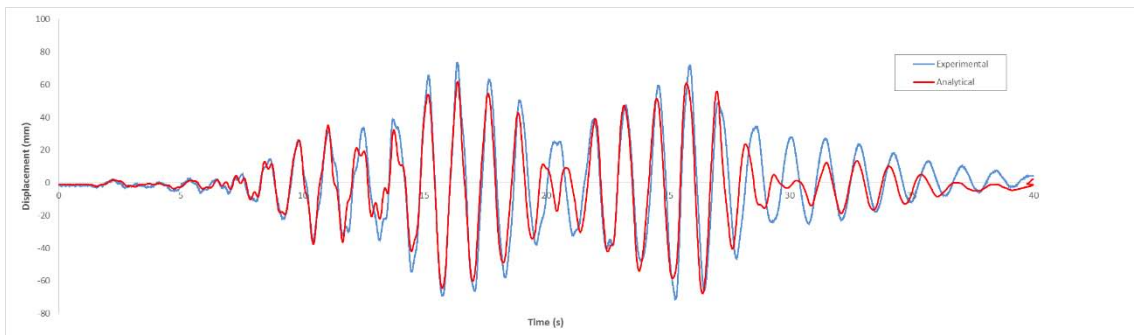


Figure 6.48: Displacement time-history for node 2010 under 0.35g PGA

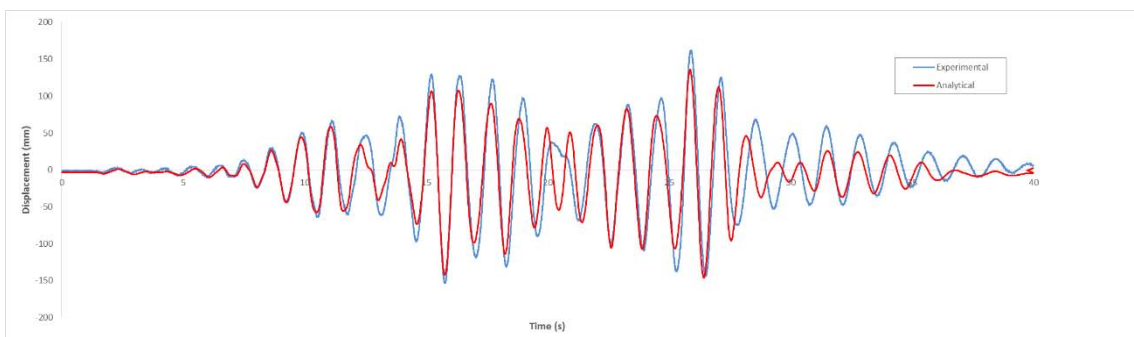


Figure 6.49: Displacement time-history for node 3010 under 0.35g PGA

### 6.11. Analytical and experimental comparisons in terms of period modes

The comparison of the analytical time-history analyses results and the experimental tests suggests that the analysis technique adopted is very satisfactory and thus, DRAIN-3DX analyses can be performed to examine the seismic behaviour of RC frames strengthened with FRP. The following tables (6-10) and (6-11) contain the analytical results of first and second period modes obtained from the seismic excitations at PGA levels from 0.025g to 0.15g on the bare frame and from 0.05g on 0.35g in the CFRP reinforced frame. These values are compared with the experimental period modes measured during the tests.

<b>Test sequence 1</b>				
<b>Condition</b>	<b>Analytical results (X-direction)</b>		<b>Experimental values (X-direction)</b>	
	First mode (s)	Second mode (s)	First mode (s)	Second mode (s)
Undamaged	0.58	0.21	0.48	0.18
After 0.025g	0.67	0.24	0.53	0.20
After 0.05g	0.76	0.26	0.60	0.22
After 0.10g	0.79	0.28	0.68	0.25
After 0.15g	0.86	0.30	0.88	0.29

**Table 6-10: Comparison of modal periods from analytical results during test sequence 1**

<b>Test sequence 4</b>				
<b>Condition</b>	<b>Analytical results (Y-direction)</b>		<b>Experimental values (Y-direction)</b>	
	First mode (s)	Second mode (s)	First mode (s)	Second mode (s)
Damaged	0.78	0.25	0.84	0.25
After 0.05g	0.97	0.31	0.88	0.25
After 0.10g	1.10	0.35	0.93	0.27
After 0.20g	1.12	0.35	0.99	0.28
After 0.30g	1.21	0.36	1.03	0.29
After 0.35g	1.26	0.39	1.11	0.30

**Table 6-11: Comparison of modal periods from analytical results during test sequence 4**

## 7. FEASIBILITY OF THE INTERVENTION

---

### 7.1. Introduction

In order to evaluate the feasibility of the intervention, it is possible to compare this intervention with the building of a new structure, with reference to resistance and also economic aspects.

First of all it is necessary to examine the earthquake resistance of the frame retrofitted with CFRP, with reference to the current seismic norms (EC8, NTC 2008). The BANDIT frame retrofitted with CFRP has been able to withstand an earthquake of 0.35g PGA without huge damages, in fact all the retrofitting materials remained sound and in place after the tests. In order to compare this technique with the building of a new structure, it is necessary to consider where the structure could be erected. In this case, for the reasons that will be explained in the next paragraph, the new structure is designed to be built in Treviso (Italy). According with new criteria for seismic classification published in 2003 and then updated, Treviso is situated in zone 3 (municipalities in this area may be subject to modest shock). Accelerations with probability of exceedance equal to 10% in 50 years ( $ag$ ) in seismic zone 3 are  $0.05 < ag \leq 0.15$ . The new structure is designed to maintain the same geometry and materials of the BANDIT specimen, but it must comply with current seismic codes. Longitudinal and transversal reinforcement are redesigned to include appropriate detailing, such as adequate shear link distribution, confinement of the nodes, anchorage lengths. Dynamic Time-History analysis of the new frame is performed through DRAIN-3DX and the results are compared to those of the frame retrofitted with CFRP, in order to evaluate the behaviour of the frame under seismic loads. Finally, an estimate of costs is performed for CFRP retrofitting and the building of the new frame, so as to evaluate the convenience of the intervention.

### 7.2. Damage limitation for CFRP retrofitted frame

According to EC8 and also NTC 2008, the “damage limitation requirement” is considered to have been satisfied. In the case of RC building, EC8 and NCT 2008 provide some damage limitations. Assuming importance class II for this structure, EC8 provides a limitation of interstorey drift based on the damage limitation state considered. On the basis of NTC 2008 and the Circolare esplicativa n.617 of 02/02/2009, damage limitation has to be considered for both the damage limit state (SLD) and operability limit state (SLO).

The following limits shall be observed for RC structures without non-structural elements:

- $d_r \cdot v \leq 0.010 \cdot h$  (SLD)
- $d_r \cdot v \leq \frac{2}{3} \cdot 0.010 \cdot h$  (SLO)

Where  $d_r$  is the design interstorey drift, evaluated as the difference of the average lateral displacements  $d_s$  at the top and bottom of the storey under consideration;  $v$  is the reduction factor which takes into account the lower return of period of the



seismic action associated with the damage limitation requirement. According with norm n.617 of 02/02/2009 and EC8, the value of the reduction  $v$  is equal to 0.5 for importance classes II. The parameter  $h$  is the storey height (equal to 3.3 m). Table (7-1) shows the damage limitation requirement for the CFRP retrofitted frame under some of the PGA levels investigated during the tests.

PGA level	First storey $d_r \cdot v$ (mm)	Second storey $d_r \cdot v$ (mm)	SLO damage limitation (mm)	SLD damage limitation (mm)
0.05g	5.55	5.46	22	33
0.10g	12.61	11.88		
0.15g	15.59	14.94		
0.20g	21.26	24.08		
0.30g	35.59	34.34		
0.35g	38.06	45.25		

Table 7-1: Damage limitation requirement for CFRP retrofitted frame

As can be seen in the table, the CFRP retrofitted frame is able to comply with the norms up to a seismic level of 0.15g, which corresponds to a seismic zone 3. For this reason, the retrofitted frame can be situated in Treviso.

### 7.3. New earthquake-proof structure design

#### 7.3.1. Design criteria and structural type

The new structure is designed to be built in Treviso, in seismic zone 3 ( $0.05 < ag \leq 0.15$ ). According with §7.1 of NCT 2008, the structure comply with all the limit-state design principles when damage limit state (SLD) and life safety limit state (SLV) are checked. Modal response spectrum analysis (linear dynamic) is applied to this building, according with §7.8.1.5.3 of NTC 2008. Straus 7 is the finite element programme used to perform the analysis. Solver capabilities in Straus 7 include: linear and non-linear static analysis; linear and non-linear transient dynamic analysis; linear buckling analysis; natural frequency; harmonic response; spectral response. This software has a graphic interface. The pre-processing environment includes a set of tools for manipulating both geometry and the elements. All element types can be fully rendered to aid in the visualisation of the model. The post-processing environment has been designed to allow easy extraction of the results: graphically on the screen, in spreadsheet format and in printed report form. As has been said, the new structure is designed to be built in Treviso. The ground type is B, characterised by deposit of very dense sand, gravel, or very stiff clay, at least several tens of metres in thickness, characterised by a gradual increase of mechanical properties with depth. The topographic category is T1, characterised by low incline slope (less than  $15^\circ$ ). The structure is a framed RC building and it is regular in plan and in elevation. The hysteretic dissipation capacity is low, therefore the ductility class chosen for the new structure is DCM (medium ductility). The building is dimensioned and detailed in accordance with specific earthquake resistant provisions, enabling the structure to develop stable mechanisms associated

with large dissipation of hysteretic energy under repeated reversed loading, without suffering brittle failures. According with §7.4.3.2 of NCT 2008, the behaviour factor is 3.6, in fact the structural type is a two-storey one bay frame system.

### 7.3.2. Modal response spectrum analysis with Straus 7

The design ground acceleration is considered only for horizontal direction, because the transversal component can be neglected, according with §7.2.1 of NCT 2008. In order to design and detailing the elements of the structure, only the life safety limit state (SLV) is considered. The inelastic horizontal ground acceleration response spectrum, also called “inelastic response spectrum”, is evaluated according with §3.2.3.2 of NCT 2008 through the programme Spettri-NTCver.1.0.3 and the results are shown in figures (7.1), (7.2), (7.3).



Figure 7.1: Identification of the site danger with Spettri-NTCver 1.0.03

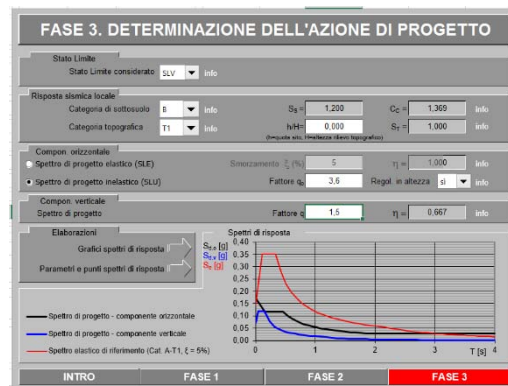


Figure 7.2: Identification of the design action with Spettri-NTCver 1.0.03

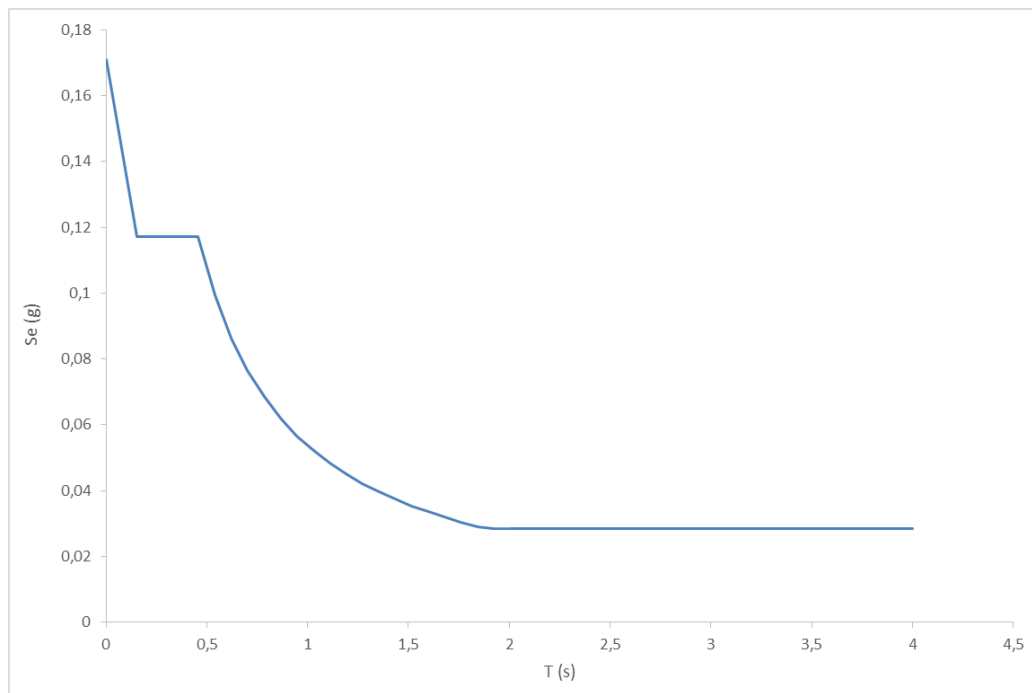


Figure 7.3: Inelastic response spectrum with Spettri-NTCver 1.0.03

$T_B = 0.153s$  is the lower limit of the period of the constant spectral acceleration branch.  $T_C = 0.458s$  is the upper limit of the period of the constant spectral acceleration branch.  $T_D = 2.170s$  is the value defining the beginning of the constant displacement response range of the spectrum. The frame is modelled in Straus 7 with beams and plates, as shown in figure (7.4).

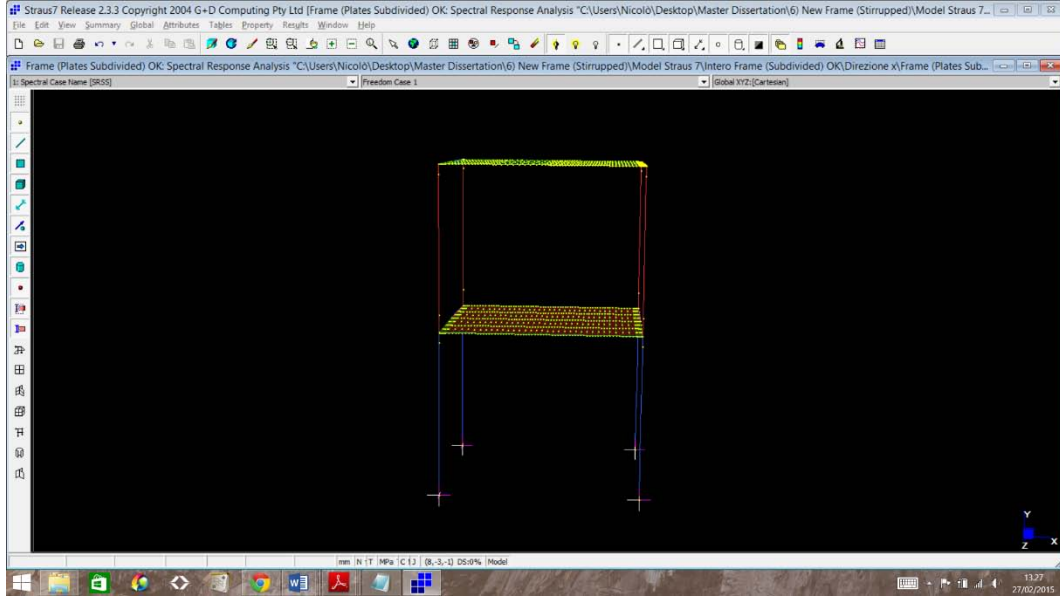


Figure 7.4: New frame implemented in Straus 7

The combination of the seismic action with other actions used in seismic analysis is given below:

$$E + G_1 + G_2 + P + \psi_{21} \cdot Q_{k1} + \psi_{22} \cdot Q_{k2} + \dots$$

Where  $\psi_{2i} = 0.3$  is the combination coefficient for the quasi-permanent value of a variable action  $i$ . The effects of actions in the structure are determined in accordance with §7.3.5 of NTC 2008 through the following expression:

$$1.00 \cdot E_x + 0.30 \cdot E_y + 0.30 \cdot E_z$$

The results of the analysis in terms of design action effects for each element are shown in tables (7-2). The sign “-“ means compressive axial force, instead sign “+” means tensile axial force.

Element	Storey	$N_{Ed}$ (compressive, KN)	$N_{Ed}$ (tensile KN)	$T_{Ed}$ (plane 1, KN)	$T_{Ed}$ (plane 2, KN)	$M_{Ed}$ (plane 1, KNm)	$M_{Ed}$ (plane 2, KNm)
Column	1	-89.73	-84.46	5.12	13.58	12.10	33.14
Column	2	-46.08	-40.83	5.76	11.35	9.44	19.70

Beam 300	1	+1.20	+1.20	0.013	5.33	0.045	7.92
Beam 300	2	-0.27	-0.27	0.019	4.40	0.044	5.83
Beam 400	1	+0.91	+4.37	0.94	60.93	0.08	30.59
Beam 400	2	-0.40	+1.70	1.49	43.99	0.14	17.22

Table 7-2: Design action effects for each element of the frame

### 7.3.3. Design and detailing of beams and columns

The geometry and the dimensions of the elements are kept the same as for the BANDIT frame. Longitudinal and transversal reinforcement are checked in order to satisfy the actual seismic provisions. The concrete cover thickness is increased to 25 mm. According with §7.4.6.1.2 of NCT 2008, the critical region length for columns is 550 mm. Critical regions are present at both ends of the columns. The length of critical region for the beams (300 · 260) are 300 mm, instead the length for the beams (400 · 260) are 400 mm, in accordance with §7.4.6.1.1 of NCT 2008. The cross-section of beams and columns of the new frame are shown in figures (7.5) ÷ (7.8). The disposition of the longitudinal and transversal reinforcement in the structure is shown in figures (7.9), (7.10). In contrast with the bare frame, in this new frame there are adequate anchorage length for beam and column ends ( $l_{anc} > 60 \cdot \Phi_t = 840 \text{ mm}$ ). Additional measures for anchorage are taken, in fact at the bottom of longitudinal bars of both transversal and horizontal elements there are hooks, so as to improve the adherence between concrete and bars. According with §7.4.6.2 of NCT 2008, stirrups of both beams and columns are closed with 135° hooks and extensions of length  $10 \cdot \phi_t$  are used.

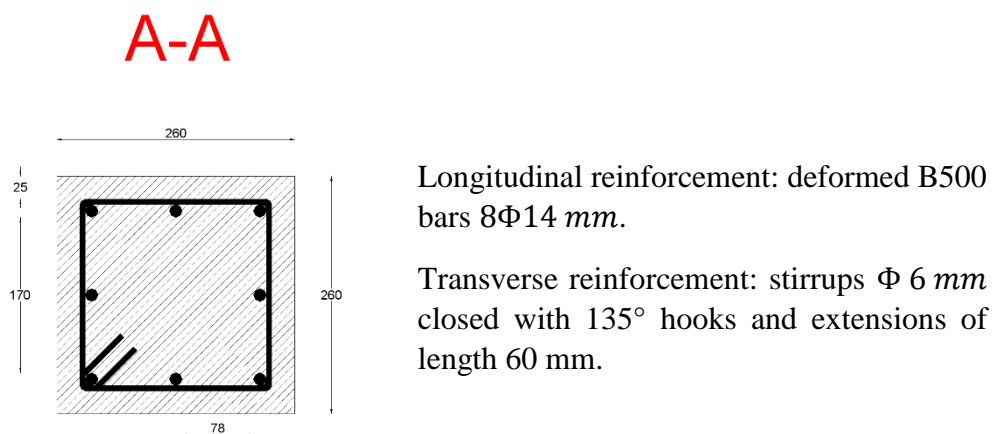
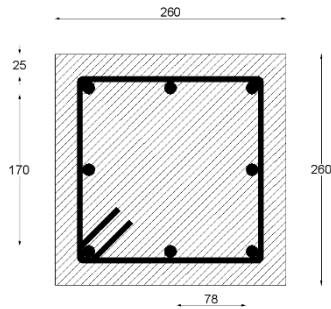


Figure 7.5: Cross-section of first-storey columns

## B-B

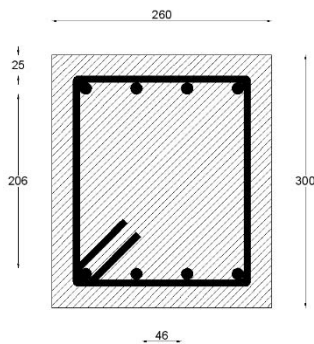


Longitudinal reinforcement: deformed B500 bars  $8\Phi 14 \text{ mm}$ .

Transverse reinforcement: stirrups  $\Phi 6 \text{ mm}$  closed with  $135^\circ$  hooks and extensions of length 60 mm.

Figure 7.6: Cross-section of second-storey columns

## C-C

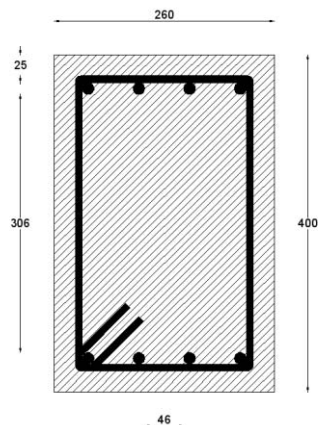


Longitudinal reinforcement: deformed B500 bars  $8\Phi 14 \text{ mm}$ .

Transverse reinforcement: stirrups  $\Phi 8 \text{ mm}$  closed with  $135^\circ$  hooks and extensions of length 80 mm.

Figure 7.7: Cross-section of beams (300 · 260)

## D-D



Longitudinal reinforcement: deformed B500 bars  $8\Phi 14 \text{ mm}$ .

Transverse reinforcement: stirrups  $\Phi 8 \text{ mm}$  closed with  $135^\circ$  hooks and extensions of length 80 mm.

Figure 7.8: Cross-section of beams (400 · 260)

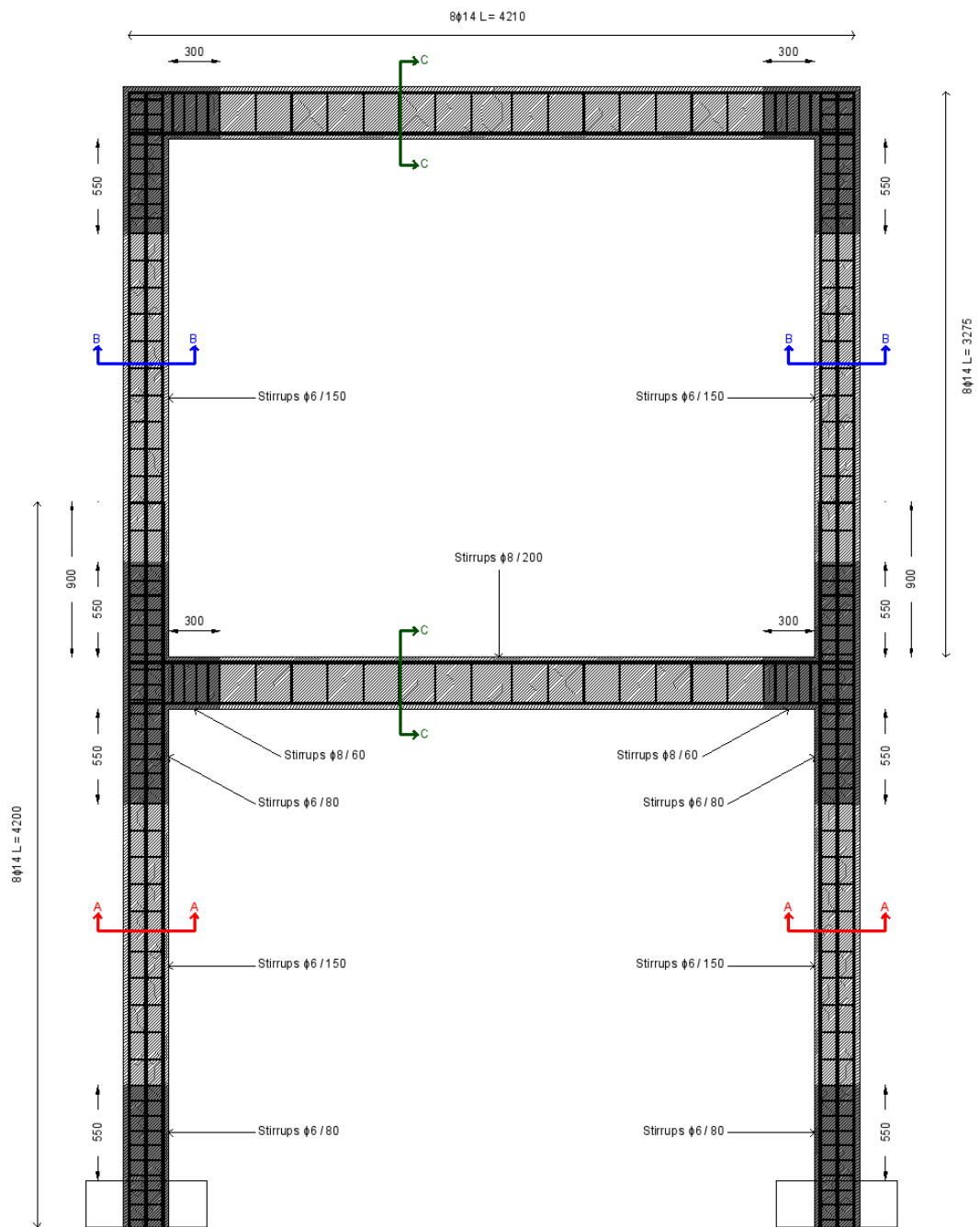


Figure 7.9: Longitudinal and transversal reinforcement in the frame (beams 300 · 260)

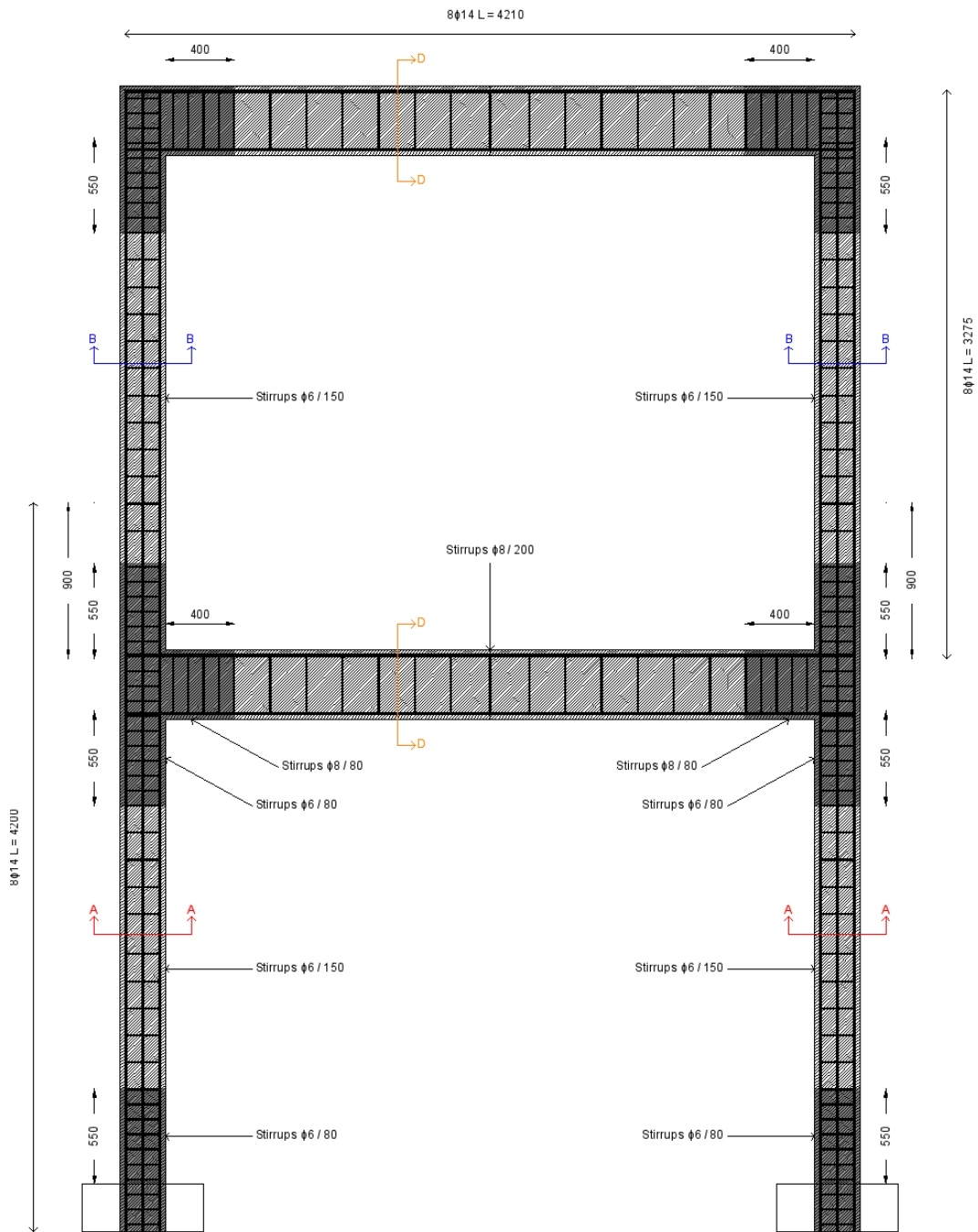


Figure 7.10: Longitudinal and transversal reinforcement in the frame (beams 400 · 260)

### 7.3.3.1. Geometrical and reinforcement constraints for columns

According with §4.1.6, §7.4.6 of NCT 2008, and §9.5.1 of EC 2, there are some geometrical provisions and reinforcement limitations for the columns. The length of the critical region for the columns is 550 mm. The minimum cross-sectional dimension of primary seismic columns has to be not less than 250 mm. The minimum diameter of the longitudinal rebars is 12 mm and the spacing of longitudinal bars cannot exceed 250 mm for seismic resistant elements. The longitudinal reinforcement ratio is 1.82%, inside the limits (minimum 1% and maximum 4%). The total area of the longitudinal reinforcement is  $1231.5 \text{ mm}^2$ , inside the limits (maximum  $2704 \text{ mm}^2$  outside the overlapping region and  $5408 \text{ mm}^2$  in the overlapping region). The minimum diameter of the stirrups is 6 mm. The spacing of confining hoops outside the critical region cannot exceed 168 mm and in the critical region this distance is reduced to 112 mm. The minimum amount of stirrups is 0.71 mm, larger than the limit 0.58 mm.

### 7.3.3.2. Geometrical and reinforcement constraints for beams

According with §4.1.6 and §7.4.6 of NCT 2008, there are some geometrical provisions and reinforcement limitations also for the beams. The length of the critical region for the beams (300 · 260) is 300 mm, but the for the (400 · 260) is 400 mm. The minimum cross-sectional dimension of beams has to be at least 200 mm. The height-to-width ratio ( $h/b$ ) of the beams has to be less than 4. The total area of the longitudinal reinforcement is  $1231.5 \text{ mm}^2$ , inside the limits (maximum  $3120 \text{ mm}^2$  for the beams (300 · 260) and  $4160 \text{ mm}^2$  for the beams (400 · 260) outside the overlapping region). The part of beam longitudinal reinforcement bent in joints for anchorage is placed inside the corresponding column hoops. The minimum anchorage length of longitudinal rebars is 150 mm. The spacing of confining hoops outside the critical region cannot exceed 220 mm for beams (300 · 260) and 300 mm for beams (400 · 260). Inside the critical region this distance is reduced to 69 mm for beams (300 · 260) and 94 mm for beams (400 · 260). The reinforcement ratio of stirrups (for each meter) is 1675.5 mm for beams (300 · 260) and 1256.6 mm for beams (400 · 260), larger than the lower limit 390 mm. Stirrups have to be closed with  $135^\circ$  hooks and extensions of length  $10 \cdot \phi_t$  have to be used.

### 7.3.4. Design resistance of the elements

Figures (7.11) ÷ (7.16) and tables (7-3) ÷ (7-8) show the interaction domains M-N of the elements, the design bending moment capacity, and the resistance to design shear forces. These parameters are referred to design action effects on table (7-2).



## First-storey columns

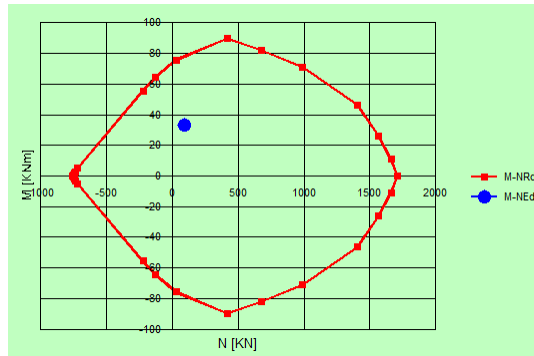


Figure 7.11: Interaction domain M-N for 1<sup>st</sup> floor columns

Bending moment capacity	Inside the critical region			Outside the critical region		
$M_u$ (KNm)	$\Phi_s$ (mm)	$s$ (mm)	$V_{Rd}$ (KN)	$\Phi_s$ (mm)	$s$ (mm)	$V_{Rd}$ (KN)
78.32	6	80	74.62	6	150	39.80

Table 7-3: Design bending moment capacity and shear resistance for 1<sup>st</sup> floor columns

## Second-storey columns

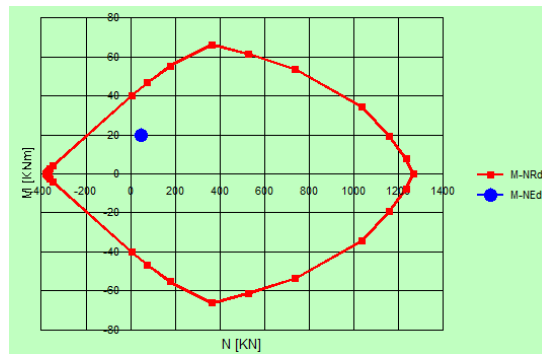


Figure 7.12: Interaction domain M-N for 2<sup>nd</sup> floor columns

Bending moment capacity	Inside the critical region			Outside the critical region		
$M_u$ (KNm)	$\Phi_s$ (mm)	$s$ (mm)	$V_{Rd}$ (KN)	$\Phi_s$ (mm)	$s$ (mm)	$V_{Rd}$ (KN)
44.07	6	80	74.62	6	150	39.80

Table 7-4: Design bending moment capacity and shear resistance for 2<sup>nd</sup> floor columns

### First-storey beams (300 · 260)

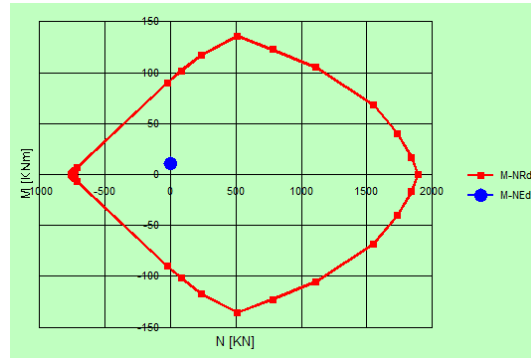


Figure 7.13: Interaction domain M-N for 1<sup>st</sup> floor beams (300 · 260)

Bending moment capacity	Inside the critical region			Outside the critical region		
	$M_u$ (KNm)	$\Phi_s$ (mm)	$s$ (mm)	$V_{Rd}$ (KN)	$\Phi_s$ (mm)	$s$ (mm)
92.57	8	60	196.17	8	200	58.85

Table 7-5: Design bending moment capacity and shear resistance for 1<sup>st</sup> floor beams (300 · 260)

### Second-storey beams (300 · 260)

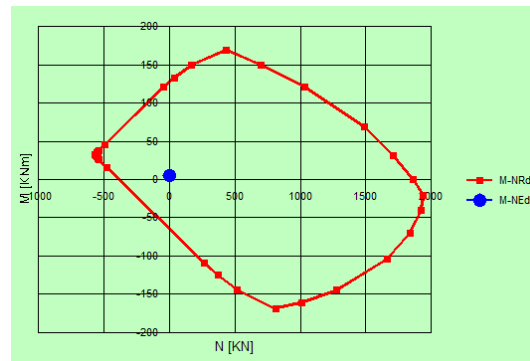


Figure 7.14: Interaction domain M-N for 2<sup>nd</sup> floor beams (300 · 260)

Bending moment capacity	Inside the critical region			Outside the critical region		
	$M_u$ (KNm)	$\Phi_s$ (mm)	$s$ (mm)	$V_{Rd}$ (KN)	$\Phi_s$ (mm)	$s$ (mm)
128.6	8	60	196.17	8	200	58.85

Table 7-6: Design bending moment capacity and shear resistance for 2<sup>nd</sup> floor beams (300 · 260)

### First-storey beams (400 · 260)

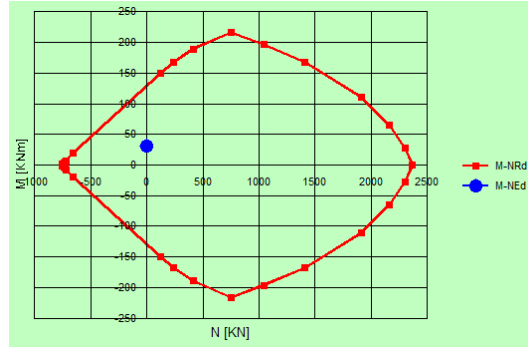


Figure 7.15: Interaction domain M-N for 1<sup>st</sup> floor beams (400 · 260)

Bending moment capacity	Inside the critical region			Outside the critical region		
	$M_u$ (KNm)	$\Phi_s$ (mm)	$s$ (mm)	$V_{Rd}$ (KN)	$\Phi_s$ (mm)	$s$ (mm)
130	8	80	200.62	8	250	64.20

Table 7-7: Design bending moment capacity and shear resistance for 1<sup>st</sup> floor beams (400 · 260)

### Second-storey beams (400 · 260)

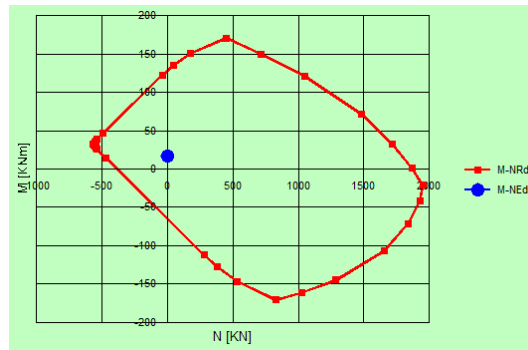


Figure 7.16: Interaction domain M-N for 2<sup>nd</sup> floor beams (400 · 260)

Bending moment capacity	Inside the critical region			Outside the critical region		
	$M_u$ (KNm)	$\Phi_s$ (mm)	$s$ (mm)	$V_{Rd}$ (KN)	$\Phi_s$ (mm)	$s$ (mm)
128.3	8	60	200.62	8	200	64.20

Table 7-8: Design bending moment capacity and shear resistance for 2<sup>nd</sup> floor beams (400 · 260)

### 7.3.5. Damping of the frame

The coefficients  $\alpha$  and  $\beta$  are the same of the bare frame described in §6.3. This is due to the same geometrical and material conditions among the frames. Furthermore, the new frame is not damaged. Table (7-7) shows the damping coefficient values used in this analysis.

Mass Damping Coefficient ( $\alpha$ )	Element Stiffness Coefficient ( $\beta$ )
0.757841	0.001301

Table 7-9: Mass damping coefficient and element stiffness coefficient for the new frame

### 7.3.6. Material properties

In relation to the bare frame, in this case only concrete properties differ, whereas steel properties are the same.

#### 7.3.6.1. Concrete confined with stirrups for the new frame

Concrete parameters change because of the different amount of transversal reinforcement in the elements. The stress-strain relationship used for confined concrete fibers is CEB model (2010) for compression and Carreira and Chu model (1986) for tension, with  $f_t = 2.3 \text{ MPa}$  and  $\beta = 2.26$ . Four points are used to describe compressive concrete behaviour and two points are used to describe tensile concrete behaviour. Figure (7.15) displays DRAIN-3DX model for 1<sup>st</sup> storey columns outside the critical region and relative values. The same is done for 1<sup>st</sup> storey columns in the critical region and the results are shown in figure (7.16). Stress-strain values used in DRAIN-3DX for all the other elements can be found in Appendices A3 and A4.

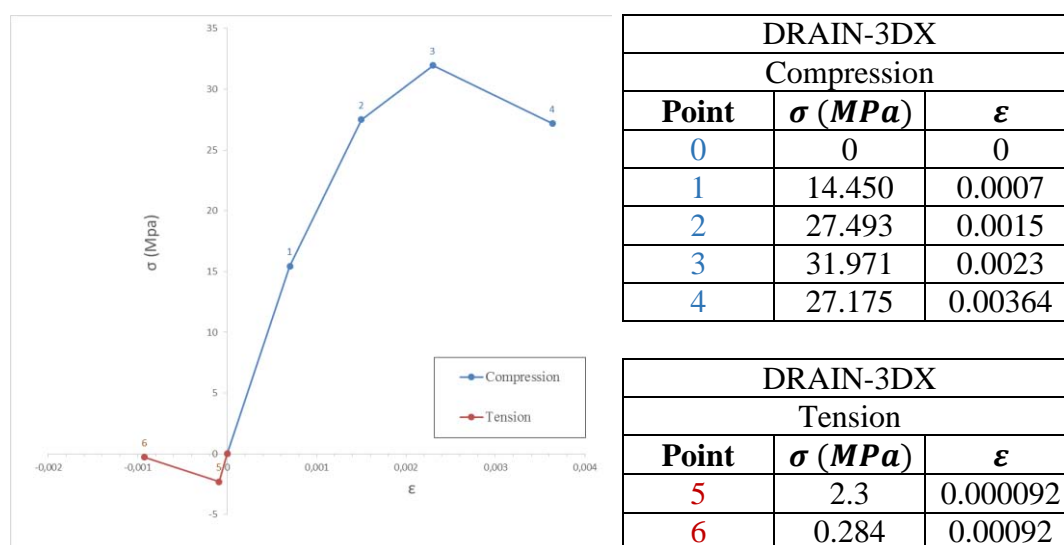


Figure 7.17: DRAIN-3DX model for confined concrete in 1<sup>st</sup> floor columns outside the critical region

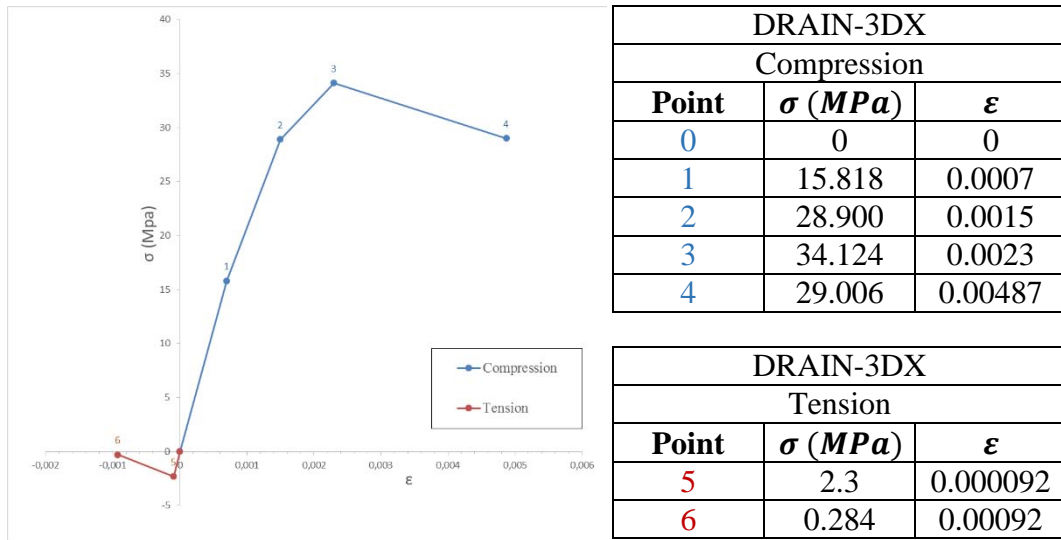


Figure 7.18: DRAIN-3DX model for confined concrete in 1<sup>st</sup> floor columns in the critical region

### 7.3.7. Analytical geometry of the frame in DRAIN-3DX

The structure is modelled in DRAIN-3DX as a two dimensional frame, with columns (260 · 260) and beams (300 · 260), in order to be then compared with the CFRP retrofitted frame. The foundation nodes (1010, 1020) are restrained by a stiff support spring which allows the frame to move with no relative displacement to the ground, as in previous cases. Figure (7.17) describes nodes, elements and groups of the frame.

1<sup>st</sup> floor column consists in four segments (groups 1, 5, 10, 11):

- Groups 10 and 11 represent the critical region of the first storey columns for the height of 550 mm.
- Group 1 represents middle stirrups column;
- Group 5 represents 1<sup>st</sup> floor beam-column joint in vertical direction.

2<sup>nd</sup> floor column consists in five segments (groups 2, 6, 9, 12, 13):

- Group 6 represents 1<sup>st</sup> floor beam-column joint in vertical direction.
- Groups 12 and 13 represent the critical region of the second storey columns for the height of 550 mm each.
- Group 2 represents middle stirrups column;
- Group 9 represents 2<sup>nd</sup> floor beam-column joint in vertical direction.

Regarding the beams, both beams of 1<sup>st</sup> and 2<sup>nd</sup> floor are divided into 9 intermediate points. Lateral segments are used to represent beam-column joints in horizontal direction. These segments are rigid joints, as in the BANDIT bare frame. 1<sup>st</sup> and 2<sup>nd</sup> floor beams consists in five segments each (groups 3, 7, 14 for 1<sup>st</sup> floor beams and groups 4, 8, 15 for 2<sup>nd</sup> floor beams):

- Group 3 (and group 4) represents middle stirrups beam;
- Group 7 (and group 8) represents 1<sup>st</sup> (and 2<sup>nd</sup>) floor beam-column joint in horizontal direction.
- Group 14 (and group 15) represents the critical region of the first (and second) storey beams for the height of 300 mm each.

In contrast with the previous frames, in this case all the elements can be considered perfectly bonded, therefore no pullout and gap properties for connection fibers are used. This is due to the attention for details, e.g. adequate anchorage length for columns, the presence of hooks at the bottom of longitudinal bars of both transversal and horizontal elements.

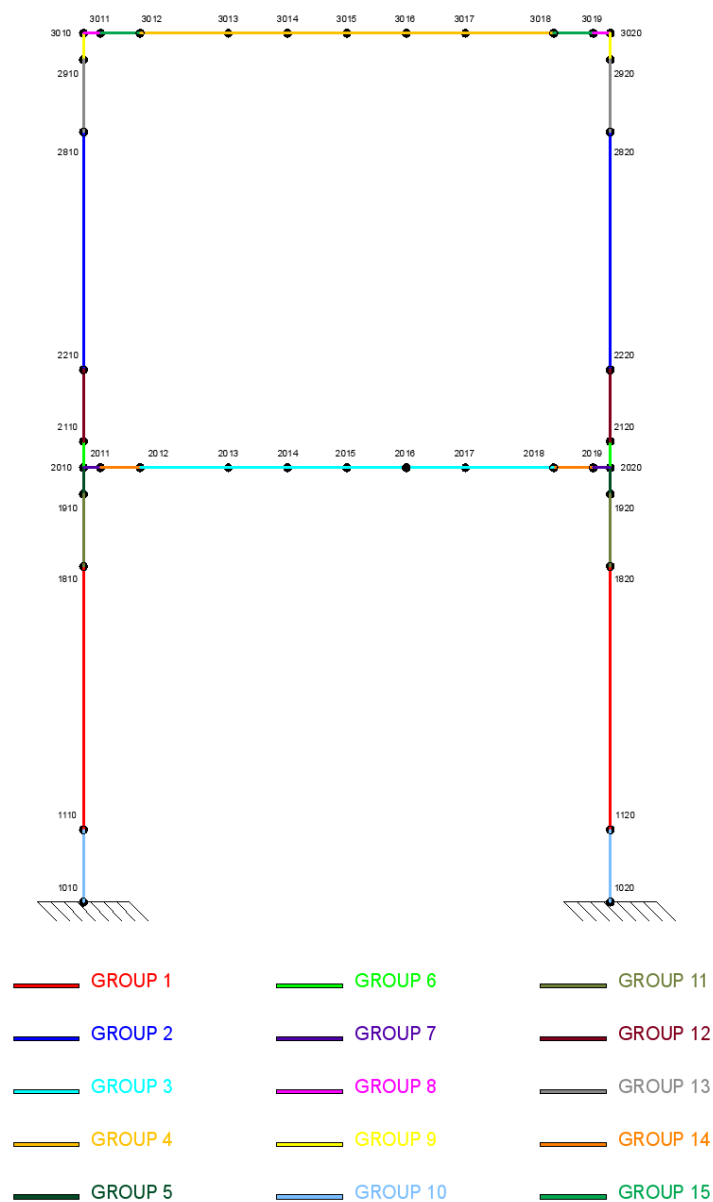


Figure 7.19: Analytical modelling of the new frame in DRAIN-3DX

### 7.3.8. Time-history analysis results

The new frame is designed to withstand the design seismic action described earlier, therefore the highest PGA level bearable is 0.15g. In order to compare the performances of the new frame with those of the CFRP retrofitted frame, a time-history analysis on the new frame is performed. The analysis is performed with reference to the first two tests of test sequence 4 (until seismic level of 0.10g), moreover an analytical test under PGA=0.15g is performed for both frames. In fact, the new frame is not designed to sustain a seismic test of 0.20g acceleration or higher, therefore the failure of the structure could occur and this failure cannot be seen from the programme. Nodes 2010 and 3010 are considered in the analysis.

#### 7.3.8.1. Displacement time-history in test sequence 4

The results of the analysis are presented in the following paragraphs. The time-history input file for the new frame is shown in Appendix D3.

##### 7.3.8.1.1. Response of the new frame under 0.05g PGA

The analytical displacement time-history of the new frame and the experimental displacement time-history of the CFRP retrofitted frame for nodes 2010 and 3010 under 0.05g PGA are shown in figures (7.18) and (7.19) respectively. The new frame seems to be more rigid than the CFRP retrofitted frame. This applies to both nodes.

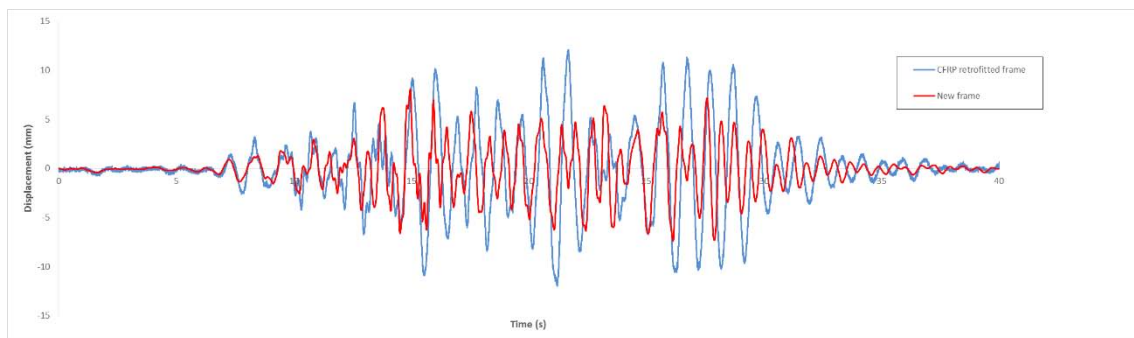


Figure 7.20: Displacement time-history for node 2010 under 0.05g PGA

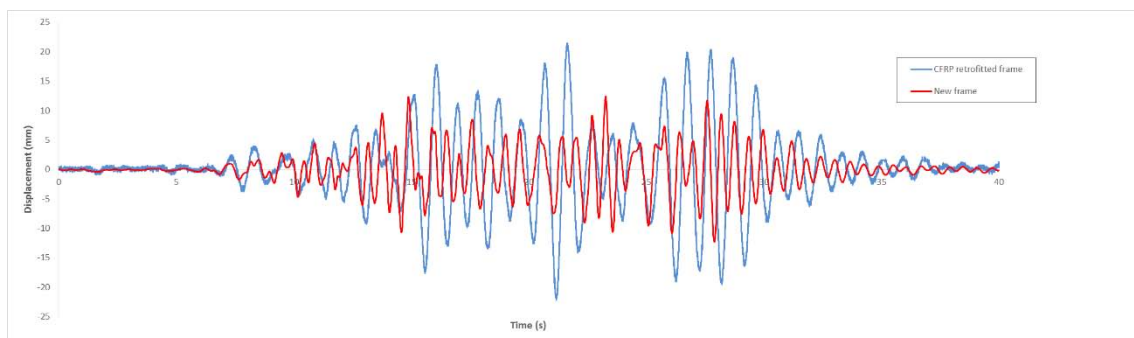


Figure 7.21: Displacement time-history for node 3010 under 0.05g PGA

### 7.3.8.1.2. Response of the new frame under 0.10g PGA

The analytical displacement time-history of the new frame and the experimental displacement time-history of the CFRP retrofitted frame for nodes 2010 and 3010 under 0.10g PGA are shown in figures (7.20) and (7.21) respectively. In contrast with the previous case, here the new frame seems to be more ductile in the first phase, but then it is stiffer than the CFRP retrofitted frame.

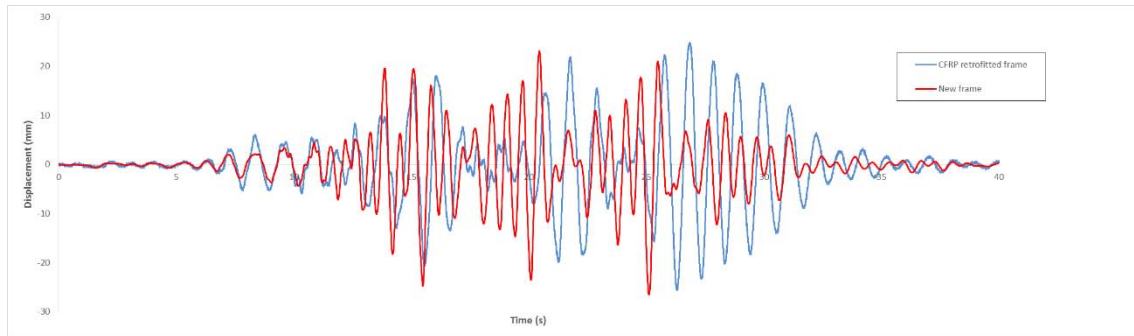


Figure 7.22: Displacement time-history for node 2010 under 0.10g PGA

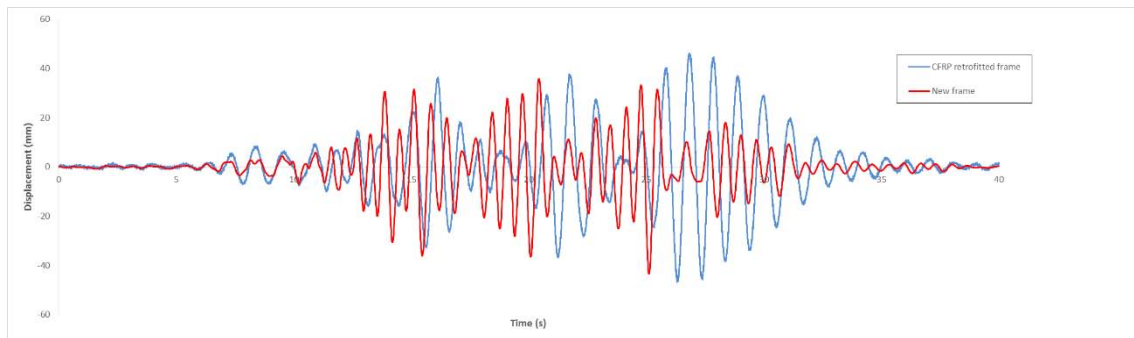


Figure 7.23: Displacement time-history for node 3010 under 0.10g PGA

### 7.3.8.1.3. Response of the new frame under 0.15g PGA

The analytical displacements time-history of both frames for nodes 2010 and 3010 under 0.15g PGA are shown in figures (7.22) and (7.23) respectively. As in the previous case, here the new frame behaves differently to the CFRP retrofitted frame.



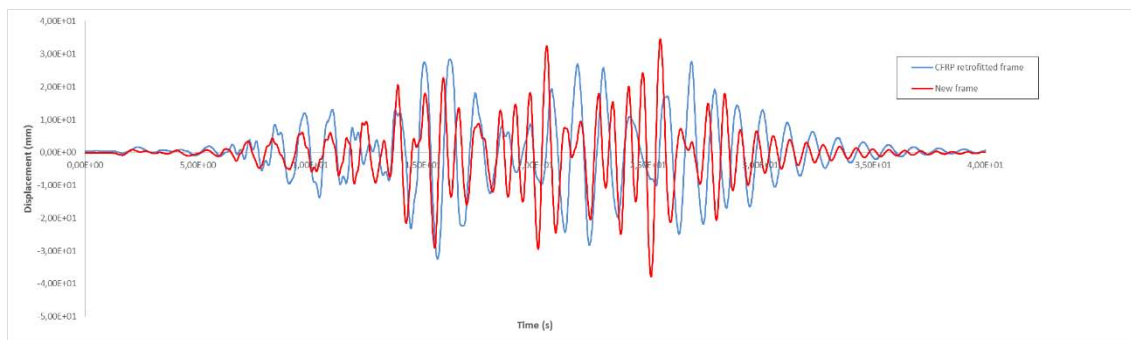


Figure 7.24: Displacement time-history for node 2010 under 0.15g PGA

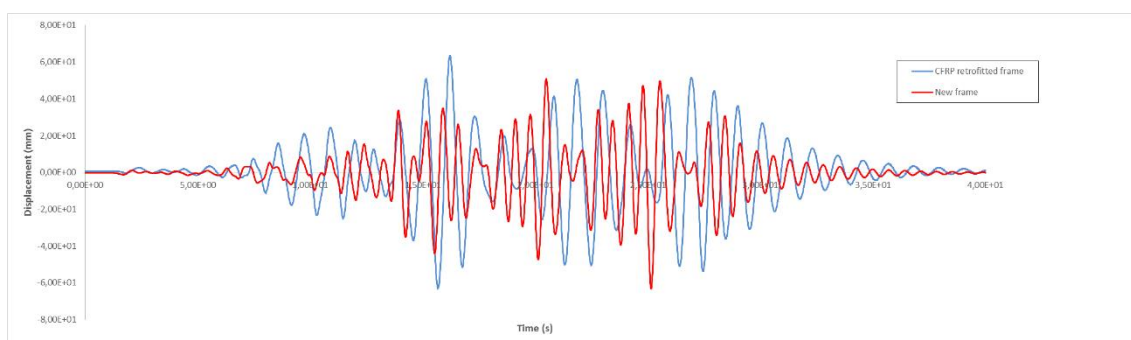


Figure 7.23: Displacement time-history for node 3010 under 0.15g PGA

### 7.3.9. Damage limitation for the new frame

As in the CFRP retrofitted frame, even in this case the “damage limitation requirement” has to be satisfied. According with §7.2, it is necessary to respect the same provisions. Importance class II is assumed even for this structure, therefore the value of the reduction  $v$  is equal to 0.5. Table (7-8) shows the damage limitation requirement for the new frame under the PGA levels investigated compared with the value for the CFRP retrofitted frame.

PGA level	New frame $d_r \cdot v$ (mm)	CFRP retrofitted frame $d_r \cdot v$ (mm)	SLO damage limitation (mm)	SLD damage limitation (mm)
0.05g	3.29	5.55	22	33
0.10g	8.50	12.61		
0.15g	17.49	15.59		

Table 7-10: Damage limitation requirement for the new frame and comparison with the CFRP retrofitted frame

As can be seen in the table, the new frame is able to comply with the norms at least up to a seismic level of 0.15g. For the first two seismic levels, the interstorey drift for the new frame is lower than that of the CFRP retrofitted frame. In the last case,

the interstorey drift for the new frame is higher than that of the CFRP retrofitted frame, but it is within the normative limit.

#### **7.4. Economic evaluation of the intervention**

For the purpose of evaluating the feasibility of the intervention, a cost analysis is performed. In particular, the cost of the CFRP intervention is compared with the cost of the new structure with regard to the particular case of BANDIT frame. CFRP technique has been implemented in the context of BANDIT program, therefore it is difficult to estimate the likely costs of the CFRP intervention. In this project, the complete system used for CFRP techniques has been provided by FREYSSINET Company and some industrial partners. Assuming Treviso as the place of the intervention, a rough cost estimate can be given with reference to MapeWrap C BI-AX system provided by the Italian company Mapei. This system is suitable for the confinement of axially loaded or damaged concrete elements and it is also suitable for the seismic strengthening and restoration of RC structures. According with §4.3, the CFRP technique used in this experiment can be compared with the dry system, where the dry fabric is placed directly on a layer of Madewrap 31 which has been applied to the concrete element that need reinforcement. In the next paragraph this system will be analysed from the viewpoint of the costs and performances.

##### **7.4.1. CFRP retrofitting rough cost estimate**

Mapewrap C BI-AX is a bidirectional continuous carbon fibre fabric with balanced weight characterized by high modulus of elasticity (comparable to steel) and very high tensile strength that can be placed using dry system method. The components used in this intervention are:

- Mapewrap Primer 1, strengthening for the treatment of the substrate;
- Mapewrap 12, smoothing compounds to smooth any rough areas or to seal porous surfaces;
- Mapewrap 31, impregnating agent for fabrics by “dry system”;
- Mapewrap C BI-AX 230, weight  $238 \text{ g}/\text{m}^2$ , fabric equivalent thickness 0.064 mm, tensile strength >4800 MPa, tensile modulus of elasticity >230 GPa, elongation at breaking point 2.1%.

The directions for use are:

1. Preparing the substrate with Mapewrap Primer 1;
2. Apply an approximately 1 mm thick coat of Mapewrap 12 over the concrete surface pre-treated;
3. Impregnate the fabric with Mapewrap 31;
4. Place the Mapewrap C BI-AX fabric.

For the installation of several layers of Mapewrap C BI-AX:

5. Apply a first coat of Mapewrap 31;
6. Place the Mapewrap C BI-AX fabric;
7. Apply another coat of Mapewrap 31.

Table (7-9) shows the retail prices valid for March 2015 of the materials used for the intervention and table (7-10) shows the estimate of materials costs for the CFRP intervention on BANDIT frame using Mapewrap C BI-AX. Lastly, the final estimate of costs for the intervention can be seen in table (7-11). The quantities of materials have been calculated in order to achieve the same performances of the CFRP system used on BANDIT experimental program. The prices are based on the maximum epoxy system consumptions, as suggested in the explanatory manual of the product. The total costs include supply and installation of the materials.

<b>Component</b>	<b>Quantity (kg)</b>	<b>Retail price (€)</b>	<b>Max. consumption (<math>g/m^2</math>)</b>	<b>Max. consumption (<math>g/m</math>)</b>	<b>Retail price (€/ml)</b>
Mapewrap Primer 1	2	13.90	300	-	-
Mapewrap 12	6	7.50	1600	-	-
Mapewrap 31	5	14.60	-	440	-
Mapewrap C BI-AX 230/20	-	-	-	-	23.00

Table 7-11: Retail prices of the materials used for the CFRP intervention on BANDIT frame using Mapewrap C BI-AX

<b>Component</b>	<b>Use</b>	<b>Area to be covered (<math>m^2</math>)</b>	<b>Number of layers</b>	<b>Price (€)</b>
Mapewrap Primer 1		32.64		68.06
Mapewrap 12		32.64		65.28
Mapewrap 31	Long. reinf. + wrapping	334.09	6+6	1073.09
Mapewrap C BI-AX 230/20	Wrapping	97.73	3	5619.36
Mapewrap C BI-AX 230/20	Long. reinf. (columns)	25.92	3	1490.40
Mapewrap C BI-AX 230/20	Long. reinf. (beams)	36.10	4	2075.73
<b>TOTAL COST OF MATERIALS</b>				<b>10391.94</b>

Table 7-12: Estimate of materials costs for the CFRP intervention on BANDIT frame using Mapewrap C BI-AX

<b>Item of expenditure</b>	<b>Price (€)</b>
Materials	10391.94
Supply and installation	5280.00
<b>TOTAL COST OF THE INTERVENTION</b>	<b>15671.94</b>

Table 7-13: Final estimate of costs for the CFRP intervention on BANDIT frame using Mapewrap C BI-AX

### 7.5. New frame rough cost estimate

As told in §7.4, the cost of the intervention is compared with the cost of the new frame. The new frame is designed to be built in Treviso, therefore the current prices of that zone are taken into consideration. The total cost of the new frame includes:

- The destruction of the previous building;
- The price of the materials that constitute the backbone of the structure;
- The price of the two slabs;
- The cost of supply and installation.

When a new structure is built, it is necessary to demolish the previous building. Furthermore, it is necessary to rebuild entirely the structure, including the non-structural parts. Table (7-12) shows the total cost of the new building valid for March 2015.

<b>Item of expenditure</b>	<b>Cost (€)</b>
Demolition of the previous building	3500.00
Final cost of the backbone of the frame	4810.00
Final cost of the two slabs	6015.00
<b>TOTAL COST OF THE NEW BUILDING</b>	<b>14325.00</b>

Table 7-12: Final estimate of costs for the new structure

## 8. CONCLUSIONS

---

### 8.1. Concluding Remarks

Many of the existing buildings in Europe, as well as in developing countries, have been designed according to old standards and have little or no seismic provision and often suffers from poor material and construction practices.

Beam-column joints have been identified as one of the leading causes of collapse of such structures during earthquakes. Joints have a very limited capacity in dissipating energy and maintaining their strength, therefore they can be considered to have a brittle mode of failure. Moreover, these failures limit the ductility of the structure. In order to improve the seismic behaviour of the joints, sufficient transverse reinforcement and anchorage of the longitudinal bars within the joint core should be provided.

Various rehabilitation techniques such as epoxy repair, concrete jackets, steel jackets, and externally bonded Fibre-Reinforced Polymeric reinforcements have been proposed to remedy their deficiencies.

The aim of this dissertation is to investigate the CFRP strengthening on RC structures, in order to provide a seismic resistance. In particular, the confinement of the columns with CFRP jackets has been analysed, with especially reference to the increment of the local ductility of the elements. Stress-strain models for columns confined with FRP jackets have been analysed in order to evaluate the ultimate conditions of the columns.

A two storey one bay reinforced concrete frame with poor detailing of reinforcement within the joints has been tested on a shake table as part of the BANDIT project. Experimental reports have shown that maximum deformation was observed in the second floor and thus experiment has been stopped after PGA level of 0.15g because the structure was about to collapse because of the damages clearly visible in all the joints at both levels, but mainly in the second level joint. The bare frame is modelled with fibre elements with non-linear material using DRAIN-3DX software. A non-linear dynamic (time-history) analysis is performed in order to analyse the structural response under seismic loading.

The time-history analysis results show a good correlation with the experimental results obtained from the BANDIT project, in particular at higher PGA levels. The model aims to simulate the deficiencies in the joints by including the pullout and gap fibres at joints to model the bond-slip behaviour of the reinforcement and the concrete crack opening. Bond-slip behaviour occurs especially at joints but even in the second floor beam.

The first and second modal frequencies are measured in the experimental case and the results are compared with those calculated in the analytical frame. In the

analytical frame there is a significant increase in the natural period compared to the experimental frame. The first modal frequency calculated in the analytical frame is over 22.4% than the experimental measurement at the 0.05g PGA level.

The BANDIT frame has been strengthened with CFRP technique, especially at joints, in order to provide a seismic resistance to the structure. The structure has been tested on the shaking table until 0.35g PGA level. The results of the shaking table test have demonstrated that the adopted local strengthening strategy using CFRP materials was effective at changing the plastic hinge mechanism from column-sway to beam-sway, which is in line with the modern seismic design philosophy. Before the strengthening of the structure, the holes have been filled with grout and the crack system have been filled up with epoxy resin. This technique was effective at restoring the initial dynamic characteristics of the RC frame. Even in this case the CFRP retrofitted frame is modelled with fibre elements with non-linear material using DRAIN-3DX software. A non-linear dynamic (time-history) analysis is then performed and the results are compared with the experimental results.

The time-history analysis results show a very good correlation with the experimental results obtained from the BANDIT project at all PGA levels. The model includes the pullout and gap fibres at joints. Even in this case bond-slip behaviour occurs, but this phenomenon is present even in the first floor beam. In the analytical frame there is a relevant increase in the natural period compared to the experimental frame, except for the natural period measured before the test sequence. The first modal frequency calculated in the analytical frame is over 15.5% than the experimental measurement at the 0.10g PGA level.

In the last chapter, the feasibility of the intervention with CFRP is evaluated and it is compared with the building of a new structure. A cost-benefits analysis is carried out and even an evaluation of the performance reached is considered. Assuming Treviso as the place where the structure is designed to be built, a new frame is designed in accordance with the current seismic legislation. The building is designed to withstand an earthquake of 0.15g PGA level and it complies with the rules provided by NTC 2008 and EC 8. The CFRP retrofitted frame has been able to withstand an earthquake of 0.35g PGA without clearly damages, but according with damage limitation provided by the norms, the maximum interstorey drift for the SLO limits the resistance of the structure until 0.20g PGA. For this reason, seismic zone 3 is taken as the design constraint for the rising of the new structure. A time-history analysis is performed for the new frame under 0.05g, 0.10g and 0.15g PGA. The results are compared with those of the CFRP retrofitted frame. Except for 0.05g PGA level, there is bad correlation between the results. Therefore, the global behaviours of the frames are different under the same earthquake simulation. There is apparently no prevalence in terms of stiffness between the CFRP retrofitted frame and the new frame during the simulations. After the analysis, the maximum interstorey drift for the new frame is evaluated and it was

always found to be within the limits recommended for the damage limit state (up to 0.15g PGA).

At the end of the chapter, an economic evaluation of the intervention is performed. The results of the rough cost estimate show that the intervention with CFRP is more expensive than the building of the new frame. Indeed, the final cost of the intervention with CFRP (Mapewrap C BI-AX system provided by the Italian company MAPEI) is 15671.94 €, whereas the cost of the new building is 14325.00 €.

There are wider considerations that it is important to take into account as part of the evaluation. These attentions are determinant when an evaluation of feasibility of the intervention is performed in a specific situation.

1. In this case, the ultimate resistance of the CFRP retrofitted frame is higher than the new frame, although the interstorey drift is not verified for high PGA levels. The interstorey drift may be limited with the introduction of non-structural elements such as infill walls.
2. In some cases, it may be not possible to rebuild entirely the structure, for instance for the renovation of buildings under particular artistical and architectural constraints. Therefore, the intervention with CFRP is to take into account
3. It is necessary to design even the foundation system when a new building is planned to be built.
4. In order to choose which type of intervention is the most appropriate, the economic evaluation and the analysis of the performance have to be performed for each particular situation. In some cases the intervention with CFRP may be economically more convenient than the building of a new structure.
5. The intervention with CFRP is more rapid than the design and building of the new structure.
6. The intervention with CFRP normally provides more ductility to the elements and the joints than the building of a new structure. Furthermore, joints retrofitting provide a ductile mode of failure for the structure.

## REFERENCES

---

ACI 352R-02 (2002). "Recommendations for design of beam-column-joints in monolithic reinforced concrete structures". The American Concrete Institute, ACI-ASCE, Committee 352, Detroit.

ACI 440 (2008). "Guide for the Design and Construction of Externally Bonded FRP systems for Strengthening Concrete Structures".

Adam T. G. (2005). Modeling the Earthquake Response of Older Reinforced Concrete Beam-Column Joints. MSc Dissertation, Department of Civil and Environmental Engineering, University of Washington.

Beres A., Pessiki S.P., White R.N., and Gergely P. (1996). "Implications of Experiments on the Seismic Behavior of Gravity Load Designed RC Beam-to-Column Connections". Earthquake Spectra, pp.185-98.

Bulletin 14 of CEB-FIP, "Externally bonded FRP reinforcement for RC structures" (2001).

Carreira D.J., Chu K.-H. (1986). "Stress-strain relationship of reinforced concrete in tension". ACI.

CEB (1996), "RC Frames under Earthquake Loading: state of art report". Thomas Telford publishing.

CEB-FIP (2010), "Model Code for Concrete Structures". Ernst and Sohn.

Chopra A.K. (2001). "Dynamics of structures: theory and applications to earthquake engineering". Upper Saddle River, NJ, London, Prentice Hall. Prentice-Hall International.

Circolare esplicativa 2 Febbraio 2009 n.617.

Circolare esplicativa n.617 (2009).

Costa J.L.D. (2003). "Reinforced Concrete under Large Seismic Action". Danmarks Tekniske Universitet.

El-Amoury T.A. (2004). "Seismic Rehabilitation of Concrete Frame Beam-Column Joints". Ph.D. thesis Mc Master University.

Eligehausen R., Popov E., and Bertero V. (1983). "Local bond stress-slip relationships of deformed bars under generalized excitations, Report No.



UCB/EERC-83/23". Earthquake Engineering Research Center, College of Engineering, University of Berkeley.

Engindeniz M., Kahn L.F. and Zureick A. (2005). "Repair and Strengthening of Reinforced Concrete Beam-Column Joints: State of the Art". *ACI Structural Journal*.

EUROCODE 2 (2004). "Design of Concrete Structures - Part1-1: General rules, and rules for buildings". Brussels, British Standard (BSI).

EUROCODE 8 (2004). "Design of structures for earthquake resistance - part1: General rules, seismic actions and rules for buildings". Brussels, British Standard (BSI).

FEMA 308 (1998), "Repair of earthquake damaged concrete and masonry wall buildings".

Ghobarah A. and El-Amoury T. (2005). "Seismic rehabilitation of deficient exterior concrete frame joints". *Journal of Composites for Construction*, ASCE, 9(1), pp.408-16.

Kwak H. and Filippou (1990). "Finite element analysis of reinforced concrete structures under monotonic loads". Report No. UCB/SEMM-90/14. University of California, Berkeley.

Kyriakides N. (2007). "Vulnerability of RC buildings and risk assessment for Cyprus". Ph.D. Thesis. UK: Department of civil and structural engineering, University of Sheffield.

Lam L. and Teng J.-G. (2003). "Design-oriented Stress-Strain Model for FRP-confined Concrete in Rectangular Columns". Department of civil and structural engineering. The Hong Kong Polytechnic University.

Mongabure P., Vasic S., Poupin S., Le Corre M., Mahe M. (2012). "European Series Project Bandit Program, Seismic Tests on a Reinforce Concrete frame with Post-Tensioned Metal Strips retrofitting".

National Research Council (2004). "Guide for the design and construction of externally bonded FRP systems for strengthening existing structures. Materials, RC and PC structures, masonry structures".

Norme Tecniche per le Costruzioni (D.M. 2008).

Pagni, C., and Lowes, Laura (2004). "Prediction Earthquake Damage in Older Reinforced Concrete Beam-Column Joints". PEER Report 2003/17, Pacific

Earthquake Engineering Research Center, College of Engineering, University of California, Berkeley.

Pampanin S., Calvi G.M., and Moratti M. (2002). "Seismic Behaviour of R.C Beam-Column Joints Designed For Gravity Loads". 12th European Conference on Earthquake Engineering. University of Pavia, Italy, Elsevier Science Ltd.

Paulay T. and Priestley M.J.N. (1992) – "Seismic design of reinforcement concrete and masonry buildings". J. Wiley & Sons, New York.

Penelis, G.G. and Kappos, A.J. (1997) – "Earthquake-Resistant concrete structures", E&FN Spon.

Pilakoutas K. (2014). "T5 Notes on Confinement of concrete using FRP, Lecture notes distributed in CIV 6170" – FRP Composites in Construction at The University of Sheffield on 2014.

Powell G.H., Campbell S. (1994). "Drain-3dx element description and user guide for element type01, type04, type05, type08, type09, type15, and type17". Version 1.10. Department of Civil Engineering, University of California, Berkeley.

Prakash V., Powell G.H. and Campbell S. (1994). "Drain-3dx base program description and user guide". Version 1.10. Department of Civil Engineering, University of California, Berkeley.

Priestley M.J.N. and Seible F. (1995). "Design of seismic retrofit measures for concrete and masonry structures. Construction and Building Materials".

Richart F.E., Brandtzaeg A. and Brown R.L. (1928). "A study of the failure of concrete under combined compressive stresses". Engineering Experiment Station Bulletin No. 185, University of Illinois, Urbana.

Scarpas A. (1981). "The inelastic behavior of earthquake resistant reinforced concrete exterior beam-column joints", Master of Eng. Thesis, University of Canterbury, Christchurch, New Zealand.

Sharma A., Reddy G.R., K.K. Vaze, A.K. Ghosh, and H.S. Kushwaha (2009). "Experimental investigations and evaluation of strength and deflections of reinforced concrete beam-column joints using nonlinear static analysis". Reactor Safety Division, HS&E Group.

Sezen H. (2002). "Seismic behaviour and modelling of RC building columns". University of California, PhD Thesis.

Triantafyllou T. (2003). "Seismic retrofitting using Externally Bonded Fibre Reinforced Polymers (FRP)". University of Patras.

## APPENDIX A

### A1. Stress-strain model for concrete confined with stirrups before test sequence 1

#### 2<sup>nd</sup> Floor columns

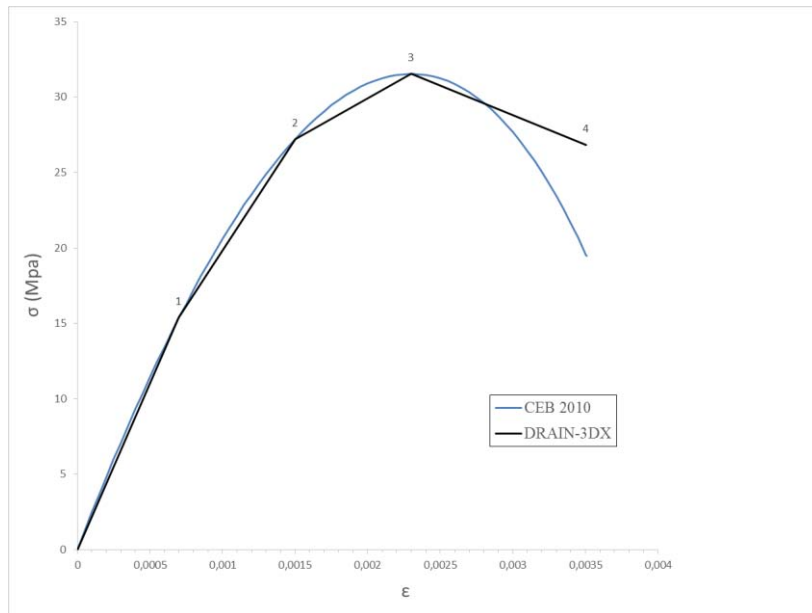
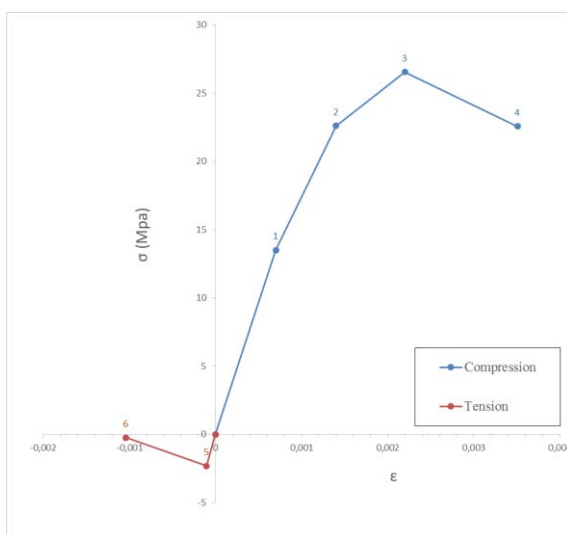


Figure A.1: Compressive Stress-strain model from CEB (2010) and DRAIN-3DX for confined concrete in 2<sup>nd</sup> floor columns.



DRAIN-3DX		
Compression		
Point	$\sigma$ (MPa)	$\epsilon$
0	0	0
1	13.506	0.0007
2	22.612	0.0014
3	26.543	0.0022
4	22.562	0.00351

Tension		
Point	$\sigma$ (MPa)	$\epsilon$
5	2.3	0.000104
6	0.284	0.00104

Figure A.2: DRAIN-3DX stress-strain model and values for confined concrete in 2<sup>nd</sup> floor columns.

### 1<sup>st</sup> Floor beams (400 · 260 mm)

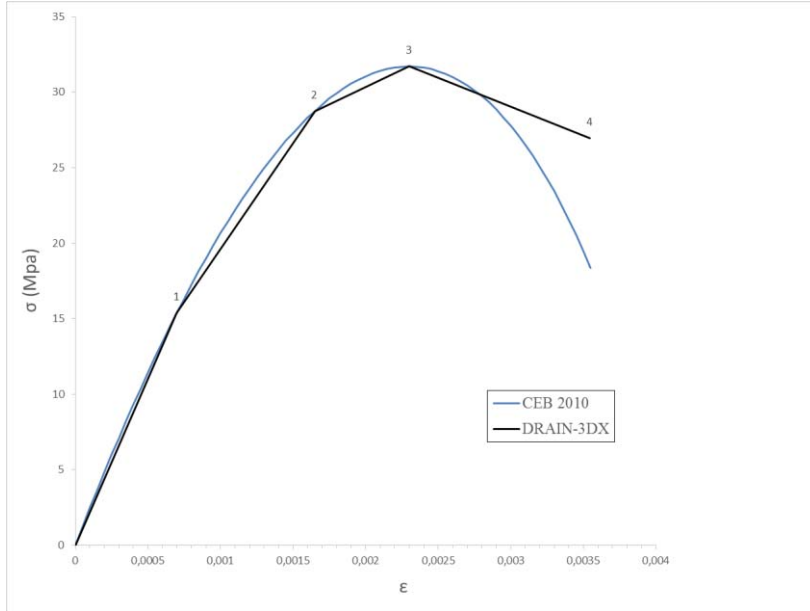
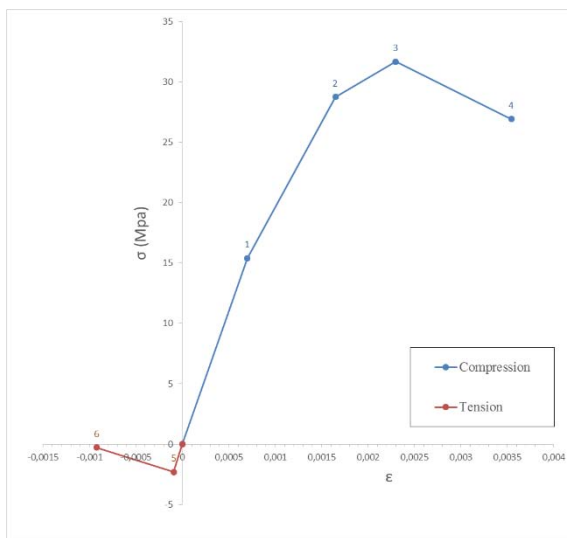


Figure A.3: Compressive Stress-strain model from CEB (2010) and DRAIN-3DX for confined concrete in 1<sup>st</sup> floor beams (400).



DRAIN-3DX		
Compression		
Point	$\sigma$ (MPa)	$\epsilon$
0	0	0
1	15.400	0.0007
2	28.761	0.00165
3	31.700	0.0023
4	26.945	0.00354

Tension		
Point	$\sigma$ (MPa)	$\epsilon$
5	2.3	0.000092
6	0.284	0.00092

Figure A.4: DRAIN-3DX stress-strain model and values for confined concrete in 1<sup>st</sup> floor beams (400).

## 2<sup>nd</sup> Floor beams (400 · 260 mm)

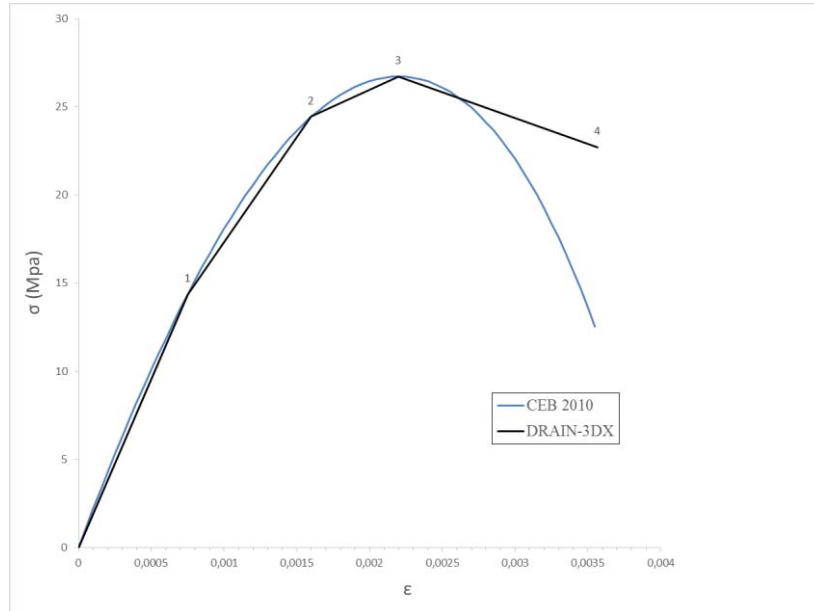
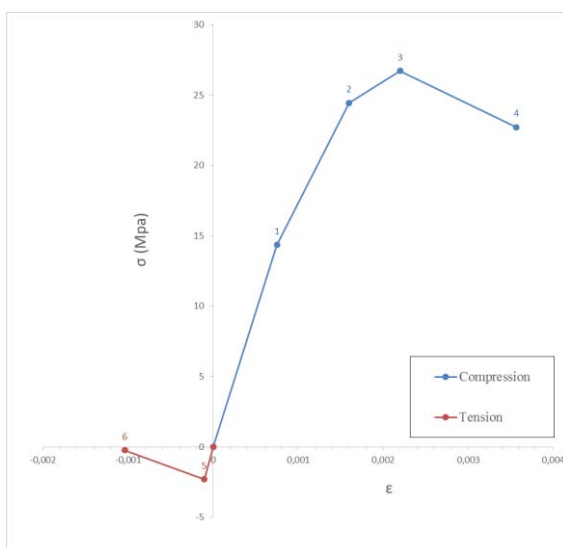


Figure A.5: Compressive Stress-strain model from CEB (2010) and DRAIN-3DX for confined concrete in 2<sup>nd</sup> floor beams (400).



DRAIN-3DX		
Compression		
Point	$\sigma$ (MPa)	$\epsilon$
0	0	0
1	14.353	0.00075
2	24.436	0.0016
3	26.725	0.0022
4	22.716	0.00357

Tension		
Point	$\sigma$ (MPa)	$\epsilon$
5	2.3	0.000104
6	0.284	0.00104

Figure A.6: DRAIN-3DX stress-strain model and values for confined concrete in 2<sup>nd</sup> floor beams (400).

### 1<sup>st</sup> Floor beams (300 · 260 mm)

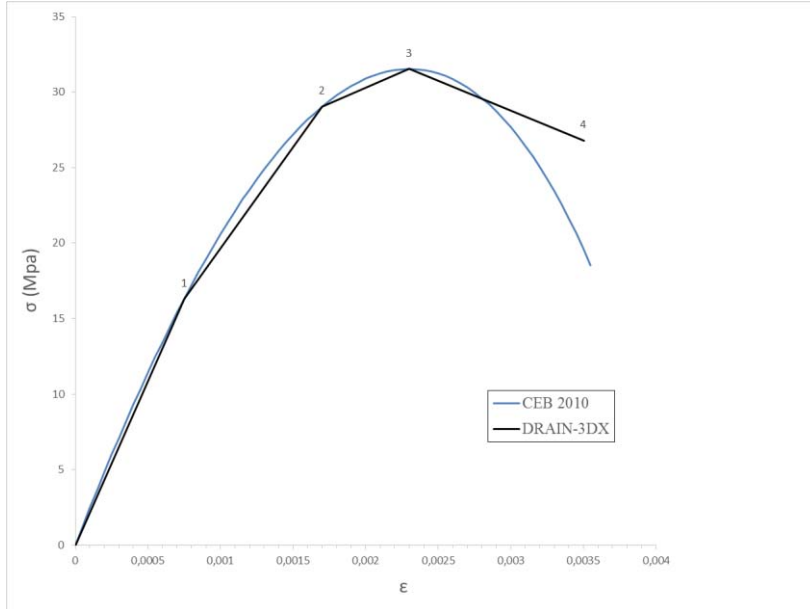
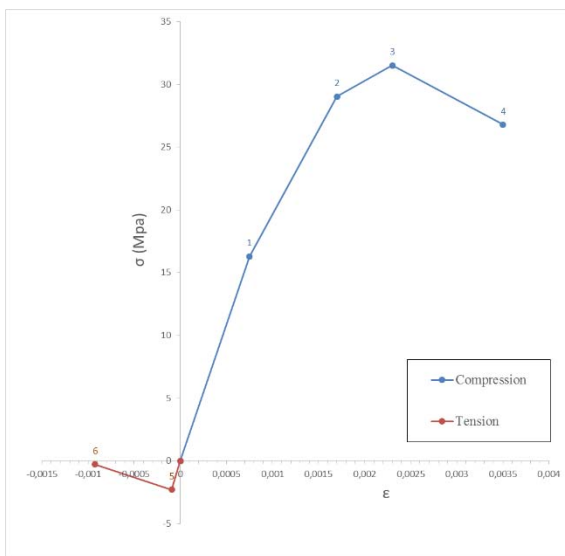


Figure A.7: Compressive Stress-strain model from CEB (2010) and DRAIN-3DX for confined concrete in 1<sup>st</sup> floor beams (300).



DRAIN-3DX		
Compression		
Point	$\sigma$ (MPa)	$\epsilon$
0	0	0
1	16.297	0.00075
2	29.041	0.0017
3	31.522	0.0023
4	26.793	0.0035

Tension		
Point	$\sigma$ (MPa)	$\epsilon$
5	2.3	0.00092
6	0.284	0.00092

Figure A.8: DRAIN-3DX stress-strain model and values for confined concrete in 1<sup>st</sup> floor beams (300).

## 2<sup>nd</sup> Floor beams (300 · 260 mm)

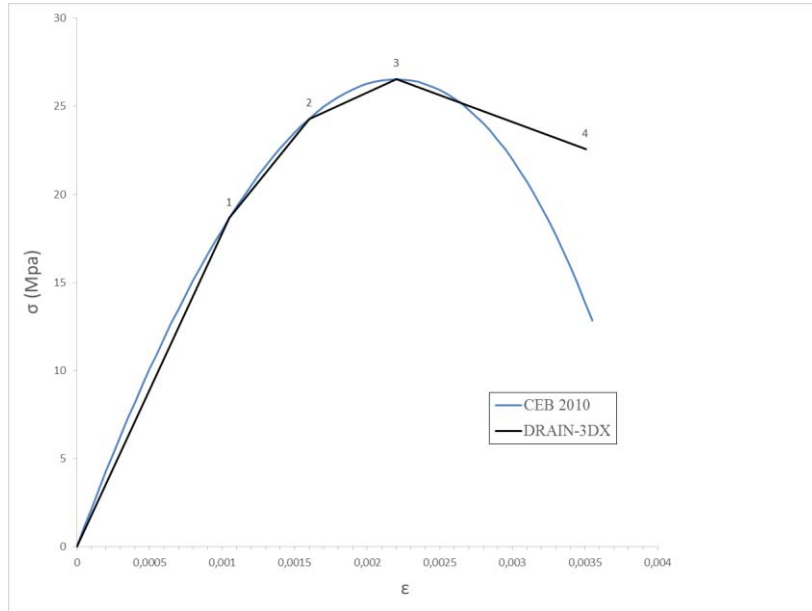
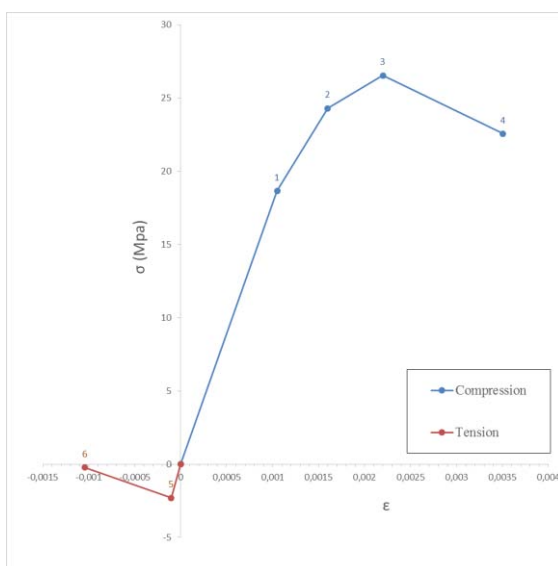


Figure A.9: Compressive Stress-strain model from CEB (2010) and DRAIN-3DX for confined concrete in 2<sup>nd</sup> floor beams (300).



DRAIN-3DX		
Compression		
Point	$\sigma$ (MPa)	$\epsilon$
0	0	0
1	18.653	0.00105
2	24.286	0.0016
3	26.534	0.0022
4	22.554	0.00351

Tension		
Point	$\sigma$ (MPa)	$\epsilon$
5	2.3	0.000104
6	0.284	0.00104

Figure A.10: DRAIN-3DX stress-strain model and values for confined concrete in 2<sup>nd</sup> floor beams (300).

**A2. Stress-strain model for concrete confined with stirrups before test sequence 4**

**2<sup>nd</sup> Floor columns**

DRAIN-3DX		
Compression		
Point	$\sigma$ (MPa)	$\epsilon$
0	0	0
1	12.648	0.0007
2	20.737	0.0014
3	24.042	0.0022
4	20.436	0.00351

Tension		
Point	$\sigma$ (MPa)	$\epsilon$
5	2.3	0.000109
6	0.284	0.00109

Table A-1: DRAIN-3DX values for confined concrete in 2<sup>nd</sup> floor columns before test sequence 4.

**1<sup>st</sup> Floor beams (400 · 260 mm)**

DRAIN-3DX		
Compression		
Point	$\sigma$ (MPa)	$\epsilon$
0	0	0
1	14.223	0.0007
2	26.846	0.00165
3	29.697	0.0023
4	25.242	0.00355

Tension		
Point	$\sigma$ (MPa)	$\epsilon$
5	3	0.000132
6	0.37	0.00132

Table A-2: DRAIN-3DX values for confined concrete in 1<sup>st</sup> floor beams (400) before test sequence 4.



**2<sup>nd</sup> Floor beams (400 · 260 mm)**

DRAIN-3DX		
Compression		
Point	$\sigma$ (MPa)	$\epsilon$
0	0	0
1	13.425	0.00075
2	22.315	0.0016
3	24.219	0.0022
4	20.586	0.00357

Tension		
Point	$\sigma$ (MPa)	$\epsilon$
5	2.3	0.000109
6	0.284	0.00109

Table A-3: DRAIN-3DX values for confined concrete in 2<sup>nd</sup> floor beams (400) before test sequence 4.

**1<sup>st</sup> Floor beams (300 · 260 mm)**

DRAIN-3DX		
Compression		
Point	$\sigma$ (MPa)	$\epsilon$
0	0	0
1	15.059	0.00075
2	27.114	0.0017
3	29.521	0.0023
4	25.093	0.00350

Tension		
Point	$\sigma$ (MPa)	$\epsilon$
5	3	0.000132
6	0.37	0.00132

Table A-4: DRAIN-3DX values for confined concrete in 1<sup>st</sup> floor beams (300) before test sequence 4.

### 2<sup>nd</sup> Floor beams (300 · 260 mm)

DRAIN-3DX		
Compression		
Point	$\sigma$ (MPa)	$\epsilon$
0	0	0
1	17.275	0.00105
2	22.165	0.0016
3	24.033	0.0022
4	20.428	0.00351

Tension		
Point	$\sigma$ (MPa)	$\epsilon$
5	2.3	0.000109
6	0.284	0.00109

Table A-5: DRAIN-3DX values for confined concrete in 2<sup>nd</sup> floor beams (300) before test sequence 4.

### A3. Stress-strain model for concrete confined with stirrups in the new frame (outside the critical region)

#### 2<sup>nd</sup> Floor columns

DRAIN-3DX		
Compression		
Point	$\sigma$ (MPa)	$\epsilon$
0	0	0
1	13.589	0.0007
2	22.879	0.0014
3	26.951	0.0022
4	22.908	0.00366

Tension		
Point	$\sigma$ (MPa)	$\epsilon$
5	2.3	0.000104
6	0.284	0.00104

Table A-6: DRAIN-3DX values for confined concrete in 2<sup>nd</sup> floor columns outside the critical region

**1<sup>st</sup> Floor beams (400 · 260 mm)**

DRAIN-3DX		
Compression		
Point	$\sigma$ (MPa)	$\epsilon$
0	0	0
1	15.369	0.0007
2	28.633	0.00165
3	31.535	0.0023
4	26.805	0.0035

Tension		
Point	$\sigma$ (MPa)	$\epsilon$
5	2.3	0.000092
6	0.284	0.00092

Table A-7: DRAIN-3DX values for confined concrete in 1<sup>st</sup> floor beams (400) outside the critical region

**1<sup>st</sup> Floor beams (400 · 260 mm)**

DRAIN-3DX		
Compression		
Point	$\sigma$ (MPa)	$\epsilon$
0	0	0
1	14.315	0.00075
2	24.306	0.0016
3	26.559	0.0022
4	22.575	0.00351

Tension		
Point	$\sigma$ (MPa)	$\epsilon$
5	2.3	0.000104
6	0.284	0.00104

Table A-8: DRAIN-3DX values for confined concrete in 2<sup>nd</sup> floor beams (400) outside the critical region

### 1<sup>st</sup> Floor beams (300 · 260 mm)

DRAIN-3DX		
Compression		
Point	$\sigma$ (MPa)	$\epsilon$
0	0	0
1	16.298	0.00075
2	29.047	0.0017
3	31.530	0.0023
4	26.801	0.0035

Tension		
Point	$\sigma$ (MPa)	$\epsilon$
5	2.3	0.000092
6	0.284	0.00092

Table A-9: DRAIN-3DX values for confined concrete in 1<sup>st</sup> floor beams (300) outside the critical region

### 2<sup>nd</sup> Floor beams (300 · 260 mm)

DRAIN-3DX		
Compression		
Point	$\sigma$ (MPa)	$\epsilon$
0	0	0
1	18.660	0.00105
2	24.300	0.0016
3	26.551	0.0022
4	22.568	0.00351

Tension		
Point	$\sigma$ (MPa)	$\epsilon$
5	2.3	0.000104
6	0.284	0.00104

Table A-10: DRAIN-3DX values for confined concrete in 2<sup>nd</sup> floor beams (300) outside the critical region

#### A.4 Stress-strain model for concrete confined with stirrups in the new frame (critical region)

##### 2<sup>nd</sup> Floor columns

DRAIN-3DX		
Compression		
Point	$\sigma$ (MPa)	$\epsilon$
0	0	0
1	13.974	0.0007
2	24.180	0.0014
3	29.014	0.0022
4	24.661	0.00513

Tension		
Point	$\sigma$ (MPa)	$\epsilon$
5	2.3	0.000104
6	0.284	0.00104

Table A-11: DRAIN-3DX values for confined concrete in 2<sup>nd</sup> floor columns in the critical region

##### 1<sup>st</sup> Floor beams (400 · 260 mm)

DRAIN-3DX		
Compression		
Point	$\sigma$ (MPa)	$\epsilon$
0	0	0
1	15.782	0.0007
2	30.416	0.00165
3	33.899	0.0023
4	28.815	0.00472

Tension		
Point	$\sigma$ (MPa)	$\epsilon$
5	2.3	0.000092
6	0.284	0.00092

Table A-12: DRAIN-3DX values for confined concrete in 1<sup>st</sup> floor beams (400) in the critical region

**2<sup>nd</sup> Floor beams (400 · 260 mm)**

DRAIN-3DX		
Compression		
Point	$\sigma$ (MPa)	$\epsilon$
0	0	0
1	14.824	0.00075
2	26.113	0.0016
3	28.911	0.0022
4	24.575	0.00504

Tension		
Point	$\sigma$ (MPa)	$\epsilon$
5	2.3	0.000104
6	0.284	0.00104

Table A-13: DRAIN-3DX values for confined concrete in 2<sup>nd</sup> floor beams (400) in the critical region

**1<sup>st</sup> Floor beams (300 · 260 mm)**

DRAIN-3DX		
Compression		
Point	$\sigma$ (MPa)	$\epsilon$
0	0	0
1	17.285	0.00075
2	33.194	0.0017
3	39.967	0.0023
4	31.422	0.00714

Tension		
Point	$\sigma$ (MPa)	$\epsilon$
5	2.3	0.000092
6	0.284	0.00092

Table A-14: DRAIN-3DX values for confined concrete in 1<sup>st</sup> floor beams (300) in the critical region

**2<sup>nd</sup> Floor beams (300 · 260 mm)**

DRAIN-3DX		
Compression		
Point	$\sigma$ (MPa)	$\epsilon$
0	0	0
1	20.627	0.00105
2	28.283	0.0016
3	31.916	0.0022
4	27.129	0.00803

Tension		
Point	$\sigma$ (MPa)	$\epsilon$
5	2.3	0.000104
6	0.284	0.00104

**Table A-15: DRAIN-3DX values for confined concrete in 2<sup>nd</sup> floor beams (300) in the critical region**

## APPENDIX B

### Stress-strain model for concrete confined with CFRP

#### 2<sup>nd</sup> Floor columns

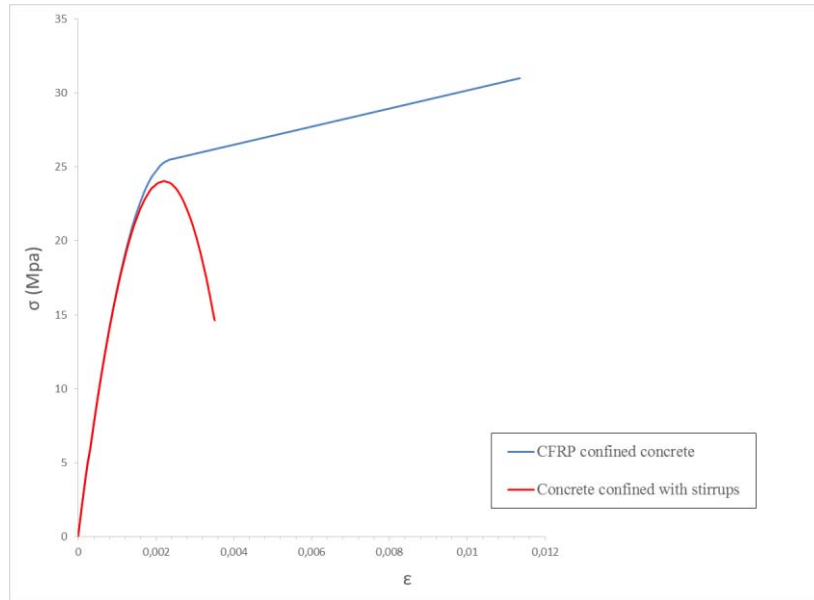
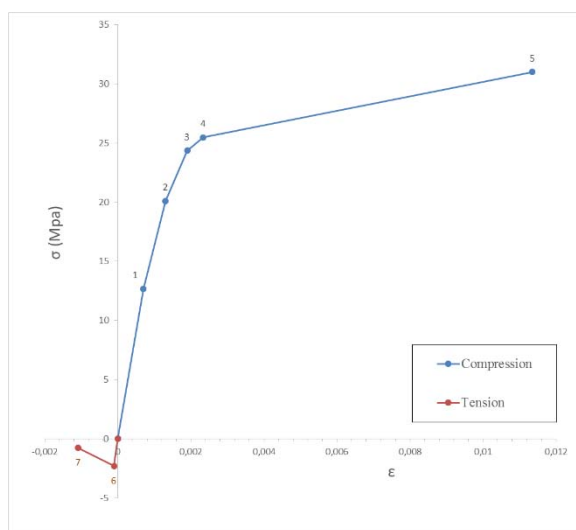


Figure B.1: Comparison between compressive stress-strain model for concrete confined with stirrups and CFRP confined concrete in 2<sup>nd</sup> floor columns.



DRAIN-3DX		
Compression		
Point	$\sigma$ (MPa)	$\epsilon$
0	0	0
1	12.681	0.0007
2	20.112	0.0013
3	24.371	0.0019
4	25.475	0.00234
5	31.003	0.0113

Tension		
Point	$\sigma$ (MPa)	$\epsilon$
6	2.3	0.000109
7	0.769	0.00109

Figure B.2: DRAIN-3DX stress-strain model and values for CFRP confined concrete in 2<sup>nd</sup> floor columns.



### 1<sup>st</sup> Floor beams (400 · 260 mm)

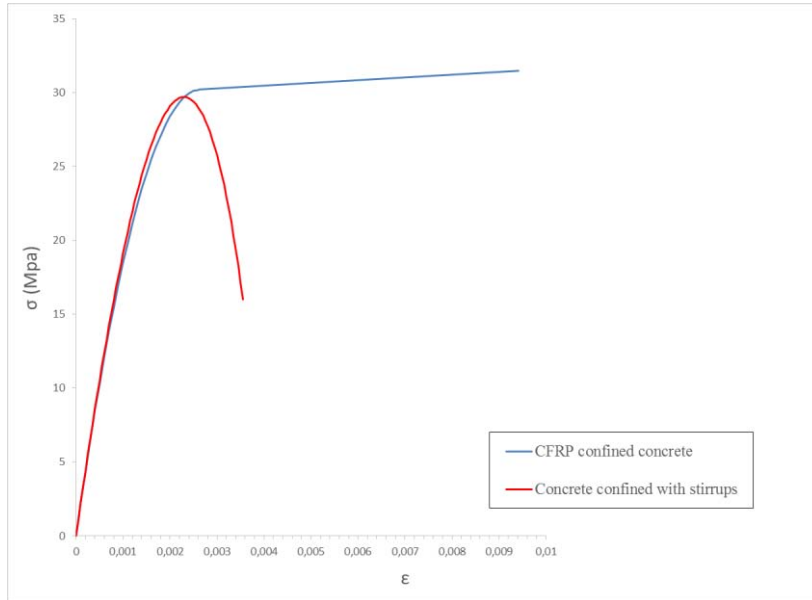
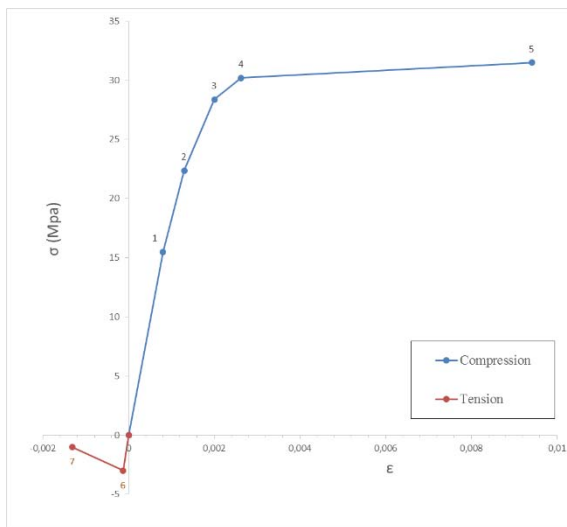


Figure B.3: Comparison between compressive stress-strain model for concrete confined with stirrups and CFRP confined concrete in 1<sup>st</sup> floor beams (400)



DRAIN-3DX		
Compression		
Point	$\sigma$ (MPa)	$\epsilon$
0	0	0
1	15.486	0.0008
2	22.367	0.0013
3	28.386	0.002
4	30.197	0.00263
5	31.489	0.00941

Tension		
Point	$\sigma$ (MPa)	$\epsilon$
6	3	0.000132
7	0.37	0.00132

Figure B.4: DRAIN-3DX stress-strain model and values for confined concrete in 1<sup>st</sup> floor beams (400).

## 2<sup>nd</sup> Floor beams (400 · 260 mm)

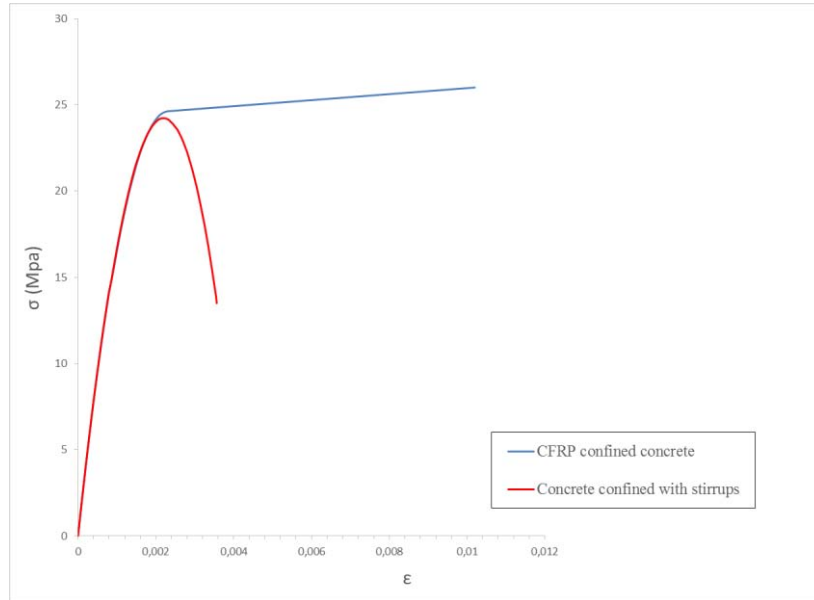
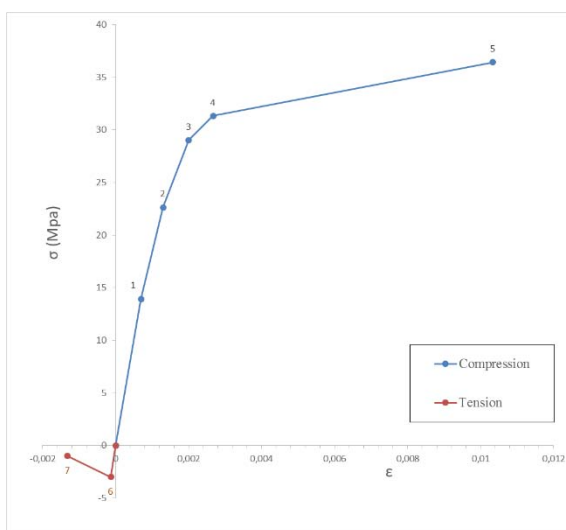


Figure B.5: Comparison between compressive stress-strain model for concrete confined with stirrups and CFRP confined concrete in 2<sup>nd</sup> floor beams (400)



DRAIN-3DX		
Compression		
Point	$\sigma$ (MPa)	$\epsilon$
0	0	0
1	17.799	0.0011
2	21.534	0.0015
3	24.149	0.002
4	24.624	0.0023
5	26.011	0.0102

Tension		
Point	$\sigma$ (MPa)	$\epsilon$
6	2.3	0.000109
7	0.769	0.00109

Figure B.6: DRAIN-3DX stress-strain model and values for confined concrete in 2<sup>nd</sup> floor beams (400).

## 1<sup>st</sup> Floor beams (300 · 260 mm)

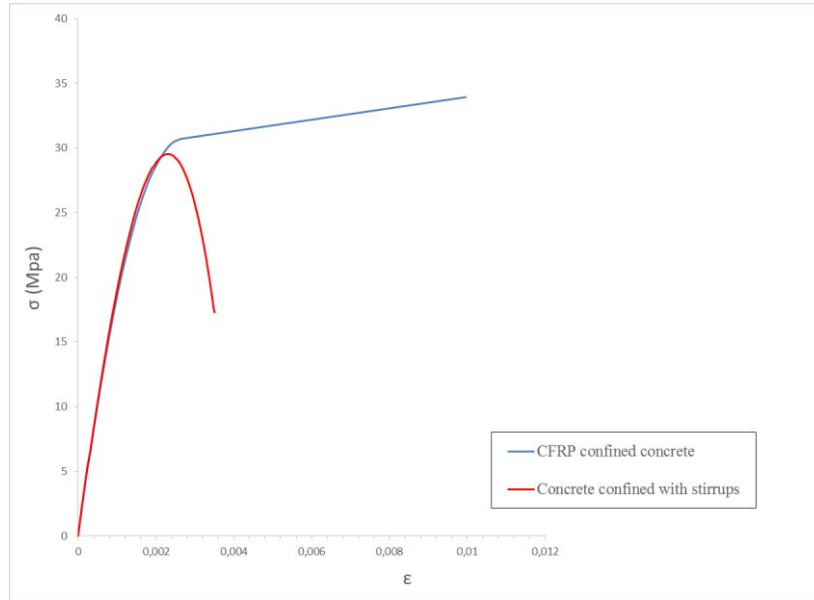
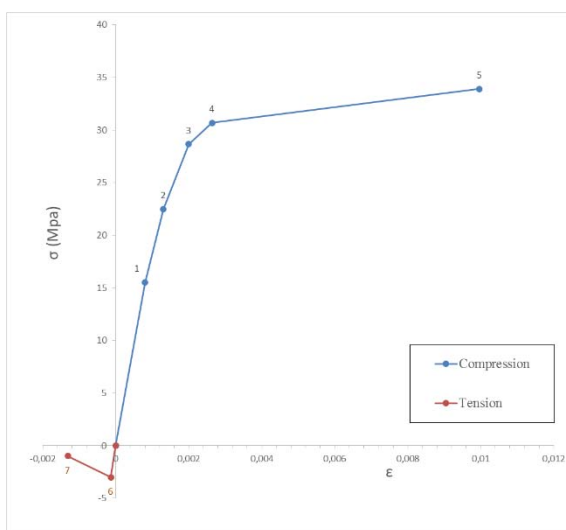


Figure B.7: Comparison between compressive stress-strain model for concrete confined with stirrups and CFRP confined concrete in 1<sup>st</sup> floor beams (300)



DRAIN-3DX		
Compression		
Point	$\sigma$ (MPa)	$\epsilon$
0	0	0
1	15.531	0.0008
2	22.486	0.0013
3	28.667	0.002
4	30.687	0.0026
5	33.921	0.01

Tension		
Point	$\sigma$ (MPa)	$\epsilon$
6	3	0.000132
7	0.37	0.00132

Figure B.8: DRAIN-3DX stress-strain model and values for confined concrete in 1<sup>st</sup> floor beams (300).

## 2<sup>nd</sup> Floor beams (300 · 260 mm)

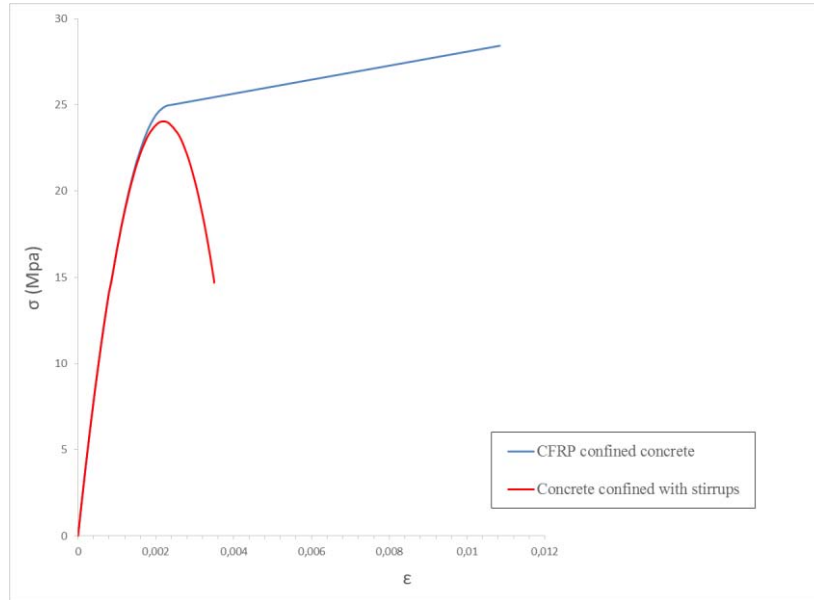
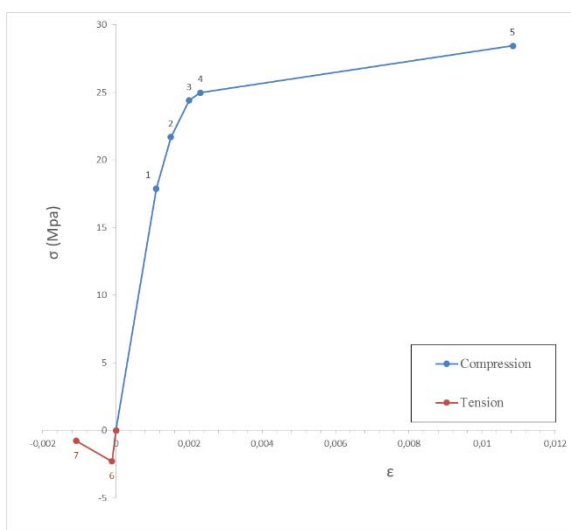


Figure B.9: Comparison between compressive stress-strain model for concrete confined with stirrups and CFRP confined concrete in 2<sup>nd</sup> floor beams (300)



DRAIN-3DX		
Compression		
Point	$\sigma$ (MPa)	$\epsilon$
0	0	0
1	17.877	0.0011
2	21.680	0.0015
3	24.408	0.002
4	24.971	0.00231
5	28.433	0.0108

Tension		
Point	$\sigma$ (MPa)	$\epsilon$
6	2.3	0.000109
7	0.769	0.00109

Figure B.10: DRAIN-3DX stress-strain model and values for confined concrete in 2<sup>nd</sup> floor beams (300).

# APPENDIX C

## Element segments and cross section fibers

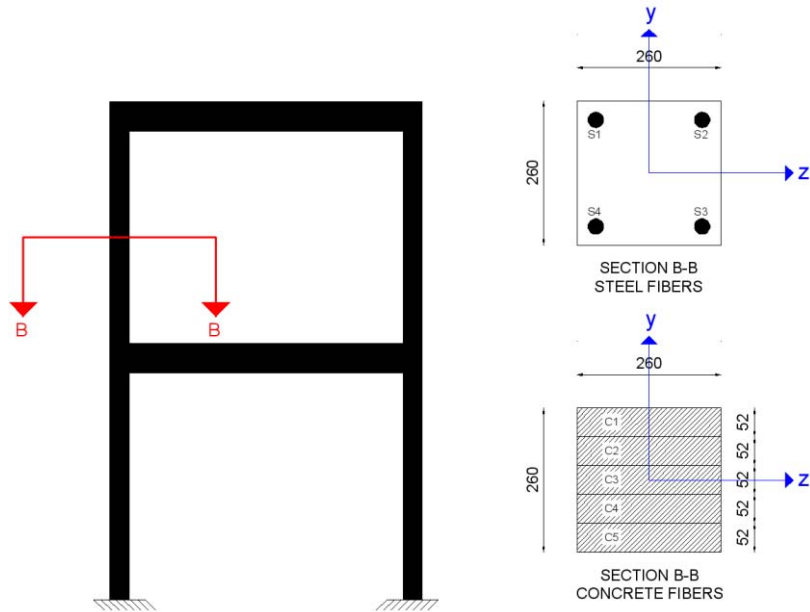


Figure C.1: Fibers cross section for 2<sup>nd</sup> floor columns in both bare frame and CFRP retrofitted frame.

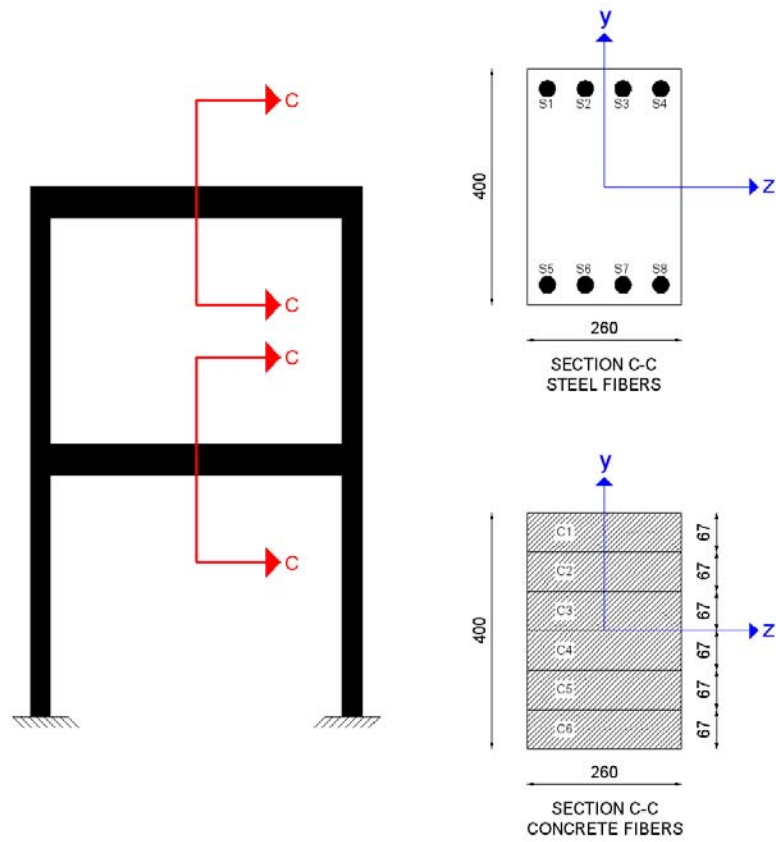


Figure C.2: Fibers cross section for 1<sup>st</sup> and 2<sup>nd</sup> floor beams (400 · 260) in bare frame.

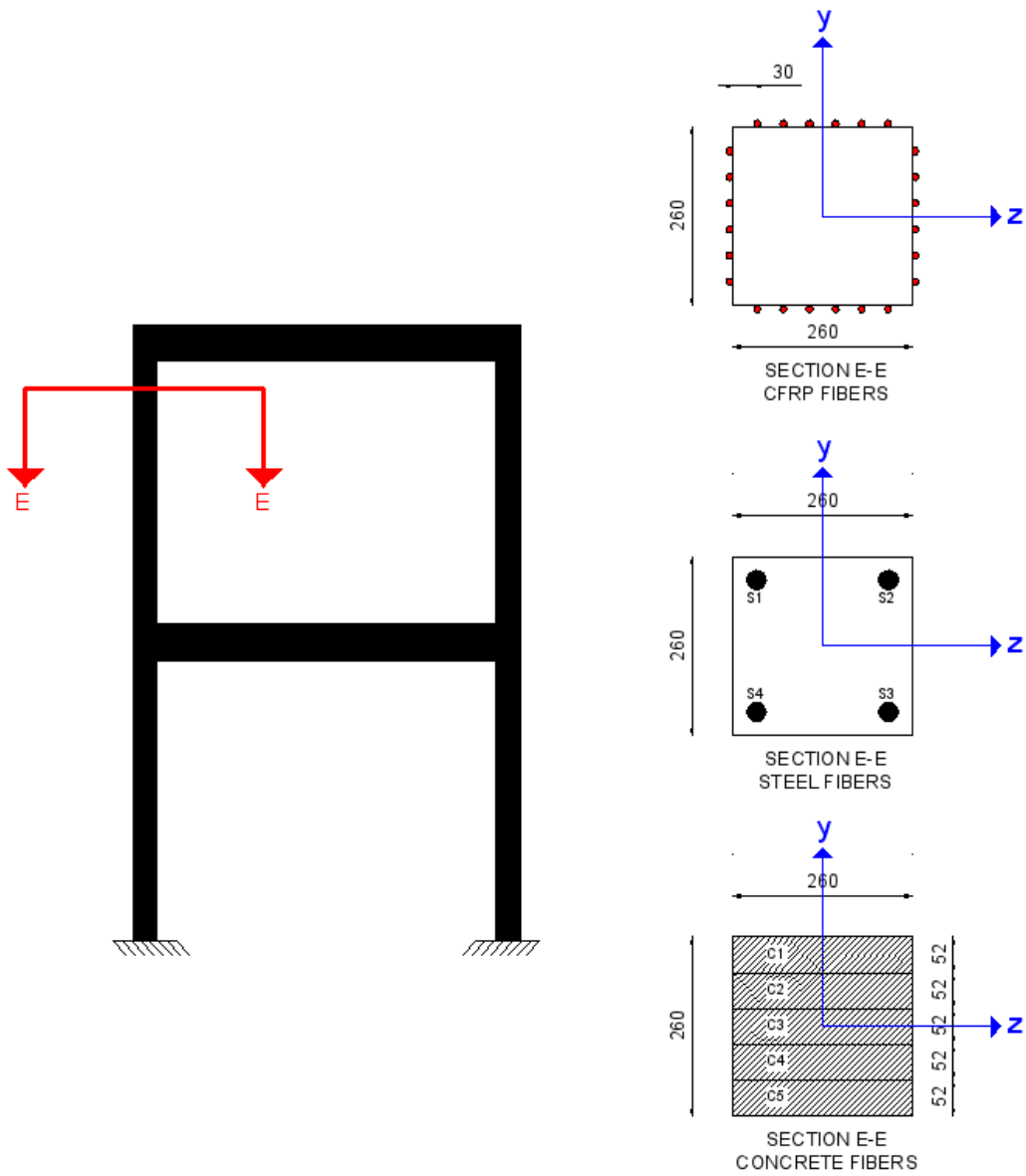


Figure C.3: Fibers cross section for 2<sup>nd</sup> floor columns in CFRP retrofitted frame.

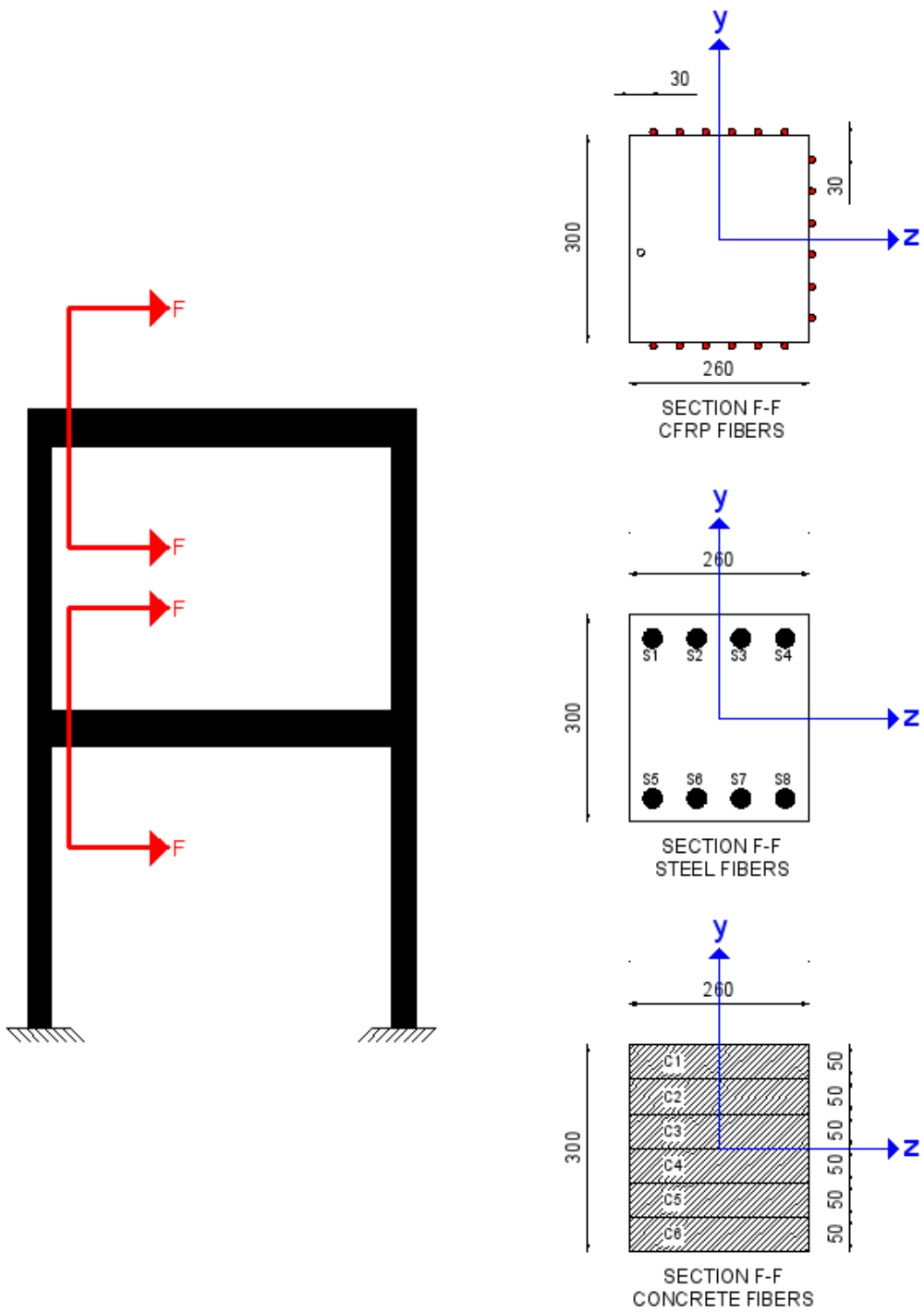


Figure C.4: Fibers cross section for 1<sup>st</sup> and 2<sup>nd</sup> floor beams (300 · 260) in CFRP retrofitted frame.

## APPENDIX D

---

### Input files of DRAIN-3DX

#### D1. Test sequence 1 – Bare frame

\*STARTXX

! Nodal Restraints: Sequential Generation

TimeH 0 1 1 0 time history Units: kNm

!

\*NODECOORDS

! Control Nodes (C-lines)

C 1010 0 0 0  
C 1020 4 0 0  
C 2010 0 3.3 0  
C 2020 4 3.3 0  
C 3010 0 6.6 0  
C 3020 4 6.6 0  
C 2011 0.13 3.3 0  
C 2012 0.65 3.3 0  
C 2013 1.1 3.3 0  
C 2014 1.55 3.3 0  
C 2015 2 3.3 0  
C 2016 2.45 3.3 0  
C 2017 2.9 3.3 0  
C 2018 3.35 3.3 0  
C 2019 3.87 3.3 0  
C 3011 0.13 6.6 0  
C 3012 0.65 6.6 0  
C 3013 1.1 6.6 0  
C 3014 1.55 6.6 0  
C 3015 2 6.6 0  
C 3016 2.45 6.6 0  
C 3017 2.9 6.6 0  
C 3018 3.35 6.6 0  
C 3019 3.87 6.6 0  
C 1910 0 3.1 0  
C 2110 0 3.5 0  
C 2910 0 6.4 0  
C 1920 4 3.1 0  
C 2120 4 3.5 0  
C 2920 4 6.4 0  
! Control Nodes  
C 1111 0 0 1  
C 2222 0 10 0



```

C 3333 4 0 1
!
!
*RESTRAINTS
! Nodal Restraints: Sequential Generation
S 222222 1010 1020 10
S 001110 2010 2020 1
S 001110 3010 3020 1
S 111111 1111 3333 1111
S 001110 1910 1920 10
S 001110 2110 2120 10
S 001110 2910 2920 10
!
*MASSES
! Nodal Masses: Sequential Generation
S 100 5.927 2010 2020 10 1.0 0.757841
S 100 5.029 3010 3020 10
!
*ELEMENTGROUP
! Group 1
! Element Group Definition
15 1 1 0.001301 COL-1
!
! Controle information
!
1 1 1 0 0 0 0 0 1
!
! Concrete Material Properties
! Controle Line
4 2 0.5 100
!
! Stress Strain Points for Compression
! Stress Strain
15371 0.0007
27207 0.0015
31545 0.0023
26813 0.00351
!
! Stress Strain Points for Tension
! Stress Strain
2300 0.000092
284 0.00092
!
! Steel Material Properties
! Controle Line

```

```

2 100
!
! Stress Strain Points for Steel
! Stress  Strain
526000 0.0026
616000 0.19
!
! Fiber Cross Section Types
! Controle Line
13 1
!
! Fibers Data
!
-0.110 0.110 0.000154 S1
0 0.110 0.000154 S1
0.110 0.110 0.000154 S1
-0.110 0 0.000154 S1
0.110 0 0.000154 S1
-0.110 -0.110 0.000154 S1
0 -0.110 0.000154 S1
0.110 -0.110 0.000154 S1
0 0.104 0.01352 C1
0 0.052 0.01352 C1
0 0 0.01352 C1
0 -0.052 0.01352 C1
0 -0.104 0.01352 C1
!
! Fiber Cross Section Types
! Controle Line
!
! Fibers Data
!
! Element Geometry Types
! Controle Line
1
!
! Segment data, Element Geometry Types
!
1 F01
!
! Element Generation Commands
!
1 1010 1910 900 1111 1
2 1020 1920 900 3333 1
!

```

```

*ELEMENTGROUP
! Group 2
! Element Group Definition
15  1  1  0.001301      COL-2
!
! Controle information
!
1  1  1  0  0  0  0  0  1
!
! Concrete Material Properties
! Controle Line
4  2  0.5  100
!
! Stress Strain Points for Compression
! Stress   Strain
13506  0.0007
22612  0.0014
26543  0.0022
22562  0.00351
!
! Stress Strain Points for Tension
! Stress   Strain
2300  0.000104
284  0.00104
!
! Steel Material Properties
! Controle Line
2  100
!
! Stress Strain Points for Steel
! Stress   Strain
526000  0.0026
616000  0.19
!
! Fiber Cross Section Types
! Controle Line
9  1
!
! Fibers Data
!
-0.110  0.110  0.000154  S1
0.110  0.110  0.000154  S1
-0.110  -0.110  0.000154  S1
0.110  -0.110  0.000154  S1
0  0.104  0.01352  C1

```

```

0    0.052  0.01352  C1
0    0      0.01352  C1
0    -0.052 0.01352  C1
0    -0.104 0.01352  C1
!
! Fiber Cross Section Types
! Controle Line
!
! Fibers Data
!
! Element Geometry Types
! Controle Line
1
!
! Segment data, Element Geometry Types
!
1    F01
!
! Element Generation Commands
!
1  2110  2910  800  1111  1
2  2120  2920  800  3333  1
!
*ELEMENTGROUP
! Group 3
! Element Group Definition
15  1  1  0.001301  BEAMS-MID1
!
! Controle information
!
1  1  1  0  0  0  0  0  1
!
! Concrete Material Properties
! Controle Line
4  2  0.5  100
!
! Stress Strain Points for Compression
! Stress  Strain
15400  0.0007
28761  0.00165
31700  0.0023
26945  0.00354
!
! Stress Strain Points for Tension
! Stress  Strain

```

```

2300  0.000092
284   0.00092
!
! Steel Material Properties
! Controle Line
2  100
!
! Stress Strain Points for Steel
! Stress   Strain
526000  0.0026
616000  0.19
!
! Fiber Cross Section Types
! Controle Line
14  1
!
! Fibers Data
!
-0.180  0.110  0.000154  S1
0.180   0.110  0.000154  S1
-0.180  0.0333 0.000154  S1
0.180   0.0333 0.000154  S1
-0.180 -0.0333 0.000154  S1
0.180  -0.0333 0.000154  S1
-0.180 -0.110  0.000154  S1
0.180  -0.110  0.000154  S1
-0.168  0      0.017333  C1
-0.101  0      0.017333  C1
-0.034  0      0.017333  C1
0.034   0      0.017333  C1
0.101   0      0.017333  C1
0.168   0      0.017333  C1
!
! Element Geometry Types
! Controle Line
1
!
! Segment data, Element Geometry Types
!
1      F01
!
! Element Generation Commands
!
1  2012  2013  0001  2222  1
2  2013  2014  0001  2222  1

```

```

3 2014 2015 0001 2222 1
4 2015 2016 0001 2222 1
5 2016 2017 0001 2222 1
6 2017 2018 0001 2222 1
!
*ELEMENTGROUP
! Group 4
! Element Group Definition
15 1 1 0.001301 BEAMS-MID2
!
! Controle information
!
1 1 1 0 0 0 0 0 1
!
! Concrete Material Properties
! Controle Line
4 2 0.5 100
!
! Stress Strain Points for Compression
! Stress Strain
14353 0.00075
24436 0.0016
26725 0.0022
22716 0.00357
!
! Stress Strain Points for Tension
! Stress Strain
2300 0.000104
284 0.00104
!
! Steel Material Properties
! Controle Line
2 100
!
! Stress Strain Points for Steel
! Stress Strain
526000 0.0026
616000 0.19
!
! Fiber Cross Section Types
! Controle Line
14 1
!
! Fibers Data
!
```

```

-0.180  0.110  0.000154  S1
0.180   0.110  0.000154  S1
-0.180  0.0333  0.000154  S1
0.180   0.0333  0.000154  S1
-0.180 -0.0333  0.000154  S1
0.180  -0.0333  0.000154  S1
-0.180 -0.110  0.000154  S1
0.180  -0.110  0.000154  S1
-0.168  0      0.017333  C1
-0.101  0      0.017333  C1
-0.034  0      0.017333  C1
0.034   0      0.017333  C1
0.101   0      0.017333  C1
0.168   0      0.017333  C1
!
! Element Geometry Types
! Controle Line
1
!
! Segment data, Element Geometry Types
!
1      F01
!
! Element Generation Commands
!
1  3012  3013  0001  2222  1
2  3013  3014  0001  2222  1
3  3014  3015  0001  2222  1
4  3015  3016  0001  2222  1
5  3016  3017  0001  2222  1
6  3017  3018  0001  2222  1
!
*ELEMENTGROUP
! Group 5
! Element Group Definition
15  1  1  0.001301      COL-JOINT1
!
! Controle information
!
1  1  1  0  1  1  1  0  1
!
! Concrete Material Properties
! Controle Line
4  2  0.5  100
!

```

! Stress Strain Points for Compression

! Stress Strain

15371 0.0007

27207 0.0015

31545 0.0023

26813 0.00351

!

! Stress Strain Points for Tension

! Stress Strain

2300 0.000092

284 0.00092

!

! Steel Material Properties

! Controle Line

2 100

!

! Stress Strain Points for Steel

! Stress Strain

526000 0.0026

616000 0.19

!

! Fiber Cross Section Types

! Controle Line

13 1

!

! Fibers Data

!

-0.110 0.110 0.000154 S1

0 0.110 0.000154 S1

0.110 0.110 0.000154 S1

-0.110 0 0.000154 S1

0.110 0 0.000154 S1

-0.110 -0.110 0.000154 S1

0 -0.110 0.000154 S1

0.110 -0.110 0.000154 S1

0 0.104 0.01352 C1

0 0.052 0.01352 C1

0 0 0.01352 C1

0 -0.052 0.01352 C1

0 -0.104 0.01352 C1

!

! Fiber Cross Section Types

! Controle Line

!

! Fibers Data



```

!
! Pullout properties for connection Hinge Fibers
! Basic Properties (1)
2.92E+08 6.56E+07 0.01 526000 616000 526000 616000 0.01 1
! Degradation Parameters (1)
1 1 1 0.005 0.005 1 1 1
!
! Gap Properties for Connection Hinge Fibers
!
8000 17033 2.45E+07 1.37E+07 7.95E+06 0.5 0.01
!
! Connection Hinge Types
! Control Line
13
!
! Fibers Data for Connection Hinge types
!
-0.105 0.105 0.000154 P1
0 0.105 0.000154 P1
0.105 0.105 0.000154 P1
-0.105 0 0.000154 P1
0.105 0 0.000154 P1
-0.105 -0.105 0.000154 P1
0 -0.105 0.000154 P1
0.105 -0.105 0.000154 P1
0 0.104 0.01352 G1
0 0.052 0.01352 G1
0 0 0.01352 G1
0 -0.052 0.01352 G1
0 -0.104 0.01352 G1
!
! Element Geometry Types
! Controle Line
3 1
!
! Segment data, Element Geometry Types
!
0.1 F01
0.8 F01
0.1 F01
!
! Element Generation Commands
!
1 1910 2010 100 1111 1
2 1920 2020 100 3333 1

```

```

!
*ELEMENTGROUP
! Group 6
! Element Group Definition
15  1  1  0.001301      COL-JOINT2-DOWN
!
! Controle information
!
1  1  1  0  0  0  0  0  1
!
! Concrete Material Properties
! Controle Line
4  2  0.5  100
!
! Stress Strain Points for Compression
! Stress   Strain
13506  0.0007
22612  0.0014
26543  0.0022
22562  0.00351
!
! Stress Strain Points for Tension
! Stress   Strain
2300  0.000104
284   0.00104
!
! Steel Material Properties
! Controle Line
2  100
!
! Stress Strain Points for Steel
! Stress   Strain
526000  0.0026
616000  0.19
!
! Fiber Cross Section Types
! Controle Line
9  1
!
! Fibers Data
!
-0.110  0.110  0.000154  S1
0.110  0.110  0.000154  S1
-0.110 -0.110  0.000154  S1
0.110  -0.110  0.000154  S1

```

```

0    0.104  0.01352  C1
0    0.052  0.01352  C1
0    0      0.01352  C1
0   -0.052  0.01352  C1
0   -0.104  0.01352  C1
!
! Fiber Cross Section Types
! Controle Line
!
! Fibers Data
!
! Element Geometry Types
! Controle Line
1
!
! Segment data, Element Geometry Types
!
1    F01
!
! Element Generation Commands
!
1  2010  2110  100  1111  1
2  2020  2120  100  3333  1
!
!
*ELEMENTGROUP
! Group 7
! Element Group Definition
15  1  1  0.001301      BEAM-JOINT1
!
! Controle information
!
1  1  1  0  1  1  1  1  1
!
! Concrete Material Properties
! Controle Line
4  2  0.5  100
!
! Stress Strain Points for Compression
! Stress  Strain
15400  0.0007
28761  0.00165
31700  0.0023
26945  0.00354
!

```

```

! Stress Strain Points for Tension
! Stress   Strain
2300   0.000092
284    0.00092
!
! Steel Material Properties
! Controle Line
2   100
!
! Stress Strain Points for Steel
! Stress   Strain
526000 0.0026
616000 0.19
!
! Fiber Cross Section Types
! Controle Line
14  1
!
! Fibers Data
!
-0.180 0.110 0.000154 S1
0.180 0.110 0.000154 S1
-0.180 0.0333 0.000154 S1
0.180 0.0333 0.000154 S1
-0.180 -0.0333 0.000154 S1
0.180 -0.0333 0.000154 S1
-0.180 -0.110 0.000154 S1
0.180 -0.110 0.000154 S1
-0.168 0 0.017333 C1
-0.101 0 0.017333 C1
-0.034 0 0.017333 C1
0.034 0 0.017333 C1
0.101 0 0.017333 C1
0.168 0 0.017333 C1
!
! Pullout properties for connection Hinge Fibers
! Basic Properties (1)
2.92E+08 1.00E+00 0.01 467000 468000 467000 468000 0.01 1
! Degradation Parameters (1)
1 1 1 0.005 0.005 1 1 1
!
! Gap Properties for Connection Hinge Fibers
!
8000 17033 2.45E+07 1.37E+07 7.95E+06 0.5 0.01
!

```

```

! Connection Hinge Types
! Control Line
14
!
! Fibers Data for Connection Hinge types
!
-0.175  0.105  0.000154  P1
0.175   0.105  0.000154  P1
-0.175  0.0333 0.000154  P1
0.175   0.0333 0.000154  P1
-0.175 -0.0333 0.000154  P1
0.175  -0.0333 0.000154  P1
-0.175 -0.105  0.000154  P1
0.175  -0.105  0.000154  P1
-0.168  0      0.017333  G1
-0.101  0      0.017333  G1
-0.034  0      0.017333  G1
0.034   0      0.017333  G1
0.101   0      0.017333  G1
0.168   0      0.017333  G1
!
! Rigid End Zone Types
!
0.12
!
! Element Geometry Types
! Control Line
1  1  1
!
! Segment data, Element Geometry Types
!
1      F01
!
! Element Generation Commands
!
1  2010  2011  1  1111  1
2  2019  2020  1  1111  1
!
*ELEMENTGROUP
! Group 8
! Element Group Definition
15  1  1  0.001301  BEAM-JOINT2
!
! Control information
!

```

```

1 1 1 0 1 1 1 1 1
!
! Concrete Material Properties
! Controle Line
4 2 0.5 100
!
! Stress Strain Points for Compression
! Stress Strain
14353 0.00075
24436 0.0016
26725 0.0022
22716 0.00357
!
! Stress Strain Points for Tension
! Stress Strain
2300 0.000104
284 0.00104
!
! Steel Material Properties
! Controle Line
2 100
!
! Stress Strain Points for Steel
! Stress Strain
526000 0.0026
616000 0.19
!
! Fiber Cross Section Types
! Controle Line
14 1
!
! Fibers Data
!
-0.180 0.110 0.000154 S1
0.180 0.110 0.000154 S1
-0.180 0.0333 0.000154 S1
0.180 0.0333 0.000154 S1
-0.180 -0.0333 0.000154 S1
0.180 -0.0333 0.000154 S1
-0.180 -0.110 0.000154 S1
0.180 -0.110 0.000154 S1
-0.168 0 0.017333 C1
-0.101 0 0.017333 C1
-0.034 0 0.017333 C1
0.034 0 0.017333 C1

```

```

0.101  0    0.017333  C1
0.168  0    0.017333  C1
!
! Pullout properties for connection Hinge Fibers
! Basic Properties (1)
2.92E+08  1.00E+00  0.01  428000  429000  428000  429000  0.01  1
! Degradation Parameters (1)
1    1    1    0.005  0.005  1    1    1
!
! Gap Properties for Connection Hinge Fibers
!
8000    17033    2.45E+07  1.37E+07  7.95E+06  0.5    0.01
!
! Connection Hinge Types
! Control Line
14
!
! Fibers Data for Connection Hinge types
!
-0.175  0.105  0.000154  P1
0.175  0.105  0.000154  P1
-0.175  0.0333  0.000154  P1
0.175  0.0333  0.000154  P1
-0.175  -0.0333  0.000154  P1
0.175  -0.0333  0.000154  P1
-0.175  -0.105  0.000154  P1
0.175  -0.105  0.000154  P1
-0.168  0    0.017333  G1
-0.101  0    0.017333  G1
-0.034  0    0.017333  G1
0.034  0    0.017333  G1
0.101  0    0.017333  G1
0.168  0    0.017333  G1
!
! Rigid End Zone Types
!
0.12
!
! Element Geometry Types
! Control Line
1    1    1
!
! Segment data, Element Geometry Types
!
1    F01

```

```

!
! Element Generation Commands
!
1 3010 3011 1 1111 1
2 3019 3020 1 1111 1
!
*ELEMENTGROUP
! Group 9
! Element Group Definition
15 1 1 0.001301 BEAM-1RIGHT
!
! Controle information
!
1 1 1 0 0 0 0 0 1
!
! Concrete Material Properties
! Controle Line
4 2 0.5 100
!
! Stress Strain Points for Compression
! Stress Strain
15400 0.0007
28761 0.00165
31700 0.0023
26945 0.00354
!
! Stress Strain Points for Tension
! Stress Strain
2300 0.000092
284 0.00092
!
! Steel Material Properties
! Controle Line
2 100
!
! Stress Strain Points for Steel
! Stress Strain
526000 0.0026
616000 0.19
!
! Fiber Cross Section Types
! Controle Line
14 1
!
! Fibers Data

```



```

!
-0.180 0.110 0.000154 S1
0.180 0.110 0.000154 S1
-0.180 0.0333 0.000154 S1
0.180 0.0333 0.000154 S1
-0.180 -0.0333 0.000154 S1
0.180 -0.0333 0.000154 S1
-0.180 -0.110 0.000154 S1
0.180 -0.110 0.000154 S1
-0.168 0 0.017333 C1
-0.101 0 0.017333 C1
-0.034 0 0.017333 C1
0.034 0 0.017333 C1
0.101 0 0.017333 C1
0.168 0 0.017333 C1
!
! Element Geometry Types
! Controle Line
1
!
! Segment data, Element Geometry Types
!
1 F01
!
! Element Generation Commands
!
1 2018 2019 0001 2222 1
!
*ELEMENTGROUP
! Group 10
! Element Group Definition
15 1 1 0.001301 BEAM-2RIGHT
!
! Controle information
!
1 1 1 0 1 1 1 0 1
!
! Concrete Material Properties
! Controle Line
4 2 0.5 100
!
! Stress Strain Points for Compression
! Stress Strain
14353 0.00075
24436 0.0016

```

```

26725 0.0022
22716 0.00357
!
! Stress Strain Points for Tension
! Stress Strain
2300 0.000104
284 0.00104
!
! Steel Material Properties
! Controle Line
2 100
!
! Stress Strain Points for Steel
! Stress Strain
526000 0.0026
616000 0.19
!
! Fiber Cross Section Types
! Controle Line
14 1
!
! Fibers Data
!
-0.180 0.110 0.000154 S1
0.180 0.110 0.000154 S1
-0.180 0.0333 0.000154 S1
0.180 0.0333 0.000154 S1
-0.180 -0.0333 0.000154 S1
0.180 -0.0333 0.000154 S1
-0.180 -0.110 0.000154 S1
0.180 -0.110 0.000154 S1
-0.168 0 0.017333 C1
-0.101 0 0.017333 C1
-0.034 0 0.017333 C1
0.034 0 0.017333 C1
0.101 0 0.017333 C1
0.168 0 0.017333 C1
!
! Pullout properties for connection Hinge Fibers
! Basic Properties (1)
2.92E+08 1.00E+00 0.01 428000 429000 428000 429000 0.01 1
! Degradation Parameters (1)
1 1 1 0.005 0.005 1 1 1
!
! Gap Properties for Connection Hinge Fibers

```

```

!
8000  17033  2.45E+07  1.37E+07  7.95E+06  0.5  0.01
!
! Connection Hinge Types
! Control Line
14
!
! Fibers Data for Connection Hinge types
!
-0.175  0.105  0.000154  P1
0.175  0.105  0.000154  P1
-0.175  0.0333  0.000154  P1
0.175  0.0333  0.000154  P1
-0.175  -0.0333  0.000154  P1
0.175  -0.0333  0.000154  P1
-0.175  -0.105  0.000154  P1
0.175  -0.105  0.000154  P1
-0.168  0  0.017333  G1
-0.101  0  0.017333  G1
-0.034  0  0.017333  G1
0.034  0  0.017333  G1
0.101  0  0.017333  G1
0.168  0  0.017333  G1
!
! Element Geometry Types
! Control Line
1  1
!
! Segment data, Element Geometry Types
!
1  F01
!
! Element Generation Commands
!
1  3018  3019  0001  2222  1
!
*ELEMENTGROUP
! Group 11
! Element Group Definition
15  1  1  0.001301  BEAM-1LEFT
!
! Control information
!
1  1  1  0  0  0  0  0  1
!

```

```

! Concrete Material Properties
! Controle Line
4 2 0.5 100
!
! Stress Strain Points for Compression
! Stress Strain
15400 0.0007
28761 0.00165
31700 0.0023
26945 0.00354
!
! Stress Strain Points for Tension
! Stress Strain
2300 0.000092
284 0.00092
!
! Steel Material Properties
! Controle Line
2 100
!
! Stress Strain Points for Steel
! Stress Strain
526000 0.0026
616000 0.19
!
! Fiber Cross Section Types
! Controle Line
14 1
!
! Fibers Data
!
-0.180 0.110 0.000154 S1
0.180 0.110 0.000154 S1
-0.180 0.0333 0.000154 S1
0.180 0.0333 0.000154 S1
-0.180 -0.0333 0.000154 S1
0.180 -0.0333 0.000154 S1
-0.180 -0.110 0.000154 S1
0.180 -0.110 0.000154 S1
-0.168 0 0.017333 C1
-0.101 0 0.017333 C1
-0.034 0 0.017333 C1
0.034 0 0.017333 C1
0.101 0 0.017333 C1
0.168 0 0.017333 C1

```

```

!
! Element Geometry Types
! Controle Line
1
!
! Segment data, Element Geometry Types
!
1      F01
!
! Element Generation Commands
!
1 2011  2012  0001  2222  1
!
*ELEMENTGROUP
! Group 12
! Element Group Definition
15  1  1  0.001301      BEAM-2LEFT
!
! Controle information
!
1  1  1  0  1  1  1  0  1
!
! Concrete Material Properties
! Controle Line
4  2  0.5  100
!
! Stress Strain Points for Compression
! Stress   Strain
14353  0.00075
24436  0.0016
26725  0.0022
22716  0.00357
!
! Stress Strain Points for Tension
! Stress   Strain
2300  0.000104
284   0.00104
!
! Steel Material Properties
! Controle Line
2  100
!
! Stress Strain Points for Steel
! Stress   Strain
526000  0.0026

```

```

616000 0.19
!
! Fiber Cross Section Types
! Control Line
14 1
!
! Fibers Data
!
-0.180 0.110 0.000154 S1
0.180 0.110 0.000154 S1
-0.180 0.0333 0.000154 S1
0.180 0.0333 0.000154 S1
-0.180 -0.0333 0.000154 S1
0.180 -0.0333 0.000154 S1
-0.180 -0.110 0.000154 S1
0.180 -0.110 0.000154 S1
-0.168 0 0.017333 C1
-0.101 0 0.017333 C1
-0.034 0 0.017333 C1
0.034 0 0.017333 C1
0.101 0 0.017333 C1
0.168 0 0.017333 C1
!
! Pullout properties for connection Hinge Fibers
! Basic Properties (1)
2.92E+08 1.00E+00 0.01 428000 429000 428000 429000 0.01 1
! Degradation Parameters (1)
1 1 1 0.005 0.005 1 1 1
!
! Gap Properties for Connection Hinge Fibers
!
8000 17033 2.45E+07 1.37E+07 7.95E+06 0.5 0.01
!
! Connection Hinge Types
! Control Line
14
!
! Fibers Data for Connection Hinge types
!
-0.175 0.105 0.000154 P1
0.175 0.105 0.000154 P1
-0.175 0.0333 0.000154 P1
0.175 0.0333 0.000154 P1
-0.175 -0.0333 0.000154 P1
0.175 -0.0333 0.000154 P1

```

```

-0.175 -0.105 0.000154 P1
0.175 -0.105 0.000154 P1
-0.168 0 0.017333 G1
-0.101 0 0.017333 G1
-0.034 0 0.017333 G1
0.034 0 0.017333 G1
0.101 0 0.017333 G1
0.168 0 0.017333 G1
!
! Element Geometry Types
! Controle Line
1 1
!
! Segment data, Element Geometry Types
!
1 F01
!
! Element Generation Commands
!
1 3011 3012 0001 2222 1
!
*ELEMENTGROUP
! Group 13
! Element Group Definition
15 1 1 0.001301 COL-JOINT2-UP
!
! Controle information
!
1 1 1 0 0 0 0 0 1
!
! Concrete Material Properties
! Controle Line
4 2 0.5 100
!
! Stress Strain Points for Compression
! Stress Strain
13506 0.0007
22612 0.0014
26543 0.0022
22562 0.00351
!
! Stress Strain Points for Tension
! Stress Strain
2300 0.000104
284 0.00104

```

```

!
! Steel Material Properties
! Controle Line
2 100
!
! Stress Strain Points for Steel
! Stress Strain
526000 0.0026
616000 0.19
!
! Fiber Cross Section Types
! Controle Line
9 1
!
! Fibers Data
!
-0.110 0.110 0.000154 S1
0.110 0.110 0.000154 S1
-0.110 -0.110 0.000154 S1
0.110 -0.110 0.000154 S1
0 0.104 0.01352 C1
0 0.052 0.01352 C1
0 0 0.01352 C1
0 -0.052 0.01352 C1
0 -0.104 0.01352 C1
!
! Fiber Cross Section Types
! Controle Line
!
! Fibers Data
!
! Element Geometry Types
! Controle Line
1
!
! Segment data, Element Geometry Types
!
1 F01
!
! Element Generation Commands
!
1 2910 3010 100 1111 1
2 2920 3020 100 3333 1
!
*RESULTS

```



```

! Nodal Results: Sequential Generation
!
NSD  001 2020
!
! Element Results: Sequential Generation
!
!!E  001 1  1
!!E  001 1  2
!
*NODALOAD
! Pattern 1
! Pattern Name          Title
VERT                    Permanent Loads
!
! Nodal Loads: Sequential Generation
SF 0  -6    0    2010  2020  10
SF 0  -3    0    3010  3020  10
SF 0 -13.2  0    2012  2018   1
SF 0 -11.6  0    3012  3018   1
SF 0  -6.6  0    2011  2019   8
SF 0  -5.83 0    3011  3019   8
!
*DISPREC
! Ground Displacement Record
! Record Name
D05 0.05    (F14.12)    Elcentro Displacement Record 0.05
!
! Control Information
300301    0  0  1    1    0.001667  0
!
*DISPREC
! Ground Displacement Record
! Record Name
D10 0.10    (F14.12)    Elcentro Displacement Record 0.10
!
! Control Information
300301    0  0  1    1    0.001667  0
!
*DISPREC
! Ground Displacement Record
! Record Name
D20 0.20    (F14.12)    Elcentro Displacement Record 0.20
!
! Control Information
300301    0  0  1    1    0.001667  0

```

```

!
*DISPREC
! Ground Displacement Record
! Record Name
D30 0.30      (F14.12)      Elcentro Displacement Record 0.30
!
! Control Information
132011      0  0 1      1      0.001667  0
!
*DISPREC
! Ground Displacement Record
! Record Name
D40 0.40      (F14.12)      Elcentro Displacement Record 0.25
!
! Control Information
180011      0  0 1      1      0.001667  0
!
*PARAMETERS
! Analysis Parameters
! Event Overshoot Scale Factors
!
F 1  0.01      0.01
F 2  0.01      0.01
F 3  0.01      0.01
F 4  0.01      0.01
F 5  0.01      0.01
F 6  0.01      0.01
F 7  0.01      0.01
F 8  0.01      0.01
F 9  0.01      0.01
F 10 0.01      0.01
F 11 0.01      0.01
F 12 0.01      0.01
F 13 0.01      0.01
!
! Output Intervals for Dynamic Analysis
!
OD  0      0      1  0      0  0      0  0
!
! Controle Parameters for Dynamic Analysis
!
DC  1  0  00
!
! Time Step Parameters for Dynamic Analysis
!

```

```

DT 0.01 0.01
!
!!*GRAV                PERM + Variable
!
! Static Gravity Load Analysis
!
! Nodal Loads
!!N  VERT1.0
!
!!*STAT                Permanent Load Analysis
!
! Static Analysis
!
! Nodal Loads
!
!!N  VERT 1.0
!
! Load Control
!
!!L 1  1
!
*MODE                Mode Shapes
!
! Control Information
!
2      0 0 0
!
*DISN                Dynamic Analysis 01
!
! Control Information
!
40    60000 1
! Ground Displacement Records
!
R  D05 1  1
!
! Degrees of Freedom
! Nodal Loads: Sequential Generation
D 1  11  1010  1020  10
!
*REST
!
*DISN                Dynamic Analysis 02
!
! Control Information

```

```

!
40    60000  1
! Ground Displacement Records
!
R   D10 1    1
!
! Degrees of Freedom
! Nodal Loads: Sequential Generation
D 1  11    1010  1020  10
!
*REST
!
*DISN                      Dynamic Analysis 03
!
! Control Information
!
40    60000  1
! Ground Displacement Records
!
R   D20 1    1
!
! Degrees of Freedom
! Nodal Loads: Sequential Generation
D 1  11    1010  1020  10
!
!
*REST
!
*DISN                      Dynamic Analysis 04
!
! Control Information
!
40    60000  1
! Ground Displacement Records
!
R   D30 1    1
!
! Degrees of Freedom
! Nodal Loads: Sequential Generation
D 1  11    1010  1020  10
!
*REST
!
*DISN                      Dynamic Analysis 05
!

```

```

! Control Information
!
40    60000  1
! Ground Displacement Records
!
R   D40 1    1
!
! Degrees of Freedom
! Nodal Loads: Sequential Generation
D 1  11    1010  1020  10
!
*STOP

```

## **D2. Test sequence 4 – CFRP retrofitted frame**

```

*STARTXX
! Nodal Restraints: Sequential Generation
TimeH      0 1 1 0      time history Units:kNm
!
*NODECOORDS
! Controle Nodes (C-lines)
C 1010  0    0    0
C 1020  4    0    0
C 2010  0    3.3  0
C 2020  4    3.3  0
C 3010  0    6.6  0
C 3020  4    6.6  0
C 2011  0.13  3.3  0
C 2012  0.62  3.3  0
C 2013  1.1   3.3  0
C 2014  1.55  3.3  0
C 2015  2     3.3  0
C 2016  2.45  3.3  0
C 2017  2.9   3.3  0
C 2018  3.38  3.3  0
C 2019  3.87  3.3  0
C 3011  0.13  6.6  0
C 3012  0.65  6.6  0
C 3013  1.1   6.6  0
C 3014  1.55  6.6  0
C 3015  2     6.6  0
C 3016  2.45  6.6  0
C 3017  2.9   6.6  0
C 3018  3.35  6.6  0
C 3019  3.87  6.6  0

```

```

C 1910 0 3.1 0
C 2110 0 3.5 0
C 2910 0 6.4 0
C 1920 4 3.1 0
C 2120 4 3.5 0
C 2920 4 6.4 0
! Control Nodes
C 1111 0 0 1
C 2222 0 10 0
C 3333 4 0 1
! CFRP Nodes
C 1110 0 0.9 0
C 1120 4 0.9 0
C 1810 0 2.5 0
C 1820 4 2.5 0
C 2210 0 4.05 0
C 2220 4 4.05 0
C 2810 0 5.8 0
C 2820 4 5.8 0
!
*RESTRAINTS
! Nodal Restraints: Sequential Generation
S 222222 1010 1020 10
S 001110 2010 2020 1
S 001110 3010 3020 1
S 111111 1111 3333 1111
S 001110 1910 1920 10
S 001110 2110 2120 10
S 001110 2910 2920 10
!
*MASSES
! Nodal Masses: Sequential Generation
S 100 5.927 2010 2020 10 1.0 0.467541
S 100 5.029 3010 3020 10
!
*ELEMENTGROUP
! Group 1
! Element Group Definition
15 1 1 0.002186 COL-1-CONFINED-NOLONGSTRIPS
!
! Controle information
!
1 1 1 0 0 0 0 0 1
!
! Concrete Material Properties

```

```

! Controle Line
5 2 0.5 100
!
! Stress Strain Points for Compression
! Stress Strain
13929 0.0007
22635 0.0013
29020 0.002
31326 0.00267
36444 0.01034
!
! Stress Strain Points for Tension
! Stress Strain
3000 0.0001316
1000 0.001316
!
! Steel Material Properties
! Controle Line
2 100
!
! Stress Strain Points for Steel
! Stress Strain
526000 0.0026
616000 0.19
!
! Fiber Cross Section Types
! Controle Line
13 1
!
! Fibers Data
!
-0.110 0.110 0.000154 S1
0 0.110 0.000154 S1
0.110 0.110 0.000154 S1
-0.110 0 0.000154 S1
0.110 0 0.000154 S1
-0.110 -0.110 0.000154 S1
0 -0.110 0.000154 S1
0.110 -0.110 0.000154 S1
0 0.104 0.01352 C1
0 0.052 0.01352 C1
0 0 0.01352 C1
0 -0.052 0.01352 C1
0 -0.104 0.01352 C1
!

```

```

! Element Geometry Types
! Controle Line
3
!
! Segment data, Element Geometry Types
!
0.1    F01
0.8    F01
0.1    F01
!
! Element Generation Commands
!
1  1010  1110  100  1111  1
2  1020  1120  100  3333  1
!
*ELEMENTGROUP
! Group 2
! Element Group Definition
15  1  1  0.002186  COL-1-NOCONFINED
!
! Controle information
!
1  1  1  0  0  0  0  0  1
!
! Concrete Material Properties
! Controle Line
4  2  0.5  100
!
! Stress Strain Points for Compression
! Stress  Strain
14196  0.0007
25355  0.0015
29544  0.0023
25113  0.00351
!
! Stress Strain Points for Tension
! Stress  Strain
3000  0.000132
370  0.00132
!
! Steel Material Properties
! Controle Line
2  100
!
! Stress Strain Points for Steel

```



```

! Stress   Strain
526000  0.0026
616000  0.19
!
! Fiber Cross Section Types
! Controle Line
13  1
!
! Fibers Data
!
-0.110  0.110  0.000154  S1
0      0.110  0.000154  S1
0.110  0.110  0.000154  S1
-0.110  0      0.000154  S1
0.110  0      0.000154  S1
-0.110 -0.110  0.000154  S1
0      -0.110  0.000154  S1
0.110  -0.110  0.000154  S1
0      0.104  0.01352  C1
0      0.052  0.01352  C1
0      0      0.01352  C1
0      -0.052  0.01352  C1
0      -0.104  0.01352  C1
!
! Element Geometry Types
! Controle Line
3
!
! Segment data, Element Geometry Types
!
0.1    F01
0.8    F01
0.1    F01
!
! Element Generation Commands
!
1  1110  1810  700  1111  1
2  1120  1820  700  3333  1
!
*ELEMENTGROUP
! Group 3
! Element Group Definition
15  1  1  0.002186  COL-2-NOCONFINED
!
! Controle information

```

```

!
1 1 1 0 0 0 0 0 1
!
! Concrete Material Properties
! Controle Line
4 2 0.5 100
!
! Stress Strain Points for Compression
! Stress Strain
12648 0.0007
20737 0.0014
24042 0.0022
20436 0.00351
!
! Stress Strain Points for Tension
! Stress Strain
2300 0.0001085
284 0.001085
!
! Steel Material Properties
! Controle Line
2 100
!
! Stress Strain Points for Steel
! Stress Strain
526000 0.0026
616000 0.19
!
! Fiber Cross Section Types
! Controle Line
9 1
!
! Fibers Data
!
-0.110 0.110 0.000154 S1
0.110 0.110 0.000154 S1
-0.110 -0.110 0.000154 S1
0.110 -0.110 0.000154 S1
0 0.104 0.01352 C1
0 0.052 0.01352 C1
0 0 0.01352 C1
0 -0.052 0.01352 C1
0 -0.104 0.01352 C1
!
! Element Geometry Types

```

```

! Controle Line
3
!
! Segment data, Element Geometry Types
!
0.1    F01
0.8    F01
0.1    F01
!
! Element Generation Commands
!
1  2210  2810  600  1111  1
2  2220  2820  600  3333  1
!
!
*ELEMENTGROUP
! Group 4
! Element Group Definition
15  1  1  0.002186      COL-1-CONFINED-YESLONGSTRIPS
!
! Controle information
!
1  2  1  0  0  0  0  0  1
!
! Concrete Material Properties
! Controle Line
5  2  0.5  100
!
! Stress Strain Points for Compression
! Stress   Strain
13929  0.0007
22635  0.0013
29020  0.002
31326  0.00267
36444  0.01034
!
! Stress Strain Points for Tension
! Stress   Strain
3000  0.0001316
1000  0.001316
!
! Steel Material Properties
! Controle Line
2  100
!

```

```

! Stress Strain Points for Steel
! Stress  Strain
526000  0.0026
616000  0.19
!
! Steel Material Properties
! Controle Line
1  100
!
! Stress Strain Points for CFRP
! Stress  Strain
1350000  0.0129
!
! Fiber Cross Section Types
! Controle Line
37  1
!
! Fibers Data
!
-0.110  0.110  0.000154  S1
0  0.110  0.000154  S1
0.110  0.110  0.000154  S1
-0.110  0  0.000154  S1
0.110  0  0.000154  S1
-0.110  -0.110  0.000154  S1
0  -0.110  0.000154  S1
0.110  -0.110  0.000154  S1
0  0.104  0.01352  C1
0  0.052  0.01352  C1
0  0  0.01352  C1
0  -0.052  0.01352  C1
0  -0.104  0.01352  C1
-0.13  0.093  0.0000164  S2
-0.13  0.056  0.0000164  S2
-0.13  0.019  0.0000164  S2
-0.13  -0.093  0.0000164  S2
-0.13  -0.056  0.0000164  S2
-0.13  -0.019  0.0000164  S2
0.093  -0.13  0.0000164  S2
0.056  -0.13  0.0000164  S2
0.019  -0.13  0.0000164  S2
-0.093  -0.13  0.0000164  S2
-0.056  -0.13  0.0000164  S2
-0.019  -0.13  0.0000164  S2
0.13  0.093  0.0000164  S2

```

```

0.13  0.056  0.0000164  S2
0.13  0.019  0.0000164  S2
0.13  -0.093  0.0000164  S2
0.13  -0.056  0.0000164  S2
0.13  -0.019  0.0000164  S2
0.093  0.13  0.0000164  S2
0.056  0.13  0.0000164  S2
0.019  0.13  0.0000164  S2
-0.093  0.13  0.0000164  S2
-0.056  0.13  0.0000164  S2
-0.019  0.13  0.0000164  S2
!
! Element Geometry Types
! Controle Line
3
!
! Segment data, Element Geometry Types
!
0.1    F01
0.8    F01
0.1    F01
!
! Element Generation Commands
!
1  1810  1910  100  1111  1
2  1820  1920  100  3333  1
!
*ELEMENTGROUP
! Group 5
! Element Group Definition
15  1  1  0.002186  COL-2-CONFINED-YESLONGSTRIPS(DOWN)
!
! Controle information
!
1  2  1  0  0  0  0  0  1
!
! Concrete Material Properties
! Controle Line
5  2  0.5  100
!
! Stress Strain Points for Compression
! Stress  Strain
12681  0.0007
20112  0.0013
24371  0.0019

```

```

25475  0.00234
31003  0.0113
!
! Stress Strain Points for Tension
! Stress  Strain
2300   0.0001085
770    0.001085
!
! Steel Material Properties
! Controle Line
2  100
!
! Stress Strain Points for Steel
! Stress  Strain
526000 0.0026
616000 0.19
!
! Steel Material Properties
! Controle Line
1  100
!
! Stress Strain Points for CFRP
! Stress  Strain
1350000 0.0129
!
! Fiber Cross Section Types
! Controle Line
33  1
!
! Fibers Data
!
-0.110  0.110  0.000154  S1
0.110   0.110  0.000154  S1
-0.110 -0.110  0.000154  S1
0.110  -0.110  0.000154  S1
0      0.104   0.01352   C1
0      0.052   0.01352   C1
0      0       0.01352   C1
0     -0.052   0.01352   C1
0     -0.104   0.01352   C1
-0.13  0.093   0.0000164  S2
-0.13  0.056   0.0000164  S2
-0.13  0.019   0.0000164  S2
-0.13 -0.093   0.0000164  S2
-0.13 -0.056   0.0000164  S2

```

```

-0.13  -0.019  0.0000164  S2
0.093  -0.13   0.0000164  S2
0.056  -0.13   0.0000164  S2
0.019  -0.13   0.0000164  S2
-0.093 -0.13   0.0000164  S2
-0.056 -0.13   0.0000164  S2
-0.019 -0.13   0.0000164  S2
0.13   0.093   0.0000164  S2
0.13   0.056   0.0000164  S2
0.13   0.019   0.0000164  S2
0.13   -0.093  0.0000164  S2
0.13   -0.056  0.0000164  S2
0.13   -0.019  0.0000164  S2
0.093  0.13    0.0000164  S2
0.056  0.13    0.0000164  S2
0.019  0.13    0.0000164  S2
-0.093 0.13    0.0000164  S2
-0.056 0.13    0.0000164  S2
-0.019 0.13    0.0000164  S2

```

!

! Element Geometry Types

! Controle Line

3

!

! Segment data, Element Geometry Types

!

0.1 F01

0.8 F01

0.1 F01

!

! Element Generation Commands

!

1 2110 2210 100 1111 1

2 2120 2220 100 3333 1

!

\*ELEMENTGROUP

! Group 6

! Element Group Definition

15 1 1 0.002186 COL-2-CONFINED-YESLONGSTRIPS(UP)

!

! Controle information

!

1 2 1 0 0 0 0 0 1

!

! Concrete Material Properties

```

! Controle Line
5 2 0.5 100
!
! Stress Strain Points for Compression
! Stress Strain
12681 0.0007
20112 0.0013
24371 0.0019
25475 0.00234
31003 0.0113
!
! Stress Strain Points for Tension
! Stress Strain
2300 0.0001085
770 0.001085
!
! Steel Material Properties
! Controle Line
2 100
!
! Stress Strain Points for Steel
! Stress Strain
526000 0.0026
616000 0.19
!
! Steel Material Properties
! Controle Line
1 100
!
! Stress Strain Points for CFRP
! Stress Strain
1350000 0.0129
!
! Fiber Cross Section Types
! Controle Line
33 1
!
! Fibers Data
!
-0.110 0.110 0.000154 S1
0.110 0.110 0.000154 S1
-0.110 -0.110 0.000154 S1
0.110 -0.110 0.000154 S1
0 0.104 0.01352 C1
0 0.052 0.01352 C1

```



```

0    0    0.01352  C1
0   -0.052 0.01352  C1
0   -0.104 0.01352  C1
-0.13  0.093  0.0000164  S2
-0.13  0.056  0.0000164  S2
-0.13  0.019  0.0000164  S2
-0.13 -0.093  0.0000164  S2
-0.13 -0.056  0.0000164  S2
-0.13 -0.019  0.0000164  S2
0.093 -0.13  0.0000164  S2
0.056 -0.13  0.0000164  S2
0.019 -0.13  0.0000164  S2
-0.093 -0.13  0.0000164  S2
-0.056 -0.13  0.0000164  S2
-0.019 -0.13  0.0000164  S2
0.13  0.093  0.0000164  S2
0.13  0.056  0.0000164  S2
0.13  0.019  0.0000164  S2
0.13 -0.093  0.0000164  S2
0.13 -0.056  0.0000164  S2
0.13 -0.019  0.0000164  S2
0.093  0.13  0.0000164  S2
0.056  0.13  0.0000164  S2
0.019  0.13  0.0000164  S2
-0.093  0.13  0.0000164  S2
-0.056  0.13  0.0000164  S2
-0.019  0.13  0.0000164  S2
!
! Element Geometry Types
! Controle Line
3
!
! Segment data, Element Geometry Types
!
0.1    F01
0.8    F01
0.1    F01
!
! Element Generation Commands
!
1  2810  2910  100  1111  1
2  2820  2920  100  3333  1
!
*ELEMENTGROUP
! Group 7

```

```

! Element Group Definition
15  1  1  0.002186      COL-JOINTS1-YESLONGSTRIPS
!
! Controle information
!
1  2  1  0  1  1  1  0  1
!
! Concrete Material Properties
! Controle Line
4  2  0.5  100
!
! Stress Strain Points for Compression
! Stress   Strain
14196  0.0007
25355  0.0015
29544  0.0023
25113  0.00351
!
! Stress Strain Points for Tension
! Stress   Strain
3000   0.000132
370    0.00132
!
! Steel Material Properties
! Controle Line
2  100
!
! Stress Strain Points for Steel
! Stress   Strain
526000 0.0026
616000 0.19
!
! Steel Material Properties
! Controle Line
1  100
!
! Stress Strain Points for CFRP
! Stress   Strain
1350000 0.0129
!
! Fiber Cross Section Types
! Controle Line
25  1
!
! Fibers Data

```

```

!
-0.110 0.110 0.000154 S1
0 0.110 0.000154 S1
0.110 0.110 0.000154 S1
-0.110 0 0.000154 S1
0.110 0 0.000154 S1
-0.110 -0.110 0.000154 S1
0 -0.110 0.000154 S1
0.110 -0.110 0.000154 S1
0 0.104 0.01352 C1
0 0.052 0.01352 C1
0 0 0.01352 C1
0 -0.052 0.01352 C1
0 -0.104 0.01352 C1
-0.13 0.093 0.0000164 S2
-0.13 0.056 0.0000164 S2
-0.13 0.019 0.0000164 S2
-0.13 -0.093 0.0000164 S2
-0.13 -0.056 0.0000164 S2
-0.13 -0.019 0.0000164 S2
0.093 -0.13 0.0000164 S2
0.056 -0.13 0.0000164 S2
0.019 -0.13 0.0000164 S2
-0.093 -0.13 0.0000164 S2
-0.056 -0.13 0.0000164 S2
-0.019 -0.13 0.0000164 S2
!
! Pullout properties for connection Hinge Fibers
! Basic Properties (1)
2.92E+08 7.82E+07 0.001 526000 616000 526000 616000 0.01 1
! Degradation Parameters (1)
1 1 1 0.005 0.005 1 1 1
!
! Gap Properties for Connection Hinge Fibers
!
8000 17033 2.45E+07 1.37E+07 7.95E+06 0.5 0.01
!
! Connection Hinge Types
! Control Line
13
!
! Fibers Data for Connection Hinge types
!
-0.105 0.105 0.000154 P1
0 0.105 0.000154 P1

```

```

0.105  0.105  0.000154  P1
-0.105  0      0.000154  P1
0.105  0      0.000154  P1
-0.105 -0.105  0.000154  P1
0      -0.105  0.000154  P1
0.105  -0.105  0.000154  P1
0      0.104   0.01352   G1
0      0.052   0.01352   G1
0      0       0.01352   G1
0      -0.052  0.01352   G1
0      -0.104  0.01352   G1
!
! Element Geometry Types
! Controle Line
3  1  1
!
! Segment data, Element Geometry Types
!
0.1    F01
0.8    F01
0.1    F01
!
! Element Generation Commands
!
1  1910  2010  100  1111  1
2  1920  2020  100  3333  1
!
*ELEMENTGROUP
! Group 8
! Element Group Definition
15  1  1  0.002186  COL-JOINTS2-YESLONGSTRIPS
!
! Controle information
!
1  2  1  0  0  0  0  0  1
!
! Concrete Material Properties
! Controle Line
4  2  0.5  100
!
! Stress Strain Points for Compression
! Stress  Strain
12648  0.0007
20737  0.0014
24042  0.0022

```

```

20436  0.00351
!
! Stress Strain Points for Tension
! Stress  Strain
2300   0.0001085
284    0.001085
!
! Steel Material Properties
! Controle Line
2  100
!
! Stress Strain Points for Steel
! Stress  Strain
526000 0.0026
616000  0.19
!
! Steel Material Properties
! Controle Line
1  100
!
! Stress Strain Points for CFRP
! Stress  Strain
1350000 0.0129
!
! Fiber Cross Section Types
! Controle Line
21  1
!
! Fibers Data
!
-0.110  0.110  0.000154  S1
0.110   0.110  0.000154  S1
-0.110 -0.110  0.000154  S1
0.110  -0.110  0.000154  S1
0      0.104  0.01352   C1
0      0.052  0.01352   C1
0      0      0.01352   C1
0     -0.052  0.01352   C1
0     -0.104  0.01352   C1
-0.13  0.093  0.0000164  S2
-0.13  0.056  0.0000164  S2
-0.13  0.019  0.0000164  S2
-0.13 -0.093  0.0000164  S2
-0.13 -0.056  0.0000164  S2
-0.13 -0.019  0.0000164  S2

```

```

0.093  -0.13  0.0000164  S2
0.056  -0.13  0.0000164  S2
0.019  -0.13  0.0000164  S2
-0.093 -0.13  0.0000164  S2
-0.056 -0.13  0.0000164  S2
-0.019 -0.13  0.0000164  S2
!
! Element Geometry Types
! Controle Line
3
!
! Segment data, Element Geometry Types
!
0.1    F01
0.8    F01
0.1    F01
!
! Element Generation Commands
!
1  2010  2110  100  1111  1
2  2020  2120  100  3333  1
!
*ELEMENTGROUP
! Group 9
! Element Group Definition
15  2  1  0.002186  BEAMS-MID1-NOCONFINED
!
! Controle information
!
1  1  1  0  0  0  0  0  1
!
! Concrete Material Properties
! Controle Line
4  2  0.5  100
!
! Stress Strain Points for Compression
! Stress  Strain
15059  0.00075
27114  0.0017
29521  0.0023
25093  0.00350
!
! Stress Strain Points for Tension
! Stress  Strain
3000  0.000132

```

```

370    0.00132
!
! Steel Material Properties
! Controle Line
2    100
!
! Stress Strain Points for Steel
! Stress    Strain
526000    0.0026
616000    0.19
!
! Fiber Cross Section Types
! Controle Line
14    1
!
! Fibers Data
!
-0.130    0.110    0.000154    S1
0.130    0.110    0.000154    S1
-0.130    0.0333    0.000154    S1
0.130    0.0333    0.000154    S1
-0.130    -0.0333    0.000154    S1
0.130    -0.0333    0.000154    S1
-0.130    -0.110    0.000154    S1
0.130    -0.110    0.000154    S1
-0.125    0        0.013        C1
-0.075    0        0.013        C1
-0.025    0        0.013        C1
0.025    0        0.013        C1
0.075    0        0.013        C1
0.125    0        0.013        C1
!
! Element Geometry Types
! Controle Line
1
!
! Segment data, Element Geometry Types
!
1        F01
!
! Element Generation Commands
!
1    2012    2013    0001    2222    1
2    2013    2014    0001    2222    1
3    2014    2015    0001    2222    1

```

```

4  2015  2016  0001  2222  1
5  2016  2017  0001  2222  1
6  2017  2018  0001  2222  1
!
*ELEMENTGROUP
! Group 10
! Element Group Definition
15  1  1  0.002186      BEAM-MID2-NOCONFINED
!
! Controle information
!
1  1  1  0  0  0  0  0  1
!
! Concrete Material Properties
! Controle Line
4  2  0.5  100
!
! Stress Strain Points for Compression
! Stress   Strain
17275  0.00105
22165  0.0016
24033  0.0022
20428  0.00351
!
! Stress Strain Points for Tension
! Stress   Strain
2300  0.000109
284  0.00109
!
! Steel Material Properties
! Controle Line
2  100
!
! Stress Strain Points for Steel
! Stress   Strain
526000  0.0026
616000  0.19
!
! Fiber Cross Section Types
! Controle Line
14  1
!
! Fibers Data
!
-0.130  0.110  0.000154  S1

```



```

0.130  0.110  0.000154  S1
-0.130  0.0333  0.000154  S1
0.130  0.0333  0.000154  S1
-0.130  -0.0333  0.000154  S1
0.130  -0.0333  0.000154  S1
-0.130  -0.110  0.000154  S1
0.130  -0.110  0.000154  S1
-0.125  0  0.013  C1
-0.075  0  0.013  C1
-0.025  0  0.013  C1
0.025  0  0.013  C1
0.075  0  0.013  C1
0.125  0  0.013  C1
!
! Element Geometry Types
! Controle Line
1
!
! Segment data, Element Geometry Types
!
1      F01
!
! Element Generation Commands
!
1  3012  3013  0001  2222  1
2  3013  3014  0001  2222  1
3  3014  3015  0001  2222  1
4  3015  3016  0001  2222  1
5  3016  3017  0001  2222  1
6  3017  3018  0001  2222  1
!
*ELEMENTGROUP
! Group 11
! Element Group Definition
15  1  1  0.002186      BEAM-JOINT1-CONFINED-YESLONGSTRIPS
!
! Controle information
!
1  2  1  0  1  1  1  0  1
!
! Concrete Material Properties
! Controle Line
4  2  0.5  100
!
! Stress Strain Points for Compression

```

```

! Stress  Strain
15059  0.00075
27114  0.0017
29521  0.0023
25093  0.00350
!
! Stress Strain Points for Tension
! Stress  Strain
3000  0.000132
370  0.00132
!
! Steel Material Properties
! Controle Line
2  100
!
! Stress Strain Points for Steel
! Stress  Strain
526000  0.0026
616000  0.18
!
! Steel Material Properties
! Controle Line
1  100
!
! Stress Strain Points for CFRP
! Stress  Strain
1350000  0.0129
!
! Fiber Cross Section Types
! Controle Line
38  1
!
! Fibers Data
!
-0.130  0.110  0.000154  S1
0.130  0.110  0.000154  S1
-0.130  0.0333  0.000154  S1
0.130  0.0333  0.000154  S1
-0.130  -0.0333  0.000154  S1
0.130  -0.0333  0.000154  S1
-0.130  -0.110  0.000154  S1
0.130  -0.110  0.000154  S1
-0.125  0  0.013  C1
-0.075  0  0.013  C1
-0.025  0  0.013  C1

```

```

0.025  0    0.013  C1
0.075  0    0.013  C1
0.125  0    0.013  C1
-0.2   0.093 0.0000164 S2
-0.2   0.056 0.0000164 S2
-0.2   0.019 0.0000164 S2
-0.2   -0.093 0.0000164 S2
-0.2   -0.056 0.0000164 S2
-0.2   -0.019 0.0000164 S2
0.093  -0.2  0.0000164 S2
0.056  -0.2  0.0000164 S2
0.019  -0.2  0.0000164 S2
-0.093 -0.2  0.0000164 S2
-0.056 -0.2  0.0000164 S2
-0.019 -0.2  0.0000164 S2
0.2    0.093 0.0000164 S2
0.2    0.056 0.0000164 S2
0.2    0.019 0.0000164 S2
0.2    -0.093 0.0000164 S2
0.2    -0.056 0.0000164 S2
0.2    -0.019 0.0000164 S2
0.093  0.2  0.0000164 S2
0.056  0.2  0.0000164 S2
0.019  0.2  0.0000164 S2
-0.093 0.2  0.0000164 S2
-0.056 0.2  0.0000164 S2
-0.019 0.2  0.0000164 S2
!
! Pullout properties for connection Hinge Fibers
! Basic Properties (1)
2.92E+08 1.00E+00 0.01  478000  479000  478000  479000  0.01  1
! Degradation Parameters (1)
1    1    1    0.005  0.005  1    1    1
!
! Gap Properties for Connection Hinge Fibers
!
8000  17033  2.45E+07 1.37E+07 7.95E+06 0.5  0.01
!
! Connection Hinge Types
! Control Line
14
!
! Fibers Data for Connection Hinge types
!
-0.125  0.105  0.000154  P1

```

```

0.125  0.105  0.000154  P1
-0.125  0.0333  0.000154  P1
0.125  0.0333  0.000154  P1
-0.125  -0.0333  0.000154  P1
0.125  -0.0333  0.000154  P1
-0.125  -0.105  0.000154  P1
0.125  -0.105  0.000154  P1
-0.125  0  0.013  G1
-0.075  0  0.013  G1
-0.025  0  0.013  G1
0.025  0  0.013  G1
0.075  0  0.013  G1
0.125  0  0.013  G1
!
! Element Geometry Types
! Controle Line
1  1  1
!
! Segment data, Element Geometry Types
!
1  F01
!
! Element Generation Commands
!
1  2010  2011  1  1111  1
2  2019  2020  1  1111  1
!
*ELEMENTGROUP
! Group 12
! Element Group Definition
15  1  1  0.002186  BEAM-JOINT2-CONFINED-YESLONGSTRIPS
!
! Controle information
!
1  2  1  0  1  1  1  0  1
!
! Concrete Material Properties
! Controle Line
4  2  0.5  100
!
! Stress Strain Points for Compression
! Stress  Strain
17275  0.00105
22165  0.0016
24033  0.0022

```

```

20428  0.00351
!
! Stress Strain Points for Tension
! Stress  Strain
2300   0.000109
284    0.00109
!
! Steel Material Properties
! Controle Line
2  100
!
! Stress Strain Points for Steel
! Stress  Strain
526000 0.0026
616000 0.19
!
! Steel Material Properties
! Controle Line
1  100
!
! Stress Strain Points for CFRP
! Stress  Strain
1350000 0.0129
!
! Fiber Cross Section Types
! Controle Line
38  1
!
! Fibers Data
!
-0.130  0.110  0.000154  S1
0.130   0.110  0.000154  S1
-0.130  0.0333 0.000154  S1
0.130   0.0333 0.000154  S1
-0.130 -0.0333 0.000154  S1
0.130  -0.0333 0.000154  S1
-0.130 -0.110  0.000154  S1
0.130  -0.110  0.000154  S1
-0.125  0      0.013    C1
-0.075  0      0.013    C1
-0.025  0      0.013    C1
0.025   0      0.013    C1
0.075   0      0.013    C1
0.125   0      0.013    C1
-0.2    0.093  0.0000164  S2

```

```

-0.2  0.056  0.0000164  S2
-0.2  0.019  0.0000164  S2
-0.2  -0.093  0.0000164  S2
-0.2  -0.056  0.0000164  S2
-0.2  -0.019  0.0000164  S2
0.093  -0.2  0.0000164  S2
0.056  -0.2  0.0000164  S2
0.019  -0.2  0.0000164  S2
-0.093  -0.2  0.0000164  S2
-0.056  -0.2  0.0000164  S2
-0.019  -0.2  0.0000164  S2
0.2  0.093  0.0000164  S2
0.2  0.056  0.0000164  S2
0.2  0.019  0.0000164  S2
0.2  -0.093  0.0000164  S2
0.2  -0.056  0.0000164  S2
0.2  -0.019  0.0000164  S2
0.093  0.2  0.0000164  S2
0.056  0.2  0.0000164  S2
0.019  0.2  0.0000164  S2
-0.093  0.2  0.0000164  S2
-0.056  0.2  0.0000164  S2
-0.019  0.2  0.0000164  S2
!
! Pullout properties for connection Hinge Fibers
! Basic Properties (1)
2.92E+08  1.00E+00  0.01  438000  439000  438000  439000  0.01  1
! Degradation Parameters (1)
1  1  1  0.005  0.005  1  1  1
!
! Gap Properties for Connection Hinge Fibers
!
8000  17033  2.45E+07  1.37E+07  7.95E+06  0.5  0.01
!
! Connection Hinge Types
! Control Line
14
!
! Fibers Data for Connection Hinge types
!
-0.125  0.105  0.000154  P1
0.125  0.105  0.000154  P1
-0.125  0.0333  0.000154  P1
0.125  0.0333  0.000154  P1
-0.125  -0.0333  0.000154  P1

```

```

0.125  -0.0333  0.000154  P1
-0.125 -0.105  0.000154  P1
0.125  -0.105  0.000154  P1
-0.125  0      0.013    G1
-0.075  0      0.013    G1
-0.025  0      0.013    G1
0.025   0      0.013    G1
0.075   0      0.013    G1
0.125   0      0.013    G1
!
! Element Geometry Types
! Controle Line
1  1  1
!
! Segment data, Element Geometry Types
!
1      F01
!
! Element Generation Commands
!
1  3010  3011  1      1111  1
2  3019  3020  1      1111  1
!
*ELEMENTGROUP
! Group 13
! Element Group Definition
15  1  1  0.002186      BEAM-JOINT1-CONFINED-YESLONGSTRIPS
!
! Controle information
!
1  2  1  0  1  1  1  0  1
!
! Concrete Material Properties
! Controle Line
5  2  0.5  100
!
! Stress Strain Points for Compression
! Stress  Strain
15530  0.0008
22486  0.0013
28667  0.002
30687  0.00264
33921  0.00996
!
! Stress Strain Points for Tension

```

```

! Stress   Strain
3000   0.0001316
370    0.001316
!
! Steel Material Properties
! Controle Line
2   100
!
! Stress Strain Points for Steel
! Stress   Strain
526000   0.0026
616000   0.19
!
! Steel Material Properties
! Controle Line
1   100
!
! Stress Strain Points for Steel2
! Stress   Strain
1350000  0.0129
!
! Fiber Cross Section Types
! Controle Line
38  1
!
! Fibers Data
!
-0.130  0.110  0.000154  S1
0.130   0.110  0.000154  S1
-0.130  0.0333 0.000154  S1
0.130   0.0333 0.000154  S1
-0.130 -0.0333 0.000154  S1
0.130  -0.0333 0.000154  S1
-0.130 -0.110  0.000154  S1
0.130  -0.110  0.000154  S1
-0.125  0      0.013    C1
-0.075  0      0.013    C1
-0.025  0      0.013    C1
0.025   0      0.013    C1
0.075   0      0.013    C1
0.125   0      0.013    C1
-0.2    0.093  0.0000164  S2
-0.2    0.056  0.0000164  S2
-0.2    0.019  0.0000164  S2
-0.2    -0.093 0.0000164  S2

```



```

-0.2  -0.056  0.0000164  S2
-0.2  -0.019  0.0000164  S2
0.093  -0.2    0.0000164  S2
0.056  -0.2    0.0000164  S2
0.019  -0.2    0.0000164  S2
-0.093 -0.2    0.0000164  S2
-0.056 -0.2    0.0000164  S2
-0.019 -0.2    0.0000164  S2
0.2    0.093  0.0000164  S2
0.2    0.056  0.0000164  S2
0.2    0.019  0.0000164  S2
0.2    -0.093 0.0000164  S2
0.2    -0.056 0.0000164  S2
0.2    -0.019 0.0000164  S2
0.093  0.2    0.0000164  S2
0.056  0.2    0.0000164  S2
0.019  0.2    0.0000164  S2
-0.093 0.2    0.0000164  S2
-0.056 0.2    0.0000164  S2
-0.019 0.2    0.0000164  S2
!
! Pullout properties for connection Hinge Fibers
! Basic Properties (1)
2.92E+08 1.00E+00 0.01  478000  479000  478000  479000  0.01  1
! Degradation Parameters (1)
1  1  1  0.005  0.005  1  1  1
!
! Gap Properties for Connection Hinge Fibers
!
8000  17033  2.45E+07 1.37E+07 7.95E+06 0.5  0.01
!
! Connection Hinge Types
! Control Line
14
!
! Fibers Data for Connection Hinge types
!
-0.125  0.105  0.000154  P1
0.125  0.105  0.000154  P1
-0.125  0.0333  0.000154  P1
0.125  0.0333  0.000154  P1
-0.125  -0.0333  0.000154  P1
0.125  -0.0333  0.000154  P1
-0.125  -0.105  0.000154  P1
0.125  -0.105  0.000154  P1

```

```

-0.125  0    0.013  G1
-0.075  0    0.013  G1
-0.025  0    0.013  G1
0.025   0    0.013  G1
0.075   0    0.013  G1
0.125   0    0.013  G1
!
! Element Geometry Types
! Controle Line
1  1
!
! Segment data, Element Geometry Types
!
1      F01
!
! Element Generation Commands
!
1  2011  2012  0001  2222  1
2  2018  2019  0001  2222  1
!
!
*ELEMENTGROUP
! Group 14
! Element Group Definition
15  1  1  0.002186      BEAM-JOINT2-CONFINED-YESLONGSTRIPS
!
! Controle information
!
1  2  1  0  1  1  1  0  1
!
! Concrete Material Properties
! Controle Line
5  2  0.5  100
!
! Stress Strain Points for Compression
! Stress  Strain
17877  0.0011
21680  0.0015
24408  0.002
24971  0.00231
28433  0.0108
!
! Stress Strain Points for Tension
! Stress  Strain
2300  0.0001085

```

```

770 0.001085
!
! Steel Material Properties
! Controle Line
2 100
!
! Stress Strain Points for Steel
! Stress Strain
526000 0.0026
616000 0.19
!
! Steel Material Properties
! Controle Line
1 100
!
! Stress Strain Points for CFRP
! Stress Strain
1350000 0.0129
!
! Fiber Cross Section Types
! Controle Line
38 1
!
! Fibers Data
!
-0.130 0.110 0.000154 S1
0.130 0.110 0.000154 S1
-0.130 0.0333 0.000154 S1
0.130 0.0333 0.000154 S1
-0.130 -0.0333 0.000154 S1
0.130 -0.0333 0.000154 S1
-0.130 -0.110 0.000154 S1
0.130 -0.110 0.000154 S1
-0.125 0 0.013 C1
-0.075 0 0.013 C1
-0.025 0 0.013 C1
0.025 0 0.013 C1
0.075 0 0.013 C1
0.125 0 0.013 C1
-0.2 0.093 0.0000164 S2
-0.2 0.056 0.0000164 S2
-0.2 0.019 0.0000164 S2
-0.2 -0.093 0.0000164 S2
-0.2 -0.056 0.0000164 S2
-0.2 -0.019 0.0000164 S2

```

```

0.093  -0.2  0.0000164  S2
0.056  -0.2  0.0000164  S2
0.019  -0.2  0.0000164  S2
-0.093 -0.2  0.0000164  S2
-0.056 -0.2  0.0000164  S2
-0.019 -0.2  0.0000164  S2
0.2    0.093 0.0000164  S2
0.2    0.056 0.0000164  S2
0.2    0.019 0.0000164  S2
0.2    -0.093 0.0000164  S2
0.2    -0.056 0.0000164  S2
0.2    -0.019 0.0000164  S2
0.093  0.2   0.0000164  S2
0.056  0.2   0.0000164  S2
0.019  0.2   0.0000164  S2
-0.093 0.2   0.0000164  S2
-0.056 0.2   0.0000164  S2
-0.019 0.2   0.0000164  S2
!
! Pullout properties for connection Hinge Fibers
! Basic Properties (1)
2.92E+08 1.00E+00 0.01  438000  439000  438000  439000  0.01  1
! Degradation Parameters (1)
1      1      1      0.005  0.005  1      1      1
!
! Gap Properties for Connection Hinge Fibers
!
8000   17033  2.45E+07 1.37E+07 7.95E+06 0.5    0.01
!
! Connection Hinge Types
! Control Line
14
!
! Fibers Data for Connection Hinge types
!
-0.125 0.105 0.000154 P1
0.125  0.105 0.000154 P1
-0.125 0.0333 0.000154 P1
0.125  0.0333 0.000154 P1
-0.125 -0.0333 0.000154 P1
0.125  -0.0333 0.000154 P1
-0.125 -0.105 0.000154 P1
0.125  -0.105 0.000154 P1
-0.125 0      0.013    G1
-0.075 0      0.013    G1

```

```

-0.025  0    0.013  G1
0.025   0    0.013  G1
0.075   0    0.013  G1
0.125   0    0.013  G1
!
! Element Geometry Types
! Controle Line
1  1
!
! Segment data, Element Geometry Types
!
1      F01
!
! Element Generation Commands
!
1  3011  3012  0001  2222  1
2  3018  3019  0001  2222  1
!
*ELEMENTGROUP
! Group 15
! Element Group Definition
15  1  1  0.002186      COL-JOINTS2-YESLONGSTRIPS
!
! Controle information
!
1  2  1  0  0  0  0  0  1
!
! Concrete Material Properties
! Controle Line
4  2  0.5  100
!
! Stress Strain Points for Compression
! Stress  Strain
12648  0.0007
20737  0.0014
24042  0.0022
20436  0.00351
!
! Stress Strain Points for Tension
! Stress  Strain
2300  0.0001085
284  0.001085
!
! Steel Material Properties
! Controle Line

```

```

2 100
!
! Stress Strain Points for Steel
! Stress   Strain
526000 0.0026
616000 0.19
!
! Steel Material Properties
! Controle Line
1 100
!
! Stress Strain Points for CFRP
! Stress   Strain
1350000 0.0129
!
! Fiber Cross Section Types
! Controle Line
21 1
!
! Fibers Data
!
-0.110 0.110 0.000154 S1
0.110 0.110 0.000154 S1
-0.110 -0.110 0.000154 S1
0.110 -0.110 0.000154 S1
0 0.104 0.01352 C1
0 0.052 0.01352 C1
0 0 0.01352 C1
0 -0.052 0.01352 C1
0 -0.104 0.01352 C1
-0.13 0.093 0.0000164 S2
-0.13 0.056 0.0000164 S2
-0.13 0.019 0.0000164 S2
-0.13 -0.093 0.0000164 S2
-0.13 -0.056 0.0000164 S2
-0.13 -0.019 0.0000164 S2
0.093 -0.13 0.0000164 S2
0.056 -0.13 0.0000164 S2
0.019 -0.13 0.0000164 S2
-0.093 -0.13 0.0000164 S2
-0.056 -0.13 0.0000164 S2
-0.019 -0.13 0.0000164 S2
!
! Fiber Cross Section Types
! Controle Line

```

```

!
! Fibers Data
!
! Element Geometry Types
! Controle Line
3
!
! Segment data, Element Geometry Types
!
0.1    F01
0.8    F01
0.1    F01
!
! Element Generation Commands
!
1  2910  3010  100  1111  1
2  2920  3020  100  3333  1
!
*RESULTS
! Nodal Results: Sequential Generation
!
NSD  001 2010
!
! Element Results: Sequential Generation
!
!!E  001 1  1
!!E  001 1  2
!
*NODALOAD
! Pattern 1
! Pattern Name          Title
VERT                    Permanent Loads
!
! Nodal Loads: Sequential Generation
SF 0  -6    0    2010  2020  10
SF 0  -3    0    3010  3020  10
SF 0  -13.2  0    2012  2018  1
SF 0  -11.6  0    3012  3018  1
SF 0  -6.6   0    2011  2019  8
SF 0  -5.83  0    3011  3019  8
!
*DISPREC
! Ground Displacement Record
! Record Name
D05 0.05    (F14.12)    Elcentro Displacement Record 0.05

```

```

!
! Control Information
300301  0  0 1  1  0.001667  0
!
*DISPREC
! Ground Displacement Record
! Record Name
D10 0.10  (F14.12)  Elcentro Displacement Record 0.10
!
! Control Information
300301  0  0 1  1  0.001667  0
!
*DISPREC
! Ground Displacement Record
! Record Name
D20 0.20  (F14.12)  Elcentro Displacement Record 0.20
!
! Control Information
300301  0  0 1  1  0.001667  0
!
*DISPREC
! Ground Displacement Record
! Record Name
D30 0.30  (F14.12)  Elcentro Displacement Record 0.30
!
! Control Information
300301  0  0 1  1  0.001667  0
!
*DISPREC
! Ground Displacement Record
! Record Name
D40 0.40  (F14.12)  Elcentro Displacement Record 0.25
!
! Control Information
300301  0  0 1  1  0.001667  0
!
!
*PARAMETERS
! Analysis Parameters
! Event Overshoot Scale Factors
!
F 1 0.01  0.01
F 2 0.01  0.01
F 3 0.01  0.01
F 4 0.01  0.01

```



```

F 5 0.01 0.01
F 6 0.01 0.01
F 7 0.01 0.01
F 8 0.01 0.01
F 9 0.01 0.01
F 10 0.01 0.01
F 11 0.01 0.01
F 12 0.01 0.01
F 13 0.01 0.01
F 14 0.01 0.01
F 15 0.01 0.01
!
! Output Intervals for Dynamic Analysis
!
OD 0 0 1 0 0 0 0 0
!
! Controle Parameters for Dynamic Analysis
!
DC 1 0 00
!
! Time Step Parameters for Dynamic Analysis
!
DT 0.01 0.01
!
!!*GRAV PERM + Variable
!
! Static Gravity Load Analysis
!
! Nodal Loads
!!N VERT1.0
!
!!*STAT Permanent Load Analysis
!
! Static Analysis
!
! Nodal Loads
!
!!N VERT 1.0
!
! Load Controle
!
!!L 1 1
!
*MODE Mode Shapes
!

```

```

! Controle Information
!
2      0  0  0
!
*DISN          Dynamic Analysis 01
!
! Control Information
!
40    60000  1
! Ground Displacement Records
!
R   D05 1    1
!
! Degrees of Freedom
! Nodal Loads: Sequential Generation
D 1  11    1010  1020  10
!
*REST
!
*DISN          Dynamic Analysis 02
!
! Control Information
!
40    60000  1
! Ground Displacement Records
!
R   D10 1    1
!
! Degrees of Freedom
! Nodal Loads: Sequential Generation
D 1  11    1010  1020  10
!
*REST
!
*DISN          Dynamic Analysis 03
!
! Control Information
!
40    60000  1
! Ground Displacement Records
!
R   D20 1    1
!
! Degrees of Freedom
! Nodal Loads: Sequential Generation

```

```

D 1 11 1010 1020 10
!
*REST
!
!
*DISN Dynamic Analysis 04
!
! Control Information
!
40 60000 1
! Ground Displacement Records
!
R D30 1 1
!
! Degrees of Freedom
! Nodal Loads: Sequential Generation
D 1 11 1010 1020 10
!
*REST
!
*DISN Dynamic Analysis 05
!
! Control Information
!
40 60000 1
! Ground Displacement Records
!
R D40 1 1
!
! Degrees of Freedom
! Nodal Loads: Sequential Generation
D 1 11 1010 1020 10
!
*STOP

```

### **D3. Test sequence 4 – New frame**

```

*STARTXX
! Nodal Restraints: Sequential Generation
TimeH 0 1 1 0 time history Units:kNm
!
*NODECOORDS

```

! Controle Nodes (C-lines)

C 1010	0	0	0
C 1020	4	0	0
C 2010	0	3.3	0
C 2020	4	3.3	0
C 3010	0	6.6	0
C 3020	4	6.6	0
C 2011	0.13	3.3	0
C 2012	0.43	3.3	0
C 2013	1.1	3.3	0
C 2014	1.55	3.3	0
C 2015	2	3.3	0
C 2016	2.45	3.3	0
C 2017	2.9	3.3	0
C 2018	3.47	3.3	0
C 2019	3.87	3.3	0
C 3011	0.13	6.6	0
C 3012	0.53	6.6	0
C 3013	1.1	6.6	0
C 3014	1.55	6.6	0
C 3015	2	6.6	0
C 3016	2.45	6.6	0
C 3017	2.9	6.6	0
C 3018	3.57	6.6	0
C 3019	3.87	6.6	0
C 1910	0	3.1	0
C 2110	0	3.5	0
C 2910	0	6.4	0
C 1920	4	3.1	0

C 2120 4 3.5 0

C 2920 4 6.4 0

!Other Nodes

C 1110 0 0.55 0

C 1120 4 0.55 0

C 1810 0 2.55 0

C 1820 4 2.55 0

C 2210 0 4.05 0

C 2220 4 4.05 0

C 2810 0 5.85 0

C 2820 4 5.85 0

! Control Nodes

C 1111 0 0 1

C 2222 0 10 0

C 3333 4 0 1

!

\*RESTRAINTS

! Nodal Restraints: Sequential Generation

S 222222 1010 1020 10

S 001110 2010 2020 1

S 001110 3010 3020 1

S 111111 1111 3333 1111

S 001110 1910 1920 10

S 001110 2110 2120 10

S 001110 2910 2920 10

!

\*MASSES

! Nodal Masses: Sequential Generation

S 100 5.927 2010 2020 10 1.0 0.533896

```

S 100 5.029 3010 3020 10
!
*ELEMENTGROUP
! Group 1
! Element Group Definition
15 1 1 0.000644 COL-1(ZNC)
!
! Controle information
!
1 1 1 0 0 0 0 0 1
!
! Concrete Material Properties
! Controle Line
4 2 0.5 100
!
! Stress Strain Points for Compression
! Stress Strain
15450 0.0007
27493 0.0015
31970 0.0023
27175 0.0064
!
! Stress Strain Points for Tension
! Stress Strain
2300 0.0001
284 0.001
!
! Steel Material Properties
! Controle Line

```

```

2 100
!
! Stress Strain Points for Steel
! Stress   Strain
526000  0.0026
616000  0.19
!
! Fiber Cross Section Types
! Controle Line
13 1
!
! Fibers Data
!
-0.105  0.105  0.000154  S1
0       0.105  0.000154  S1
0.105   0.105  0.000154  S1
-0.105  0      0.000154  S1
0.105   0      0.000154  S1
-0.105  -0.105 0.000154  S1
0       -0.105 0.000154  S1
0.105   -0.105 0.000154  S1
0       0.104  0.01352   C1
0       0.052  0.01352   C1
0       0     0.01352   C1
0       -0.052 0.01352   C1
0       -0.104 0.01352   C1
!
! Fiber Cross Section Types
! Controle Line

```

```

!
! Fibers Data
!
! Element Geometry Types
! Controle Line
1
!
! Segment data, Eement Geometry Types
!
1      F01
!
! Element Generation Commands
!
1  1110  1810  700  1111  1
2  1120  1820  700  3333  1
!
*ELEMENTGROUP
! Group 2
! Element Group Definition
15  1  1  0.000644  COL-2(ZNC)
!
! Controle information
!
1  1  1  0  0  0  0  0  1
!
! Concrete Material Properties
! Controle Line
4  2  0.5  100
!

```



! Stress Strain Points for Compression

! Stress Strain

13589 0.0007

22879 0.0014

26951 0.0022

22908 0.00366

!

! Stress Strain Points for Tension

! Stress Strain

2300 0.0001

284 0.001

!

! Steel Material Properties

! Controle Line

2 100

!

! Stress Strain Points for Steel

! Stress Strain

526000 0.0026

616000 0.19

!

! Fiber Cross Section Types

! Controle Line

13 1

!

! Fibers Data

!

-0.105 0.105 0.000154 S1

0 0.105 0.000154 S1

```

0.105  0.105  0.000154  S1
-0.105  0    0.000154  S1
0.105  0    0.000154  S1
-0.105 -0.105 0.000154  S1
0    -0.105 0.000154  S1
0.105 -0.105 0.000154  S1
0    0.104  0.01352  C1
0    0.052  0.01352  C1
0    0    0.01352  C1
0    -0.052 0.01352  C1
0    -0.104 0.01352  C1
!
! Fiber Cross Section Types
! Controle Line
!
! Fibers Data
!
! Element Geometry Types
! Controle Line
1
!
! Segment data, Eement Geometry Types
!
1    F01
!
! Element Generation Commands
!
1  2210  2810  600  1111  1
2  2220  2820  600  3333  1

```

```

!
*ELEMENTGROUP
! Group 3
! Element Group Definition
15  1  1  0.000644  BEAMS-mid1
!
! Controle information
!
1  1  1  0  0  0  0  0  1
!
! Concrete Material Properties
! Controle Line
4  2  0.5  100
!
! Stress Strain Points for Compression
! Stress  Strain
16298  0.00075
29047  0.0017
31530  0.0023
26801  0.0035
!
! Stress Strain Points for Tension
! Stress  Strain
2300  0.0001
284  0.001
!
! Steel Material Properties
! Controle Line
2  100

```

```

!
! Stress Strain Points for Steel
! Stress   Strain
526000  0.0026
616000  0.19
!
! Fiber Cross Section Types
! Controle Line
14  1
!
! Fibers Data
!
-0.125  0.105  0.000154  S1
0.125  0.105  0.000154  S1
-0.125  0.0333  0.000154  S1
0.125  0.0333  0.000154  S1
-0.125  -0.0333  0.000154  S1
0.125  -0.0333  0.000154  S1
-0.125  -0.105  0.000154  S1
0.125  -0.105  0.000154  S1
-0.125  0  0.013  C1
-0.075  0  0.013  C1
-0.025  0  0.013  C1
0.025  0  0.013  C1
0.075  0  0.013  C1
0.125  0  0.013  C1
!
! Element Geometry Types
! Controle Line

```

```

1
!
! Segment data, Element Geometry Types
!
1      F01
!
! Element Generation Commands
!
1  2012  2013  0001  2222  1
2  2013  2014  0001  2222  1
3  2014  2015  0001  2222  1
4  2015  2016  0001  2222  1
5  2016  2017  0001  2222  1
6  2017  2018  0001  2222  1
!
*ELEMENTGROUP
! Group 4
! Element Group Definition
15  1  1  0.000644      BEAMS-mid2
!
! Controle information
!
1  1  1  0  0  0  0  0  1
!
! Concrete Material Properties
! Controle Line
4  2  0.5  100
!
! Stress Strain Points for Compression

```

```

! Stress   Strain
18660    0.00105
24300    0.0016
26551    0.0022
22568    0.00351
!
! Stress Strain Points for Tension
! Stress   Strain
2300     0.0001
284      0.001
!
! Steel Material Properties
! Controle Line
2  100
!
! Stress Strain Points for Steel
! Stress   Strain
526000   0.0026
616000   0.19
!
! Fiber Cross Section Types
! Controle Line
14  1
!
! Fibers Data
!
-0.125  0.105  0.000154  S1
0.125   0.105  0.000154  S1
-0.125  0.0333 0.000154  S1

```

```

0.125  0.0333  0.000154  S1
-0.125 -0.0333  0.000154  S1
0.125  -0.0333  0.000154  S1
-0.125 -0.105  0.000154  S1
0.125  -0.105  0.000154  S1
-0.125  0      0.013    C1
-0.075  0      0.013    C1
-0.025  0      0.013    C1
0.025   0      0.013    C1
0.075   0      0.013    C1
0.125   0      0.013    C1
!
! Element Geometry Types
! Controle Line
1
!
! Segment data, Element Geometry Types
!
1      F01
!
! Element Generation Commands
!
1  3012  3013  0001  2222  1
2  3013  3014  0001  2222  1
3  3014  3015  0001  2222  1
4  3015  3016  0001  2222  1
5  3016  3017  0001  2222  1
6  3017  3018  0001  2222  1
!

```

```

*ELEMENTGROUP
! Group 5
! Element Group Definition
15  1  1  0.000644      COL-joint1
!
! Controle information
!
1  1  1  0  0  0  0  0  1
!
! Concrete Material Properties
! Controle Line
4  2  0.5  100
!
! Stress Strain Points for Compression
! Stress   Strain
15818  0.0007
28900  0.0015
34124  0.0023
29006  0.00487
!
! Stress Strain Points for Tension
! Stress   Strain
2300  0.0001
284  0.001
!
! Steel Material Properties
! Controle Line
2  100
!

```



! Stress Strain Points for Steel

! Stress Strain

526000 0.0026

616000 0.19

!

! Fiber Cross Section Types

! Controle Line

13 1

!

! Fibers Data

!

-0.105 0.105 0.000154 S1

0 0.105 0.000154 S1

0.105 0.105 0.000154 S1

-0.105 0 0.000154 S1

0.105 0 0.000154 S1

-0.105 -0.105 0.000154 S1

0 -0.105 0.000154 S1

0.105 -0.105 0.000154 S1

0 0.104 0.01352 C1

0 0.052 0.01352 C1

0 0 0.01352 C1

0 -0.052 0.01352 C1

0 -0.104 0.01352 C1

!

! Fiber Cross Section Types

! Controle Line

!

! Fibers Data

```

!
!
! Element Geometry Types
! Controle Line
1
!
! Segment data, Element Geometry Types
!
1      F01
!
! Element Generation Commands
!
1  1910  2010  100  1111  1
2  1920  2020  100  3333  1
!
*ELEMENTGROUP
! Group 6
! Element Group Definition
15  1  1  0.000644      COL-joint2DOWN
!
! Controle information
!
1  1  1  0  0  0  0  0  1
!
! Concrete Material Properties
! Controle Line
4  2  0.5  100
!
! Stress Strain Points for Compression

```

```

! Stress   Strain
15818    0.0007
28900    0.0015
34124    0.0023
29006    0.00487
!
! Stress Strain Points for Tension
! Stress   Strain
2300     0.0001
284      0.001
!
! Steel Material Properties
! Controle Line
2  100
!
! Stress Strain Points for Steel
! Stress   Strain
526000   0.0026
616000   0.19
!
! Fiber Cross Section Types
! Controle Line
9  1
!
! Fibers Data
!
-0.105   0.105   0.000154   S1
0.105    0.105   0.000154   S1
-0.105   -0.105   0.000154   S1

```

```

0.105  -0.105  0.000154  S1
0      0.104   0.01352   C1
0      0.052   0.01352   C1
0      0       0.01352   C1
0      -0.052  0.01352   C1
0      -0.104  0.01352   C1
!
! Fiber Cross Section Types
! Controle Line
!
! Fibers Data
!
! Element Geometry Types
! Controle Line
1
!
! Segment data, Element Geometry Types
!
1      F01
!
! Element Generation Commands
!
1  2010  2110  100  1111  1
2  2020  2120  100  3333  1
!
*ELEMENTGROUP
! Group 7
! Element Group Definition
15    1  1  0.000644    Beam-Joint1

```

```

!
! Controle information
!
1 1 1 0 0 0 0 1 1
!
! Concrete Material Properties
! Controle Line
4 2 0.5 100
!
! Stress Strain Points for Compression
! Stress Strain
15503 0.0007
29190 0.00165
32263 0.0023
27424 0.0038
!
! Stress Strain Points for Tension
! Stress Strain
2300 0.0001
284 0.001
!
! Steel Material Properties
! Controle Line
2 100
!
! Stress Strain Points for Steel
! Stress Strain
526000 0.0026
616000 0.19

```

```

!
! Fiber Cross Section Types
! Controle Line
14 1
!
! Fibers Data
!
-0.125 0.105 0.000154 S1
0.125 0.105 0.000154 S1
-0.125 0.0333 0.000154 S1
0.125 0.0333 0.000154 S1
-0.125 -0.0333 0.000154 S1
0.125 -0.0333 0.000154 S1
-0.125 -0.105 0.000154 S1
0.125 -0.105 0.000154 S1
-0.125 0 0.013 C1
-0.075 0 0.013 C1
-0.025 0 0.013 C1
0.025 0 0.013 C1
0.075 0 0.013 C1
0.125 0 0.013 C1
!
! Rigid End Zone Types
!
0.12
!
! Element Geometry Types
! Controle Line
1 1

```

```

!
! Segment data, Element Geometry Types
!
1      F01
!
! Element Generation Commands
!
1  2010  2011  1  1111  1
2  2019  2020  1  1111  1
!
*ELEMENTGROUP
! Group 8
! Element Group Definition
15  1  1  0.000644      Beam-Joint2
!
! Controle information
!
1  1  1  0  0  0  0  1  1
!
! Concrete Material Properties
! Controle Line
4  2  0.5  100
!
! Stress Strain Points for Compression
! Stress   Strain
14463  0.00075
24813  0.0016
27208  0.0022
23127  0.00389

```

```

!
! Stress Strain Points for Tension
! Stress   Strain
2300   0.0001
284    0.001
!
! Steel Material Properties
! Controle Line
2   100
!
! Stress Strain Points for Steel
! Stress   Strain
526000  0.0026
616000  0.19
!
! Fiber Cross Section Types
! Controle Line
14  1
!
! Fibers Data
!
-0.125  0.105  0.000154  S1
0.125   0.105  0.000154  S1
-0.125  0.0333 0.000154  S1
0.125   0.0333 0.000154  S1
-0.125  -0.0333 0.000154  S1
0.125   -0.0333 0.000154  S1
-0.125  -0.105  0.000154  S1
0.125   -0.105  0.000154  S1

```



```

-0.125  0    0.013  C1
-0.075  0    0.013  C1
-0.025  0    0.013  C1
0.025   0    0.013  C1
0.075   0    0.013  C1
0.125   0    0.013  C1
!
! Rigid End Zone Types
!
0.12
!
! Element Geometry Types
! Controle Line
1      1
!
! Segment data, Element Geometry Types
!
1      F01
!
! Element Generation Commands
!
1  3010  3011  1    1111  1
2  3019  3020  1    1111  1
!
*ELEMENTGROUP
! Group 9
! Element Group Definition
15   1  1  0.000644    COL-joint2UP
!

```

! Controle information

!

1 1 1 0 0 0 0 0 1

!

! Concrete Material Properties

! Controle Line

4 2 0.5 100

!

! Stress Strain Points for Compression

! Stress Strain

13974 0.0007

24180 0.0014

29014 0.0022

24661 0.00513

!

! Stress Strain Points for Tension

! Stress Strain

2300 0.0001

284 0.001

!

! Steel Material Properties

! Controle Line

2 100

!

! Stress Strain Points for Steel

! Stress Strain

526000 0.0026

616000 0.19

!

```

! Fiber Cross Section Types
! Controle Line
13 1
!
! Fibers Data
!
-0.105 0.105 0.000154 S1
0 0.105 0.000154 S1
0.105 0.105 0.000154 S1
-0.105 0 0.000154 S1
0.105 0 0.000154 S1
-0.105 -0.105 0.000154 S1
0 -0.105 0.000154 S1
0.105 -0.105 0.000154 S1
0 0.104 0.01352 C1
0 0.052 0.01352 C1
0 0 0.01352 C1
0 -0.052 0.01352 C1
0 -0.104 0.01352 C1
!
! Fiber Cross Section Types
! Controle Line
!
! Fibers Data
!
! Element Geometry Types
! Controle Line
1
!

```

```

! Segment data, Element Geometry Types
!
1      F01
!
! Element Generation Commands
!
1  2910  3010  100  1111  1
2  2920  3020  100  3333  1
!
*ELEMENTGROUP
! Group 10
! Element Group Definition
15  1  1  0.000644      COL-story1(ZCDOWN)
!
! Controle information
!
1  1  1  0  0  0  0  0  1
!
! Concrete Material Properties
! Controle Line
4  2  0.5  100
!
! Stress Strain Points for Compression
! Stress   Strain
15818  0.0007
28900  0.0015
34124  0.0023
29006  0.00487
!

```

! Stress Strain Points for Tension

! Stress Strain

2300 0.0001

284 0.001

!

! Steel Material Properties

! Controle Line

2 100

!

! Stress Strain Points for Steel

! Stress Strain

526000 0.0026

616000 0.19

!

! Fiber Cross Section Types

! Controle Line

13 1

!

! Fibers Data

!

-0.105 0.105 0.000154 S1

0 0.105 0.000154 S1

0.105 0.105 0.000154 S1

-0.105 0 0.000154 S1

0.105 0 0.000154 S1

-0.105 -0.105 0.000154 S1

0 -0.105 0.000154 S1

0.105 -0.105 0.000154 S1

0 0.104 0.01352 C1

```

0    0.052  0.01352  C1
0    0      0.01352  C1
0    -0.052 0.01352  C1
0    -0.104 0.01352  C1
!
! Fiber Cross Section Types
! Controle Line
!
! Fibers Data
!
! Element Geometry Types
! Controle Line
1
!
! Segment data, Eement Geometry Types
!
1    F01
!
! Element Generation Commands
!
1  1010  1110  100  1111  1
2  1020  1120  100  3333  1
!
*ELEMENTGROUP
! Group 11
! Element Group Definition
15  1  1  0.000644  COL-story1(ZCUP)
!
! Controle information

```

```

!
1 1 1 0 0 0 0 0 1
!
! Concrete Material Properties
! Controle Line
4 2 0.5 100
!
! Stress Strain Points for Compression
! Stress Strain
15818 0.0007
28900 0.0015
34124 0.0023
29006 0.00487
!
! Stress Strain Points for Tension
! Stress Strain
2300 0.0001
284 0.001
!
! Steel Material Properties
! Controle Line
2 100
!
! Stress Strain Points for Steel
! Stress Strain
526000 0.0026
616000 0.19
!
! Fiber Cross Section Types

```

```

! Controle Line
13 1
!
! Fibers Data
!
-0.105 0.105 0.000154 S1
0 0.105 0.000154 S1
0.105 0.105 0.000154 S1
-0.105 0 0.000154 S1
0.105 0 0.000154 S1
-0.105 -0.105 0.000154 S1
0 -0.105 0.000154 S1
0.105 -0.105 0.000154 S1
0 0.104 0.01352 C1
0 0.052 0.01352 C1
0 0 0.01352 C1
0 -0.052 0.01352 C1
0 -0.104 0.01352 C1
!
! Fiber Cross Section Types
! Controle Line
!
! Fibers Data
!
! Element Geometry Types
! Controle Line
1
!
! Segment data, Eement Geometry Types

```



```

!
1      F01
!
! Element Generation Commands
!
1  1810  1910  100  1111  1
2  1820  1920  100  3333  1
!
*ELEMENTGROUP
! Group 12
! Element Group Definition
15  1  1  0.000644      COL-2(ZCDOWN)
!
! Controle information
!
1  1  1  0  0  0  0  0  1
!
! Concrete Material Properties
! Controle Line
4  2  0.5  100
!
! Stress Strain Points for Compression
! Stress   Strain
13974  0.0007
24180  0.0014
29014  0.0022
24661  0.00513
!
! Stress Strain Points for Tension

```

```

! Stress   Strain
2300   0.0001
284   0.001
!
! Steel Material Properties
! Controle Line
2   100
!
! Stress Strain Points for Steel
! Stress   Strain
526000  0.0026
616000  0.19
!
! Fiber Cross Section Types
! Controle Line
13  1
!
! Fibers Data
!
-0.105  0.105  0.000154  S1
0       0.105  0.000154  S1
0.105   0.105  0.000154  S1
-0.105  0      0.000154  S1
0.105   0      0.000154  S1
-0.105  -0.105 0.000154  S1
0       -0.105 0.000154  S1
0.105   -0.105 0.000154  S1
0       0.104  0.01352   C1
0       0.052  0.01352   C1

```

```

0    0    0.01352  C1
0    -0.052  0.01352  C1
0    -0.104  0.01352  C1
!
! Fiber Cross Section Types
! Controle Line
!
! Fibers Data
!
! Element Geometry Types
! Controle Line
1
!
! Segment data, Eement Geometry Types
!
1    F01
!
! Element Generation Commands
!
1  2110  2210  100  1111  1
2  2120  2220  100  3333  1
!
*ELEMENTGROUP
! Group 13
! Element Group Definition
15  1  1  0.000644  COL-2(ZCUP)
!
! Controle information
!

```

1 1 1 0 0 0 0 0 1

!

! Concrete Material Properties

! Controle Line

4 2 0.5 100

!

! Stress Strain Points for Compression

! Stress Strain

13974 0.0007

24180 0.0014

29014 0.0022

24661 0.00513

!

! Stress Strain Points for Tension

! Stress Strain

2300 0.0001

284 0.001

!

! Steel Material Properties

! Controle Line

2 100

!

! Stress Strain Points for Steel

! Stress Strain

526000 0.0026

616000 0.19

!

! Fiber Cross Section Types

! Controle Line

```

13 1
!
! Fibers Data
!
-0.105 0.105 0.000154 S1
0 0.105 0.000154 S1
0.105 0.105 0.000154 S1
-0.105 0 0.000154 S1
0.105 0 0.000154 S1
-0.105 -0.105 0.000154 S1
0 -0.105 0.000154 S1
0.105 -0.105 0.000154 S1
0 0.104 0.01352 C1
0 0.052 0.01352 C1
0 0 0.01352 C1
0 -0.052 0.01352 C1
0 -0.104 0.01352 C1
!
1
!
! Segment data, Element Geometry Types
!
1 F01
!
! Element Generation Commands
!
1 2810 2910 100 1111 1
2 2820 2920 100 3333 1
!

```

```

*ELEMENTGROUP
! Group 14
! Element Group Definition
15  1  1  0.000644      BEAMS-1 (ZC)
!
! Controle information
!
1  1  1  0  0  0  0  0  1
!
! Concrete Material Properties
! Controle Line
4  2  0.5  100
!
! Stress Strain Points for Compression
! Stress   Strain
17285  0.00075
33194  0.0017
36967  0.0023
31421  0.00714
!
! Stress Strain Points for Tension
! Stress   Strain
2300  0.0001
284  0.001
!
! Steel Material Properties
! Controle Line
2  100
!

```

! Stress Strain Points for Steel

! Stress Strain

526000 0.0026

616000 0.19

!

! Fiber Cross Section Types

! Controle Line

14 1

!

! Fibers Data

!

-0.125 0.105 0.000154 S1

0.125 0.105 0.000154 S1

-0.125 0.0333 0.000154 S1

0.125 0.0333 0.000154 S1

-0.125 -0.0333 0.000154 S1

0.125 -0.0333 0.000154 S1

-0.125 -0.105 0.000154 S1

0.125 -0.105 0.000154 S1

-0.125 0 0.013 C1

-0.075 0 0.013 C1

-0.025 0 0.013 C1

0.025 0 0.013 C1

0.075 0 0.013 C1

0.125 0 0.013 C1

!

! Element Geometry Types

! Controle Line

1

```

!
! Segment data, Element Geometry Types
!
1      F01
!
! Element Generation Commands
!
1  2011  2012  0001  2222  1
2  2018  2019  0001  2222  1
!
*ELEMENTGROUP
! Group 15
! Element Group Definition
15  1  1  0.000644      BEAMS-2(ZC)
!
! Controle information
!
1  1  1  0  0  0  0  0  1
!
! Concrete Material Properties
! Controle Line
4  2  0.5  100
!
! Stress Strain Points for Compression
! Stress   Strain
20627  0.00105
28283  0.0016
31916  0.0022
27127  0.00803

```



```

!
! Stress Strain Points for Tension
! Stress   Strain
2300    0.0001
284     0.001
!
! Steel Material Properties
! Controle Line
2  100
!
! Stress Strain Points for Steel
! Stress   Strain
526000  0.0026
616000  0.19
!
! Fiber Cross Section Types
! Controle Line
14  1
!
! Fibers Data
!
-0.125  0.105  0.000154  S1
0.125   0.105  0.000154  S1
-0.125  0.0333 0.000154  S1
0.125   0.0333 0.000154  S1
-0.125  -0.0333 0.000154  S1
0.125   -0.0333 0.000154  S1
-0.125  -0.105  0.000154  S1
0.125   -0.105  0.000154  S1

```

```

-0.125  0    0.013  C1
-0.075  0    0.013  C1
-0.025  0    0.013  C1
0.025   0    0.013  C1
0.075   0    0.013  C1
0.125   0    0.013  C1
!
! Element Geometry Types
! Controle Line
1
!
! Segment data, Element Geometry Types
!
1      F01
!
! Element Generation Commands
!
1  3011  3012  0001  2222  1
2  3018  3019  0001  2222  1
!
*RESULTS
! Nodal Results: Sequential Generation
!
NSD  001 2010
!
! Element Results: Sequential Generation
!
!!E  001 1  1
!!E  001 1  2

```

```

!
*NODALOAD
! Pattern 1
! Pattern Name          Title
VERT                    Permanent Loads
!
! Nodal Loads: Sequential Generation
SF 0  -6    0    2010  2020  10
SF 0  -3    0    3010  3020  10
SF 0  -13.2  0    2012  2018  1
SF 0  -11.6  0    3012  3018  1
SF 0  -6.6   0    2011  2019  8
SF 0  -5.83  0    3011  3019  8
!
*DISPREC
! Ground Displacement Record
! Record Name
D05 0.05    (F14.12)    Elcentro Displacement Record 0.05
!
! Control Information
300301    0  0  1    1    0.001667  0
!
*DISPREC
! Ground Displacement Record
! Record Name
D10 0.10    (F14.12)    Elcentro Displacement Record 0.10
!
! Control Information
300301    0  0  1    1    0.001667  0

```

```

!
*DISPREC
! Ground Displacement Record
! Record Name
D20 0.20      (F14.12)      Elcentro Displacement Record 0.20
!
! Control Information
300301      0  0 1      1      0.001667  0
!
*DISPREC
! Ground Displacement Record
! Record Name
D30 0.30      (F14.12)      Elcentro Displacement Record 0.30
!
! Control Information
132011      0  0 1      1      0.001667  0
!
*DISPREC
! Ground Displacement Record
! Record Name
D40 0.40      (F14.12)      Elcentro Displacement Record 0.25
!
! Control Information
180011      0  0 1      1      0.001667  0
!
*PARAMETERS
! Analysis Parameters
! Event Overshoot Scale Factors
!

```

F 1 0.01 0.01  
F 2 0.01 0.01  
F 3 0.01 0.01  
F 4 0.01 0.01  
F 5 0.01 0.01  
F 6 0.01 0.01  
F 7 0.01 0.01  
F 8 0.01 0.01  
F 9 0.01 0.01  
F 10 0.01 0.01  
F 11 0.01 0.01  
F 12 0.01 0.01  
F 13 0.01 0.01  
F 14 0.01 0.01  
F 15 0.01 0.01

!

! Output Intervals for Dynamic Analysis

!

OD 0 0 1 0 0 0 0 0

!

! Control Parameters for Dynamic Analysis

!

DC 1 0 00

!

! Time Step Parameters for Dynamic Analysis

!

DT 0.01 0.01

!

!!\*GRAV PERM + Variable

```
!  
! Static Gravity Load Analysis  
!  
! Nodal Loads  
!!N VERT1.0  
!  
!!*STAT Permanent Load Analysis  
!  
! Static Analysis  
!  
! Nodal Loads  
!  
!!N VERT 1.0  
!  
! Load Controle  
!  
!!L 1 1  
!  
*MODE Mode Shapes  
!  
! Controle Information  
!  
2 0 0 0  
!  
*DISN Dynamic Analysis 01  
!  
! Control Information  
!  
40 60000 1
```

```

! Ground Displacement Records
!
R   D05 1    1
!
! Degrees of Freedom
! Nodal Loads: Sequential Generation
D 1  11    1010  1020  10
!
*REST
!
!
*DISN                      Dynamic Analysis 02
!
! Control Information
!
40   60000  1
! Ground Displacement Records
!
R   D10 1    1
!
! Degrees of Freedom
! Nodal Loads: Sequential Generation
D 1  11    1010  1020  10
!
*REST
!
!
*DISN                      Dynamic Analysis 03
!

```

```

! Control Information
!
40    60000  1
! Ground Displacement Records
!
R   D20 1    1
!
! Degrees of Freedom
! Nodal Loads: Sequential Generation
D 1  11    1010  1020  10
!
*REST
!
!
*DISN                Dynamic Analysis 04
!
! Control Information
!
40    60000  1
! Ground Displacement Records
!
R   D30 1    1
!
! Degrees of Freedom
! Nodal Loads: Sequential Generation
D 1  11    1010  1020  10
!
*REST
!

```



```
!  
*DISN                      Dynamic Analysis 05  
!  
! Control Information  
!  
40    60000  1  
!  
! Ground Displacement Records  
!  
R   D40 1    1  
!  
! Degrees of Freedom  
!  
! Nodal Loads: Sequential Generation  
D 1  11    1010  1020  10  
!  
*STOP
```